PhD Thesis

The Role of Growth Associated Transcription Factors c-Jun and ATMIN in Neuronal Regeneration and Repair.

Crystal Ann Delores Blaylock Ruff

Department of Perinatal Brain Repair/

Department of Cell and Developmental Biology

University College London

Supervisors: Professors Gennadij Raivich and Stephen P. Hunt

This Thesis is Submitted for the Degree of:

Doctor of Philosophy (PhD) in Neuroscience

DECLARATION

I, Crystal Ann Delores Blaylock Ruff, confirm that the work presented in this thesis is my own. Where information has been derived from other sources, I confirm that this has been indicated in the thesis.

Signed:_____ Date:_____

ABSTRACT

1.1 The Role of Growth-Associated Transcription Factors c-Jun and ATMIN in Neuronal Regeneration and Repair

Subsequent to neuronal injury, increased levels of protein synthesis accompany associated rises in transcription factor expression. Two transcription factors involved in the cellular stress response are *c-Jun* and *ATMIN*.

Neuron-specific deletion of c-Jun resulted in defects in perineuronal sprouting, lymphocyte recruitment and microglial activation. Motoneurons also exhibited an atrophic phenotype, reduced target reinnervation and resistance to cell death. Additionally, mutants lacking Jun expression in peripheral Schwann Cells exhibited decreased regeneration and target muscle reinnervation, with accompanying deficits in cell survival, which highlights the dual role of c-Jun in response to stress. Homozygous deletion of JNK1, JNK2 or JNK3, or substitution of the c-Jun N-terminal serine phosphoacceptor sites (ser63&73), with alanines (JunAA), did not produce a difference in response to injury. This evidence indicates that N-terminal phosphorylation of ser63&73 does not play an essential function for axonal regeneration in vivo, while the whole c-Jun is clearly needed to successfully mount a regenerative response.

$ATMIN^{\Delta N}$ mutants, which have CNS-specific Nestin::Cre-mediated ATMIN deletion, exhibited higher transcription factor expression (c-Jun, Activating Transcription Factor-3/ATF3) in facial motoneurons – both baseline and following peripheral facial axotomy - and increased central post-traumatic sprouting of CGRP-and galanin-immunoreactive motoneurites. Although there was no effect on gross functional recovery or neuronal cell death, retrograde transport of florescent markers (Fluoro-Gold, MiniRuby) revealed augmented branching under normal conditions and during the reinnervation of peripheral

motor targets. In the spinal cord injury model, ATMIN$^{\Delta n}$ animals showed increased numbers of corticospinal tract (CST) axons projecting to both dorsal horns and contralateral CST, as well as bilateral impairment in precise co-ordinated motor behaviour following dorsolateral hemisection. This highlights the role of ATMIN as an important regulator of axonal guidance and pruning in neuronal development and regeneration.

Altogether, these findings demonstrate the essential roles of c-Jun and ATMIN in the neuronal stress response following nerve transection.

ACKNOWLEDGEMENTS

First and foremost, I would like to thank the Big Guy for getting me where I am today.

Secondly, I would like to thank my parents, Delores and Charles Ruff. All the praise and kind words in the world could not do you justice. Through your constant support, hard work, guidance and most importantly – your unconditional love - you made me what I am today. I've said it before and I'll say it again – I have the best parents in the world! Thank you.

To my amazing family, wonderful aunts and uncles and my exemplary grandparents, Ann and Roy Blaylock, and Phil and Greta Ruff – I Love You, I Love You, I Love You. You are the 'wind beneath my wings' and the source of my strength. Thank you for your constant, loving presence. Granddad, I know you're looking out for me from Heaven and hope I've made you proud!

To my Primary Supervisor, Professor Gennadij Raivich – Thank you for the valuable training you have provided. You taught me how to be a strong, independent scientist and how to critically evaluate research. You taught me how to 'frame frame frame' and the value of hard work. For that I will always be grateful. Thank you for the past 3 years!

To my Second Supervisor, Professor Stephen P. Hunt – I will always be grateful for your ears and your Kleenex (and your wisdom). You have been a beacon, shining a path of light through this whole process. Thank you for the strong guidance and soft shoulder.

To my Departmental Head, Professor Donald Peebles, you have been a constant source of positivity and solid leadership. You helped me (several times) when you didn't have to and that is an irrefutable testament to your character. You are everything a good leader should be and I am proud to have worked with you.

To my Colleague and Mentor, Patrick N. Anderson – There aren't words to describe my gratitude to you. For your guidance and wisdom, without which I would be scientifically lost, your patience during all the long hours of stereotactic surgery, your kind words, which got me through the tough days and your unwavering willingness to help when I really needed it! You are a unique and exceptional human being, not to mention an extraordinary scientist, and I consider it a great honour and privilege to have had the opportunity to work with you.

To Nnennaya Kanu – Thanks for Lunch! And for being the embodiment of the strong, capable, intelligent and well-rounded female scientist I would like to be one day. I will always admire your strength in science and strength of character.

To Eridan, my self-proclaimed lab minion and honorary science angel – you came into my life and lab just when I needed you most! I will always be grateful for your mind and heart... and overall brilliance and wonderfulness! *Because we love science!*

To my lab-mates and work colleagues, both past and present – Lab Manager, Dr. Mariya Hristova, Postdoctoral fellow, Dr. Prakasham Rumajogee, PhD students Dr. Milan Makwana, Dr. Giles Kendall, Alejandro Acosta-Saltos, Alex Liang, Laura Thei and Smriti Patodia for your teamwork and cheer in the face of intense stress - and for your 'best hugs'. To Eleonora, Emily and Judy on the admin team, thanks for all the blank CDs! And to the PGD girls and our 'winning' office - thank you for team Fridays.

To Marianne, Rachel, Jen, and Eddy Goh - thanks for your unflappable guidance. Out of the goodness of your big hearts, you shared your wisdom and time with me. For no other reason than the fact that you were good people (and maybe some swimming lessons), you provided me with invaluable help and guidance. May your blessings be surpassed only by your good looks! And my gratitude toward you.

To my flatmates, both past and present, who have looked out for me and tolerated my late nights and constant stressing – and still found it in their hearts to share their chocolate and make me kofte, polenta and chicken fajitas on the weekends. You are exquisite.

To my supportive and loving friends –I couldn't have made it here without you. Thanks for holding my hand and heart.

TABLE OF CONTENTS

TABLE OF FIGURES

TABLE OF EQUATIONS

TABLE OF TABLES

LIST OF ABBREVIATIONS

A	Astrocytes
a4B1y1	Alpha4 chain in laminin 8
AAD	Acute Axonal Degeneration
ALS	Amyotrophic Lateral Sclerosis
AP1	Activator Protein 1
APC	Antigen Presenting Cell
ASCIZ	Ataxia Telangiectasia Mutated/Ataxia Telangiectasia and Rad3 related substrate Chk2-interacting Zn^{2+}-finger protein
ATF	Activating Transcription Factor
ATM	Ataxia Telangiectasia Mutated
ATMIN	Ataxia Telangiectasia Mutated Interacting Protein
$ATMIN^{\Delta N}$	Mice lacking ATMIN in neural cells
$ATMIN^{F/F}$	Floxed ATMIN allele
ATR	Ataxia Telangiectasia and Rad3 related
B2-MG	Beta2-microglobulin
BBB	Blood Brain Barrier
BDNF	Brain –Derived Neurotrophic Factor
BIM	BcI2-interacting mediator of cell death
Bs	Brain stem
CaM kinase I	Ca^{2+}/calmodulin-dependent protein kinase I
cAMP	Cyclic adenosine monophosphate
Cb	Cerebellum
CD44	Hyaluronic acid receptor
cdc	Cyclin-dependent protein kinase
ced-3	Caenorhabditis elegans correlate – cell death abnormality-3
CGRP	Calcitonin Gene Related Peptide
Cip 1/WAF 1	Cyclin-dependent-kinase inhibitor p21
$c\text{-}Jun^{\Delta N}$	Mice lacking c-Jun in neural cells
$c\text{-}Jun^{\Delta S}$	Mice lacking c-Jun in neurons
CNS	Central Nervous System
CNTF	Ciliary Neurotrophic Factor
CNTFR	CNTF receptor
CR1, 2, and 4	Complement receptors

CRE	Cyclic AMP response element
CREB	Cyclic AMP response element-binding protein
CRTC1	Cyclic AMP response element-binding protein-regulated transcription coactivator 1
CSPGs	Chondroitin Sulfate Proteoglycans
CST	Corticospinal tract
Cx	Cortex
D	Mean diameter of nucleolus perpendicular to sectioning direction
d04	Day 4
d14	Day 14
DHH	Desert Hedgehog
DRG	Dorsal Root Ganglia
Egr	Early Growth Response Protein
ERK	Extracellular signal-related kinase
ES	Embryonic stem
EST	Expressed sequence tag
F1	Heterozygous offspring
F2	Homozygous offspring
FBW7L	FBW7 ubiquitin ligase
FG	Fluorogold
FGF	Fibroblast Growth Factor
floxed	Lox P tagged
FMN	Facial motor nucleus
FNA	Facial Nerve Axotomy
GAG	Glycos –aminoglycan
GDNF	Glial-cell derived neurotrophic factor
GFAP	Glial Fibrilatory Acidic Protein
GMC	GAP43, MARCKS and CAP23 cytoplasmic proteins
GRASP-1	GRIP1 associated protein 1
Gt	Goat
H&E	Haematoxylin and Eosin
Hc	Hippocampus
Hm	Hamster
ICAM-1	Intercellular adhesion molecule-1
ICE/ caspase-1	Interleukin-1B-converting enzyme

IFN	Interferon
IGF-1	Insulin-like Growth Factor 1
IkAP	IkB Kinase complex-associated protein
IL	Interleukin
IL-4	Interleukin-4
IR	Immunoreactivity
JDP	Jun dimerization Protein
JIPs	JNK interacting proteins
JNK	Jun N-Terminal Kinase
Jun AA	Mice with c-Jun N-Terminal serines mutated to Alanines
$jun^{f/f}$	Floxed c-jun allele
kDa	KiloDalton
KO	Knock Out
L2/HNK-1	L2 Carbohydrate
LIF	Leukaemia Inhibitory Factor
MAC-1	aM integrin
MAGs	Associated glycoproteins
MAP	Mitogen Activated Protein
MAPK	Mitogen-Activated Protein Kinase
MAPKK, MEK	MAPK Kinase
MAPKKK	MAPK Kinase Kinase
MBP	Myelin Basic Protein
MCSF	Monocyte Colony Stimulating Factor
MHC	Major Histocompatibility Complex
MN	Motor Neuron
MPF	Maturation/M-phase promoting factor
MR	Miniruby
MU	Mutant
N	Neurons
N_A	Uncorrected profile estimate per unit of area
NBS -1	Nibrin
Ncd	Neuronal Cell Death
Nes::cre	Nestin promoter-driven Cre Recombinase
NESC	Neuroepithelial Stem Cell
NeuN	Neuronal Nuclei

NF kappa-b	Nuclear factor kappa-b
NGF	Nerve Growth Factor
NO	Nitric oxide
NP	Neuropeptide
NOD	Non-Obese Diabetic
NRSF/REST	Neuron-restrictive silencer factor/RE-1 silencing transcription factor
NT -3	Neurotropin 3
N_V	Corrected estimate of object number per unit of volume (numerical density)
O	Oligodendrocytes
O2-	Superoxide
OLV	Optical luminosity value
P0 x $jun^{f/f}$	Mice lacking c-Jun in Schwann cells
P0	Myelin Protein 0
P0::cre	P0 promoter-driven Cre Recombinase
pAPCs	Professional antigen presenting cells
PB	Phosphate Buffer
PB/BSA	Bovine Serum Albumin in 0.1M PB
PBS	Phosphate buffered saline
PCR	Polymerase chain reaction
PFA	Paraformaldehyde
PI(4,5)P2	Phosphoinositol-4,5-diphosphate
PI3K	Phosphatidyl-inositol-3 kinase
PKA	Protein Kinase A
PMP22	Peripheral myelin protein-22
PNS	Peripheral Nervous system
POSH	Plenty of SH3
Rb	Rabbit
ROS	Reactive Oxygen Species
RST	Rubrospinal tract
Rt	Rat
SC	Schwann Cell
SCID	Severe Combined Immunodeficiency
SEM	Standard Error of the Mean
Ser63&73	Serine 63 and 73

SHH	Sonic Hedgehog
SI	Staining intensity
SKRP-1	Stress –activated protein kinase pathway-regulating phosphatase 1
SQ/TQ motifs	Serine or threonine residues followed by glutamine
SRS	Systematic Randomly Sampled
STAT-3	Signal transducer and activator of transcription-3
Syn::cre	Synapsin promoter-driven Cre Recombinase
T	Mean thickness of the section
TF	Transcription Factor
TFC	Transcription Factor Complex
TGF	Transforming Growth Factor
Thr91&93	Threonines 91 and 93
TNFR	Tumour necrosis factor receptors
TPA	12-O- Tetradecanoylphorbol-13 acetate
TRAIL	TNF-related apoptosis-inducing ligand
TRE	12-O- Tetradecanoylphorbol-13 acetate Response Element
TUNEL	TDT UTP Nick End Labelling
uSTT	Unpaired Student’s t test
VAChT	Vesicular Acetyl Choline Transporter
WT	Wild type
$Zn2^{+}$	Zinc

CHAPTER 2: INTRODUCTION

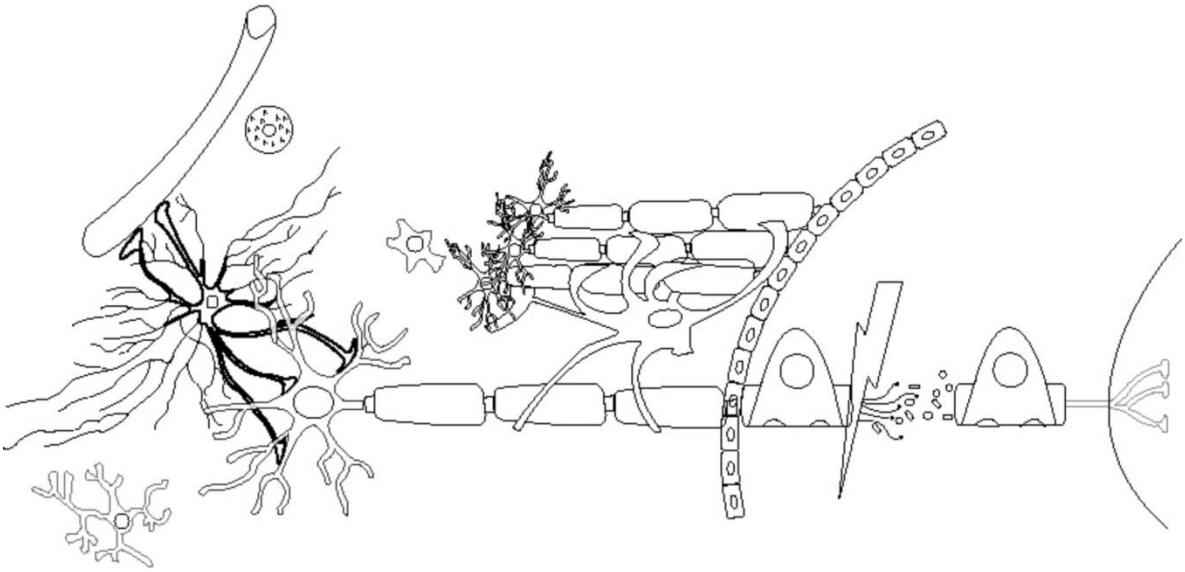

Nerve injury results in weakness, altered sensation, pain and loss of function below the level of the injury. Here, the extent of nerve injury (and also the resulting pain) can range from mild to severe, necessitating the need for better understanding of the underlying mechanisms in injury management.

Axonal injury – particularly peripheral nerve injury – can affect several different neurological systems. One of the most common peripheral nerves affected by injury is the facial motor nerve, of which the most prevalent type of injury is Bell's palsy. Each year, roughly one in 5000 individuals in the UK develops this condition (BUPA, 2009). Although Bell's palsy usually arises spontaneously from edema caused by viral infection or diabetes, eighty percent of facial motor nerve trauma also results in Bell's palsy.

From a research point of view, the assembly of facial motoneurons into a tightly packed, easily identifiable nucleus with high homogeneity, the separation by the Blood Brain Barrier (BBB) of facial motor neurons from their axons and the well characterized, successful regenerative response of the facial motor nerve also makes it an ideal paradigm in which to study the cellular response to injury.

2.1 Peripheral Regeneration

In anatomical terms, the central nervous system (CNS) consists of the brain and spinal cord; the peripheral nervous system (PNS) consists of all other nerve tissue located peripherally to the CNS. After injury, the PNS regenerates spontaneously whereas the CNS does not. These mechanisms are poorly understood, but involve synchronization of several key factors and systems, including the expression of both neuronal growth signals and trophic cues from the local microenvironment.

2.1.1 Wallerian Degeneration

In the injured peripheral nerve, a series of events will take place. First, neurofilaments and microtubules in the axoplasm of the distal nerve segment begin to deteriorate. This process was first characterized by Augustus Waller (Waller, 1850) and is called *Wallerian Degeneration. Wallerian Degeneration* is powered by a Ca2+ proteolytic mechanism that involves Calpain (Nixon et al., 1994; Schlaepfer and Hasler, 1979). Severed neurite ends retract via a vesicle-mediated process (Krause et al., 1994) and as early as thirty minutes after injury, both proximal and distal axons degenerate several hundreds of micrometres, a process termed *Acute Axonal Degeneration* (AAD, Kerschensteiner et al. 2005). Schwann cells degrade myelin into smaller units called ovoids, which are marked for opsonisation by peripheral macrophages (Vargas and Barres, 2007). *Wallerian Degeneration* proceeds down the distal nerve segment in a particular fashion, with the axotomized portion of the distal tip degrading within hours, neuromuscular denervation occurring within 12-24 hours and axonal shaft degradation around 3 days following injury (Chaudhry et al., 1992; Griffin and Thompson, 2008; Griffin et al., 1996; Gillingwater and Ribchester, 2003; Raivich et al., 1991). It is essential that peripheral macrophages and Schwann Cells quickly phagocytose

the extracellular debris created by this process, since extracellular myelin has been shown to be inhibitory to axonal sprouting (McGee and Strittmatter, 2003).

2.1.2 Schwann Cell Activation

Two to three days post-injury, Schwann cells become activated and begin to proliferate (Salonen et al., 1988). Schwann cells separate from their myelin sheath at Schmidt-Lanterman incisures and create *Bands of Büngner* which guide axons to their appropriate targets (Williams and Hall, 1971b, 1971a; Ghabriel and Allt, 1979a, 1979b). They also release cytoplasmic Ciliary Neurotrophic Factor (CNTF) stores and express several growth and survival associated factors such as Brain-Derived Neurotrophic Factor (BDNF), Glial Cell-Derived Neurotrophic factor (GDNF) and Leukaemia Inhibitory Factor (LIF, Boyd and Gordon 2002, 2003; Meyer et al. 1992; Sendtner et al. 1994; Terenghi 1999).

Although the Schwann cells separate from the myelin, the basal lamina remains intact. Studies show that as long as the basal lamina remains intact, elongation can proceed – even in the absence of Schwann cells (Fugleholm et al., 1994).

2.1.3 Developmental Regulation of Schwann Cells

Schwann cells originate from neuroepithelial stem cell precursors in the neural crest. Upon regulatory signals like Sox-10 upregulation, they differentiate into Schwann Cell precursors, which express Myelin Protein 0 (P0) and brain fatty acid binding protein, as well as Cadherin 19 (Takahashi and Osumi, 2005; Jessen, 2004). Morphologically, their processes begin to envelop bundles of axons – indicating differentiation into the immature SC phenotype, which express markers S100 protein, GFAP and O4 glycolipid.

At this point, a fate decision is made to either become myelinating or non-myelinating; this decision is influenced by neuregulin-1 expression, which inhibits P0 and subsequent myelination signals (Cheng and Mudge, 1996). In addition, transcription factor Krox-20 (also known as Early Growth Response Protein 2/Egr2) is indispensable for Schwann cell myelination, although it is not required for oligodendrocyte myelination (Parkinson et al., 2004; Lee et al., 1997; Jessen, 2004). Other pro-myelin cues are provided by Nab1 and 2, Oct-6, Brn2 and NFκB (Yoon et al., 2008; Ghislain and Charnay, 2006; Le et al., 2005; Nickols et al., 2003; Jaegle et al., 2003; Topilko et al., 1994).

Schwann Cells can revert back from myelinating or non-myelinating SCs to immature SCs in the presence of high levels of c-Jun and via cyclic adenosine monophosphate (cAMP) and the inhibition of the Krox-20 pathways (Parkinson et al., 2008; Mirsky et al., 2008). Here, c-jun and Krox-20 have antagonistic functions in Schwann Cell differentiation (Krox-20) and de-differentiation (c-Jun).

2.1.4 Chromatolytic Response

Following nerve injury, lesioned neurons initiate a *chromatolytic response.* The neuronal cell body cytoplasm swells and displaces the nucleus to the periphery of the cell soma (Bishop, 1982). Restructuring of the rough endoplasmic reticulum causes basophilic material in the cytoplasm to be more evenly distributed. Several electrophysiological processes are affected: chromatolytic cells exhibit decreased resting potential, conduction velocity and duration of after-hyperpolarization as well as increases in action potential overshoot (Huizar et al., 1977). There is also the onset of proximal sprouting. This regenerative sprouting refers to the growth cones that project from the proximal tip of the injured axon and extend filopodia along bands of Büngner toward extracellular targets, expressing markers CGRP, Galanin and Vesicular Acetyl Choline Transporter (VAChT)

(Makwana et al., 2009). Motor neuron axons extend processes preferentially toward their target distal segment along a chemotactic gradient – a process known as *Neurotropism* – and sometimes innervate several different Schwann cell tubes in the distal segment (Cajal, 1928).

Experiments using peripheral nerve grafts in the CNS show that some CNS neurons, in particular retinal ganglion cells, medullary and pontine reticular neurons, as well as striatal, cerebellar and thalamic neurons, can extend axonal processes through a peripheral nerve graft (Campbell et al., 2005; Hüll and Bähr, 1994; Schuetz et al., 2003; Tom and Houle, 2008; Houle et al., 2006; Zhang et al., 1995; Woolhead et al., 1998; Vaudano et al., 1995, 1998, 1996). Since these neuronal populations do not spontaneously regenerate in the CNS, this differential growth response indicates that the extracellular Schwann Cell environment might play a pivotal role in successful regeneration.

2.1.5 Preferential Motor Reinnervation

Not all Schwann Cells are created equal. Peripheral motor neurons exhibit a phenomenon known as *preferential motor reinnervation* (Brushart, 1988, 1993; Brushart and Seiler, 1987). Motor axons preferentially reinnervate motor targets and not sensory targets or cutaneous tissue. This is thought to be due primarily to the differential nature of Schwann cells that surround sensory and motor axons. Schwann cells surrounding sensory axons exhibit a pruning phenotype, whereas those surrounding motor neuron axons encourage growth. L2 Carbohydrate (L2/HNK-1) is expressed primarily on Schwann cells that innervate motor pathways rather than sensory ones. Through association with cell adhesion molecules, L2 Carbohydrate is thought to play a role in *preferential motor reinnervation;* it is present both during and after *Wallerian Degeneration*, which highlights its omnipresent role in this phenomenon (Nieke and Schachner, 1985a; Martini et al.,

1994). However, preferential reinnervation is not unique to motor neurons; studies using the transected femoral nerve show that, after sequential labelling, transected femoral sensory neurons show preferential sensory reinnervation (Madison et al., 1996) and more recent studies suggest an alternative trophic hierarchy model, with muscle contact at the top, followed by terminal branch length and/or contact with skin (Robinson and Madison, 2004).

2.1.6 Rate of Regeneration

Speed of regeneration varies depending on degree of nerve injury. Characterized by Sunderland (Sunderland, 1951), a first degree injury, which affects only myelination, can take up to twelve weeks to heal fully. Second through sixth degree injuries, which involve much more damage and also *Wallerian Degeneration*, sometimes never regenerate fully, although, in rodents, reinnervation is generally believed to proceed at a rate of 2-6 mm per day (Hadlock et al., 2005).

Due primarily to the extracellular environment, damaged neurons in the PNS tend to regenerate spontaneously whereas their CNS counterparts do not (Vaudano et al., 1995). As such, approaches to CNS repair commonly consist of attempts to shape the CNS environment in a way that would closely mimic that of the growth-permissive PNS. In particular, if one modifies or deletes a particular type of gene, especially one involved in growth, death or repair, it could affect regrowth of damaged axons.

2.2 Central Regeneration

Shortly after injury, neuronal cells express immediate early genes – such as transcription factors (TFs) c-jun, c-fos and ATF3. In the PNS, upregulation remains consistent

throughout the course of regeneration; in the CNS, this reaction is quickly quenched. Nerve Growth Factor (NGF), Brain-Derived Neurotrophic Factor (BDNF),as well as Laminin and several cell adhesion molecules also show lower levels of expression in response to CNS rather than PNS injury. Additionally, sprouting growth cones that are integral for PNS regeneration are quickly dampened by the CNS extracellular environment. Several key factors found in CNS glia and not PNS glia are commonly attributed to this differential growth.

2.2.1 Oligodendrocytes

First, the CNS contains three major types of glia – Oligodendrocytes (or Oligodendroglia), Astrocytes (or Astroglia) and Microglia. Microglia are a special population derived from a monocytic lineage which behave primarily in an immune surveillance and phagocytic function; their role will be discussed later. Oligodendrocytes are bulbous glia primarily responsible for producing CNS myelin. However, oligodendrocytes function differentially to their peripheral counterparts – the Schwann cells. Some of the most pronounced differences involve their role in myelination and phagocytosis. While peripheral Schwann cells myelinate axons in a strictly 1 to 1 fashion – that is, one Schwann Cell will myelinate only one axon – each oligodendrocyte can myelinate several axons simultaneously (Melli and Höke, 2007). After injury, Wallerian degeneration occurs in the distal nerve segment of CNS axons as well as PNS axons; however failure of these CNS axons to regenerate is partially attributable to differential glial activation. As mentioned previously, Schwann Cells are capable of phagocytosing extracellular debris when ‘activated’ by neuronal damage, whereas oligodendrocytes are not – thus they are unable to make the myelin ovoid bodies present in regenerating peripheral nerves. After injury, oligodendroglia continue to produce myelin whereas Schwann cells decrease synthesis of both myelin lipids and proteins within 48h following injury (Trapp et al., 1988; White et al., 1989; Morrison et al., 1991). Myelin

contains several cell surface proteoglycans that inhibit neuronal growth, some of which are called *nogo* (Filbin, 2003; Schwab, 2004), myelin associated glycoprotein (MAG) and oligodendrocyte-myelin glycoprotein (OMGP,Spencer, 2004). It has been shown that all three of these molecules bind to the nogo receptor present in neuronal growth cones and cause the cones' subsequent collapse (Giger et al., 2008). Also, due to the tight regulation of the Blood Brain Barrier (BBB), less monocytic infiltration (which helps clean up extracellular myelin and debris) is present in the CNS compared to the PNS.

2.2.2 Astrocytes

Astrocytes are star-shaped glia that, under normal circumstances, provide structural integrity within the brain. They display a multitude of immune cell signalling receptors, including Toll-like receptors, nucleotide-binding oligomerization domains, double-stranded RNA-dependent protein kinase, scavenger receptors, mannose receptors and components of the complement system (Farina et al., 2007). They also have a role in promoting brain metabolic processes and helping to maintain the BBB. Astrocytes express two main intermediate filament proteins – vimentin and Glial Fibrilatory Acidic Protein (GFAP). During development, vimentin immunoreactivity predominates, but is slowly replaced by GFAP in differentiated neurons. Once Astrocytes become activated, usually as a result of neural injury or trauma, they upregulate GFAP, and after severe trauma, also vimentin (Bramanti et al., 2010). They then extend processes to injured neurons and begin to secrete reactive oxygen intermediates like interleukin (IL)-1β, inducible nitric oxide (NO) synthase, the NO metabolite nitrite and superoxide (O2-), *in vitro* studies link this with the ERK1/2, p38 MAPK and JNK signalling pathways (Tichauer et al., 2007; Ranaivo and Wainwright, 2009). Astrocyte reaction also leads to the production of growth factors, like GM-CSF, that promote microglial growth and activation (Ovanesov et al., 2008; Lee et al., 1994) and initiate the cell response to damage (Liu et al., 1994). Recent data shows

Astrocyte activation can also induce oligodendrocyte proliferation in response to injury via the sonic Hedgehog (SHH) pathway (Amankulor et al., 2009) and that astrocytes and microglia function cooperatively in the neuronal response to injury (Pifarré et al., 2009; Butchi et al., 2009; Martin et al., 1994; Ranaivo et al., 2009).

Astrocytes also exhibit unique properties that inhibit central regeneration. Notably, after injury, reactive astrocytes as well as oligodendroglial precursors, contribute to glial scar formation– which is largely inhibitory to growing axons due to the enhanced expression of Chondroitin Sulfate Proteoglycans (CSPGs). Common CNS repair strategies consist of using a compound called chondroitinase ABC to degrade certain disaccharide glycosamino glycan (GAG) chains in these CSPGs. This alleviates the inhibitory effects of CSPGs and promotes axonal passage through the glial scar (Bradbury et al., 2002; Curinga et al., 2007).

2.2.3 Synaptic Stripping

Along with brain resident microglia, Astrocytes participate in a CNS process called *synaptic stripping* (Blinzinger and Kreutzberg, 1968) During this process, presynaptic clefts between dendrites of damaged neurons and terminal boutons of undamaged neurons are filled and separated by processes of activated astrocytes and microglia. It is unclear whether microglia and astrocytes invade these clefts to separate the presynaptic boutons from the postsynaptic dendrites or whether neurons first create the space; however microglia are present in stripped synapses from day 2-4 following injury and activated astrocytes invade soon after (Graeber et al., 1988; Streit and Kreutzberg, 1988; Graeber and Kreutzberg, 1986; Aldskogius et al., 1999). Recent studies using focal cortical inflammation models suggest that *synaptic stripping,* at least by microglia, is

neuroprotective, due to the absence of pathology following both acute and immune-mediated lesion using injection of killed bacteria (Trapp et al., 2007).

2.2.4 T Cells

A T-cell is a type of immune effector cell that homes to the site of injury and there can exert its trophic effects as a mediator of either the pro-inflammatory or anti-inflammatory response. Pro-inflammatory responses in the central nervous system are thought to be neurodestructive, while anti-inflammatory responses are considered neuroprotective. Th1 and Th17 subsets of T-cells are pro-inflammatory, whereas Th2, Tr1, and Foxp3(+) Treg cells are anti-inflammatory. Furthermore, CD4(+) T helper (Th) 2 cells, but not Th1 cells, have been shown to participate in the rescue of mouse facial motoneurons (FMN) from axotomy-induced cell death (Xin et al., 2008), possibly through NTF-dependent mechanisms that support motoneuron survival before target reconnection occurs (Serpe et al., 2005). Furthermore, these CD4(+) T cells can initially be activated peripherally and subsequently reactivated centrally. (Sanders and Jones, 2006).

T cells enter the injury site within the first 24 hours following insult. Although initial rate of infiltration is consistent, there is evidence that after 14 days, at the peak of the injury response, the number of invading T-cells in the facial motor nucleus is proportional to the severity of insult and resulting cell death – animals with crush injury showed fewer T-Cells in the facial motor nucleus than did animals with facial nerve resections (Ha et al., 2008). In addition, there is evidence of indirect microglial regulation of CD3 positive lymphocyte recruitment following injury through monocyte colony stimulating factor (MCSF) secretion, but T cells do not moderate microglial reactivity in the axotomized FMN (Ha et al., 2006). Although this early phase of microglial activation is not involved in regeneration following

peripheral nerve injury (Kalla et al., 2001), later interactions between T cells and microglia do seem to confer modest neuroprotection to injured motoneurons (Ha et al., 2006).

2.3 Inflammation and Regeneration- Microglia and Macrophages in the Nervous System

In the brain, resident microglia play a significant role in clearing debris within the CNS. In several types of injury models, damage to the BBB allows peripheral macrophages to invade the brain and participate in the injury response; this can affect experimental outcome.

However, recent studies show microglia and macrophages have different roles in the regenerative response and that invading peripheral macrophages can regulate local inflammation, as well as repress microglial activation (Shechter et al., 2009). Because of this, several researchers use injury models like the axotomized facial motor nucleus where the BBB remains intact and peripheral macrophages do not enter the nucleus itself.

2.3.1 Microglia

Microglia are perhaps the most important inflammatory mediators in the CNS; they comprise almost twenty percent of the CNS glial population and are loosely deemed brain-resident macrophages. Like their PNS counterparts, they originate from myeloid precursors. However, as their name suggests, these cells are also glia and form structural support for neurons as well. Microglia constantly circulate and patrol the brain and are quick to detect neuronal injury. In their ramified (or inactivated) form, microglia have a small nucleus and long, extended processes that they use to scan the environment. These surveillance cells do not express any type of cell surface Major Histocompatibility Complex

(MHC), which is characteristic of other antigen presenting cells (APCs, Aloisi, 2001). However, when microglia are activated - due to cues from the neuronal cellular response - they develop large, bulbous nuclei and start to express cell surface αM integrin subunit, MHC (either type I or II), as well as CD40, CD11b, Fc receptors I–III, complement receptors (CR1, 2, and 4), β2 integrins, the co-stimulatory molecules CD80, CD86, and intercellular adhesion molecule-1 (ICAM-1, Matsumoto et al. 1986; P. L. McGeer et al. 1993; Hickey & H. Kimura 1988; Minagar et al. 2002; Woodroofe et al. 1991). They are then able to secrete reactive intermediates like TNF-α, NO, IL-6 or TGF-β1, IL-1β and IL-10 and participate in the injury response as chemical signalling cells (Dopp et al., 1997; Woo et al., 2003; Kraft et al., 2009; Jana et al., 2002). Interestingly, depending on the stimulus, microglia play different roles in the injury response; for example, microglia show a neurotoxic phenotype following treatment with lipopolysaccharides (LPS) but show neuroprotection when primed with interleukin-4 (IL-4, Butovsky et al. 2006). In response to cellular debris, microglia upregulate cell-surface TNF receptors (TNFRs) 1 and 2 (Dopp et al., 1997), as well as transcription factors AP1 and STAT3 (Qin et al., 2007; Suh et al., 2005). Phagocytic microglia express αXβ2 integrin subunit on their cell surface and are known effector cells that can engulf debris and participate in the clearing response to neuronal insult (Bohatschek et al., 2004, 2001). Inside the cell, chemically destructive lysozomes form and chemotoxic intermediates are secreted. Phagocytic microglia found in periventricular zones preferentially cannibalise other phagocytic microglia during normal development (Hristova et al., 2009). Although some authors claimed that, after axotomy, a significant proportion of activated microglia are derived from peripheral hematopoietic cells that enter the CNS and differentiate into microglia in situ (Priller et al., 2001), this has been disproved in many experiments (Fluegel 2001, Bohatschek 2001).

2.3.2 Macrophages

Peripheral macrophages play a similar role to microglia; however they are generally more efficient due to their activation. They express MHC on their cell surfaces and are able to ingest debris, degrade axons and present antigen to T-Cells (which are identifiable by CD3 immunoreactivity). Activated macrophages can act as pro- or anti-inflammatory mediators, dependent on the means by which they are activated (DiPietro et al., 1998; Gallin and Goldstein, 1992) Interferon-(IFN-)γ is the classical macrophage activating factor leading to synthesis and release of inflammatory mediators, enhanced phagocytosis and upregulation of MHC class II and co-stimulatory molecules (North, 1978; Murray, 1988). However, other stimuli such as interleukin-(IL-) 4 can initiate a state of 'alternative activation' with the development of anti-inflammatory characteristics (Goerdt and Orfanos, 1999). In addition, invading macrophages, through ILβ upregulation, enhance NGF expression; NGF is an important intermediate in axonal regeneration, which will be discussed later (Lindholm et al. 1987; Nathan and Sieff 1987). Furthermore, there is evidence that axonal outgrowth is increased by macrophage application (Stolz et al., 1991; Miyauchi et al., 1997) and that inflammation near the nerve cell body enhances regeneration of DRGs (Lu and Richardson, 1991).

2.4 Injury Associated Molecules

Nerve transection rapidly induces several different molecular pathways in the injured neuron. These include cell death signals, neurotrophic factors, cell adhesion molecules, cell surface interactors and intracellular signalling molecules.

2.4.1 Cell Death Signals

There are several cell surface molecules associated with signalling cell death. For example, CD95 (fas, APO-1), TNF-related apoptosis-inducing ligand (TRAIL) R1/R2 (DR4 and DR5, respectively) and tumour necrosis factor receptors (TNFR) 1 and 2 have been linked to neuronal cell death following injury; all but TNFR2 carry identified cytoplasmic death domains (Terrado et al., 2000; Raivich et al., 2002; Ugolini et al., 2003; Schutze et al., 2008) However, not every time that these signals are induced does it lead to cell death. Thus, Fas and TNFR1 are capable of transducing anti-apoptotic signals through activation of a MAPK cascade or nuclear factor kappa-b (NF kappa-b) downstream activation (Schutze et al., 2008) .

Other factors found further downstream include the caspase and bax systems. Genetic deletion of both of these systems has been shown to prevent cell death (Chan et al., 2003; Yick et al., 2003; Sun and Chang, 2003; Sun and Oppenheim, 2003). Caspase systems consist of cysteine proteases that cleave after an aspartate residue (Alnemri et al., 1996) in their substrates and are a conserved family of enzymes that irreversibly commit a cell to die. The first caspase identified in humans was interleukin-1β-converting enzyme (ICE), also known as caspase-1, (Cerretti et al., 1992; Thornberry et al., 1992) . However, the role of caspase-1 in apoptosis was not properly characterized until its nematode worm Caenorhabditis elegans correlate - cell-death abnormality-3 (ced-3) was found and its role was elucidated (Yuan et al., 1993; Xue et al., 1996). Since then, at least 14 separate caspases have been identified in mammalian systems, of which 11 exist in humans (Shi, 2002). Furthermore, caspase action seems to be regulated at a post-translational level, due to the need for rapid activation after injury. Caspases are first synthesized as pro-caspases and once they are activated by death receptors like FAS, TRAIL 1 /2 and TNFR and the like, active caspases aggregate in a cluster formation where they proceed to

establish an effector phenotype (Yuan and Horvitz, 2004). Both Bax and caspases act downstream of c-Jun phosphorylation by JNKs (Chan et al., 2003; Sun et al., 2003; Sun et al., 2003); this suggests that cellular atrophy, as a result of c-Jun n-terminal phosphorylation, could induce Bax and subsequent caspase cascades.

2.4.2 Neurotrophic Factors

Not only is the cellular response to damage mediated by death signals, but it is also controlled by neurotrophins released into and by the local microenvironment. Leukaemia Inhibitory Factor (LIF), Ciliary Neurotrophic Factor (CNTF), Fibroblast Growth Factor (FGF), Nerve Growth Factor (NGF) and neurotropin 3 (NT-3) are factors secreted near the site of injury that help mediate the axonal response by acting on regenerating proximal axonal tips (Eckenstein et al., 1991; Funakoshi et al., 1993; Sendtner et al., 1994a).

CNTF binds to and activates the CNTF receptor (CNTFR), subsequently inducing downstream activation of signal transducer and activator of transcription-3 (STAT-3). STAT-3 is phosphorylated in the proximal neuronal tip and is later found in the cell body, presumably via retrograde transport (Lee et al., 2004), which suggests that it could carry the injury signal from the site of injury to the cell soma. Furthermore, neuronal deletion of STAT-3 has been linked to increased levels of post-traumatic cell death (Schweizer et al., 2002). Experiments ablating CNTF function show a significant delay in the appearance of phosphorylated STAT-3 and also a delay in its nuclear translocation following neuronal stress (Dobrea et al., 1992; Rende et al., 1992). The fact that this function of STAT-3 is delayed and not ablated in CNTF-deficient animals suggests that there are other compensatory, albeit less efficient, mechanisms at work upstream of STAT-3. Another moderator of CNTF action is Reg2 (rat) or RegIIIβ in mice. This 16 kDa secretory protein helps to preserve the integrity of motor neurons during development and is a powerful

Schwann cell mitogen. Normally, following facial nerve section, CNTF applied locally will enhance regeneration and help rescue the injured neonatal facial motor nerve. This response was absent in globally deleted RegIIIβ mutants, although motoneurons do show delayed myelination (Tebar et al., 2008). This illustrates the role of CNTF as an integral intermediate in chemical neuromodulation of the regenerative response after injury.

Another important neurotrophic mediator is NGF. As discussed earlier in the introduction, it can be induced by ILβ upregulation by macrophages. NGF has been described as a regulator of the negative, denervation response following nerve injury (Raivich and Makwana, 2007). Normally, similar to STAT-3, NGF is retrogradely transported to the cell body after injury. However, after axonal damage, particularly to the sciatic nerve, levels of endogenous NGF retrogradely transported to the soma decrease by almost tenfold (Raivich et al., 1991). This decrease lasts for roughly 48 hours, after which NGF levels reach threefold reduction from baseline, and this threefold reduction continues until the onset of regeneration. Interestingly, NGF neutralization using specific antibodies results in a conditioning lesion-like effect in sympathetic neurons (Shoemaker et al., 2006) and axotomy-like changes even to intact cells, especially in levels of transcription factors like c-jun, and neuropeptides (NPs) like galanin, CGRP and Neuropeptide Y (Gold et al., 1993; Shadiack et al., 2001a). However, if this antibody neutralization is coupled with axotomy, there is no effect on speed of regeneration (Diamond et al., 1987). This may be due to a reduction in the amount of high-affinity NGF receptors at this time (Raivich and Kreutzberg, 1987a, 1987b; Verge et al., 1989). If NGF is applied externally, it shows variable results. *In vitro* studies link exogenous NGF application with increased neuronal sprouting (Angeletti et al., 1968). *In vivo* studies, however, show that exogenous application of NGF to axotomized neurons results in altered expression of axotomy-induced transcription factors and growth associated molecules (Verge et al., 1995; Gold, 1997; Mohiuddin et al., 1999), as well as a delay in axonal regeneration (Gold, 1997;

Hirata et al., 2002). This highlights the role of negative retrograde signalling and lack thereof in successful peripheral mechanisms of repair.

Lastly, studies characterizing speed of axonal regeneration have thus far focused on three groups of factors: Trophic Factors (like Insulin-like Growth Factor [IGF]-1, IGF-2 and Brain-Derived Neurotrophic Factor [BDNF]), transforming growth factor (TGF) Beta Superfamily members (including glial-cell derived neurotrophic factor [GDNF]) and neurokines (like LIF and IL6). In the pinch test, a universal indicator of regenerative speed, application of IGF-1 and 2, as well as overexpression of IL6 and its receptor, both resulted in improved regeneration (Kanje et al., 1989; Glazner et al., 1993; Hirota et al., 1996), whereas blocking IGF-1 and 2 with antibody, as well as genetic deletion of IL6, has been shown to reduce speed of axonal regeneration in peripheral systems (Galiano et al., 2001). Conversely, ablation of IL6 has led to reduced glial scar formation, increased sprouting in the facial motor nerve model (Galiano et al., 2001); it also enhances recovery when applied after spinal cord injury (Okada et al., 2004). BDNF and GDNF application post-injury did not improve regeneration post-injury, presumably due to the fact that expression levels of their respective receptors on axotomized neurons slowly decreases during chronic disconnection (Hammarberg et al., 2000). However, BDNF and GDNF application did promote axonal regeneration of motor neurons that had suffered chronic axotomy 3 months prior to nerve resuture (Boyd et al., 2002, 2003a). This indicates that insufficient BDNF and GDNF support might be contributing to the lack of response post-injury. Furthermore, inhibition of BDNF (Streppel et al., 2002b) and GDNF (Sun et al., 2003) also decreased collateral sprouting post-peripheral nerve transection, which highlights their integral, albeit complicated role in sprouting after neuronal injury. Taken together, these data illustrate the complex and intricate role of neurotrophic factors in engineering the neuronal response to injury.

2.4.3 Cell Adhesion Molecules

In addition to soluble molecules molecules that play a part in the orchestration of a complete cellular response, regenerating neurons also extend filopodia into the neighbouring microenvironment whose interactions within the immediate vicinity dictate the extent and direction of axonal progression. Axotomized neurons upregulate a plethora of adhesion molecules that interact with extracellular matrix and cell surface molecules in the local environment (Werner et al., 2000; Vogelezang et al., 2001; Raivich et al., 2002; Ekstrom et al., 2003; Gschwendtner et al., 2003; Wallquist et al., 2004). In response to axotomy, neurons upregulate receptors for CD44 hyaluronic acid, (Jones et al., 1997, 2000; Kloss et al., 1999) and galectin-1 (Horie and Kadoya, 2000; Akazawa et al., 2004; McGraw et al., 2004a, 2004b), as well as cell surface markers involved in homophilic binding, such as ninjurin (Araki and Milbrandt, 2000) and gicerin/CD146 (Hiroi et al., 2003). Further to this, FLRT3 – which has previously been characterised to complex with FGF receptors on cell membranes and subsequently upregulate FGF signalling (Bottcher et al., 2004) and was characterized by Robinson, (Robinson et al., 2004) also shows enhanced expression following nerve injury. As mentioned previously, Galanin immunoreactivity increases in injured neuronal cell bodies, and is transported into extending growth cones. c-Jun has been suggested as a putative mediator of the cellular response to stress and studies show that CD44 and Galanin both have AP1 sites on their gene promoters (Anouar et al., 1999; Corness and Hökfelt, 1998; Lee et al., 1993; Raivich et al., 2004b)

Eventually, modifications of neuronal cell surface markers lead to changes in expression levels of cell adhesion molecules on neighbouring non-neuronal cells. As such, adhesion molecules such as L1, NCAM and N-cadherin (Nieke and Schachner, 1985b; Bixby et al., 1988; Martini et al., 1994; Archer et al., 1999), and extracellular matrix molecules like laminin, fibronectin, tenascin and NG2 are upregulated by non-neuronal cells in the local

microenvironment after peripheral nerve injury (Manthorpe et al., 1983; Kuecherer-Ehret et al., 1990; Martini et al., 1990; Taira et al., 1994; Vogelezang et al., 2001; Rezajooi et al., 2004; Nolin et al., 2008; Buss et al., 2009). In particular, L1 has recently been characterized as a negative regulator of Schwann Cell proliferation in the PNS (Guseva et al., 2009).

Lastly, proteases and matrix inhibitors also show upregulation after neuronal injury in both neurons and their non-neuronal counterparts (Sesaki and Jensen, 2001; Demestre et al., 2004; Davies et al., 2006; Rolls et al., 2008). Chondroitin Sulphate Proteoglycans, particularly the glycos –aminoglycan (GAG) side chains thereof, have previously been characterized as major inhibitors of axonal regeneration (Asher et al., 2000; Bradbury et al., 2002; Properzi et al., 2003; Sandvig et al., 2004; Beggah et al., 2005; Buss et al., 2009)

Upregulated in the glial scar by reactive astroglia, these GAG chains are inhibitory to axonal growth. Current studies are underway mapping regeneration using Chondroitinase ABC to specifically degrade these GAG chains (Yick et al., 2003; Ikegami et al., 2005; Curinga et al., 2007; Tom et al., 2008; Nakamae et al., 2009). Currently, moderate functional improvements have been observed after topical Chondroitinase ABC application after spinal cord injury (Bradbury et al., 2002; Galtrey et al., 2007; Garcia-Alias et al., 2009; Tom et al., 2008; Ikegami et al., 2005). Similarly to GAG proteins, myelin-associated glycoproteins (MAGs) are synthesized by Schwann cells in response to injury. Ablation of MAG through specific antibody targeting has been shown to facilitate motor innervation (Mears et al., 2003) and duplication of peripheral myelin protein-22 (PMP22) gene has been shown to delay axonal maturation and remyelination in nerve xenografts (Sahenk et al., 2003).

Functional studies on cell adhesion have so far focused on the role of laminin, its alpha7 beta1 integrin receptor, galectin and beta2-microglobulin (β2-MG) in cellular adhesion during regeneration. Genetic global deletion of β2-MG—an important component of surface MHC 1 interactions—results in a 20 percent reduction of regenerating motor neuron axons to cross the proximal to distal gap in the cut peripheral nerve, as well as increased levels synaptic stripping (Oliveira et al., 2004). Furthermore, deletion of alpha7 integrin subunit causes an almost 40 percent reduction in speed of motor axon regeneration in similar peripheral systems, as well as delayed target reinnervation after facial axotomy (Werner et al., 2000). Similar responses were observed *in vitro*, which caused the disappearance of a conditioning-lesion response in sensory neurons cultured in matrigel or in collagen covered surfaces complemented with laminin – the substrate for alpha7 beta1 integrin receptors (Ekstrom et al., 2003).

Animals lacking c-Jun in the CNS show reduced alpha7 integrin subunit upregulation post facial nerve transection, which could account partially for the poor regenerative response exhibited by these animals (Raivich et al., 2004a). Ablation of all gamma 1-dependent laminin isoforms, including those that are the primary ligands for alpha7 beta1 integrin, laminins 1 (α1β1γ1), 2 (α2β1γ1) and 4 (α2β2γ1), led to similar, albeit more severe regenerative effects. Animals with cell-specific laminin 1 gamma chain deletion, renders the alpha beta gamma trimer inactive in peripheral Schwann cells. They thus exhibited lower levels of axon reinnervation into the distal segment of the crushed sciatic nerve 30 days post-injury (Chen et al., 2003; Chen and Strickland, 2003). On the other hand, deletion of alpha4 chain in laminin 8 (α4β1γ1) did not affect axonal regeneration, although it reduced the remyelination of the regenerating axons (Wallquist et al., 2005). As mentioned previously, alpha-7 deficient mutants exhibit reduced rate of motor regeneration and delayed target reinnervation. It has also been observed that these animals show massive upregulation of beta1 integrin after facial nerve injury, which coincides with a

strong increase in central axonal sprouting (Makwana et al., 2009). This might suggest that some compensatory mechanism, involving other alpha subunits, might be involved in this system.

Laminin activity is not limited to a unimolecular or bimolecular signalling system. Due to their trimeric and combinatorial structure, laminins have been known to act as ligands for several different receptors, including the integrins, gicerin/CD146, alpha-dystroglycan, and beta 1,4-galactosyltransferase (Taira et al., 1994; Powell and Kleinman, 1997; Ekblom et al., 2003). Overexpression of the latter, beta 1,4-galactosyltransferase I, in Schwann cell and sensory neuron co-cultures has led to increased axonal outgrowth (Shen et al., 2003), and may reflect the interaction of laminin/galactosyltransferase complexes with downstream axonal receptors. Either way, mounting evidence suggests that cellular adhesion molecules play a significant and essential role in the neuronal response to injury; without these molecules, neurons would not be able to extend processes into the local microenvironment which ultimately result in functional connections.

2.4.4 Cell Surface Interactions

Once cells form channels of recognition and communication, cell surface-cytoskeletal interactions permit continued ‘discourse’ between these channels. Codistribution with phosphoinositol-4,5-diphosphate, PI(4,5)P2, of GAP43, MARCKS and CAP23 cytoplasmic proteins summarised by the acronym GMC (Willard et al., 1980; Hoffman, 1989; Wiederkehr et al., 1997; Bomze et al., 2001; McNamara et al., 2003), at raft regions of the cell membrane (Laux et al., 2000) accompany cellular changes that lead to actin cytoskeleton polymerization, organization and disassembly (Caroni, 1997, 2001; Frey et al., 2000; Laux et al., 2000; Golub and Caroni, 2005) appearance of filopodia and microspikes and also initiation of neurite outgrowth (Bomze et al., 2001).

Studies show that GMC molecules, while being functionally interchangeable, bind solely to acidic phospholipids like the aforementioned PI-(4, 5)-P2, along with calcium/calmodulin, protein kinase C and actin filaments. Furthermore, calcium-containing or calcium-absent calmodulin interactions with GMC proteins (Gerendasy et al., 1995; Dunican and Doherty, 2000) provide a mechanism whereby growth cone signals can be inferred from changes in intracellular calcium levels (Hong et al., 2000; Nishiyama et al., 2003; Henley and Poo, 2004; Henley et al., 2004; Ooashi et al., 2005). For example, inhibition of calcium influx by nimodipine has been shown to enhance axonal regeneration after several types of peripheral injury – including that of the facial nerve (Andersen et al., 1990; Bar et al., 1990; Angelov et al., 1996; Bishop and Milton, 1998; Mattsson et al., 2001, 2005; Hydman et al., 2007).

Lastly, Rho GTPases, such as RhoA, Rac, Cdc42 and TC10, are known to act as regulatory switches that affect cytoskeletal structure, dynamics, and cell adhesion (Aepfelbacher et al., 1997; Murphy et al., 1999; Bass and Humphries, 2002; Aspenstrom et al., 2004; Begum et al., 2004; Coisy-Quivy et al., 2006; Bement et al., 2007; Benarroch, 2007). Rho GTPase activation is effected by receptor-linked adaptor molecules such as slit-robo GTPase-activating protein 2 (Madura et al., 2004; Lin et al., 2005). After nerve injury, rhoA, rac, cdc42 and TC10 are upregulated, however the most striking increase in expression is that exhibited by TC10 (Tanabe et al., 2000; Aspenstrom et al., 2004). As mentioned previously, CNS neurons do not tend to regenerate spontaneously like their PNS counterparts, however, inhibition of rhoA, as well as overexpression of cyclin-dependent-kinase inhibitor p21 (Cip1/WAF1), which inhibits rho-kinase function by binding, have both been shown to enhance regeneration in CNS models (Dergham et al., 2002; Ellezam et al., 2002; Tanaka et al., 2002). Moreover, studies show that enhanced expression of p21, which is accomplished by upregulating nuclear localized protein p311, also leads to increased levels of regeneration and target reinnervation following peripheral

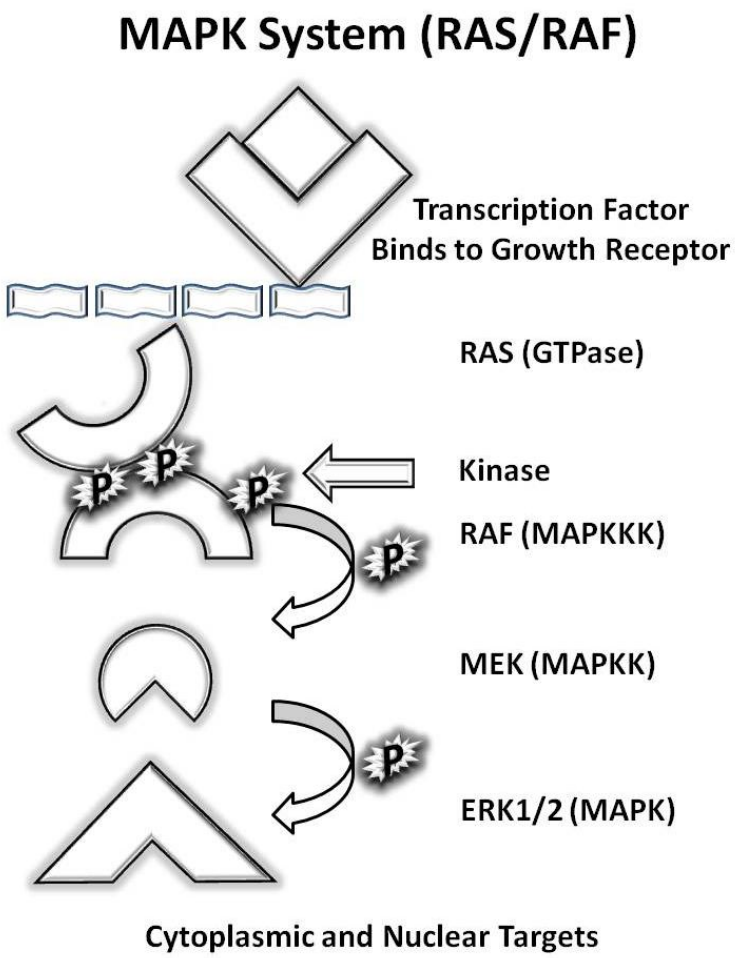

Figure 2-1: MAPK Cascade
RAS GTPase interacts with RAF, which then activates MEK, which phosphorylates ERK1/2 to induce its transcriptional activity.

motor neuron injury (Fujitani et al., 2004). Taken together, these data suggest that complex cytoskeletal interactions contribute to and maintain the neuronal regenerative response to injury.

2.4.5 Intracellular Signalling Molecules

There are several important intracellular signalling molecules involved in the regenerative response. As mentioned previously, many are kinases or activated by kinase activity – other mechanisms of action include acetylation, amino acid substitution and allosteric modification.

The Mitogen-Activated Protein Kinase (MAPK) system is one of the major intracellular signalling systems involved in proliferation, differentiation survival and death (Figure 2-1). In brief, this system generally consists of a G-Coupled ligand receptor that interacts with three kinases- a MAPK Kinase Kinase (MAPKKK), a MAPK Kinase (MAPKK, MEK) and a MAPK - of which each of the former phosphorylates and/or activates the latter in a sequential mechanism. The Ras/Raf system of activation, resulting in extracellular signal-

related kinase (ERK) one and two activation, is a classic example of a MAPK system. Upon transcription factor binding to the growth receptor, GTPase Ras activates the protein kinase Raf (a MAPKKK) via an allosteric mechanism (Kolch, 2000). Raf goes on to phosphorylate and activate MEK (a MAPKK), and this, in turn, activates ERK (a MAPK). Studies show ERK is upregulated in response to axonal injury (Kiryu et al., 1995). Inhibition of Ras, Raf, MEK and ERK1/2 has been linked to decreased survival and neurite outgrowth in embryonic neurons; this case seems to be reversed in adult neurons (Liu and Snider, 2001; Makwana et al., 2009a; Chang et al., 2003; Desbarats et al., 2003; Wiklund et al., 2002) . This illustrates that there exists a pro and anti-apoptotic dichotomy between naïve and adult Erk pathways. Erk 1 and 2 are also involved in C-terminal acetylation of c-Jun and subsequent c-Jun activation (Raivich, 2008). There is an observed increase in phosphatidyl-inositol-3 kinase (PI3K) in response to upregulation of the ERK cascade (Ito et al., 1998). PI3K is an upstream kinase of Protein Kinase B, or AKT (Owada et al., 1997; Murashov et al., 2001), which has been linked to axonal regeneration and enhanced postnatal, but not adult motor neuron survival (Namikawa et al., 2000). Another important PI3K family member, which mediates cellular response to stress, is the PI3K-related protein Ataxia Telangiectasia Mutated (ATM). Studies show that mice deficient in upstream ATM show increased AP-1 activation (Weizman et al., 2003) and that ATF3 over-expression in particular can negatively regulate cell cycle progression from G1 to S phase (Fan et al., 2002). This data highlights the importance of intracellular activation signals in propagating the neuronal response to stress and damage.

Several transcription factors have been linked to regeneration and the cellular response to stress, including c-Jun, ATMIN, JunD, ATF3, Sox 11 and STAT3 (Herdegen and Zimmermann, 1994; Pennypacker, 1997; Buschmann et al., 1998; Kenney and Kocsis, 1998; Lindwall et al., 2004; Campbell et al., 2005; Seijffers et al., 2006; Kanu, 2010). For example, STAT3 neuronal-specific deletion increases neuronal cell death after injury

(Schweizer et al., 2002) and ATF3 expression or upregulation has been linked to increased sprouting in vitro and in vivo (Nakagomi et al., 2003; Pearson et al., 2003a; Campbell et al., 2005; Seijffers et al., 2007; Kiryu-Seo et al., 2008), as well as changes in cell-cycle regulation. ATF3, when complexed with c-Jun is part of a larger transcriptional complex called AP1; because of its importance in the neuronal response to damage and this research, it will be discussed separately, as will the stress response protein ATMIN.

2.5 AP1 Transcription Factors

One of the most interesting regeneration-associated transcription factors is AP1, consisting primarily of c-Jun dimers. c-Jun is an immediate early transcription factor shown to be upregulated in cell repair and also damage. It forms both homodimers and heterodimers with other transcription factors, including members of the Jun dimerization Protein (JDP), C-Fos and ATF/CREB families. Homodimers or heterodimers containing c-Jun are collectively referred to as the Activator Protein 1 (AP1) Transcription complex. The AP1 transcription complex binds to DNA at 12-O-Tetradecanoylphorbol-13-acetate (TPA) Response Element (TRE) sequences and activates genes downstream of its binding site (Angel and Karin, 1991). Although TRE has basal activity prior to stimulation (Angel et al., 1991), it is highly activated following AP1 binding.

Depending on its dimerization partner and the system in which it functions, c-Jun has been shown to function in both pro-apoptotic and pro-regenerative roles (Raivich and Behrens, 2006; Broude et al., 1999; Vaudano et al., 1998; Hüll et al., 1994; Canettieri et al., 2009; Han et al., 1992; Smeal et al., 1989; Chiu et al., 1988; Kobayashi et al., 2009). For example, JNK phosphorylation increases stability of c-Jun against ubiquitin-mediated cellular degradation (Musti et al., 1997) but can also increase degradation dependent on its partner, for example with c-Myc (Alarcon-Vargas and Ronai, 2004). Likewise, cyclic

AMP response element (CRE)BII will heterodimerize with c-Jun when Jun is complexed with CRE but not c-Fos or JunB to mediate downstream effects (Benbrook and Jones, 1990; Macgregor et al., 1990), showing differential preference and activation based on binding partner.

Importantly, c-Jun shows prolonged upregulation in PNS, but not CNS regeneration and is expressed at high levels during the entire regenerative process in the periphery (Broude et al., 1997). c-Jun is upregulated in regenerating nerves (Utikal et al., 2009; Lindwall and Kanje, 2005a; Campbell et al., 2005; Zhou et al., 2004; Mason et al., 2003; Chaisuksunt et al., 2003) and is also involved in Heat Shock Protein (HSP) 27 upregulation when complexed with ATF3 (Nakagomi et al., 2003). Heat Shock proteins have previously been shown to play a pro-regenerative role in the injury response. *In vivo*, forced neuronal expression of ATF3, first characterized by Tsujino (2000), strongly improved DRG neurite outgrowth in the injured spinal cord (Seijffers et al., 2007). In concert, c-Jun and ATF3 have been shown to mediate *in vitro* neurite outgrowth (Pearson et al., 2003a; Nakagomi et al., 2003; Campbell et al., 2005; Kiryu-Seo et al., 2008) and cellular response to stress (Chaum et al., 2009). Since global deletion of *c-jun* is lethal in early embryogenesis, neuron-specific deletion of c-Jun using Nestin::Cre and a floxed c-Jun cassette was generated (Behrens et al., 2003), which abolished post-axotomy neuronal cell death, and strongly reduced peripheral regeneration and central axonal sprouting following injury (Raivich et al., 2004a; Makwana, Werner, et al., 2009).

c-Jun has diverse and overlapping roles in both normal biological processes and also following injury; it shows multi-faceted regulation at both the protein and transcriptional level.

2.5.1 c-Jun Protein interactions

c-Jun protein function can be influenced by physical interaction with other AP1 factors in its immediate environment. For example, c-Jun:c-Fos heterodimers are more efficient DNA binding proteins than c-Jun homodimers due to increased thermostability (Smeal et al., 1989) and, due to differences in both protein and mRNA half-life, (Angel and Karin, 1992), can affect the injury response differentially; c-Jun:c-Fos heterodimers are thought to initiate the induction response while c-Jun:c-Jun homodimers maintain it (Angel et al., 1988; Schonthal et al., 1988). Dimerization of c-Jun occurs via hydrophobic interactions in the leucine zipper region of AP1 transcription factor subunits (Kouzarides and Ziff, 1988; Ransone et al., 1989; Gentz et al., 1989; Turner and Tjian, 1989; Smeal et al., 1989), they align to form 'coiled coil arrangements.' There is also evidence of Fos:Jun Heterodimerization affecting transcriptional motility; as a monomer, Fos can translocate between nucleus and cytoplasm, however, once bound to c-Jun in the nucleus, it remains nuclearly localized (Malnou et al., 2007; Angel et al., 1991). In addition, certain AP1 subunits cannot bind to DNA or induce transcription on their own, and thus must rely on c-Jun for regulational activity (Chiu et al., 1988; Sassone-Corsi, Sisson, et al., 1988; Sassone-Corsi, Lamph, et al., 1988; Kouzarides et al., 1988; Nakabeppu et al., 1988; Halazonetis et al., 1988).

2.5.2 c-Jun transcriptional regulation

c-Jun has a very long 5' untranslated region, which extends for roughly 1 kb (Hattori et al., 1988) and, in contrast to c-Fos (Sassone-Corsi et al., 1988; Schonthal et al., 1989), *c-jun* transcription seems to be positively autoregulated (Angel et al., 1988). This is most likely due to the high-affinity AP-1 binding site in the jun promoter region; although induction of *c-jun* transcription via activators such as TPA (Kim et al., 1990) leads to a 15-fold increase

in *mRNA,* it only corresponds with a 3-4 fold increase in c-Jun protein synthesis (Angel et al., 1988) highlighting the role of both transcription and post-translational events in regulating c-Jun function. Furthermore, depending on the stimulus, maximal *c-jun* transcription levels are reached at different timepoints (Kim et al., 1990; Boyle et al., 1991) and if the SP1 or CTF sites in the *c-jun* promoter are deleted, both basal and induced transcription increase substantially after TPA treatment (Han et al., 1992; Unlap et al., 1992). Sp1 has been shown to recruit ATF3, c-Jun, and STAT3 to the TRE (Kiryu-Seo et al., 2008). Furthermore, other Jun isoforms like JunB and JunD have been shown to competitively inhibit *c-jun* transcription (Chiu et al., 1989; Schutte et al., 1989; Angel et al., 1992). While c-Jun is induced only by TPA, junB can also be induced by cAMP, and cAMP upregulation is known to inhibit *c-jun* transcription (Angel et al., 1987; Buscher et al., 1988; Chiu et al., 1988; Bravo et al., 1987; Angel et al., 1992). Recently, cyclic AMP response element-binding protein (CREB)-regulated transcription coactivator 1 (CRTC1) was found to modulate c-Jun and c-Fos transcriptional activity via AP-1 target gene promoter binding (Canettieri et al., 2009).

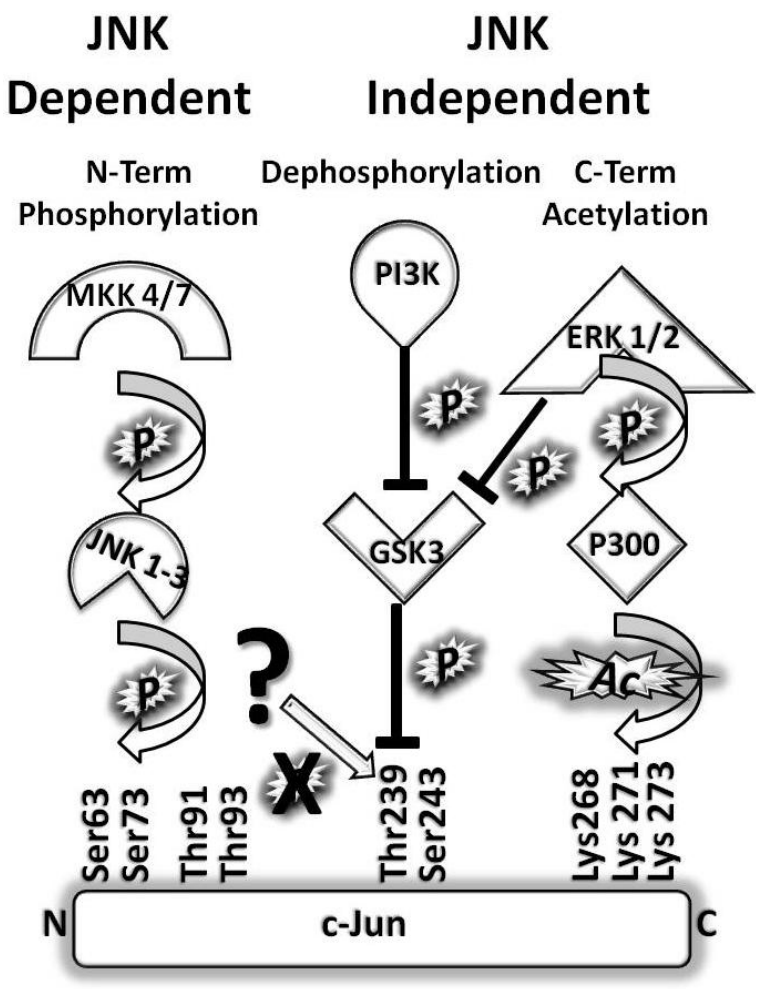

Figure 2-2: Jun Interactions
c-Jun participates in several transcriptional cascades – both phosphorylation-dependent and phosphorylation-independent. C-Jun can also function without N-Terminal activation. Activation dependent MKK4/7 activates JNKs which then phosphorylate c-Jun at serine residues 63&73. Jun function can also be affected by dephosphorylation at Threonine 239 and c-terminal acetylation involving ERK and P300.

2.5.3 JNK

Close proximity of Phosphorylation sites to 'basic region' DNA binding site and subsequent activity assays indicate that c-Jun phosphorylation alters binding activity (Boyle et al., 1991) and can do so in the absence of *de novo* protein synthesis (Angel et al., 1987). This suggests the potential of N-terminal c-Jun phosphorylation to play an integral role in the c-Jun reaction to stress and cell damage (Figure 2-2).

Mitogen Activated Protein Kinases (MAPKs) are serine/threonine kinases, which can be classified into three main subtypes: extra cellular signal-regulated kinases (ERKs), p38 MAPKs and c-Jun N-terminal kinases (JNKs, Brust et al., 2007). Jun N-Terminal Kinase (JNK) is a type of MAPK that binds specifically to and phosphorylates the c-jun N-Terminus. This has been tracked specifically to serine 63 and 73 (Ser63&73) n-terminal phosphoacceptor sites (Smeal et al., 1994) and partially threonines 91 and 93 (Thr91&93), although earlier studies proposed 5 to 7 putative targets with a pSer:pThr ratio of 5:1 (Boyle et al., 1991). JNKs are expressed in neurons, microglia, astrocytes and

oligodendrocytes in the brain (Fan et al., 2002) and are thought to initiate and participate in the chromatolytic cellular response seen after nerve injury. This hypothesis is supported by the fact that JNKs, like c-Jun, are immediately activated following peripheral nerve injury and remain so throughout the entire regenerative response – increasing the amount of phospho-c-Jun in the process (Eminel et al., 2008; Waetzig et al., 2006; Whitmarsh, 2006). JNKs can also travel anterogradely along axon microtubules via kinesin motor proteins (Verhey and Rapoport, 2001; Verhey, 2007).

There are 10 different JNK splice variants, of which functional specificity is derived from different functional domains (Gupta et al., 1996). Of the three main isoforms, JNK1, JNK2 and JNK3, JNK1 and JNK2 are ubiquitously expressed in mammals and JNK3 expression is targeted mainly to the heart, brain and testis. (Waetzig and Herdegen, 2005; Brecht et al., 2005b). Isoforms vary in their α and β docking regions, which regulate substrate specificity and subsequent biological function *in vivo* (Waetzig et al., 2005; Kuan et al., 1999b). Crystal structure analysis shows that protein structure and conformation state of JNKs can also affect their ability to be phosphorylated by upstream kinases (Heo et al., 2004; Xie et al., 1998; Takatori et al., 2008; Shaw et al., 2008) and thus their effector potential. Experiments using TNF-α induced apoptosis also showed that JNK can perform in an isoform-specific manner depending on upstream signalling cues (Liu et al., 2004). MEK1 has also been shown to preferentially activate JNK1 over JNK2 in epithelial systems via small conformational differences in JNK1 (Takatori et al., 2008). Furthermore, cellular localization of upstream signalling molecules can also affect JNK activity. Cerebellar granule neurons have MEK kinase Kinase exclusively (MKK)4 in nuclei and MKK7 expressed throughout the cell. Ablation of Nuclear MKK4 led to lower JNK, c-Jun and ATF2 activity during development, without changes in MKK7 or JNK expression (Wang et al., 2007). Therefore, isoform specific regulation of upstream kinases also affects downstream JNK effector function.

Furthermore, JNKs are primarily located in the cytoplasm and must translocate into the nucleus to affect most of their downstream signalling targets, such as c-Jun, JunD, ATF-2, Elk-1, p53, NFAT4 (Waetzig et al., 2005; Brecht et al., 2005b; Hess et al., 2004). Therefore, JNKs generally form scaffolding complexes with JNK interacting proteins (JIPs), plenty of SH3 (POSH), filamin B, β-arrestin-2, GRIP1 associated protein 1 (GRASP-1), stress-activated protein kinase pathway-regulating phosphatise 1 (SKRP-1) or IκB kinase complex-associated protein (IκAP) that give them increased mobility, stability and downstream interaction potential (Yang et al., 2007; Waetzig et al., 2006; Whitmarsh, 2006) This interaction can be generalized – as is the case with JIPs – or it can be isoform specific – as is the case with β-arrestin-2 which only binds a specific JNK3 isoform (Dickens et al., 1997; Guo and Whitmarsh, 2008). There is also evidence of JNK interactions with other AP1 transcription factors, c-Jun-E3 ligases (such as FBW7 and itch), cytoplasmic proteins and mitochondria (Widmann et al., 1999; Tararuk et al., 2006; Huang et al., 2008; Eminel et al., 2008; Zhou et al., 2008; Anzi et al., 2008).

Substitution of JNK phosphorylation motifs with those for PKA abolishes c-Jun-mediated JNK effects (Smeal et al., 1994). Similarly, substitution of ser63&73 with alanine residues (junAA) prevents JNK-mediated (Yang et al., 1997) excitotoxic cell death following exposure to kainite, as does global JNK3 deletion (Behrens et al., 1999; Brecht et al., 2005a). Although JNKs have no effect on retinal photoreceptor apoptosis (Grimm et al., 2001), JunAA and JNK3 mutants show transient improvement in outcome after targeted dopaminergic cell death (Brecht et al., 2005b). JNK1 has been linked to diabetes – global JNK1-deleted mutants are protected against type II diabetes mellitus and JNK1 expression accelerates β-cell death in the pancreas. In addition JNK2 global mutants are resistant to hypercholesterolemia-induced endothelial dysfunction (Varona-Santos et al., 2008). Complete JNK ablation – either by deletion or inhibition – leads to decreased caspase-

dependent neuronal cell death in both neuronal and non-neuronal cells (Weston and Davis, 2007).

Conversely, if JNK upregulation is induced *in vitro,* either endogenously or through transfection, all isoforms can induce neurite sprouting in PC12 cells or primary neuronal cell cultures (Waetzig and Herdegen, 2003; Riese et al., 2004; Eminel et al., 2008). JNKs – particularly JNK1 - are thought to do this through increasing microtubule stability (Chang, Jones, et al., 2003; Björkblom et al., 2005; Rosso et al., 2005; Ciani and Salinas, 2007). JNK enhancement can also increase growth rates of fibroblasts (Castellazzi et al., 1991) and transcriptional activation of AP-1 promoters (Radler-Pohl et al., 1993). Alternatively, after JNK upregulation via exposure to p75 neurotrophin receptor ligands, inflammatory stimuli or reactive oxygen species (Vollgraf et al., 1999; Casaccia-Bonnefil, 2000; Miskimins et al., 2002; Casaccia-Bonnefil et al., 2008) increased glial cell death is observable, especially in oligodendroglial precursors, via the p53 pathway (Ladiwala et al., 1999). This cell death can be prevented by incubation with JNK antagonists (Eilers et al., 2001; Senger et al., 2002; Jurewicz et al., 2003; Zhuang et al., 2006; Fernandes et al., 2007). Phospho-c-Jun has also been shown to enhance downstream expression of Bcl2-interacting mediator of cell death (BIM) and ATF3 (Mei et al., 2008b).

Extensive research points to the fact that JNK inhibition can be a useful treatment for neurodegenerative conditions (Behrens et al., 1999; Brecht et al., 2005a; Waetzig et al., 2005; Waetzig et al., 2006; Borsello and Forloni, 2007) Several clinical trials using JNK inhibition to treat neurodegeneration are currently underway (Haeusgen et al., 2009; Suckfuell et al., 2007; Behrens et al., 1999; Brecht et al., 2005a; Waetzig et al., 2005; Waetzig et al., 2006; Borsello et al., 2007). and presently, there are about 12 different JNK inhibitors (Bogoyevitch and Arthur, 2008). Derivatives of Celgene's (summit, New Jersey, USA) SP600125, CC-359 and CC-930, are JNK ATP-binding site inhibitors in trials for

neurodegenerative conditions, leukaemia and fibrotic disease (Haeusgen et al., 2009) and XG-102, from Xigen Pharm (Lausanne, Switzerland) blocks JNK binding to substrates and is in phase I trials for stroke and traumatic hearing loss (Haeusgen et al., 2009; Suckfuell et al., 2007). However, only the latter is effective after the onset of injury and is thus most clinically relevant. Pharmacologically, chemical inhibition of mixed lineage kinases - upstream regulators of JNK - with CEP-1347 enhanced survival of embryonic sensory, sympathetic and motor neurons, as well as auditory hair cells and PC12 cells following withdrawal of trophic support (Lindwall and Kanje, 2005b; Borasio et al., 1998; Maroney et al., 1998, 1999; Pirvola et al., 2000) Although there is evidence it can help prevent dopaminergic cell death *in vitro* (Saporito et al., 2002; Mathiasen et al., 2004) and *in vivo* (Saporito et al., 1999, 2000), CEP-1347 does not improve outcome for patients with early Parkinson's Disease (Wang and Johnson, 2008). Also, competitive inhibition of JNK using the DJNKI1 fragment of Jun Interacting Protein (JIP) blocked c-jun phosphorylation and also led to decreased levels of NMDA-induced cortical neuron cell death *in vitro* (Borsello et al., 2003).

2.6 ATMIN

Ataxia Telangiectasia Mutated (ATM) Interacting protein or ATMIN is an 88 kDa substrate of the phosphatidylinositol kinase-related, ATM enzyme. This enzyme will normally bind and phosphorylate the transcription factor NBS-1 (Nibrin) to promote the repair of double stranded DNA breaks. However, in the absence of double stranded breaks, for example after hypotonic stress, UV light exposure or treatment with hydroxyurea, ATM will also bind to and phosphorylate ATMIN to halt cell cycle progression, activate checkpoints and promote repair (Kanu and Behrens, 2007, 2008). First characterized in its truncated version, based on N-terminal interactions with Chk2 checkpoint kinase, as 66 kDa ATM/ Ataxia telangiectasia and Rad3 related (ATR)-substrate Chk2-interacting Zn^{2+}-finger

protein (ASCIZ, McNees et al. 2005) deletion of ATMIN also results in increased sensitivity to DNA base-damaging agents and altered immunoglobulin gene diversification following histone deacetylase inhibition in DT40 cell lines (Oka et al., 2008). DNA damage response proteins generally have SQTQ cluster domains (Traven and Heierhorst, 2005; Lee et al., 2008), which are present in the ATMIN gene, however the shorter ASCIZ version of the gene contains two N-terminal C2H2 zinc (Zn^{2+}) fingers, whereas the longer ATMIN version contains four (McNees et al., 2005; Kanu et al., 2007). Alternative splicing between exons indicates that both the 66 kDa ASCIZ and 88 kDa ATMIN forms of the gene exist but functional analysis reveals that the longer ATMIN transcript is the more prevalent in nature (McNees et al., 2005). Although its *in vitro* role during cell stress has been characterized, little is known about its involvement *in vivo.*

2.7 Cell Type-Specific Promoters of Cre Recombinase

2.7.1 Nestin

First discovered in 1985 as an antigen recognized by monoclonal antibody Rat-401 (Hisanaga and Hirokawa, 1988), Nestin was finally characterized as an intermediate filament protein in 1990 and is a 198 kDa protein spanning more than 1600 amino acids (Cooper and Hausman, 2006; Lendahl et al., 1990). Its highly conserved exon-intron structure is identical in mice, rats, and humans (Michalczyk and Ziman, 2005a). Present from E7, nestin expression is slowly downregulated as other, more cell-specific, filament proteins take over during post-natal cellular differentiation (Lothian and Lendahl, 1997; Zimmerman et al., 1994; Dahlstrand et al., 1995; Hockfield and McKay, 1985). Nestin is thought to participate in developmental regulation by stabilizing cell structure and co-ordinating changes in intracellular dynamics (Herrmann and Aebi, 2000; Michalczyk et al.,

2005a); this takes place via threonine phosphorylation at residue 316 (Eriksson et al., 1992; Sahlgren et al., 2001; Skalli et al., 1992). The principal activator of nestin is cyclin-dependent protein kinase (cdc) 2. Along with cyclin B, cdc2 forms the maturation/M-phase promoting factor (MPF), which orchestrates mitotic progression of the cell cycle from G2 phase to M phase (Dahlstrand et al., 1992). Another putative phosphorylation target is Nestin's serine-rich c-terminus – which could facilitate Nestin's interaction with other cytoskeleton components via side branch modification (Michalczyk and Ziman, 2005b). Intermediate filaments are divided into 6 classes; Nestin codes for a class 6 intermediate filament gene (Dahlstrand et al., 1995; Lendahl et al., 1990). Because of its short N-terminus, Nestin can only form heterodimers – not homodimers – and prefers to do so with class 3 intermediate filament proteins vimentin and α-internexin (Eliasson et al., 1999; Marvin et al., 1998; Michalczyk et al., 2005a). Although it is primarily characterized as an early developmental marker, nestin expression is upregulated in the adult during pathogenesis – for example in the glial scar and during regeneration (Michalczyk et al., 2005a, 2005b) Nestin is a well-characterized neuronal stem cell marker (Okuno et al., 2010; Hernández-Benítez et al., 2009; Vukojevic et al., 2009; Bramanti et al., 2010; Kozubenko et al., 2009; Pilkington, 2005), although it is also present in various other tissue, including the testes (Fröjdman et al., 1997), pancreas (Rovira et al., 2009; Ueno et al., 2005), olfactory epithelium (Minovi et al., 2010), retina (Kohno et al., 2006; Wislet-Gendebien et al., 2005), muscle (Lendahl et al., 1990), skin (Medina et al., 2006), teeth (About et al., 2000; Graham et al., 2006), liver (Forte et al., 2006; Li and Chopp, 1999), kidneys (Zou et al., 2006), adrenals (Toti et al., 2005) and mammary epithelial stem cells (Liu et al., 2009)

2.7.1.1 CNS-Specific Conditional Deletion

Nestin mediated cre excision is a well characterized mechanism for gene deletion in the CNS Successful recombination targets gene deletion to Neurons, Astrocytes, Oligodendrocytes and Schwann Cells (Hanada et al., 2009; Heffron et al., 2009; Read et al., 2009; Raivich et al., 2004a; Kanu et al., 2008; Rao, 1999). Previous studies using Nestin promoter-driven *c-jun* showed decreased cellular response, increased motoneuron survival and decreased regeneration in c-Jun deficient mice. However, since nestin is not neuron specific, it remains unclear whether the effects observed in neuronal regeneration were due to the specific action of Jun deletion in neurons or other Nestin+ progenitor-derived cells.

2.7.2 Synapsin

Synapsins are a type of phosphoprotein specifically associated with the cytoplasmic surface of pre-synaptic neurons (Huttner et al., 1983; Pieribone et al., 1995). Synapsins are encoded by three separate genes – *Synapsin I, II and III* (Rosahl et al., 1995; Kao et al., 1998; Esser et al., 1998; Hosaka and Südhof, 1998b, 1998a). Post-transcriptional modification creates three distinct Synapsin isoforms – a, b and b-like – that are distinguishable primarily by structural differences in the C-Terminus of the molecule (Hilfiker et al., 1999). The *Synapsin* N-terminal is mostly conserved, and contains a protein kinase A (PKA) and Ca^{2+}/calmodulin-dependent protein kinase I (CaM kinase I) phosphorylation site, which suggests that N-Terminal activation plays an important role in Synapsin function (Hilfiker et al., 1999). This activation is regulated, at least in part, by opiate ligands (Nah et al., 1993). The Synapsin protein consists of 3-6 primary regions, which differ based on organism; these regions are labelled A-J, and are arranged differentially according to species. The core ‘C’ region shows roughly 50% homology and

is highly conserved between species – both vertebrate and invertebrate (Hilfiker et al., 1999). Despite the somewhat dissimilar sequence structure in other regions, Synapsins share high levels of amino acid congruence – with high levels of proline, glutamine, alanine and serine, as well as MAP kinase and CaM kinase II activation sites. Synapsins are found in all neurons except those containing ribbon synapses (Usukura and Yamada, 1987), although there is conflicting morphological evidence that they are present in DRGs (Sims et al., 2008; Zhu et al., 2001).

Genetic deletion studies show that Synapsins I and II are important for presynaptic vesicle formation and repeated action potential firing (Li et al., 1995; Lonart and Simsek-Duran, 2006; Rosahl et al., 1995). Global mutants exhibit deregulation of basal neurotransmission (Lonart et al., 2006), with impairments in neurotransmitter reserve pool after high-frequency stimulation (Rosahl et al., 1993, 1995). Synapsin global mutants show increased propensity toward seizure behaviour both baseline (Synapsin II) and after electrical stimulation (Synapsin I, Li et al., 1995; Rosahl et al., 1995). Also, they show more age-related neuronal loss and gliosis in the cerebral cortex and hippocampus, with accompanying age-dependent increases in cognitive impairment (Corradi et al., 2008). Furthermore, Synapsin deletion also affects other synaptic vesicle proteins; for example, mutants show decreased abundance but increased activation of rabphilin (Lonart et al., 2006) in synaptic terminals.

2.7.2.1 Neuron-Specific Conditional Deletion

The neuronal specificity of the Synapsin gene makes its promoter an ideal candidate for conditional gene deletion strategies. Synapsin I protein is present in the presynaptic bouton at a concentration of roughly 10-20 μM, with roughly 10-30 Synapsin I molecules per vesicle (Schiebler et al., 1986; Ho et al., 1991; De Camilli et al., 1990). *Synapsin I* has

previously been characterized as a neuron-specific promoter (Usukura et al., 1987; Zhu et al., 2001; Hasue et al., 2005; He et al., 2004; Xia et al., 2003; May et al., 2004; Tamai et al., 2008; Ferguson et al., 2007; Sims et al., 2008; Kügler et al., 2001). The proximal region of the *Synapsin I* promoter is sufficient to direct neuron-specific gene expression, due to negative regulation by the zinc finger protein, neuron-restrictive silencer factor/RE-1 silencing transcription factor (NRSF/REST, Schoch et al., 1996). In contrast to Nestin, which targets floxed gene deletion to all neurons in the CNS, Synapsin I is a more specific promoter, excising the gene of interest solely in neurons. It creates the ideal system in which to investigate neuron-specific effects.

2.7.3 P0

P0 is the most abundant myelin protein in the PNS, composing roughly 50% of total myelin protein in peripheral nerves (Sommer and Suter, 1998). The P0 gene was first isolated in 1985, is found on Chromosome 1 and is activated prior to myelination in all immature SCs and also in SC precursors (Cheng et al., 1996; Lee et al., 1997, 2001; Lemke and Axel, 1985; Kuhn et al., 1990). P0 protein, an IgG family member, is stabilized by homophilic interactions and its expression is regulated by neuronal signalling cues (Sommer et al., 1998; Xu et al., 2000), although SCs in culture can express low levels of P0 even in the absence of neurites (Sommer et al., 1998; Burroni et al., 1988). Its enhanced expression provides a regulatory signal for Schwann Cells to differentiate toward a myelinating phenotype. As such, it is an ideal molecular candidate for gene deletion studies targeting Schwann Cells. Indeed, several studies have examined the effects of global and conditional mutation and deletion of this gene. P0-globally deficient mice exhibited deficits in motor coordination, tremors and occasional convulsions. Immunologically, they showed severe hypomyelination of peripheral axons, vast axonal degeneration and poor neurite integrity. Furthermore, some, but not all, molecules involved in myelination were

dysregulated in P0 deficient mice (Giese et al., 1992; Xu et al., 2000). Minimal P0 expression has also been found in other areas and subpopulations of cells, where its significance is largely unknown (Bhattacharyya et al., 1991; Lee et al., 1997; Sato et al., 1999; Sato and Endo, 2000; Yamauchi et al., 1999).

2.7.3.1 Schwann Cell Conditional Deletion

The P0 promoter can also be used for conditional mutation systems, such as Cre::LoxP, to excise certain genes specifically from all Schwann Cells; to excise a gene specifically from myelinating SCs, Myelin Basic Protein (MBP) targeted deletion has been employed (Niwa-Kawakita et al., 2000). One such gene that has been explored using P0::Cre-mediated deletion is c-Jun. To date, its role has been explored *in vitro,* where c-Jun was essential for Schwann cell proliferation and death, as well as *in vivo* following sciatic nerve injury. P0::Jun mutants showed inability to de-differentiate from a myelinating to immature phenotype and delayed demyelination in sciatic nerves after cut. This demyelination is necessary for a successful regenerative response due to the axonal inhibitory cues present in myelin. As a result of the impaired demyelination response, more debris and nerve sheaths were present in distal nerve segments 3 and 5 days post-injury (Parkinson et al., 2008; Mirsky et al., 2008). Biochemically, this system showed that c-Jun was a negatively regulated by Krox-20 and, along with NOTCH, acted as an inhibitory pathway molecule for SC myelination.

2.8 Stereology – Optical Fractionator and the Abercrombie Correction

2.8.1 Background

The tenets of stereology rely upon extrapolating 3-D volumetric analyses from a series of 2-D sampling sets. 3-D Stereology utilizes random, systematic sampling to provide “unbiased” quantitative data, whereas 2-D stereological methods derive similar conclusions from “assumption based” reasoning.

The Abercrombie Correction is a type of 2-D stereological assessment first described in histological sections (Abercrombie, 1946) that is commonly used in the context of facial motoneuron injury models (Serpe et al., 2003a, 2005; Huppenbauer et al., 2005; Wainwright et al., 2009; Makwana et al., 2009, 2007; Mills et al., 2008). The Abercrombie correction is based upon the observation that cell sections inevitably contain both whole and fragmented cells (which have been cut during sectioning), which result in a phenomenon called the split cell error. Split cell error results from cell fragments at the upper and lower surfaces of the section being counted as if they were entire cells and thus results in over-estimation of the actual cell number. Abercrombie reasoned that the true number of cells equals the number of cells/fragments counted times a correction factor equal to the ratio of the section's thickness divided by the sum of the section's thickness plus the mean diameter of the cells or nucleoli: From this, the Abercrombie Correction was born – the formula is described below:

Equation 1: Abercrombie Correction - $N_V=N_A[T/(T+D)]$

Where:

N_V= corrected estimate of object number per unit of volume (numerical density)

N_A= uncorrected profile estimate per unit of area

T= mean thickness of the section (20 μM)

D= mean diameter of nucleolus perpendicular to sectioning direction (20μM, Raivich et al., 2004a; Coggeshall, 1992)

The most common 3-D Stereological assessment is called the Optical Fractionator. It uses thick sections to estimate total cell counts from the number of cells sampled with a Systematic Randomly Sampled (SRS) set of unbiased virtual counting spaces (Micro Bright Field Bioscience, 2010). This samples the entire region of interest and places uniform distance between unbiased virtual counting spaces in X, Y and Z planes. “Guard” or “buffer” zones in the Z-plane are utilized in the optical fractionator workflow to reduce split cell error. Mean cell density is calculated within the region of interest by dividing total number of counted cells by the number of counting spaces and their uniform volume. By multiplying average cell density with the volume of the investigated region of interest, one can obtain an “unbiased” estimate of the total number of cells in the region of interest.

2.8.2 Cell Size and Split Cell Error

Both methodologies have systems in place to reduce split cell error. The Abercrombie Correction utilizes mathematical principles to account for this, whereas Optical Fractionator has a “guard” zone in place of one cell length at the top and bottom of the Z-plane. One of the main arguements against the Abercrombie correction is that bias issues become apparent and less predictable when size distribution of cells is skewed or bimodal, for example, when D varies (Hendry, 1976). Also, for non-spherical objects, the mean D will change according to the sampling direction. Thus, objects must be spheroid like the mouse facial motoneuron nucleolous. Optical Fractionator’s buffer zone accounts for this

potential drawback and individual cell diameters can be measured and accounted for; although the necessity to set the buffer zone based on the largest cell diameter as opposed to the smallest one means that large cells could be over-estimated or that smaller cells could be under-represented in final measurements. As a result, Optical Fractionator uses very thick sections to reduce the proportion of buffer/measured zone.

2.8.3 Tissue Shrinkage and Section Size

Tissue shrinkage is also an issue when using histological preparations. The Abercrombie method assumes a consistent T value, but individual section thickness can vary between and even within sections. Most histological sections that are mounted on glass slides collapse non-uniformly along the z-axis when the tissue dries. Traditional 3-D counting methods fail to take this into account, resulting in the possibility that such counts would be confounded by indeterminate degrees of distortion, depending upon where along the z-axis the optical disector is placed (Benes and Lange, 2001). The only alternative is to use thin sections, which pose the same limitations as the Abercrombie method, and also increase the buffer/measured zone ratio. For such sections, counting is done at low magnification (ex. 20x) with a large depth of field. Under these conditions, all cells along the entire z-axis can be included in the analysis. Although distortion is minimized by individual Z measurement beforehand in optical fractionator, it can never be completely controlled for in either stereological method.

2.8.4 Non-Uniform Sampling Areas

One of the central assumptions when using the Optical Fractionator and one of its main pitfalls when used in the context of the facial motor nucleus, is the necessity for a completely random distribution of measured objects. Somata in the uninjured brainstem

facial motor nucleus are roughly 15-20um size (Raivich et al., 2004a), show a distinct lateral concentration, as well as densely packed brainstem nuclei. Following injury, motoneuron distribution is more evenly spaced, but the necessity for comparison between the two might present problems with Optical Fractionator analysis, at least in determining control densities. Since 3-D techniques rely on the combination of several random sampling zones, and not quantification of all cells in all areas, cell numbers could be augmented. Theoretically, the optical fractionator counting frame could be increased to accommodate for this, but this would still provide a less precise measurement. All things considered, manual counting of all motoneurons (as performed for 2-D analysis) in the nuclei seems the best approach for this type of cell distribution.

2.8.5 Stereology Conclusions

Both 2-D and 3-D stereological techniques present with unique benefits and drawbacks. The fact remains that most facial nerve survival data has been collected using the Abercrombie system, but the ease, flexibility and novelty of the Optical Fractionator merit further investigation. Perhaps characterizing and comparing these two approaches could be a future direction in the Raivich laboratory.

AIMS

2.9 Characterizing the Regenerative Response

2.9.1 c-Jun

In 2004, Raivich et al. reported that mice with a Neuroepithelial Stem Cell Marker (Nestin)-specific c-Jun deletion, induced by the Cre::Lox P recombination system, exhibit several defects in the neuronal regenerative response. In brief, animals with this deletion showed reduced levels of neuronal cell death, target-muscle reinnervation, perineuronal sprouting, lymphocyte recruitment and microglial activation after facial nerve axotomy (Raivich et al., 2004a). Surviving motor neurons in the facial motor nucleus also exhibited an atrophic phenotype.

Since neuroepithelial stem cells differentiate into several distinct CNS populations such as neurons, oligodendrocytes, astrocytes and peripheral Schwann cells (Hanada et al., 2009; Heffron et al., 2009; Read et al., 2009; Raivich et al., 2004a; Kanu et al., 2008; Rao, 1999), it remained unknown which of these cell types is the key regulator of the phenotype exhibited by Nestin::Jun mice. In addition to different potential regulatory cell types, multiple activation sites for c-Jun have also been characterized which might affect the regenerative response. Activation of the c-Jun mediated transcriptional apparatus appears to be affected by interactions at 3 major sites: N-Terminal phosphorylation at Ser 63&73 and Thr 91&93 by JNKs (Figure 0-1, Smeal et al. 1994; Morton et al. 2003), which can also exert indirect effects by activating the transcription factor complex (TFC) which controls jun mRNA synthesis; dephosphorylation of Thr239 (Morton et al., 2003), which attracts FBW7 ubiquitin ligase (FBW7L) and targets the phosphorylated protein for

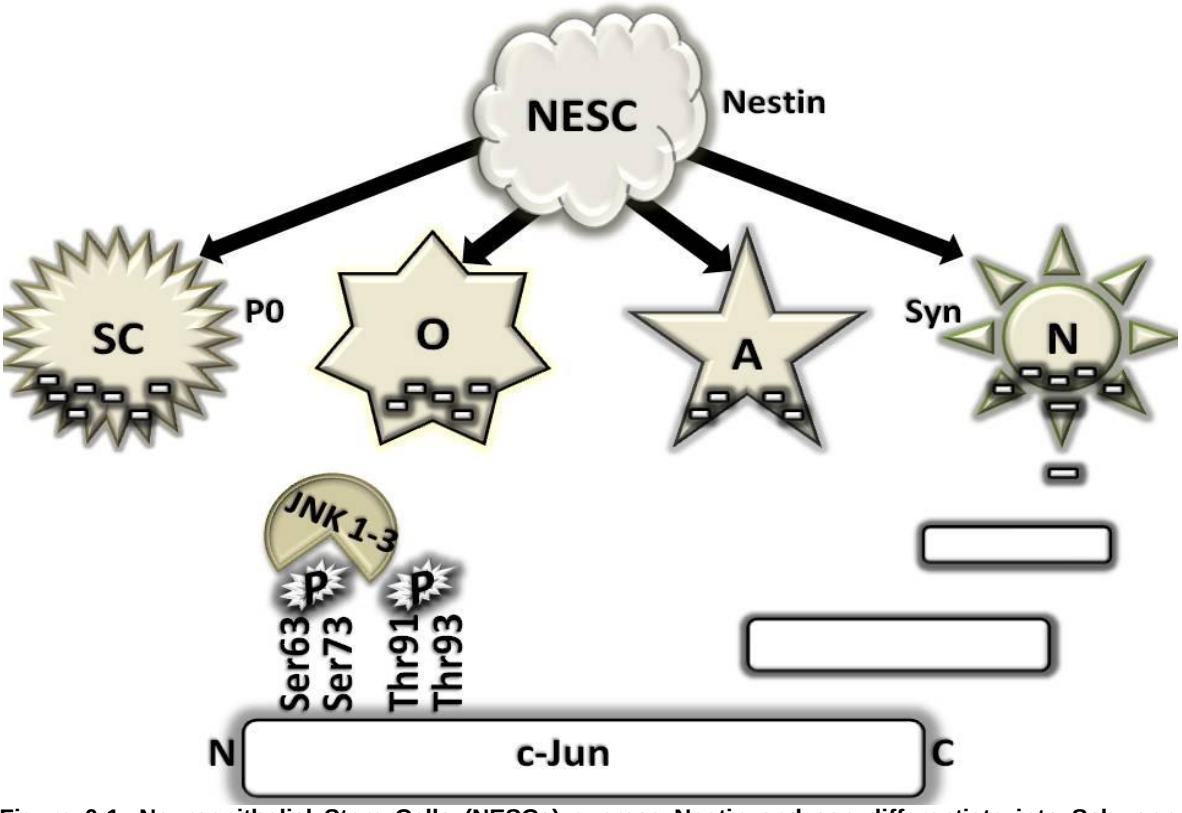

Figure 0-1: Neuroepithelial Stem Cells (NESCs) express Nestin and can differentiate into Schwann Cells (SC, marker P0), Oligodendrocytes (O), Astrocytes (A) and Neurons (N, marker Synapsin I).
All of these cell types express nuclear transcription factor c-Jun. c-Jun activation pathways are known to involve N-Terminal phosphorylation at Ser 63&73 and Thr 91&93 by JNK, dephosphorylation of Thr239 and C-terminal lysine acetylation near aa257-276 by p300.

ubiquitination and subsequent degradation; and finally, C-terminal lysine acetylation near aa257-276 (Vries et al., 2001), which results in activated c-Jun via the ERK pathway.

Here, the regulatory role of c-Jun was explored using cell-specific deletions of P0 in Schwann Cells and Synapsin in Neurons. Also examined was the role of N-Terminal Phosphorylation in c-Jun's regenerative function in response to facial motor nerve transection. Using transgenic systems, we characterize the role of c-Jun in:

- The Cellular Response to Injury – both Neuronal and Non-Neuronal
- Motor Neuron Survival
- Reinnervation – both Functional and Anatomical

As one further characterizes the cellular interactions surrounding c-Jun function in neuronal regeneration, one is better equipped to use available technology to exploit its role in cell survival after injury.

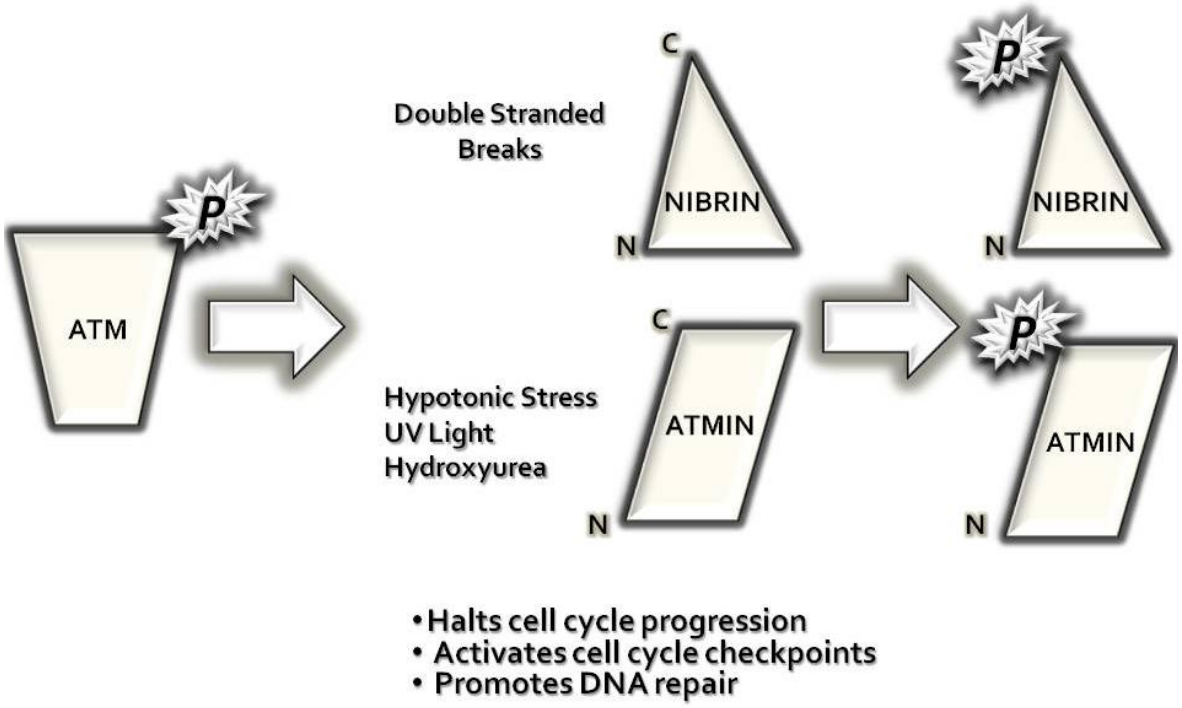

Figure 0-2: ATM activates both Nibrin and ATMIN via c-terminal phosphorylation to initiate cellular repair responses in the presence and absence (respectively) of double stranded breaks.

2.10 ATMIN

Ataxia Telangiectasia is an autosomal recessive, multisystem condition, characterized by progressive cerebellar ataxia, oculocutaneous telangiectasia (dilation of small vessels in capillary beds), radiosensitivity, predisposition to lymphoid malignancies and immunodeficiency, with defects in both cellular and humoral immunity (Lavin and Shiloh, 1997). Almost a decade ago, a mutation in Ataxia Telangiectasia Mutated (ATM), a member of the phosphatidylinositol kinase-related protein cell signalling family, was identified as the causative factor of this disease (Savitsky et al., 1995). ATM has since been well characterized and is a known mediator of cell signalling in response to DNA damage (Pandita, 2003). Active ATM phosphorylates numerous substrates including Smc1 and p53, and usually targets specifically serine or threonine residues followed by glutamine, termed ‘SQ/TQ' motifs (Kim et al., 1999; Shiloh, 2003). In particular, ATM has been shown to bind to and phosphorylate the transcription factor Nibrin (NBS-1), via c-terminal interactions, to promote DNA repair resulting from double stranded breaks (Falck

et al., 2005; Kanu et al., 2007). Recently, a novel ATM substrate protein called ASCIZ was described that contained multiple SQ/TQ sites and two N-terminal C2H2 zinc (Zn2+) fingers (McNees et al., 2005). However, expressed sequence tag (EST) analysis suggested that its amino acid sequence was incomplete, and subsequently, two additional exons (encoding Zn2+ finger domains) were characterized; the complete 88.3 kDa gene was then termed Ataxia Telangiectasia Mutated Interacting Protein (ATMIN, Kanu & Behrens 2007). Both ATMIN and Nibrin interact with ATM using similar motifs and in a stimulus-dependent manner; however, whilst ATM activates the Nibrin pathway for cellular repair in response to double stranded DNA breaks, it activates the ATMIN pathway for cellular repair in the absence of double stranded breaks - for example, after hypotonic stress, UV light exposure or treatment with hydroxyurea (Figure 0-2, Kanu & Behrens 2007). Since ATMIN is involved in cellular repair after damage, it follows naturally that it might play a role in the response to injury. CNS specific ATMIN-null mutants were created using the Cre::Lox P system of conditional mutation (Nestin::ATMIN) and neuronal response to injury will be studied. Three factors will be investigated:

- The Cellular Response to Injury – both Neuronal and Non-Neuronal
- Motor Neuron Survival
- Reinnervation – both Functional and Anatomical

These factors will be explored in both PNS and CNS paradigms to further describe the role of ATMIN in response to traumatic injury.

CHAPTER 3: MATERIALS AND METHODS

All procedures complied with the United Kingdom Animals (Scientific Procedures) Act 1986.

3.1 Generation of Mutants

3.1.1 Synapsin and P0 Jun:

Mice carrying a floxed *c-jun* allele, *c-jun*$^{f/f}$ (Behrens et al., 2002), were crossed with animals expressing cre recombinase under the control of Synapsin I promoter (Zhu et al., 2001) and then crossed again to generate the *c-jun*$^{f/f}$; Synapsin::cre+ mutant mice, in which both *c-jun* alleles are inactivated in Neurons (c-Jun$^{\Delta S}$). Sibling animals lacking the cre transgene, with functional, unrecombined homozygous *c-jun* (*jun* $^{f/f}$), and also littermates who were heterozygous for the Synapsin::cre mutation (*Syn::Cre jun* $^{f/WT}$), served as controls. To avoid possible germline inactivation of Synapsin by cre (Rempe et al., 2006) only female Synapsin I::cre+ animals were mated to male c-junf/f mice.

Mice carrying a floxed *c-jun* allele, *c-jun*$^{f/f}$ (Behrens et al., 2002), were crossed with animals expressing cre recombinase under the control of Myelin Protein 0 (P0) promoter (Feltri et al., 1999) and then crossed again to generate the *c-jun*$^{f/f}$; P0::cre+ mutant mice, in which both *c-jun* alleles are inactivated in Schwann cells (*P0 x jun* $^{f/f}$). Sibling animals lacking the cre transgene, with functional, unrecombined homozygous *c-jun* (*jun* $^{f/f}$), and also littermates who were heterozygous for the P0::cre mutation (*P0 x jun* $^{f/WT}$), served as controls.

3.1.2 JNK:

Genetic inactivation of JNK1, JNK2 and / or JNK3 in mice has been described in detail elsewhere (Yang et al., 1997, 1997; Dong et al., 1998; Kuan et al., 1999a) JNK null mutants were backcrossed once with C57 / BL6 mice. Thereafter, heterozygous F1 offspring were crossed to obtain F2 homozygous JNK knockout mice and homozygous wild type (WT) littermate controls. The F2 generation were set up in breeding pairs to produce KO and WT mice used in these experiments (F3). This breeding approach minimizes genetic strain variability between KO and WT animals and also facilitates production of large numbers of offspring necessary under guidelines of the Banburry Conference.

3.1.3 JunAA

JunAA animals carry a substitution mutation on the *Jun* allele where serines 63 and 73 are replaced with alanines; this prevents JNKs from binding to the N-terminal phosphorylation site and renders the gene product constitutively functionally inactive. Generation of these mutants is detailed elsewhere (Behrens et al., 1999). Briefly, *NotI*-linearized knock-in construct (20 mg) was electroporated into R1 embryonic stem (ES) cells. Reverse and Forward primers were used to select transfected cells, and targeting specificity was confirmed by Southern-blot analysis. Individual ES cell clones (PGKbgeo:JunWT or PGKbgeo:JunAA) were microinjected into C57BL/6 blastocysts. The floxed PGKbgeo gene was later removed from the animals' germline using Cre recombinase by pronuclear injection of a cre-expressing plasmid (Behrens et al., 1999).

3.1.4 ATMIN:

Mice carrying a floxed *ATMIN* allele, *ATMIN*$^{f/f}$ (Kanu et al., 2007), were crossed with animals expressing cre recombinase under the control of Nestin promoter and then crossed again to generate the ATMIN$^{\Delta N}$ mutant mice, in which both *ATMIN* alleles are inactivated in cells derived from neuroepithelial stem cells (Neurons, Astrocytes, Oligodendrocytes and Schwann Cells, Rao 1999). Sibling animals lacking the cre transgene, with functional, unrecombined homozygous *ATMIN* (*ATMIN*$^{f/f}$), served as controls.

3.2 Surgery

3.2.1 Facial Nerve Axotomy (FNA)

Pups were anaesthetized using cooling anaesthesia on wet ice (4°C), and the extent of anaesthesia was determined by assessing reflex responses to tail pinch. Adult mice were anesthetized with tri-bromo-ethanol (Avertin, Sigma Aldrich; 0.05mL of 2.5% solution injected intraperitoneally) or Isoflurane (5% to induce, 2% to maintain) and extent of anaesthesia was determined by assessing reflex response to ear pinch. Oxygen was administered at 1L/min. The animal was shaved beneath the right ear and the area was sterilized using 70% ethanol in ddH2O. The right facial nerve was transected at the stylomastoid foramen and both the retroauricular and main branches were severed. For crush experiments, only retroauricular branch was crushed and main branch was untouched. Nerve was crushed with fine forceps 3 times for 5 seconds. Successful facial motor nerve transection was confirmed by the absence of motor function in the ipsilateral

whisker hair. Animals were then allowed to survive for 1 (axotomy), 4 (crush), 14 (axotomy) or 30 (axotomy) days.

3.2.2 Dorsal Hemisection

Dorsal spinal cord hemisection was performed at level C5. Both central and lateral ipsilateral corticospinal tracts were severed. Animals were anaesthetized using Isoflurane (5% to induce, 1-2.5% to maintain, depending on animal) and the spinal cord was exposed. Sterile paper tissue rolls were inserted and used to visualize the area and to hold the skin and muscle apart. C5 laminectomy was performed using forceps and the spinal cord was exposed. Dura mater was punctured roughly 0.5 mm lateral of the midline on the contralateral (right) side using an insulin syringe. Fine scissors (Fine Science Tools, Heidelberg) were inserted into the hole roughly 2mm deep and a cut was made across the midline to the ipsilateral side that severed the ipsilateral and medial CST. An insulin syringe was run between distal and proximal segments to confirm complete transection.

3.2.3 Dorsolateral Hemisection

Dorsolateral spinal cord hemisection was performed at level C5. Both central and lateral ipsilateral corticospinal tracts were severed, as well as the more ventrolateral ipsilateral rubrospinal tract. Animals were anaesthetized using Isoflurane (5% to induce, 1-2.5% to maintain, depending on animal) and the spinal cord was exposed. Sterile paper tissue rolls were inserted and used to visualize the area and to hold the skin and muscle apart. C5 laminectomy was performed using forceps and the spinal cord was exposed. Dura mater was punctured roughly 0.5 mm lateral of the midline on the contralateral (right) side using an insulin syringe. Fine scissors (Fine Science Tools, Heidelberg) were inserted into the hole roughly 2.5 mm deep and a cut was made across the midline to the ipsilateral side

that severed the ipsilateral and medial CST, as well as the RST. This lesion is roughly 0.5mm deeper than a dorsal spinal cord axotomy. An insulin syringe was run between distal and proximal segments to confirm complete transection on the ipsilateral side.

3.2.4 Retrograde Tracing

Whisker pad reinnervation was assessed by applying 20-30 µL of 4% Fluorogold (Fluorochrome, Denver, CO) in ddH2O to a 2mm x 2mm piece of gelfoam (Pfizer, New York, NY) placed under both whisker pads 28 days after unilateral nerve cut. Pads were left for 30 minutes and then removed and the wound was closed. Subsequently, the number of fluorescently labelled motoneurons in the injured and contralateral facial motor nuclei was quantified 48 hr after Fluorogold implantation (Werner et al., 2000). In addition, some experiments used a double labelling system where 2-3µL of a 10% solution of MiniRuby (Invitrogen, Paisley, UK) in ddH2O was injected using a 10 µL Hamilton Syringe (Hamilton Company, Switzerland) sub-cutaneously into the contralateral and ipsilateral upper and lower eyelids on the same day as Fluorogold implantation.

3.2.5 Stereotactic Anterograde Tracer Injection

In animals that received dorsal and dorsolateral spinal cord transection, anterograde tracers were injected stereotactically at 30 days post-axotomy to visualise the lesion site and track anatomical recovery. In both cases (dorsal and dorsolateral transection), corticospinal axons were labelled with MiniRuby or FluoroRuby (Invitrogen, Paisley, UK) red fluorescent tracer injected into the contralateral (right) motor cortex. Since the corticospinal pathways cross the midline at the pyramidal decussation, tracer was injected into the right side to ultimately label the left-injured section of spinal cord. 0.5 µL of tracer was injected at 4 sites in the forebrain at 150 nL/min, according to Table 1. All injections

were performed stereotactically, using a 10 μL Hamilton syringe attached to a Micro4 MicroSyringe Pump Controller (World Precision Instruments, Sarasota, USA) micropipettor. Animals were anaesthetized using Isoflurane anaesthetic (5% to induce, 1-2.5% to maintain, depending on animal), an incision was made along the top of the skull with a size 15 or 20 scalpel and connective tissue was scraped away with the scalpel until the bregma was exposed. Measurements were taken twice before holes were drilled at the appropriate sites using a dental drill. All injections were made using a 5μL or 10μL Hamilton Syringe (Hamilton Company, Switzerland) with a pulled glass tip attached with superglue. Animals survived for 10-14 days post – injection to allow for anterograde tracer transport before undergoing transcardial perfusion.

Table 1 Stereotactic Co-Ordinates for Motor Cortex

Motor Cortex Coordinates From Bregma	Lateral (X)	Caudal/Rostral (Y)	Depth (Z)	Angle (˚)
Site 1	1.0mm	-1.0mm	1.0mm	0˚
Site 2	1.0mm	-0.5mm	1.0mm	0˚
Site 3	1.0mm	+0.2mm	1.0mm	0˚
Site 4	1.0mm	+0.5mm	1.0mm	0˚

3.3 Analgesia, Antibiotic and Hydration

All animals were given 0.05 – 0.1 mg/kg buprenorphine (vetergesic, Alstoe Animal Health, Hull, UK) sub-cutaneously as a pre-operative analgesic, as well as 0.05 – 0.1 mg/kg buprenorphine sub-cutaneously every 8 hours additionally for at least 16 hours post-injury.

Clamoxyl LA (Pfizer, Kent, UK) was given prophylactically as a pre-operative antibiotic via sub-cutaneous injection at 0.1mL/animal.

In addition, all animals were given 0.5mL saline (Braun, Melsungen, Germany) or sterile water via a sub-cutaneous bolus pre-operatively to prevent dehydration. Animals were

given an additional 0.5mL bolus (1mL total) if haemorrhage occurred during or after surgery.

3.4 Perfusion

3.4.1 Facial Nerve Cut

One, 14 or 30 days later, mice were deeply anesthetized with Intraperitoneal 2.5% Avertin (0.5mL) or Euthatal (0.5 mL) and transcardially perfused with 200mL/animal 4% paraformaldehyde (PFA) in 0.1M phosphate buffered saline (PBS) (pH 7.4) preceded by a brief wash (150mL/animal) with 0.1M PBS (pH 7.4, Moller et al. 1996). Brains were extracted and after a 2h postfix in 1% PFA or 1h in 4%, tissue was moved to 30% sucrose (Fluka) overnight in PB solution in preparation for freeze sectioning.

3.4.2 Facial Nerve Crush

Four days after facial nerve crush, animals were anesthetized with Intraperitoneal 2.5% Avertin (0.5mL) or Euthatal (0.5 mL) and transcardially perfused for 10 minutes with 4% paraformaldehyde (PFA) in 0.1M phosphate buffered saline (PBS) (pH 7.4) preceded by a brief wash (5 minutes) with 0.1M PBS (pH 7.4, Moller et al. 1996). After 5 minutes in PBS and 10 minutes in 4% PFA, animals were perfused continuously for 45 minutes with 1% PFA. Brains were extracted placed in 30% sucrose (Fluka) overnight in PB solution in preparation for freeze sectioning and facial nerves were extracted and flash frozen in boats containing OCT (BDH biochemical) put on glass slides over dry ice (-80˚C).

3.4.3 SCI

Ten to fourteen days after stereotactic tracer injection, animals were deeply anesthetized with Intraperitoneal 2.5% Avertin (0.5mL) or Euthatal (0.5 mL) and transcardially perfused with 200mL/animal 4% paraformaldehyde (PFA) in 0.1M phosphate buffered saline (PBS) (pH 7.4) preceded by a brief wash (150mL/animal) with 0.1M PBS (pH 7.4, Moller et al. 1996). Brains were extracted and spinal cords were left encased in bone/tissue. After a 2h postfix in 1% PFA or 1h in 4%, tissue was moved to 30% sucrose (Fluka) overnight in PB solution in preparation for freeze sectioning. Before freeze sectioning, spinal cords were removed from within the vertebral column and were flash frozen in boats containing OCT (BDH biochemical) using glass slides over dry ice (-80˚C).

3.5 Freeze sectioning

3.5.1 Hindbrain

Tissue was cut at the level of the facial motor nucleus (the facial nucleus is ≈700 µm in length in the anterior–posterior direction) using a freezing cryostat (Leica CM 1900), with internal temperature of -20˚C and chuck temperature -15˚C, into 20 µM sections, taken up onto 0.5% gelatine (BDH Biochemical) coated glass slides or Superfrost Plus slides (BDH Biochemical) and stored immediately on dry ice. After roughly 1 minute on dry ice, slides were placed in a chilled box and stored at -80˚C for further use.

Facial Nucleus was found by cutting the brain in half coronally post-sucrose cryoprotection to separate the hindbrain from the forebrain and then mounting the hindbrain, rostral side down, on a piece of wet filter paper on dry ice. The paper and hindbrain was allowed to freeze on the dry ice and either stored at -80˚C for future cutting or immediately processed

for cutting. Hindbrains for cutting were embedded in OCT (BDH biochemical) on a chuck in the -20˚C cryostat until the OCT solidified. Dry ice was placed around the OCT to accelerate freezing. Coronal hindbrain sections were taken and discarded until cutting reached the cerebellum, at which point a section was taken and the level was examined. If sections were in the Lateral Reticular nucleus, 30-35 sections were taken until the level of the Nucleus Ambiguus was reached. This was verified visually. Once in the Nucleus Ambiguus, landmarking was done via the Hypoglossal Nucleus, 4th Ventricle and Dorsal Motor Nucleus of the Vagus Nerve. 3-5 sections were cut and then one was examined to determine level. Once the Hypoglossal Nucleus disappeared, the Dorsal Motor Nucleus of the Vagus Nerve was laterally displaced and the 4th ventricle enlarged, single sections were taken and confirmed visually until the facial motor nucleus was reached. Abducens nuclei and the internal genu of the facial nerves were used to precisely match the location of the left (contralateral) and right (ipsilateral) sides.

3.5.2 Facial Motor Nerve

Facial Motor Nerve was cut longitudinally in 10µm sections using a freezing cryostat (Leica CM 1900), with internal temperature of -20˚C and chuck temperature -15˚C. Sections were taken up onto 0.5% gelatine (BDH Biochemical) coated glass slides or Superfrost Plus slides (BDH Biochemical) and sections were immediately frozen on dry ice. After roughly 1 minute on dry ice, slides were placed in a chilled box and stored at -80˚C for further use.

3.5.3 Spinal Cord

Spinal cord was cut longitudinally in 40µm sections using a freezing cryostat (Leica CM 1900), with internal temperature of -20˚C and chuck temperature -15˚C. Sections were taken up onto 0.5% gelatine (BDH Biochemical) coated glass slides or Superfrost Plus

slides (BDH Biochemical) and every fifth section was either spread with ddH20 and allowed to dry overnight or stored immediately on dry ice for later spreading and drying overnight. After roughly 1 minute on dry ice, slides were placed in a chilled box and stored at -80˚C for further use.

3.6 Immunohistochemistry

Tissue sections (20 µm) were rehydrated in ddH2O and spread. After drying on an angle in an indirect breeze for 15 minutes, they were circled with a DAKO pen (DAKO, Cambridgeshire). After being fixed in 4% formaldehyde (BDH biochemical) for 5 minutes, sections were then washed with 0.1M Phosphate Buffer (PB) for a minimum of 5 minutes. After defatting for 2 minutes each in 50%, 100% and 50% Acetone (VWR), then washing for 2 minutes each in 0.1M PB, 0.1M PB and 0.1% Bovine Serum Albumin in 0.1M PB (PB/BSA, BDH biochemical), sections were blocked using 5% goat (Gt) serum (Sigma) in PB for 30 minutes. They were then stained overnight at 4˚C with primary antibodies, optimized previously and diluted in PB/BSA, as described in previous studies (Galiano et al., 2001; Werner et al., 2000); dilutions are described in

Table 3 of the Appendix. Sections were then visualized using biotinylated immunoglobulin secondary antibody (1:100 in PB/BSA for one hour, Vector) after 30 minute incubation with mouse serum (ABD Serotec). They were then washed with PB ABC peroxidase complex (10% each A and B in PB for 1 hour, Vector), and stained with diaminobenzidine (25 mg in 50mL of 10mM PB, Sigma), with hydrogen peroxide (17.6 µL in 50 mL DAB solution BDH biochemical) added immediately before initiating the reaction. Reaction was stopped using 10mM PB and ddH2O. Sections were subsequently dehydrated in increasing concentrations of ethanol (70%, 70%, 90% 95%, 95%, 100%, 100%, VWR) and isopropanol (BDH biochemical), then immersed thrice in Xylene (VWR) before being

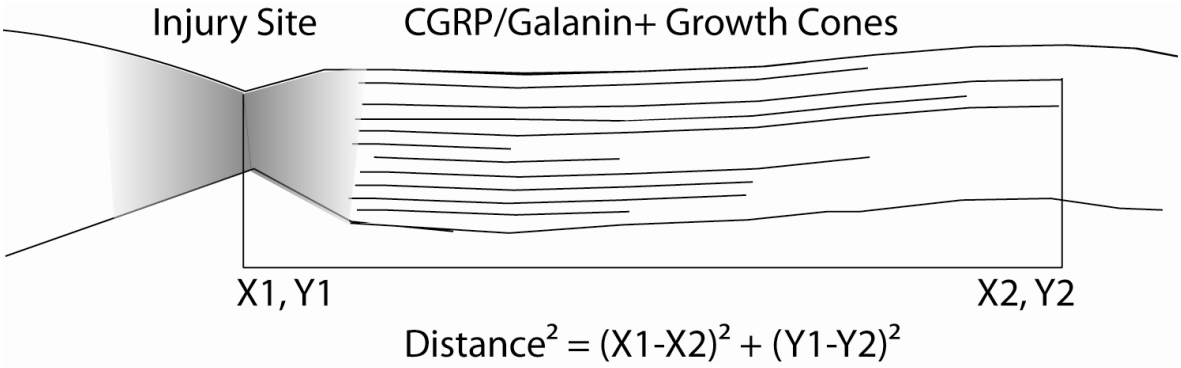

Figure 3-1: Measuring Regeneration Distance
The Pythagorean Theorem states that $Z^2 = X^2+Y^2$. By determining X and Y lengths between the injury site (X_1, Y_1) and the last regenerating growth cone front (X_2, Y_2), reinnervation distance was quantified for WT and KO animals.

covered with glass slide covers (VWR) using depex (BDH biochemical). A Sony 3 CCD video camera was used to obtain 8 bit digital images (based on a 0–255 scale of optical luminosity values) of the antibody stained sections. Immunohistochemical staining was quantified using the OPTIMAS 6.2 imaging system (Media Cybernetics Inc, Silver Spring, MD) and the Mean-SD algorithm. The overall mean optical luminosity value for the antibody staining intensity (SI) was determined for each facial motor nucleus, on both the ipsilateral and contralateral side, and subsequently the SI of the adjacent glass was subtracted.

3.7 Reinnervation Distance

Animals that survived for 4 days following a facial motor nerve crush were transcardially perfused and brains were extracted. Tissue was processed in accordance with the protocol described above and sections were stained for CGRP and Galanin immunopositive growth cones according to

Table 3 of the Appendix (Galiano et al., 2001; Werner et al., 2000). Galanin and CGRP+ growth cone lengths were measured using a Leica microscope with an attached vernier device (Figure 3-1). Measurements began at the injury site and were taken to the end of

the furthest regenerating immunoreactive growth cone front. Distance was calculated using the Pythagorean Theorem:

Equation 2: Pythagorean Theorem - $Z^2 = (X_1-X_2)^2+(Y_1-Y_2)^2$

Where X and Y line length were calculated by subtracting X and Y co-ordinates in space between the injury site (X_1, Y_1) and the furthest regenerating nerve front (X_2, Y_2). In cases where the growth cones were interrupted or crooked, individual line lengths were determined using the formula above and added or subtracted as appropriate to determine total length.

3.8 Neuronal Cell Counts

Tissue sections (20 µm) were rehydrated in ddH2O and spread. They were allowed to dry at an angle in indirect breeze for 15 minutes and then dried flat for at least 8 hours.

3.8.1 Nissl

4/5 sections were placed in 4% formaldehyde (BDH biochemical) overnight and then solution was changed to 70% ethanol (VWR) overnight. These sections were then stained with Toluidine blue (Nissl). This is made by mixing 4g cressyl violet (Merck) in 40mL 100% Ethanol (VWR), shaking and inverting for 15 minutes, then adding this mixture to 360mL ddH2O and filtering using size 4 filter paper. Neuronal cell counts were made of ipsilateral and contralateral facial motor nucleus and percentage change between the left and right sides was calculated and compared between groups. The Abercrombie Correction (Equation 1) was used to determine relative percentage change between contralateral and ipsilateral side per histological section.

3.8.2 Fluorogold and Miniruby

1/5 sections were taken and examined under a fluorescent microscope (Nikon Eclipse E600). Fluorogold positive cells were counted in the facial motor nucleus using both 64x and 16x filters at 450-490 nm wavelength. FMN neurons that were labelled with MiniRuby were also counted on these slides at 510-560 nm wavelength.

3.9 Spinal Cord Axonal Counts

Tissue sections (40 µm) were rehydrated in ddH2O and spread. They were allowed to dry at an angle in indirect breeze for 15 minutes and then dried flat for at least 8 hours. 1/5 sections were taken and examined under a fluorescent microscope (Nikon Eclipse E600). The left scope was fitted with a lens conveying a vertical line to the field of vision and MiniRuby and MiniEmerald positive axons that transected that line were counted 0, ±0.5mm, ±1.0mm and ±1.5mm past the lesion site at 450-490 nm wavelength for MiniEmerald and at 560 nm wavelength for FluoroRuby and MiniRuby.

3.10 Whisker Function Assessment

Animals received facial motor nerve transections and subsequent whisker function was recorded on both ipsilateral and contralateral sides. Measurements were taken at 2-3 day intervals until day 28, when Fluorogold implantation was carried out. Animals were rated by 5 independent observers on a scale from 0 (no movement) to 3 (normal movement).

3.11 Rearing Test

The rearing test explores gross motor co-ordination and is sensitive to limb use asymmetries (Starkey et al., 2005). Briefly, animals were placed in a Perspex cylinder (300mm height, 80mm diameter, Habitat) and spontaneous rearing was recorded using a Sony digital video camera recorder, DCR-TRV60E camera for five minutes. White paper was used as a backdrop and a mirror was placed at an angle behind the cylinder so that forepaws were visible at all times. Taped footage was later reviewed and weight bearing during each rear was quantified as right, left or both. If animals supported in one rear with alternating left and right, it was counted as both. Animals were placed in cylinders prior to surgery for habituation and also for baseline measurements. Animals were subsequently tested on days 2, 7, 14, 21 and 28 post-surgery.

3.12 Grid Test

The grid test assesses fine motor co-ordination and the animal's ability to accurately place the forepaws during spontaneous exploration (Starkey et al., 2005). Animals were placed on an elevated wire grid with 1cm x 1cm spacing. Edges were upward-facing and filed sharp to deter animals from going over the edges. A Sony digital video camera recorder, DCR-TRV60E camera was placed under the grid facing upward and spontaneous exploration was recorded for 3 minutes. Taped footage was later reviewed and foot slips were quantified for each foot during the first 100 steps. A foot slip was scored either when the paw completely missed the rung and fell through the rung or when the paw was placed correctly but subsequently fell through the rung upon weight bearing (Starkey et al., 2005; Selak and Fritzler, 2004; Lee et al., 2009; Goldshmit et al., 2008; Hsu et al., 2006). Animals were placed on the grid prior to surgery for habituation and also for baseline

measurements. Animals were subsequently tested on days 2, 7, 14, 21 and 28 post-surgery.

3.13 Statistical Analysis

All data were expressed as mean ± standard error of the mean and analysed using unpaired student t test for 2 groups and ANOVA, followed by post-hoc Tukey for 3 groups, as appropriate. In the spinal cord, MiniRuby-labelled axons in all 6 compartments were corrected as a fraction of the average number of ipsilateral CST axons 1.5-0.5mm above the injury site, and further normalised using the log (x+0.01) algorithm, as in previous studies (Galiano et al., 2001). For all statistical analysis, statistical significance was set at $P < 0.05$.

CHAPTER 4: JUNΔS RESULTS: NEURONAL JUN IS AN ESSENTIAL FACTOR IN THE CELL RESPONSE TO INJURY

Previous investigations link c-Jun deletion in the nervous system with increased neuronal survival post injury, as well as decreased reinnervation and perineuronal sprouting, increased expression of growth associated molecules and decreased non-neuronal cell activity (Raivich et al., 2004a; Makwana et al., 2009). However, since this particular gene deletion was mediated by a nestin promoter, this could have resulted in cre-mediated excision in all cells of a neuroepithelial lineage – including Schwann Cells, Neurons, Oligodendrocytes and Astrocytes.

These findings have interesting clinical implications – many neurodegenerative diseases such as MS, ALS, Huntington's disease and Parkinson's disease would benefit from treatments designed to reduce levels of neuronal apoptosis. However, the broadness of the nestin-mediated deletion means that the potential therapeutic anti-apoptotic properties of *c-Jun* targeted gene-deletion could be attributed to any one of several cellular systems that are affected by a deletion in neuroepithelial stem cells. Any one of (or combination thereof) the aforementioned daughter cell types could be contributing to the phenotype seen in nestin-jun mutants. Furthermore, these systems could be contributing separately to increased survival and decreased reinnervation; if that is the case, specific targeting of *c-Jun* deletion to one differentiated cell type and not another could selectively increase neuronal survival whilst leaving reinnervation unaffected. Therefore, it is necessary to explore *c-jun* gene deletion in terminally differentiated daughter cells (for example, neurons and Schwann cells) to determine the role it plays in each. First, the role of c-Jun was explored using the Synapsin promoter to target cre mediated *c-Jun* excision exclusively to neurons.

4.1 Generation of Mice Lacking c-Jun in Neurons

To characterize the role of neuronally expressed c-Jun in peripheral regeneration, animals were created with a neuron-specific deletion of c-Jun. This was done by crossing mice with a floxed c-jun allele (c-JunF/F) with animals expressing cre recombinase under the control of the Synapsin promoter, which targets recombination specifically to neurons (Zhu et al., 2001; Hasue et al., 2005; He et al., 2004; Xia et al., 2003; May et al., 2004; Tamai et al., 2008; Ferguson et al., 2007; Usukura et al., 1987; Sims et al., 2008; Kügler et al., 2001). The resulting F1 generation was crossed again with c-JunF/F mice to result in generation of homozygous mutant c-JunΔS and homozygous wild type animals. Since previous research shows that there is a possibility of germline recombination of Synapsin::Cre in the testes, which can affect offspring numbers in males, but not females (K. A. Street et al., 2005; Hoesche et al., 1993; Rempe et al., 2006), female cre+ animals were bred with cre- (c-JunF/WT and c-JunF/F) males. c-JunΔS animals were born with Mendelian frequency and showed normal brain structure and histology, as indicated by Haematoxylin and Eosin (H&E) staining and Neuronal Nuclei (NeuN) immunoreactivity. However, as seen in Figure 4-1, c-jun inactivation was present in several brain regions, including the cerebellum (Cb), cortex (Cx), brain stem (Bs), and hippocampus (Hc). In general, while brain organization and histology was relatively normal in c-Jun$^{\Delta S}$ mutants, facial motor nucleus counts revealed a 14% increase in facial motoneurons in c-Jun$^{\Delta S}$ animals, with 2369 ± 92 in control c-Jun$^{F/F}$ mice compared to 2699±123 in c-Jun$^{\Delta S}$ mice ($p < 0.05$ in uSTT).

To account for differences in recombination frequencies established by Cre/LoxP-mediated recombination (due to chromosomal location of recombination substrates, Vooijs et al. 2001), effects of Synapsin-mediated *c-jun* deletion were first investigated in heterozygous c-Jun$^{F/WT}$ Synapsin-I cre+ mouse. There were no differences between c-Jun$^{F/WT}$ Synapsin-cre+ and c-Jun$^{F/F}$ mice in any paradigms investigated, indicating that one

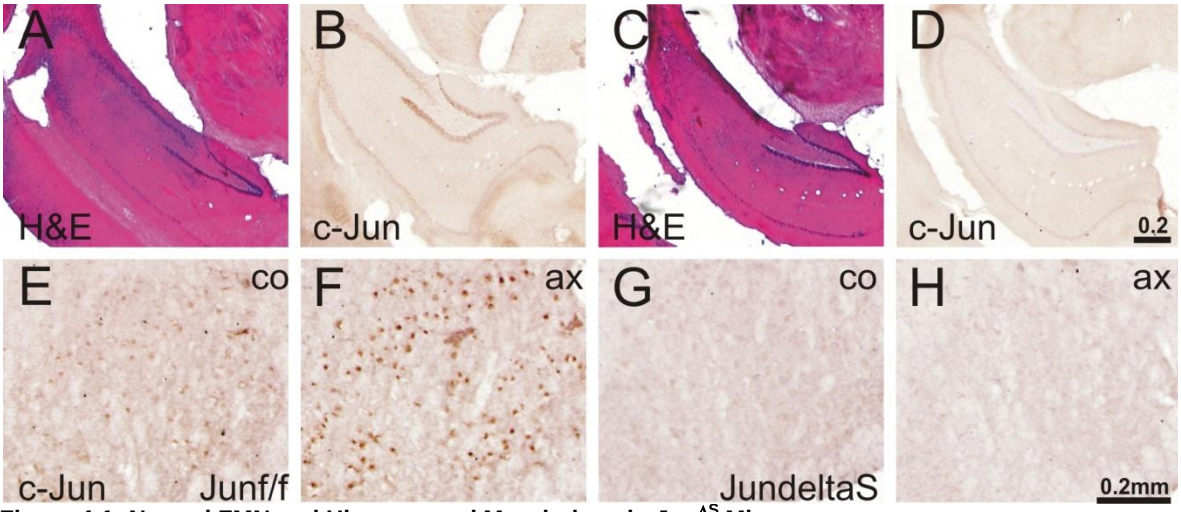

Figure 4-1: Normal FMN and Hippocampal Morphology in Jun$^{\Delta S}$ Mice
(A and C) Histological analysis (haematoxylin and eosin staining, [H&E]) of hippocampal sections of control animals (A, Jun$^{F/F}$) and Jun$^{\Delta S}$ Mice (C). (B and D) c-Jun immunostaining on hippocampal sections of Jun$^{F/F}$ (B) and Jun$^{\Delta S}$ mice (D). (E-H) shows c-Jun immunopositive motor neurons in the facial motor nucleus of c-Jun$^{F/F}$ and c-Jun$^{\Delta S}$ mice on the control (co, E, G) and operated side (ax, F, H).

copy of *c-jun* was sufficient to mediate its trophic effects. As a result, c-Jun$^{F/WT}$ Synapsin-cre+ heterozygotes and c-Jun$^{F/F}$ wild type mice were included in the same control groups for the purpose of this study.

4.2 c-jun is Induced Following Facial Nerve Transection

Previous studies point to the presence of a strong *c-jun* induction following facial nerve injury (Raivich et al., 2004a; Crocker et al., 2001). To determine whether this was the case with c-Jun$^{\Delta S}$, regeneration was explored at 4 and 14 days following cut injury. Basal c-Jun protein levels were present in uninjured wild type facial motor neuron nuclei (Figure 4-1) and facial nerve transection led to a strong and robust increase in c-Jun immunoreactivity 14 days following injury. Neither basal nor induced levels of c-Jun protein were present in facial motoneurons of c-Jun$^{\Delta S}$ mutants.

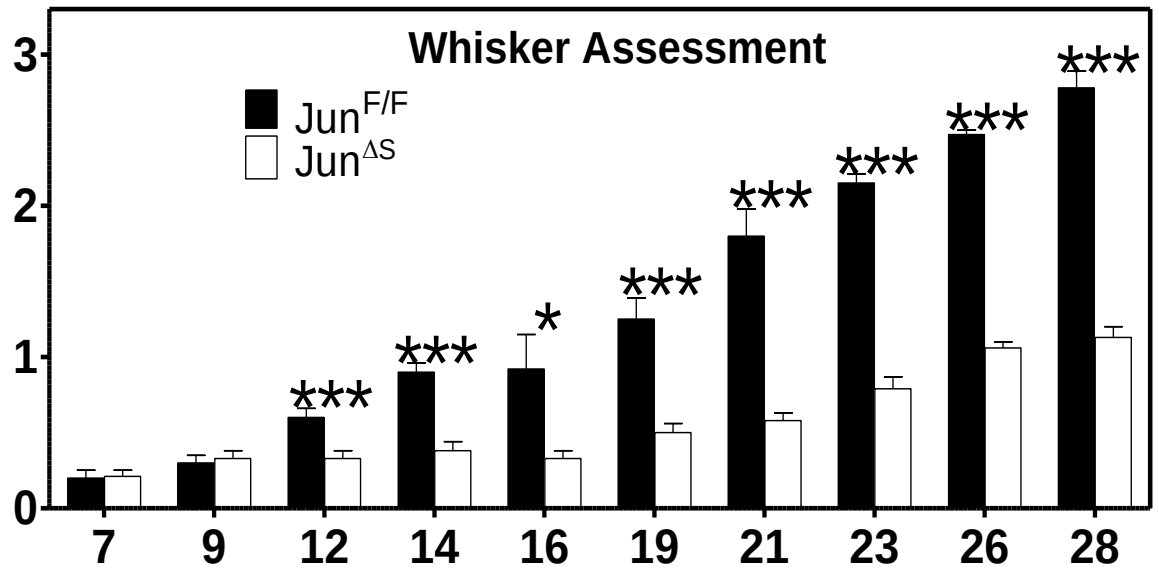

Figure 4-2: Neuronal c-Jun is Necessary for Successful Functional Reinnervation after facial nerve axotomy

Posttraumatic whisker hair motor performance was measured for 28 days after facial nerve axotomy, on a scale of 0 (no movement) to 3 (normal, strong movement similar to the contralateral side). c-Jun$^{\Delta S}$ mutants showed impaired functional recovery compared to c-Jun$^{F/F}$ counterparts; N=8 for c-Jun$^{F/F}$ and N=8 for c-Jun$^{\Delta S}$ mutants. *p<0.05 and ***p < 0.001 between c-Jun$^{F/F}$ and c-Jun$^{\Delta S}$ animals in unpaired Student's T-Test (uSTT).

4.3 Neural c-Jun is Essential for Peripheral Axonal Regeneration

Following injury, neurons participate in a complex cellular response that results in sprouting and elongation of growth cones from the proximal axonal tip. These growth cones travel along the basal lamina to eventually reinnervate target muscle. Post facial nerve injury, this reinnervation is examined using three different tests. Anatomical reinnervation was determined 30 days following facial nerve cut, and extent of regeneration is gauged via retrograde tracer transport from the site of injury to the facial motor nucleus. Functional recovery, also analyzed for 30 days following injury, determined functionality of those connections and was assessed by scoring whisker hair movement. Finally the reinnervation distance of CGRP and galanin immunopositive growth cones is measured 4 days after crush injury (Makwana et al., 2009).

4.3.1 Whisker Hair Movement

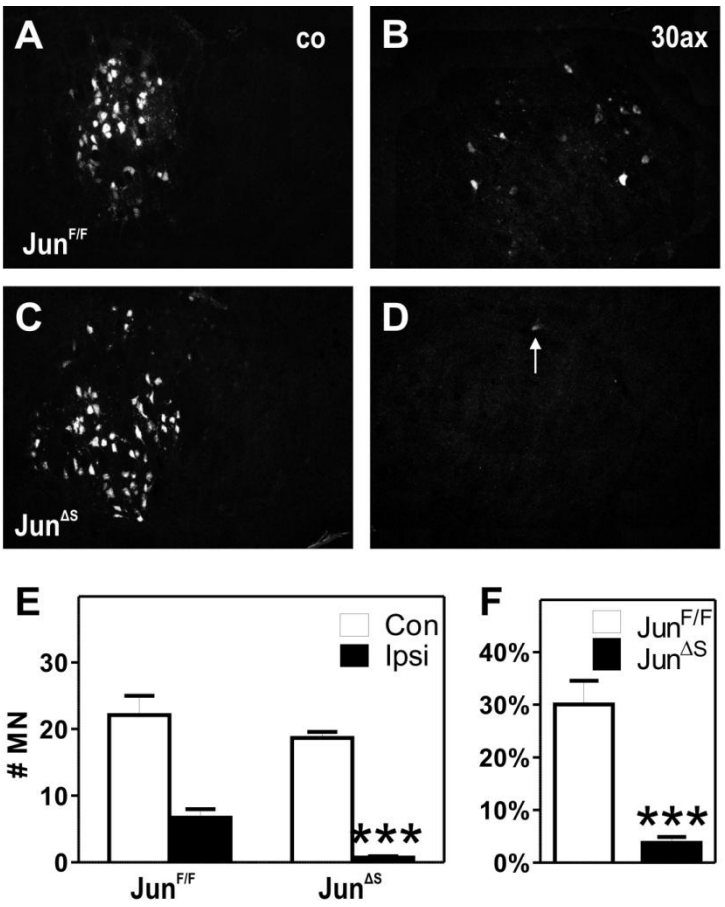

Figure 4-3 Characterizing Post-Operative Regenerative Response – Neuronally expressed c-Jun is essential for successful target reinnervation

(A-D) Fluorogold expression in c-Jun$^{F/F}$ (A, B) and c-Jun$^{\Delta S}$ (C, D) on the contralateral (A, C) and ipsilateral (B, D) sides 30 days following facial nerve transection. (E) Quantification of retrogradely labelled motoneurons in the facial motor nucleus of c-Jun$^{F/F}$ (N=8) and c-Jun$^{\Delta S}$ (N=9) animals, using FluoroGold, performed 28 days post-operatively. c-Jun$^{\Delta S}$ animals show virtually no anatomical reinnervation following peripiheral nerve injury. Contralateral side, white bars; ipsilateral side, black bars. *p<0.05 and ***p < 0.001 in uSTT between c-Jun$^{\Delta S}$ and c-Jun$^{F/F}$. (B) Ax/Co ratio of FluoroGold positive neurons is shown for c-Jun$^{F/F}$, black bars and c-Jun$^{\Delta S}$, white bars. c-Jun$^{\Delta S}$ animals show an almost 80% reduction in specific reinnervation.

Movement of whisker vibrissae was scored at 2-3 day intervals post-facial nerve axotomy by three observers unaware of genotype on a scale of 0 (no movement) to 3 (normal movement, similar to that of contralateral side). During the course of recovery, control animals showed steady improvement of whisker function, whereas c-Jun$^{\Delta S}$ animals showed only moderate recovery (Figure 4-2). Twenty-eight days after injury, all animals showed normal movement on the contralateral side (3.0). On the ipsilateral side, c-Jun$^{F/F}$ animals showed 2.78±0.11 units of recovery (N=8) and c-Jun$^{\Delta S}$ animals averaged an almost threefold lower score – 1.13±0.07 (N=8).

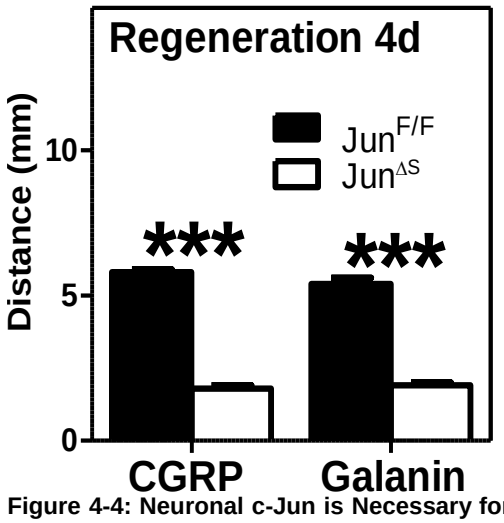

Figure 4-4: Neuronal c-Jun is Necessary for Facial Motor Nerve Regeneration and Sprouting after facial nerve axotomy
Regeneration Distance was measured 4 days after facial nerve crush in mm. Axons of c-Jun$^{\Delta S}$ mutants reinnervate less than half the distance of their c-Jun$^{F/F}$ littermates; N=6 for c-Jun$^{F/F}$ and N=4 for c-Jun$^{\Delta S}$ animals. ***p<0.001 between c-Jun$^{F/F}$ animals and c-Jun$^{\Delta S}$ mutants in uSTT.

4.3.2 Anatomical Recovery

To establish whether this deficit was due to lack of axonal reinnervation or just function of successfully reinnervated axons, a fluorescent tracer, Fluorogold (Fluorochrome, Denver, CO), was implanted via a gelfoam insert under the whisker pad 28 days following facial nerve lesion. In addition to Fluorogold, MiniRuby tracer (Invitrogen, Paisley, UK) was also injected in the area surrounding the eyelid, according to Ruff (2010) and (Popratiloff et al., 2001). Following 48 hours of retrograde transport, animals were perfused and facial motor nuclei were examined. Contralateral nuclei served as intra-animal controls. c-Jun$^{F/F}$ animals averaged 22.1 ±2.9 (N=5) Fluorogold immunopositive neurons on the contralateral side and mutants showed 18.7±0.9 (N=6, p<0.001 in unpaired Student's T-test). On the axotomized side, c-Jun$^{F/F}$ controls showed 6.7±1.3 and KOs showed 0.7±0.2 according to Figure 4-3. The ratio of labelled motoneurons on the axotomized compared to control side (ax/co ratio) was 30±4.5% for control animals and 3.8±1.1% for c-Jun$^{\Delta S}$ mutants – a more than 7-fold decrease (p<0.001 in unpaired Student's T-test) – indicating that neuronal c-Jun signalling is very important for successful axonal outgrowth. Without this anatomical connection, animals do not recover function to the same extent after peripheral nerve injury. Previous studies in animals with neuroepithelial specific deletion of c-Jun (who share this phenotype) show that functional reinnervation also did not return to normal; corresponding anatomical reinnervation still remained about 3-4 times lower (Raivich et al., 2004a).

4.3.3 Facial Nerve Regeneration

To determine whether neuronal c-Jun deletion in $Jun^{\Delta S}$ animals directly influenced the regenerative process, we measured the distance of facial motor nerve axon outgrowth 96h after nerve crush at the stylomastoid foramen. The growth front of the regenerating CGRP- and galanin-immunopositive motor neurites was quantified in longitudinally cut, fixed 10um thick facial nerve sections using DAB immunoreactivity for the axonally transported neuropeptides CGRP and galanin (Werner et al., 2000). As revealed in Figure 4-4, control c-$Jun^{F/F}$ wild-type animals averaged a regeneration distance of 5.8±0.1mm for CGRP immunopositive axon length. Mutants showed a 60% reduction in CGRP immunopositive axon length compared to wild type littermates, averaging 1.8±0.1mm for CGRP positive outgrowth. Upon comparing Galanin immunoreactive protrusions, the same threefold difference was observable: wild type axon length was 5.4±0.2mm and mutants' axons grew an average distance of 1.9±0.1mm. N=6 for c-$Jun^{F/F}$ wild type animals and N=4 for c-$Jun^{\Delta S}$ mutants; $p<0.0001$ in unpaired Student's T-test.

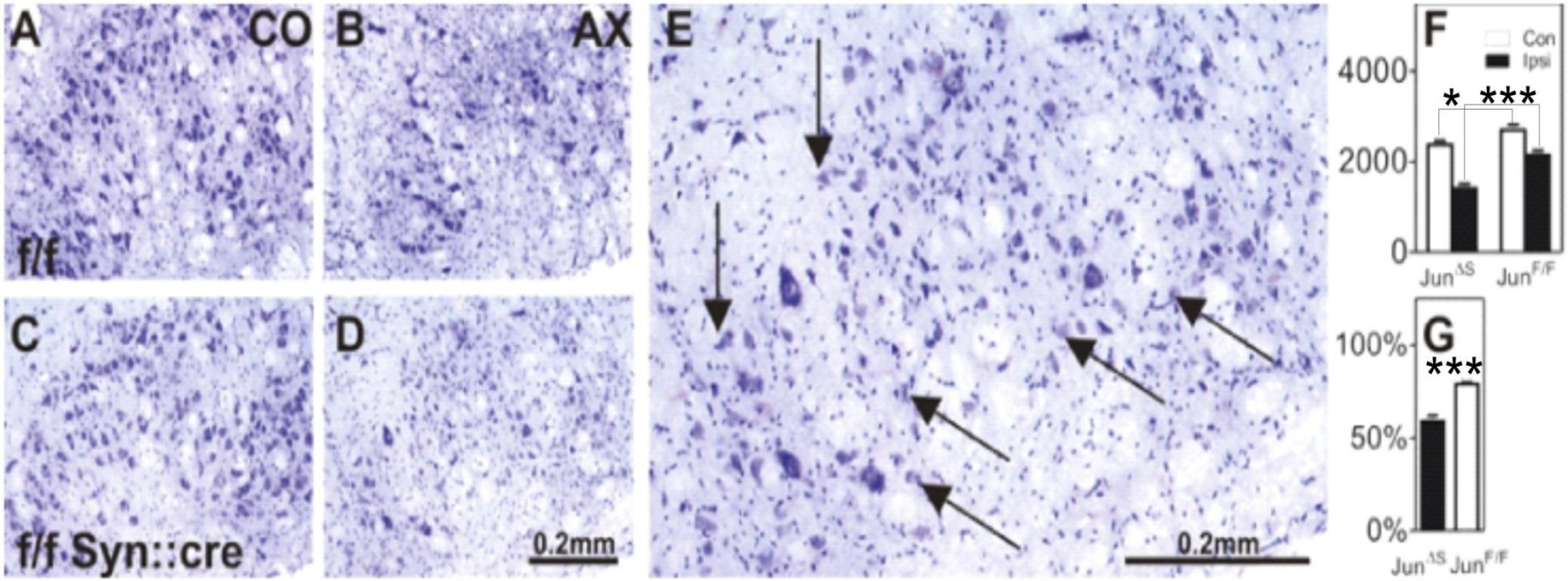

Figure 4-5 Increased Post-Facial Nerve Axotomy Cell Survival in Neuronal c-Jun-Deficient Mice.

(A-E) Neuron-Specific c-Jun deletion increases levels of motoneuron survival 30 days post-facial nerve axotomy on the contralateral side (A, C) and axotomized side (B, D). Most jun-deficient surviving motoneurons are atrophic, as shown using higher magnification (E, arrows, right). Control side (co) and Axotomized side (ax); c-Jun$^{F/F}$ and c-Jun$^{\Delta S}$. (F) Quantification of motoneuron number in facial nucleus of adult c-Jun$^{F/F}$ and c-Jun$^{\Delta S}$ mice on the contralateral (white bars) and ipsilateral side (black bars), 30 days after facial nerve transection. *$p < 0.05$ and *$p < 0.001$ in uSTT between c-Jun$^{F/F}$ and c-Jun$^{\Delta S}$ groups (F and G), N = 8 for both c-Jun$^{F/F}$ and c-Jun$^{\Delta S}$ groups in (F) and (G). (G) Quantification of specific cell death Ax/Co in the facial motor nucleus of adult c-Jun$^{F/F}$ (black bars) and c-Jun$^{\Delta S}$ (white bars) mice, 30 days after facial nerve axotomy.

4.4 Neural c-Jun Deletion Abolishes Neuronal Cell Death but Cells Display an Atrophic Phenotype

Normally, 20-40% of adult axotomized mouse facial motoneurons die within 4 weeks of nerve cut (Ferri et al., 1998b; Serpe et al., 2003a; Makwana, Serchov, et al., 2009); this is largely attributable to inadequate trophic support during the regenerative process. This experiment investigated the role of neuronally expressed c-Jun in facial nerve survival by quantifying the number of surviving motoneurons 30 days after transection. 20μm sections were taken at the level of the facial motor nucleus and 4/5 sections were stained with cresyl violet to expose surviving facial motoneurons. As seen in Figure 4-5, wild type c-Jun$^{F/F}$ animals showed 41% loss of facial motoneurons on the axotomized side – on the contralateral side, 2369±92 were present and on the injured side 1406±101 motoneurons survived. Contrastingly, c-Jun$^{\Delta S}$ mediated deletion reduced cell death by 21%. On the contralateral side, c-Jun$^{\Delta S}$ mutants showed 2699±123 surviving motoneurons and on the ipsilateral side, 2140±107. N=8 for c-Jun$^{F/F}$ littermates and N=8 for Jun$^{\Delta S}$ mutants; $p<0.05$ in unpaired Student's T-test. Many surviving motoneurons also exhibited an atrophic phenotype described in other studies targeting c-Jun deletion to CNS neuroepithelial precursor-derived cells, which include neurons (Raivich et al., 2004a). Atrophic neurons showed a roughly 20% reduction in diameter. These results indicate that c-Jun in the neuron – and not other neuroepithelium-derived cells – is responsible for the increased cell survival seen in the aforementioned study, as well as the current study and it further elucidates the role of neuronal c-Jun signalling in the cell fate decision to die; in Jun's absence, facial motor neurons are unable to die, which normally results from axonal transection, and instead become atrophic.

4.5 Neuronal c-Jun is Essential for Non-Neuronal Cell Activation

Facial nerve transection not only results in changes in the neuron itself, but it also affects neighbouring non-neuronal cells. Brain-resident Microglia and Astrocytes become activated and begin to secrete chemical signalling molecules (Pifarré et al., 2009; Butchi et al., 2009; Martin et al., 1994; Ranaivo et al., 2009). Within the first 24 hours, T-Cells invade from the vasculature (Kalla et al., 2001). While the cellular response peaks 4 days after injury, the inflammatory response does not reach a maximum until 14 days after injury (Makwana, Werner, et al., 2009; Bohatschek et al., 2004; Moller et al., 1996; Ha et al., 2008), so responses at both timepoints were measured. Normally, activated microglia upregulate αM (MAC-1) integrin expression and home to the site of injury. There, they surround dying neurons and can help participate in the injury response. As seen in Figure 4-6, 4 days after injury, wild type animals showed 12.6±1.0 αM units of optical luminosity value (OLV) on the contralateral side and 47.8±2.7 on the ipsilateral side (N=5). As seen in Figure 4-6 and Figure 4-7, by the 14th day after injury, wild type animals exhibited 13.7±2.0 on the contralateral side and 53.5±2.3 on the injured side (N=10). Jun$^{\Delta S}$ animals showed diminished microglial activation at both time-points post-injury. At 4 days, the contralateral average was 12.1±1.0 and on the injured side, only 25.7±2.3 showed αM immunoreactivity (N=5, $p<0.001$ in unpaired Student's T-test). At 14 days, mutants exhibited 12.5±3.3 baseline immunopositive cells and 21.2±3.0 on the ipsilateral side (N=5, $p<0.00001$ in unpaired Student's T-test).

They also failed to exhibit αX immunopositive nodule formation characteristic of the wild type injury response (Figure 4-6 and Figure 4-7). Upon exposure to neuronal debris following cell death, microglia adopt a phagocytic phenotype and upregulate expression of cell surface marker αXβ2 integrin and assist in the injury response by disposing of neuronal debris (Bohatschek et al., 2004, 2001; Kloss et al., 2001; Streit et al., 1988).

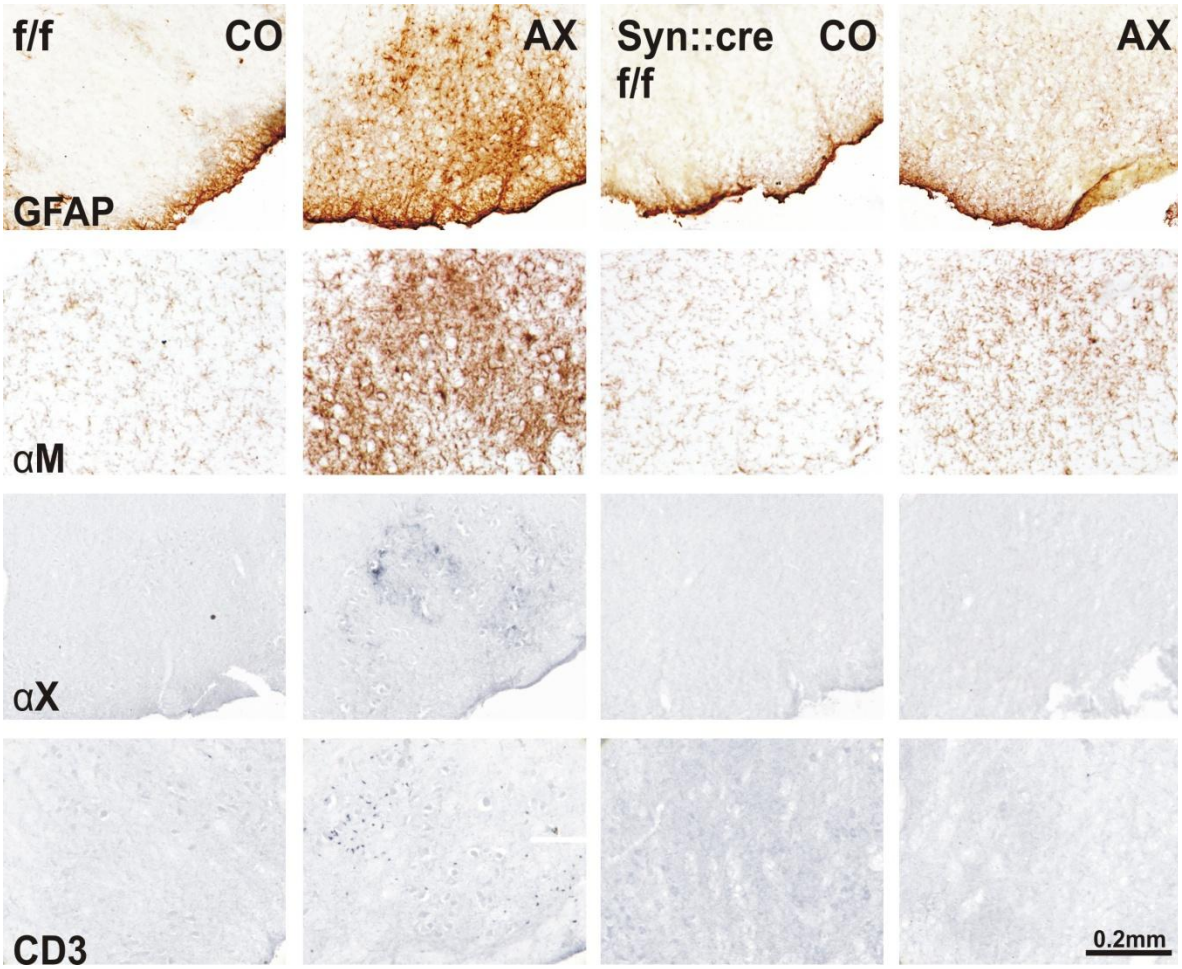

Figure 4-6 Neuronal c-Jun is Necessary for the Non-Neuronal Response to facial nerve axotomy.
Diminished non-neuronal cell response to facial nerve axotomy in c-Jun$^{\Delta S}$ mutants at day 14 (d14) after axotomy compared to c-Jun$^{F/F}$ controls. The facial motor nuclei from c-Jun$^{F/F}$ littermate controls are shown in the 1st & 2nd columns (A,B,E,F,I,J,M,N), those from the c-Jun$^{\Delta S}$ mutants are in the 3rd & 4th column (C,D,G,H,K,L,O,P). Second and 4th columns are axotomized, 1st & 3rd columns, contralateral sides, respectively. (A-D) Neuronal Jun deletion reduced axotomy-induced GFAP activation in the facial motor nucleus. (E-H) Axotomy-induced αM upregulation following injury is greatly ablated in c-Jun$^{\Delta S}$ facial motor nuclei. Phagocytic microglial infiltration (I-L), as well as CD3 immunopositive T-Cell migration (M-P) is absent in c-Jun$^{\Delta S}$ mutants following facial nerve axotomy. Scale bar 0.2mm.

Generally, levels of phagocytic microglia closely reflect levels of neuronal cell death (Raivich et al., 2004a; Makwana et al., 2009; Moller et al., 1996). While no αX immunopositive microglial nodules were present in uninjured facial motor nuclei (Figure 4-6 and Figure 4-7), wild type animals showed 23.7±4.1 phagocytic microglia on the injured side (N=10). In stark contrast, Jun deficient animals showed no phagocytic microglia in either the contralateral or the ipsilateral facial motor nucleus (N=7, $p<0.001$ in unpaired Student's T-test). Taken together, low-level microglial action reflects the much lower levels of cell death found in c-Jun$^{\Delta S}$ mice.

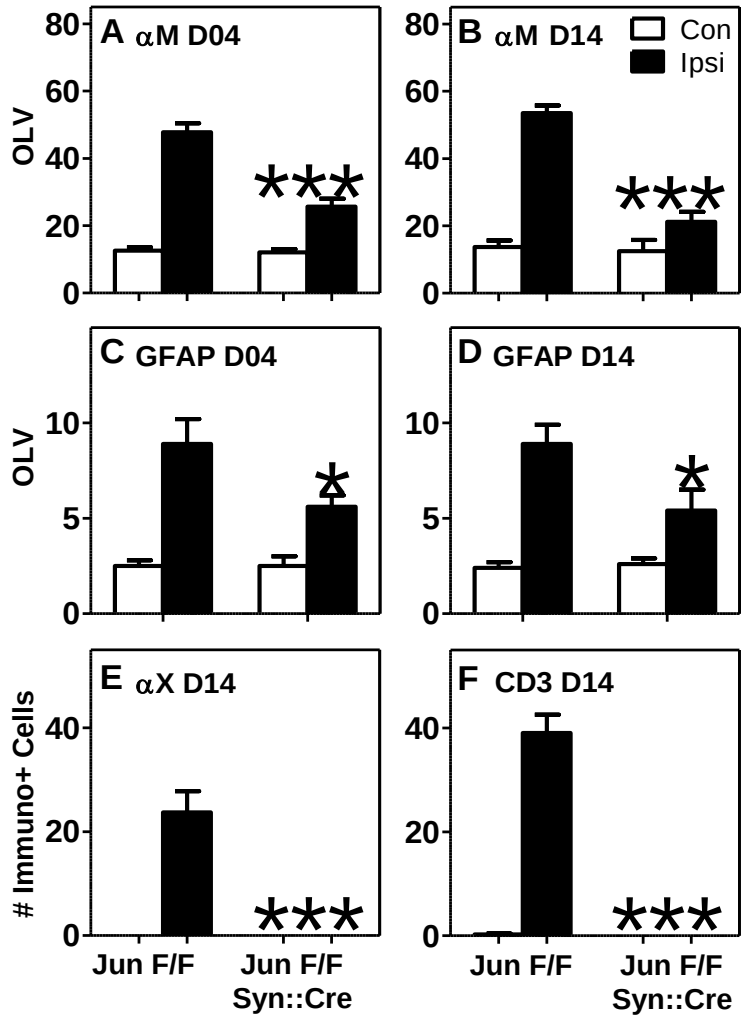

Figure 4-7 Neuronal c-Jun deletion produces severe deficits in non-neuronal cell activation after Facial Nerve Axotomy
(A, B) Quantification of microglial αM immunoreactivity at day 4 (d04, A) and day 14 (d14, B) in c-Jun$^{F/F}$ and c-Jun$^{\Delta S}$ animals after axotomy. (C-D) Quantification of GFAP immunoreactivity – an indicator of Activated Astroglia - at day 4 (d04, C) and day 14 (d14, D) in c-Jun$^{F/F}$ and c-Jun$^{\Delta S}$ animals after facial nerve transection. (E) Quantification of microglial αX immunoreactivity at day 14 in c-Jun$^{F/F}$ and c-Jun$^{\Delta S}$ animals. (F) Quantification of CD3+ T-Cell immunoreactivity at day 14 in c-Jun$^{F/F}$ and c-Jun$^{\Delta S}$ animals. Data was calculated using the MEAN-SD algorithm (Moller et al., 1996). White bars, contralateral; black bars, axotomized. *p< 0.05 and ***p< 0.001 in uSTT between c-Jun$^{F/F}$ and c-Jun$^{\Delta S}$.

Another non-neuronal cell that is an important player in the injury response is the astrocyte. Once astrocytes become activated, they upregulate expression of Glial Fibrilatory Acidic Protein (GFAP) and participate in the injury response, displaying immune cell signalling receptors such as Toll-like receptors, nucleotide-binding oligomerization domains, double-stranded RNA-dependent protein kinase, scavenger receptors, mannose receptors and components of the complement system (Farina et al., 2007) and secreting reactive intermediates like interleukin (IL)-1β, inducible nitric oxide (NO) synthase, the NO metabolite nitrite, superoxide (O2-) (Tichauer et al., 2007; Ranaivo et al., 2009). Wild type animals expressed 8.9±1.3 OLV units of GFAP luminosity (N=4) 4 days after facial nerve transection and 8.9±1.5 OLV units (N=10) 14 days after injury. This was greatly ablated, but not absent, in c-Jun$^{\Delta S}$ KOs, which expressed roughly half as much immunoreactivity at

both timepoints (5.6±0.6 at d4 [N=5] and 5.4±1.1 at d14 [N=5], $p<0.05$ in unpaired Student's T-test, see Figure 4-6 and Figure 4-7).

T-cell recruitment was abolished by neural deletion of c-Jun. c-Jun$^{\Delta S}$ animals had no CD3+ lymphocyte recruitment to the injured facial motor nucleus (N=7) whereas their wild type counterparts averaged 39.1±3.52 (N=10) CD3+ T-Cells per nucleus (Figure 4-6 and Figure 4-7).

Taken together, this data shows that the non-neuronal cell response relies heavily on the presence of neuronal c-Jun; this response is virtually non-existent without it. Microglia and Astrocytes fail to activate, CD3+ T-Cells are not recruited to the site of injury and microglia do not differentiate into a phagocytic phenotype. Lack of phagocyte activation could also be attributed to decreased levels of cell death. To determine whether lack of cell death andnon-neuronal response was due to inadequate neural cues or to Jun actions further downstream, the neuronal response to injury in Jun$^{\Delta N}$ mutants was explored.

4.6 Neuronal c-Jun is Necessary for Neuronal Cellular Response to Injury

Nerve injury not only elicits changes in the local microenvironment but it also, perhaps more importantly, induces changes in the neuron itself that promote growth and sprouting. Immediate early transcription factors like c-Jun and ATF3 are upregulated within hours. Jun heterodimerizes with ATF3 to produce a type of AP-1 transcription complex which has been implicated with downstream actions including growth, survival and sprouting (Pearson et al., 2003a; Nakagomi et al., 2003; Campbell et al., 2005; Kiryu-Seo et al., 2008). CGRP and Galanin are expressed in the neuronal cell body and are transported anterogradely into axonal growth cones (Makwana et al., 2009). Adhesion molecules like CD44 hyaluronic acid receptor and α7β1 integrin are also translated and used for

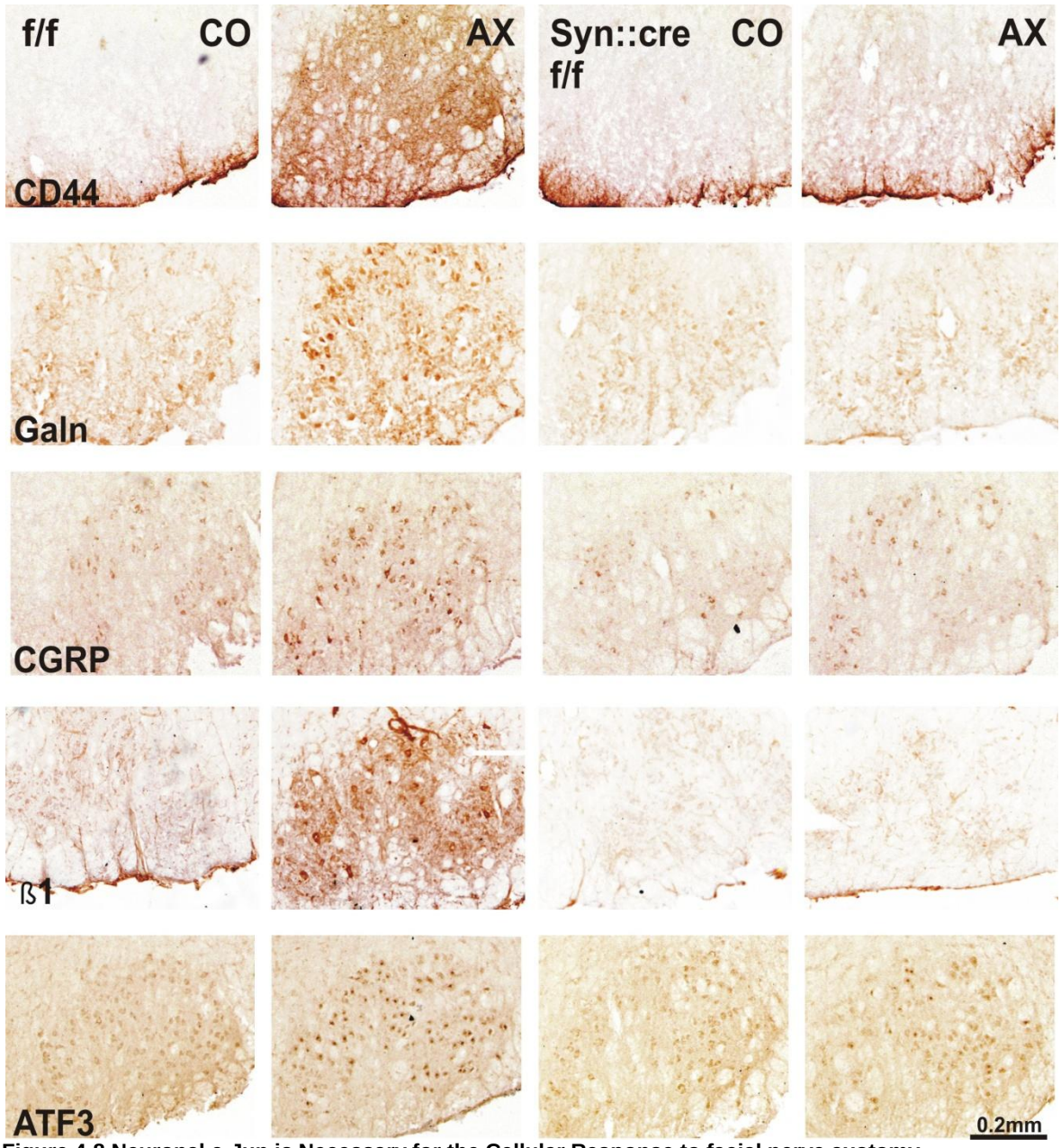

Figure 4-8 Neuronal c-Jun is Necessary for the Cellular Response to facial nerve axotomy.
Abolished neuronal cell response to facial nerve axotomy in c-Jun$^{\Delta S}$ mutants at day 14 (d14) after axotomy compared to c-Jun$^{F/F}$ controls. The facial motor nuclei from c-Jun$^{F/F}$ littermate controls are shown in the 1st & 2nd columns (A,B,E,F)(Moller et al., 1996). White bars,I,J,M,N,Q,R), those from the c-Jun$^{\Delta S}$ mutants are in the 3rd & 4th column (C,D,G,H,K,L,O,P,S,T). Second and 4th columns are axotomized, 1st & 3rd columns, contralateral sides, respectively. (A-D) Neuronal Jun deletion reduced axotomy-induced CD44 Hyaluronic acid expression in injured facial motor neurons. (E-H) Axotomy-induced galanin upregulation, as well as (I-L) CGRP and (M-P) β1 integrin expression following injury is absent in c-Jun$^{\Delta S}$ facial motor nuclei. (Q-T) ATF3 immunoreactivity is also is absent in c-Jun$^{\Delta S}$ mutants following facial nerve axotomy. Scale bar 0.2mm.

guidance and cell-cell communication (Lin and Chan, 2003; D. Wynick and McMahon, 2001). Previous studies link c-Jun deletion to absence of CD44 expression in several neuronal cell types following injury (Raivich et al., 2004a). All of these regeneration associated molecules showed strong upregulation in wild type animals after injury.

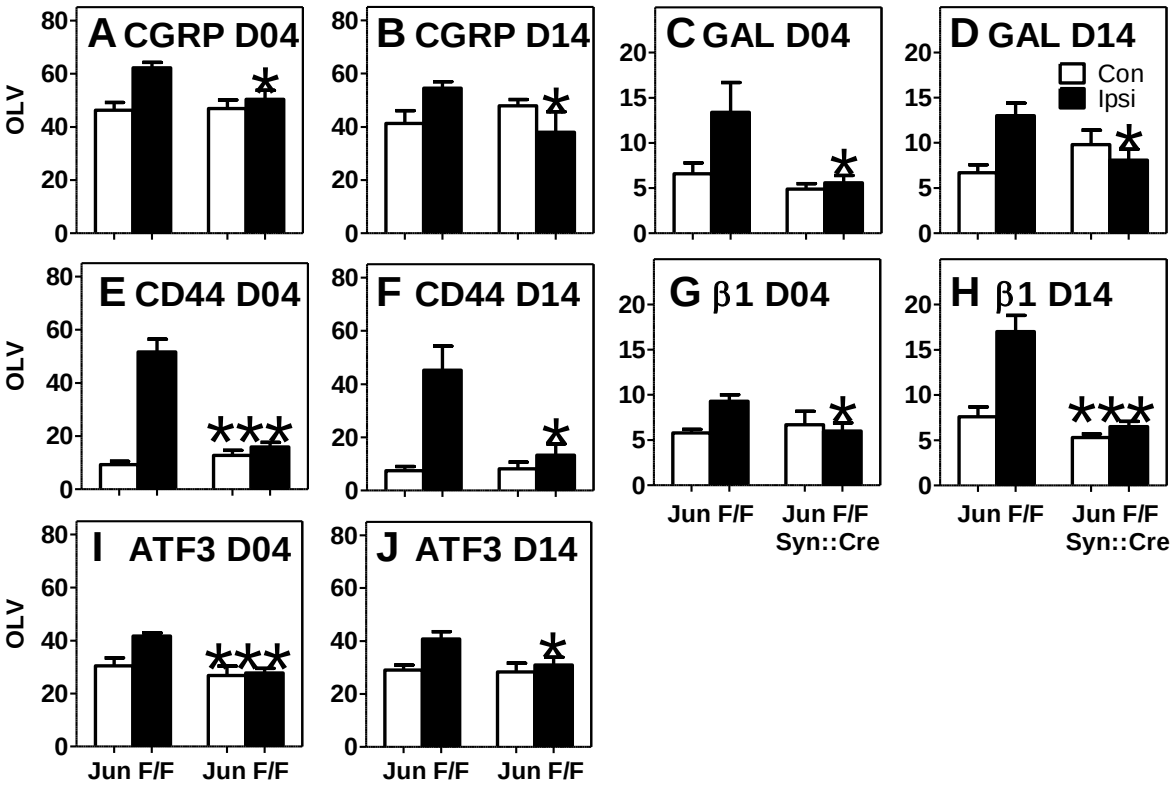

Figure 4-9: Abolished Neuronal Cell Response Following Facial Nerve Transection in c-Jun$^{\Delta S}$ mutants. (A-B) Quantification of CGRP immunoreactivity at day 4 (d04, A) and day 14 (d14, B) after axotomy. (C-D) Quantification of Galanin immunoreactivity at day 4 (d04, C) and day 14 (d14, D) after axotomy. (E-F) Quantification of CD44 Hyaluronic acid immunoreactivity at day 4 (d04, E) and day 14 (d14, F) after axotomy. (G-H) Quantification of β1 integrin immunoreactivity at day 4 (d04, G) and day 14 (d14, H) after axotomy. (I-J) Quantification of ATF3 immunoreactivity at day 4 (d04, I) and day 14 (d14, J) after axotomy using the MEAN-SD algorithm (Moller et al., 1996). White bars, contralateral side; black bars, axotomized side. *p< 0.05 and ***p< 0.001 in uSTT between c-Jun$^{F/F}$ and c-Jun$^{\Delta S}$ mice. N=5 for 4D c-Jun$^{F/F}$ and c-Jun$^{\Delta S}$. N=10 for 14D c-Jun$^{F/F}$ and N=6 for 14D c-Jun$^{\Delta S}$.

Contrastingly, they showed diminished or abolished action following facial nerve transection in activation in c-Jun$^{\Delta S}$ animals (Table 4 of the Appendix, Figure 4-8 and Figure 4-9). Galanin, CGRP, CD44 and α7β1 integrin fail to be upregulated either 4 or 14 days following facial nerve transection (Figure 4-8 and Figure 4-9) and ATF3 shows failed nuclear early upregulation 4 but not 14 days post-facial nerve axotomy (Figure 4-8 and Figure 4-9). This illustrates the importance of c-Jun for the neuronal injury response and suggests an alternate but slower mechanism of ATF3 upregulation following injury. Without upstream signalling from c-Jun, neurons are unable to initiate the cellular response that leads to non-neuronal cell recruitment and eventual death of damaged neurons.

JUN$^{\Delta S}$ DISCUSSION: NEURONAL C-JUN ORCHESTRATES THE CELLULAR RESPONSE TO INJURY AND CELL DEATH

Upon facial nerve transection, many growth and survival-associated transcription factors are immediately upregulated. One of the most important and well-characterized of these is the AP1 transcription complex, consisting of either c-Jun homodimers or heterodimers with other Jun, or ATF/CREB family members (Angel et al., 1992). Jun can also complex with c-Fos family members, although Fos is not expressed in regenerating facial motor neurons. Jun's AP1 activity has been linked to increased neuronal sprouting (Pearson et al., 2003a; Nakagomi et al., 2003; Campbell et al., 2005; Kiryu-Seo et al., 2008; Seijffers et al., 2007, 2006), cellular response to stress (Chaum et al., 2009; Chen et al., 2009; Coffey et al., 2000; Donovan et al., 2002; Johnson and Nakamura, 2007) and survival (Raivich et al., 2004a; Haeusgen et al., 2009; Wang et al., 2009; Behrens et al., 1999; Brecht et al., 2005a; Cuadrado et al., 2004) both *in vivo* and *in vitro*. This study investigated the role of neuronally expressed c-Jun in peripheral regeneration. It revealed that c-Jun is an essential regulator of the cellular response to axonal injury and also resulting neuronal survival. Neuronal c-Jun deletion affects lymphocyte recruitment and phagocyte activation, as well as survival and successful reinnervation following injury.

4.7 Increased Facial Motoneuron Number in c-Jun Deficient Mice

Despite normal brain morphology, as indicated by Haematoxylin & Eosin staining of the hippocampus and thalamus, as well as NeuN staining of the same areas, brain-deficient *c-jun* mice showed a 14% increase in baseline facial motoneuron number. This is similar to the findings of Raivich et al., who used Nestin-mediated Jun excision to show increased numbers of facial motor neurons in neuroepithelial stem cell *c-jun*-deficient animals, although they found no differences in learning, fear conditioning, motor performance, number of dorsal root ganglia (DRG) neurons or number of hypoglossal neurons (Raivich

et al., 2004a). This increase in baseline facial motor neuron number could be attributable to a lack of cell death signalling during developmental pruning, as previous studies have shown decreased neuronal cell death both *in vitro* and *in vivo* following *c-jun* deletion or inactivation (Raivich et al., 2004a; Palmada et al., 2002). In light of this research, current studies are underway to explore the role of c-Jun deletion in relation to disease models that show high levels of neuronal cell death in the absence of reinnervation, such as amyotrophic lateral sclerosis (ALS).

4.8 Cell-Type Specificity of c-Jun$^{\Delta S}$

Previous studies from Raivich et al. using Nestin::Cre deleted c-Jun targeted the Jun deletion to neuroepithelial derived cells (Raivich et al., 2004a). These include Neurons, Astrocytes, Oligodendrocytes and Schwann Cells – as well as some other cell types (Minovi et al., 2010; Kohno et al., 2006; Zou et al., 2006; Vukojevic et al., 2009; Ueno et al., 2005; Toti et al., 2005; Saito et al., 2009; Rovira et al., 2009). However, it was unclear as to whether the cellular differences observed in that study were due to the actions of neuronal Jun, or Jun deletion in the other cells with neuroepithelial origin. Here, c-Jun deletion was specifically targeted to neurons to explore the role of c-Jun in peripheral regeneration. This experiment confirmed the previous hypothesis that neuronal c-Jun was indeed orchestrating the impaired regenerative response seen in c-Jun$^{\Delta N}$ mice.

Normally, after injury, CD3+ T-Cells are recruited from the local microenvironment (Galiano et al., 2001; Ha et al., 2006). T-Cell infiltration to the site of injury was completely absent in c-Jun$^{\Delta S}$ mice, illustrating its essential role in the chemoattractant signalling cascades leading to successful T-lymphocyte recruitment. Given the fact that neuronal survival was also enhanced in c-Jun$^{\Delta N}$ mutants, lack of effector migration could also be attributed to decreased levels of cell death. Vice versa, it could be argued that lack of T-

Cell recruitment was contributing to c-Jun deficient neurons' inability to die. However, previous investigations with Non-Obese Diabetic (NOD) Severe Combined Immunodeficiency (SCID) mice show that T-Cell deficient mice – which therefore do not show T-Cell recruitment following facial nerve injury – show enhanced motoneuron cell death following peripheral injury (Serpe et al., 1999, 2000, 2002; Byram et al., 2004; Deboy et al., 2006; Xin et al., 2008). This indicates that increased cell survival or decreased cellular response – as a product of Jun ablation – caused impaired lymphocyte trafficking to the facial motor nucleus and not the other way around.

Not only was CD3+ lymphocyte recruitment ablated in c-Jun mutant mice, but signalling by activated astrocytes was also affected by neuronal c-Jun deletion. Normally, astrocytes home to the site of injury, secrete reactive oxygen intermediates and other molecules used in chemoattraction and participate in the injury response as antigen presenting cells (Farina et al., 2007). The absence neuronal cues led to impaired astroglial recruitment and activation, as well as decreased response to peripheral nerve transection. Phagocytic microglial transformation was also affected, as was microglial activation following injury. Synapsin 1 has previously been characterized as a neuron-specific promoter (Usukura et al., 1987; Zhu et al., 2001; Kügler et al., 2003; Sims et al., 2008) and does not target gene expression to monocytic cell types such as microglia. Therefore, defects in microglial response are solely attributable to defects in neuronal signalling conferred by neuron-specific *c-jun* deletion. Microglial activation, as indicated by αM integrin immunoreactivity, was impaired within 4 days following injury and remained so throughout the injury response. This indicates that microglial activation depends closely on neuronal signals put forth by c-Jun and that defects in the microglial response result from impaired neuronal cues. Additionally, there was a distinct absence of injury-associated αX integrin immunopositive monocytic nodules in the FMN of $Jun^{\Delta S}$ animals. This is probably due to the lack of cellular debris present in mutants, as a result of decreased cell death, which

abolishes the need for phagocytic cells; thus the transition of Microglia into a phagocytic phenotype does not take place due to insufficient environmental cues.

4.9 Impaired Target Reinnervation in Jun Deficient mice

To determine the role of neuronally expressed c-Jun in successful target reinnervation, three methods were utilized; functional recovery was scored for thirty days following facial nerve transection using the whisker hair assessment approach and anatomical recovery was gauged thirty days after nerve cut via retrograde labelling. In addition, physical regeneration of the facial motor nerve was gauged via anatomical tracking of CGRP and galanin immunopositive axonal sprouts in the facial nerve 4 days following crush injury. Whisker function showed an almost 3 fold deficit in recovery of motor function of c-Jun$^{\Delta S}$ mutants compared to wild type controls, which was consistent throughout the trial period. Other studies using a nestin mediated *jun* deletion showed that animals with more general neural deletion of *jun* do not recover function, even after 15 weeks, in a nonlinear manner. Likewise, anatomical assessment revealed an almost 8 fold decrease in reinnervation after 30 days in c-Jun$^{\Delta S}$ mice compared to control littermates. Previous data in c-Jun$^{\Delta N}$ mice indicates that while functional recovery returned to normal after 15 weeks in neuronally jun-deficient animals, levels of anatomical recovery remained consistently lower and the predictive value of the whisker hair test became less reliable as more neurons reconnected to the original target (Raivich et al., 2004a)

Crushed facial nerves normally exhibit a robust growth response following injury, with the extension of CGRP and galanin immunoreactive growth cones into local bands of Büngner to reinnervate neuromuscular targets, (Makwana et al., 2009; Williams et al., 1971b, 1971a; Ghabriel et al., 1979b, 1979a). Animals that were neuronally deficient in c-Jun showed a 60% reduction in the length of axons extruded distally from the injured portion of

the neuron. This difference was consistent for both CGRP and galanin immunoreactive sprouts, which indicates that neuronal c-Jun has a regulatory role in neurite elongation following peripheral nerve injury.

4.10 C-Jun is Essential for both Regeneration and Cell Death

These data illustrate the previously described dual role of c-Jun in both neuronal regeneration and apoptosis (Raivich, 2008; Raivich et al., 2006; Herdegen et al., 1997; Shaulian and Karin, 2001; Mechta-Grigoriou et al., 2001). Animals lacking c-Jun in neurons showed decreased anatomical and functional recovery with increased levels of cell survival. Normally, neurons that do not reach the neuromuscular junction die due to insufficient trophic support, however in the absence of c-Jun they were unable to die and simply atrophied.

4.11 The Cellular Response to Injury in c-Jun Null Mice– Molecular Mechanisms

Lack of reinnervation can also be attributed to the failed cellular response exhibited by c-Jun$^{\Delta S}$ neurons. Without adequate sprouting and elongation signals, as well as participation from local non-neuronal effector cells, mutant neurons were not able to mount a sufficient cellular injury response. Previous studies highlight upregulation of and describe the role of pro-regenerative factors CD44 (Jones et al., 2000), α7β1 integrin (Werner et al., 2000), ATF3 (Pearson et al., 2003a; Fan et al., 2002), CGRP and Galanin (Makwana, Serchov, et al., 2009) in the injury response. In fact, CD44, α7 and Galanin have AP1 promoters (Lee et al., 1993; Anouar et al., 1999; Jones et al., 2000; Nishida et al., 1997) and ATF3 has been described as a downstream target of c-Jun (Mei et al., 2008a). As a result of growth-enhancing adhesion molecule and neuropeptide expression from the neuronal cell body following injury, peripheral facial motor neurons are typically able to mount a successful

and robust regenerative response. $Jun^{\Delta S}$ animals showed no upregulation of any of these pro-regenerative factors following facial nerve transection. As a result, regeneration in these mutants was poor. Taken together, these data indicate that c-Jun plays a critical role in both neuronal regeneration and cellular commitment to die; future therapeutic strategies could exploit this fact to prolong neuronal survival or enhance regeneration in disease models.

CHAPTER 5: P0::JUN RESULTS: SCHWANN CELL – EXPRESSED C-JUN IS REQUIRED FOR MOTOR NEURON SURVIVAL AND SUCCESSFUL POST-INJURY PERIPHERAL REINNERVATION

5.1 Generation of Mice Lacking c-jun in Schwann Cells

To define the role of *c-jun* in the peripheral regenerative response, animals were created with a Schwann Cell specific deletion of *c-jun.* To do this, mice carrying a floxed *c-jun* allele (*jun*$^{f/f}$) were crossed with animals expressing cre recombinase under the control of the P0 promoter, which causes Schwann cell specific recombination (P0::Cre, Raivich et al. 2004; Lee et al. 1997; Rhona Mirsky et al. 2008; Behrens et al. 2002 and Tronche et al. 1999) to make homozygous *P0 x jun* $^{f/f}$ and heterozygous *P0 x jun* $^{f/WT}$ mutants. Previous studies demonstrate the efficiency and Schwann-cell specificity of the P0::Cre transgenic line (Yamauchi et al., 1999). Furthermore, it has been shown that chromosomal location of recombination substrates influences recombination frequencies in Cre/LoxP systems of gene expression, and therefore differences in recombination efficiency between different floxed genes have been observed (Vooijs et al., 2001). Thus, recombination was investigated in both homozygous *P0 x jun* $^{f/f}$ and heterozygous *P0 x jun* $^{f/WT}$ littermates to exclude the possibility of compensatory mechanisms resulting from homozygous *jun*$^{f/f}$ inactivation affecting the final result.

Mice lacking *c-jun* in Schwann cells (*P0 x jun* $^{f/f}$) were born with Mendelian frequency and were viable and fertile. Neuronal cell counts of the facial motor nucleus showed no difference in baseline numbers of facial motor neurons between *P0 x jun* $^{f/f}$ animals and their wild-type littermates.

5.2 Glial c-jun is Required in the Periphery for Effective Axonal Regeneration and Reinnervation

After nerve injury, neurons and peripheral glia upregulate several key factors involved in sprouting, elongation and growth; these factors act to establish and maintain a growth-permissive environment that supports the anatomical and functional reinnervation commonly seen in response to peripheral nerve injury. First, axons must successfully cross the site of injury toward the degrading peripheral nerve stump, and then they must form physical and functional connections at the neuromuscular junction. Schwann cells play a pivotal role in this peripheral response by engulfing axonal debris, upregulating growth associated survival factors like RegIIIβ, LIF and CNTF and also separating from the Myelin sheath to create *Bands of Büngner* which provide physical structures along which axons are guided to their appropriate targets (Williams et al., 1971b, 1971a; Ghabriel et al., 1979a, 1979b; Tebar, Géranton, et al., 2008). Therefore, it is important to characterize the role, if any, that Schwann Cell – expressed c-Jun plays in this injury response.

5.2.1 Functional Reinnervation of Peripheral Targets

First, it was determined whether transected facial motor axons were able to regenerate through a Schwann Cell environment lacking c-Jun to form functional connections with target muscle. A reliable measure of this functional reinnervation – in particular with regard to that of the facial motor nerve – is the reestablishment of function of the whisker hair post-axotomy. Extent of whisker function was scored by five observers, on a scale of 0 (no movement) to 3 (strong, normal movement). As seen in Figure 5-1, twenty-eight days post-injury, both control and mutant animals showed strong, normal movement on the uninjured side (3.0). On the injured side, control animals showed an average motor score of 2.2 ± 1.0 (n = 9). Likewise, *P0 x jun* $^{f/WT}$ heterozygotes showed 2.3 ± 1.6 units of recovery (n=2).

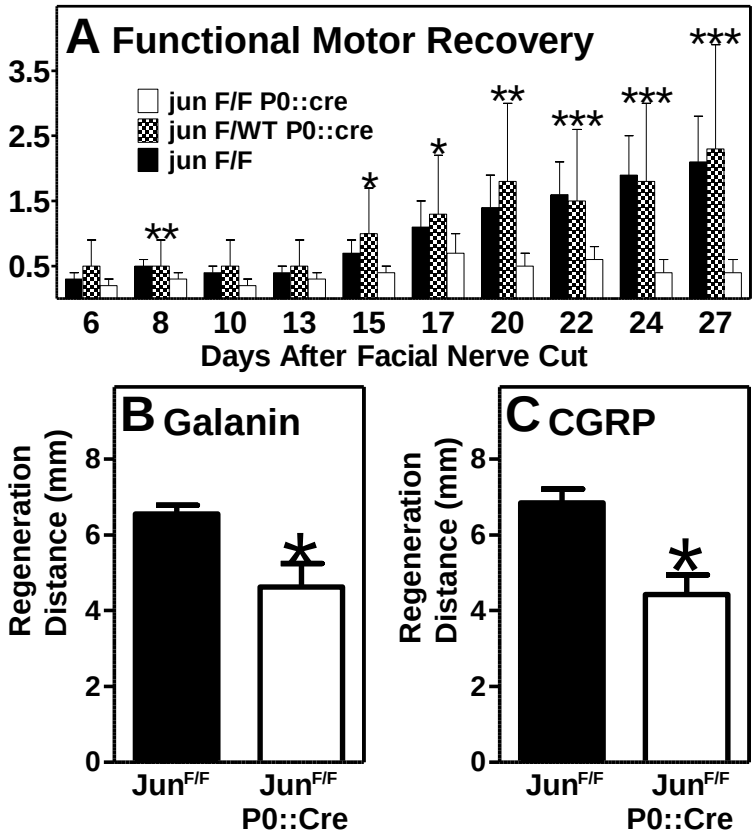

Figure 5-1: Charting the Post-Axotomy Regenerative Response – c-Jun in Schwann cells is essential for Functional Reinnervation. (A) *jun$^{f/f}$ P0::cre* animals show impaired motor recovery following facial nerve transection. Posttraumatic whisker hair motor performance was measured 28 days after facial nerve axotomy, on a scale of 0 (no movement) to 3 (normal strong movement similar to that of contralateral side); N = 5 for *jun$^{f/f}$*, N=2 for *jun$^{f/WT}$ P0::cre* and N = 3 for *jun$^{f/f}$ P0::cre* animals. Black Bars, WT; Checked Bars, Het; White Bars, KO. (B) Shorter average regeneration distance of CGRP and galanin immunopositive motor axon populations 4 days after facial nerve crush in *jun$^{f/f}$ P0::cre* mutants (Error bars indicate mean +/-standard error of mean (SEM), n=4 animals per group). *p < 0.05, **p<0.01 and ***p<0.001 between *jun$^{f/f}$* and *jun$^{f/f}$ P0::cre* in uSTT. Data collected in collaboration with D. Cuthill and M. Makwana.

Contrastingly, *P0 x jun $^{f/f}$* mice showed significantly less functional recovery on the injured side of the whisker pad (0.3 ± 0.2; n = 6, p < 0.01 between *jun$^{f/f}$* and *jun$^{f/f}$ P0::cre* in uSTT). Since n=2 for heterozygotes, for the purpose of both functional and anatomical recovery, student's T-Test between wild type and mutant was used instead of 3-way ANOVA.

To determine whether defective whisker movement exhibited by *P0 x jun $^{f/f}$* mice was due to differences in muscle reinnervation, the fluorescent tracer Fluorogold was introduced under the whisker pad as described in Materials and Methods. Fluorogold implantation on the uninjured side served as an intra-animal control. Similar numbers of retrogradely labelled neurons were visible on contralateral sides of control, heterozygote and mutant animals, but on the axotomized side, the number of retrogradely labelled neurons decreased proportionally with number of deleted copies of *c-jun.* Control animals showed 164±9 labelled motoneurons on the contralateral side and 110±10 on the axotomized side (n=9); *P0 x jun$^{f/WT}$* heterozygotes exhibited 193±22 FG+ motor neurons on the uninjured and 54±3 on the injured sides

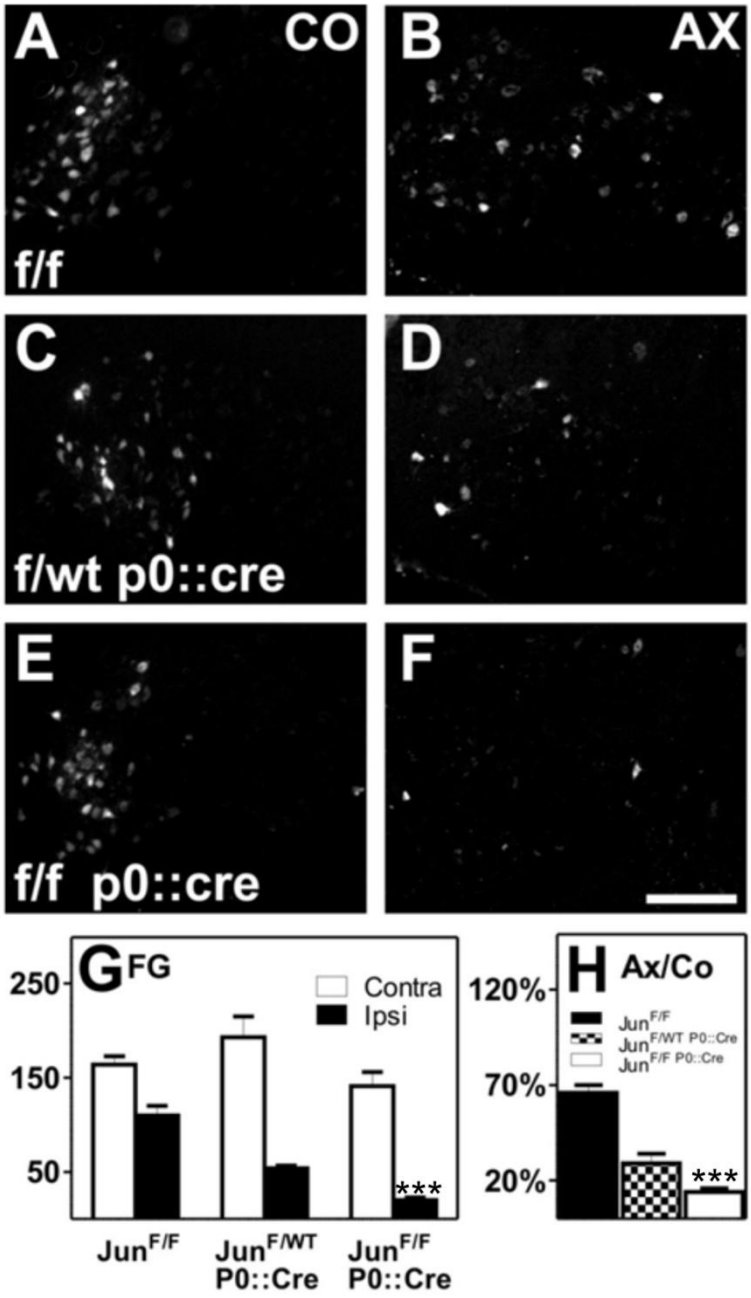

Figure 5-2: Deletion of Schwann cell c-jun using p0::cre recombinase interferes with the reinnervation of the peripheral target (Whisker Pad)

FMN Fluorogold (FG) fluorescence in jun$^{f/f}$ and jun$^{f/f}$ P0::cre mice on control (co) and operated side (ax) 28 days post-facial nerve cut with 72 hours for retrograde FG transport. (A-B) Animals with normal c-jun, (C-D) heterozygote excision of Schwann Cell (SC) c-jun and (E-F) homozygote deletion. Scale bar, 250 µm. (G) Normal numbers of FG+ motoneurons were present in the contralateral side of WT, Het and KO animals, however after injury FG+ motor neuron number reduces by about 50% with each deleted copy of *c-jun.*(N = 5 for *jun$^{f/f}$* N=2 for *jun$^{f/wt}$ P0::cre* and N = 3 for *jun$^{f/f}$ P0::cre* mice). Contralateral side, white bars; Ipsilateral side, black bars. (H) Ax/Co ratio of FG+ neurons is shown;again, note the graded decrease in FG+ motoneurons with decreasing copy numbers of *c-jun; jun$^{f/f}$* black bars; *jun$^{f/wt}$* checked bars; *P0::cre jun$^{f/f}$ P0::cre* mice, white bars. ***p<0.001 between in uSTT. Figure produced in collaboration with M. Makwana.

(n=2); *P0 x jun $^{f/f}$* mutants displayed 141±15 FG immunoreactive neurons on the control and 20±3 on the axotomized sides (n=6, Figure 5-2, * p < 0.001 between Junf/f wild type and Junf/f x P0::Cre mutants in uSTT). Overall, the ratio of labelled neurons on axotomized versus contralateral sides (ax/co ratio or specific reinnervation) in control animals was 66% ± 4% (n=9). In heterozygotes, specific reinnervation was 29%±5% (n=2) and in P0 x jun $^{f/f}$ mutants, it was 14%±2%(n=6), more than 4-fold lower (*p < 0.001 between Junf/f controls and Junf/f x P0::Cre mutants in uSTT), which suggests that failure to recover whisker movement in P0 x jun $^{f/f}$ mice is due to insufficient Schwann

Cell jun-associated signalling cues.

5.2.2 4 Day Regeneration

Within 1-2 days after injury, lesioned neurons extrude growth cones from their proximal neuronal tips. These sprouts show galanin and CGRP immunoreactivity and extend in a proximal – to – distal direction (Galiano et al., 2001; Werner et al., 2000; Makwana, Werner, et al., 2009). As seen in Figure 5-1, *c-jun*-deficiency in Schwann cells interfered with this axonal extension. Control, $jun^{f/f}$ animals showed prominent sprouting of galanin-immunoreactive growth cones averaging 6.5±0.2mm following injury and mutants showed less - 4.6±0.6mm (n=4). The same is true for CGRP immunoreactive axons; control animals' axons grew 6.8±0.4 following injury and mutants averaged 4.4±0.5mm (n=4). Neurons that lacked trophic support from *c-jun* expressing glia showed an average reduction in length of 35 percent (*$p < 0.05$ in unpaired Student's T-test) in CGRP immunoreactive growth cones and 30 percent (*$p < 0.05$ in unpaired Student's T-test) in galanin reactive growth cones compared to wild type counterparts.

5.2.2.1 Absence of Glial c-jun Increases Axotomy-Induced Cell Death

Peripheral nerves display a robust regenerative response post-injury, whereas those of the CNS do not. This is, in part, may be due to the existence or absence of appropriate trophic support – since some CNS neurons will regenerate through a peripheral nerve graft but not through native CNS glia (Cajal, 1928). Despite this, twenty to thirty percent of facial motor neurons normally fail to survive following nerve transection (Ferri et al., 1998a; Hottinger et al., 2000). To determine whether glial c-Jun plays a role in axotomy-induced cell death, quantitative measurements were made of all motoneurons in the facial motor nucleus of the brainstem using cresyl violet (Figure 5-3).

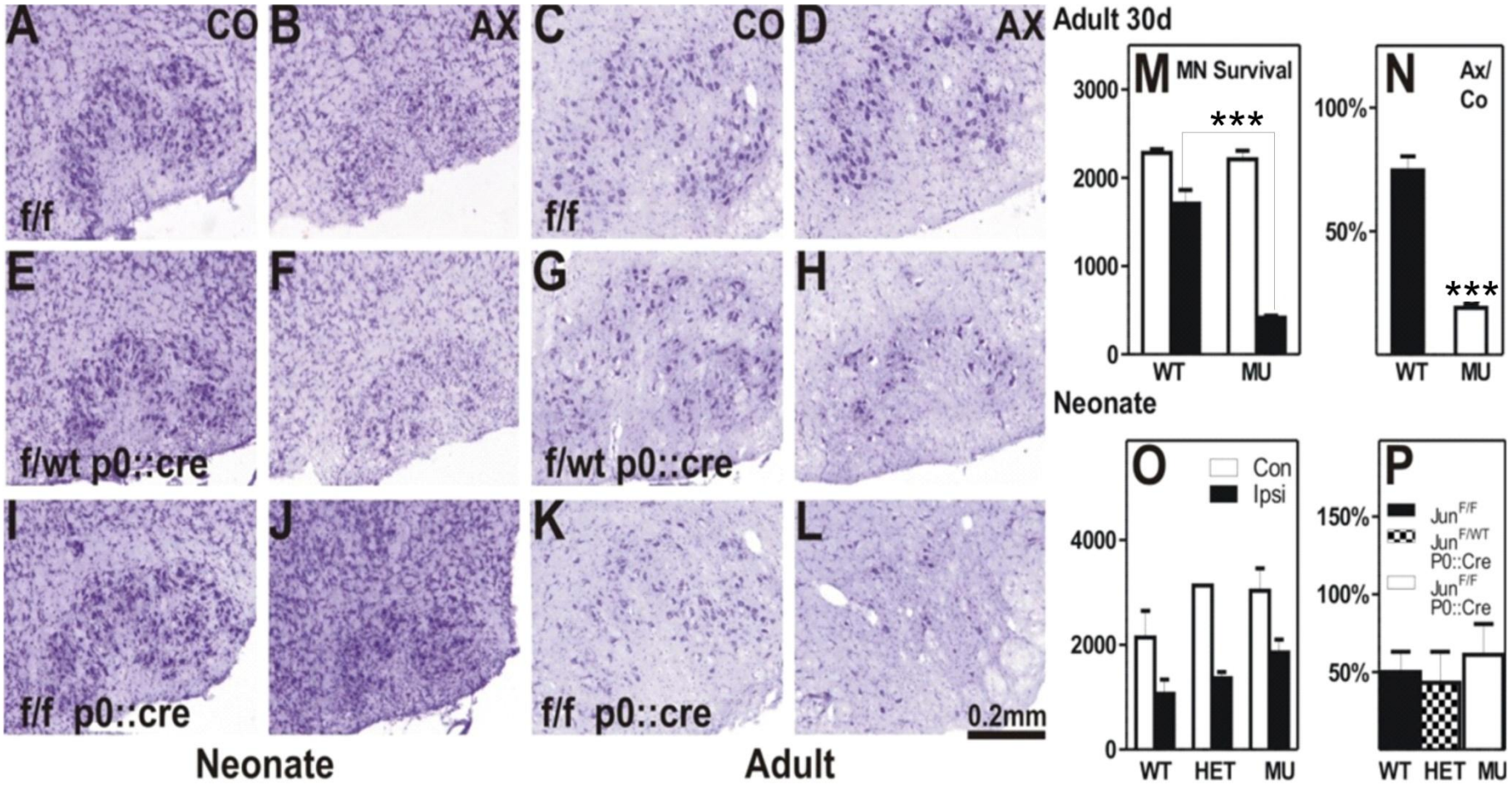

Figure 5-3: Decreased Cell Survival after Axotomy in junf/f P0::cre Motor neurons

(A) Quantification of motoneuron number in facial nucleus of adult *c-jun*$^{f/f}$ and *jun*$^{f/f}$ *P0::cre* mice on the contralateral (white bars) and ipsilateral side (black bars), 30 days after facial nerve transection. *p < 0.01% in uSTT between *jun*$^{f/f}$ *P0::cre* and *c-jun*$^{f/f}$ groups (A and B), N = 5 for *c-jun*$^{f/f}$ and N = 3 for *jun*$^{f/f}$ *P0::cre* animals in (A) and (B). (B) Quantification of specific cell death Ax/Co in the facial motor nucleus of adult *c-jun*$^{f/f}$ (black bars) and *jun*$^{f/f}$ *P0::cre* (white bars) mice, 30 days after facial nerve axotomy. (C) Quantification of motoneuron number in facial nucleus of neonate *c-jun*$^{f/f}$ and *jun*$^{f/f}$ *P0::cre* mice on the contralateral (white bars) and ipsilateral side (black bars), 30 days after facial nerve transection. **p < 0.01% in uSTT between jun*$^{f/f}$ *P0::cre and c-jun*$^{f/f}$ *groups (A and B), N = 5 for c-jun*$^{f/f}$ *and N = 3 for jun*$^{f/f}$ *P0::cre animals in (A) and (B).* (D) Quantification of specific cell death Ax/Co in the facial motor nucleus of neonate *c-jun*$^{f/f}$ (black bars) and *jun*$^{f/f}$ *P0::cre* (white bars) mice, 30 days after facial nerve axotomy.

Thirty days post- axotomy, 75% ± 6% of neurons were present in the injured facial motor nucleus of control mice (n=9), whereas only 19%± 2% were present in the facial motor nucleus of P0 x jun $^{f/f}$ animals (n=6, $p < 0.05$ in unpaired Student's T-test). Total cell counts showed increased cell death on the axotomized side ($p < 0.001$ in unpaired Student's T-test) in P0 x jun $^{f/f}$ animals, compared to wild type littermates. Control animals had 2280±43 labelled neurons in the control nucleus and 1707±154 on the axotomized side (n=9), whereas their transgenic counterparts possessed 2207 ±100 cresyl violet-stained neurons on the control side and 416 ± 22 on the operated side (n = 6). However, this difference in survival following transection was dependent on stage of development; facially transected neonate (P1) animals failed to show the same distribution. In fact, although there was vast neuronal cell death associated with neonatal transection, there was no difference between wild type, heterozygotes and mutants in facial motor neuron survival 3 days following facial nerve cut. Control animals showed 50±13% motor neuron survival (N=7), heterozygotes displayed 43±20% (N=2) and mutants had 61±20% (N=3). On the contralateral side, Jun $^{f/f}$ wild types had 1069±258 surviving motor neurons, compared to the ipsilateral side, which had 533±137. Jun$^{f/wt}$ xP0::Cre heterozygotes averaged 1567±0 on the contralateral side and 682±60 following injury. Similar levels of survival were seen in Jun$^{f/f}$ xP0::Cre mutants, who averaged 1518±926 facial motor neurons on the uninjured and 926±124 on the injured side respectively. This data suggests that glial c-jun expression creates trophic support from Schwann Cells which is essential for successful motoneuron survival in adult animals, but not during development.

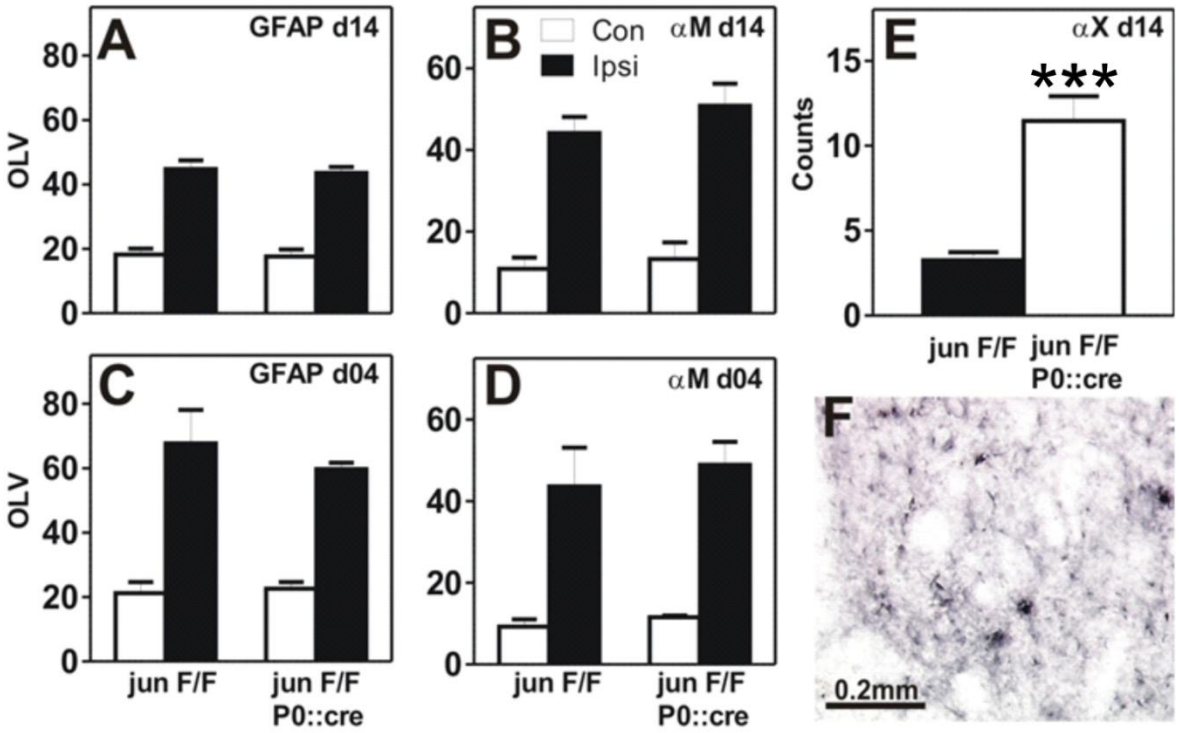

Figure 5-4: Increased Phagocytic Microglial Activation after facial nerve cut in junf/f P0::cre mice. (A and C) Quantification of astrocytic GFAP immunoreactivity at day 14 (d14) and (C) day 4 (d04) after axotomy. (B and D) Quantification of activated microglial marker αM immunoreactivity at day 14 (d14) (B) and (D) day 4 (d04) after axotomy. A-D were quantified in OLV of luminosity. White bars, contralateral side; black bars, ipsilateral side. p >0.05 in uSTT between junf/f P0::cre mice and *c-jun*$^{f/f}$ groups. N = 5 for *c-jun*$^{f/f}$ and N = 5 for *jun*$^{f/f}$ *P0::cre* in (A) and (B); N = 3 for *jun*$^{f/f}$ and N = 3 for *jun*$^{f/f}$ *P0::cre* animals in (C); N = 2 for *jun*$^{f/f}$ and N = 3 for *jun*$^{f/f}$ *P0::cre* animals in (D). (E) Quantification of phagocytic microglial marker αX integrin immunoreactivity at day 14 (d14) after axotomy in *jun*$^{f/f}$ (black bars) and *jun*$^{f/f}$ *P0::cre* (white bars) animals. ***p < 0.001 in uSTT between *jun*$^{f/f}$ *P0::cre* mice and *jun*$^{f/f}$ groups.

5.3 Changes in Non-Neuronal Cell Activation after Facial Nerve Axotomy accompanying c-Jun deletion in Schwann Cells

Peripheral nerve transection is accompanied by reactive changes in brain resident non-neuronal cells such as astrocytes and microglia (Raivich et al., 1999, 1999; Schwaiger et al., 1998; Werner et al., 2001a; Tichauer et al., 2007). Astrocytes upregulate reactive oxygen species (ROS) and GFAP and mobilize to the site of injury, where they exert their trophic effects. Microglia undergo morphological changes to become activated, in the presence of signalling cues, or to become phagocytic in response to cellular debris. There exists accompanying increase in markers αM integrin subunit and αX integrin subunit respectively in activated and phagocytic microglia. Cell survival and death signals are propagated both anterogradely, from the neuronal cell body to the regenerating proximal

axonal tip and retrogradely, from Schwann Cells in the periphery and other environmental cues into the soma; there exists a feedback loop throughout the entire regenerative process. Therefore, the resultant changes in non-neuronal cell activation and recruitment associated with ablation of c-Jun-derived signalling from the periphery were investigated.

First, the role of peripheral c-Jun signalling in clearing cellular debris after facial nerve transection was investigated. In the presence of debris, microglia adopt a phagocytic phenotype, as indicated by presence of the cell surface marker αX integrin, and form distinct nodal structures in the axotomized but not the contralateral brainstem facial motor nucleus (Streit et al., 1988; Aloisi, 2001; Bohatschek et al., 2004). These structures were counted in both control and mutant mice and, as seen in Figure 5-4, control animals exhibited an average of 3.3±0.5 αX immunopositive cells in the ipsilateral facial motor nucleus 14 days after facial nerve transection (N=5). *P0 x jun* $^{f/f}$ animals had higher levels of phagocytic microglia in the ipsilateral facial motor nucleus (11.5±1.5; n=5) compared to *jun* $^{f/f}$ controls ($p < 0.01$ in unpaired Student's T-test). Next, activation levels in microglia, as indicated by αM integrin immunoreactivity, were investigated. Schwann Cell deletion of c-Jun did not affect levels of activated microglia. 14 days post facial nerve axotomy, wild type animals exhibited 10.9±2.7 units of optical luminosity value (OLV) on the contralateral side and 44.1±4.0 on the ipsilateral side (N=5) and *P0 x jun* $^{f/f}$ animals exhibited 13.3±4.0 OLV on the contralateral side and 50.9±5.4 on the injured side (N=5, $p<0.05$ in unpaired Student's T-test). Four days after facial nerve transection, control animals showed 9.3±1.7 OLV on the contralateral side and 43.6±9.5 on the ipsilateral side (N=2) whereas mutants exhibited 11.6±0.4 OLV on the contralateral side and 48.9±5.6 on the ipsilateral side 4 days post-axotomy (N=3, $p<0.05$ in unpaired Student's T-test). Lastly, astrocyte activation, as indicated by GFAP expression, was investigated. There were no differences between wild type and mutant animals in GFAP expression at 14 days post-axotomy, with control animals showing 18.2±1.8 OLV on the contralateral side and 44.8±2.6 on the ipsilateral

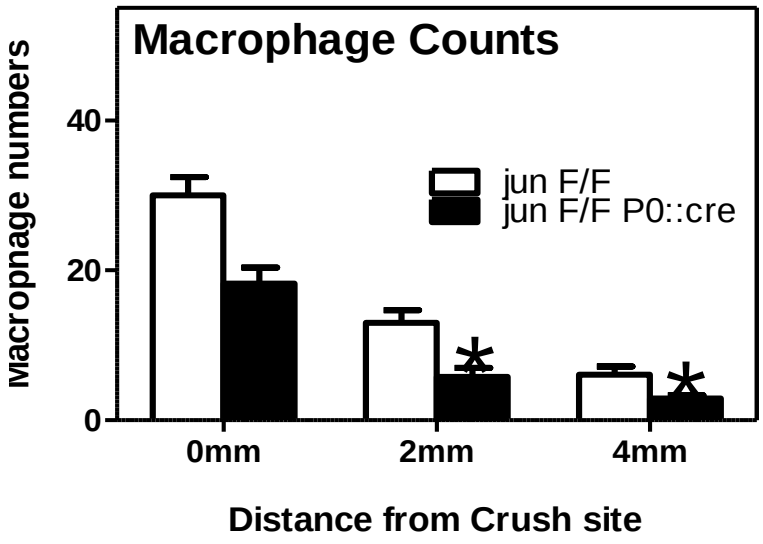

Figure 5-5: Decreased Macrophage Infiltration in P0xJunf/f Mutant Facial Motor Nerves
Quantification of Macrophages homed to site of peripheral injury 4 days following facial nerve crush, on the ipsilateral side. Data quantified in OLV of luminosity using the MEAN-SD algorithm (Moller et al., 1996). White bars, Jun f/f wild type animals; black bars (N=4), Jun f/f x P0::Cre mutants (N=3). *p<0.05 in uSTT between junf/f P0::cre mice and *c-jun*$^{f/f}$ groups. Data collected in collaboration with M. Makwana.

side (N=5) and mutants showing 17.6±2.2 on the contralateral side and 43.6±1.8 on the injured side (N=5, p<0.05 in unpaired Student's T-test). There were also no differences 4 days post-axotomy, with wild type animals exhibiting 21.2±3.5 OLV on the contralateral side and 67.7±10.4 on the ipsilateral side (N=3) and *P0 x jun* $^{f/f}$ animals showing 22.6±2.1 on the contralateral side and 59.7±2.0 on the ipsilateral side (N=3, p<0.05 in unpaired Student's T-test).

Contrastingly, monocyte recruitment at the lesion site after crush injury was less in *P0 x jun* $^{f/f}$ animals than wild type controls (Figure 5-5). This difference became less prominent progressively further from the lesion site. At the crush area (0mm), macrophage numbers averaged 3.9±2.9 in control animals (n=4). Contrastingly, *P0 x jun* $^{f/f}$ mutants displayed 19.1±4.3 macrophages, an almost 30% reduction, although this fell short of significance (P<0.1, n=3). 2mm from the lesion site, *P0 x jun* $^{f/f}$ mutants showed roughly half the infiltration of their wild type counterparts - counts were 14.9±1.3 for wild type *jun* $^{f/f}$ animals and 2.9±2.1 for *P0 x jun* $^{f/f}$ knock outs (n=4 and n=3 respectively, p <0.005 in unpaired Student's T-test). Lastly, 4mm from the lesion site, *jun* $^{f/f}$ animals averaged 6.7±1.2 macrophages and *P0 x jun* $^{f/f}$ animals averaged 1.7±1.1, again, almost fifty percent less than in wild type littermates (n=4 and n=3 respectively, p <0.05 in unpaired Student's T-test).

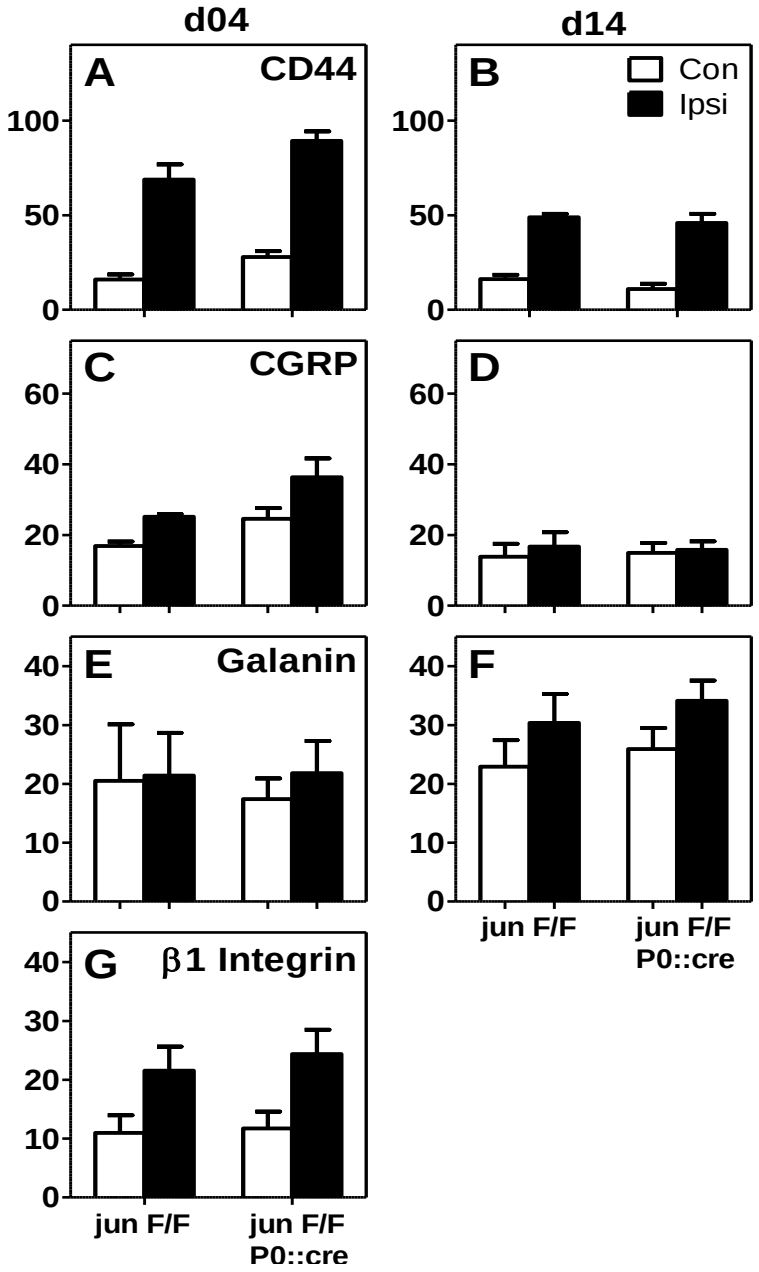

Figure 5-6: No Difference in Expression Levels of Neuronal Factors after Facial Nerve Transection in junf/f P0::cre Mice
No differences in CD44 (A–B), CGRP (C-D), Galanin (E-F) or α7β1 integrin (Integrin β1, G) immunoreactivity in the facial nucleus of *c-jun*$^{f/f}$ and *jun*$^{f/f}$ *P0::cre* mice on the contralateral (white bars) and ipsilateral (black bars) side on post-surgical day 4 (d04, A, C, E, G) and day 14 (d14, B, D, F). N=3 for *c-jun*$^{f/f}$ and *jun*$^{f/f}$ *P0::cre* in (A, C, E, G) and N=5 for *c-jun*$^{f/f}$ and *jun*$^{f/f}$ *P0::cre* in (B, D, F); p>0.05 in uSTT between *c-jun*$^{f/f}$ and *jun*$^{f/f}$ *P0::cre* animals.

Glial Expression of c-Jun does not Affect Neuronal Cell Body Response

Reciprocal interactions amongst neuronal systems are common; facial motor neurons are affected by homeostatic changes in both the axonal and the somatic cellular microenvironments. Therefore, the contribution of c-Jun, expressed by peripheral glia, to the cellular response of motor neuron soma in the facial motor nucleus was investigated. Normally, nerve transection is accompanied by upregulation of various growth-associated transcription factors – such as CGRP and Galanin, beta-1 integrin and CD44 - in the neuronal cell body. These factors can act locally, or in the proximal nerve segment via axonal transport. No significant differences were observable between wild-type and mutant animals in CD44, CGRP, Galanin or β1 integrin expression levels either 4 or 14 days post facial nerve transection (Figure 5-6).

P0::JUN DISCUSSION: THE ROLE OF SCHWANN CELL C-JUN IN REGENERATION

Heightened expression of AP1 transcription factors such as c-Jun, c-Fos and ATF/CREB proteins are some of the most immediate, consistent and well characterized changes to take place following neuronal injury; they are known to participate in the sprouting response to injury, to mediate cell survival and to direct the cellular response to stress and damage (Raivich et al., 2006; Broude et al., 1999; Vaudano et al., 1998; Hüll et al., 1994; Canettieri et al., 2009; Han et al., 1992; Smeal et al., 1989; Chiu et al., 1988; Kobayashi et al., 2009). In the current study, we have explored the role of peripheral c-Jun using a conditional Cre:: LoxP Schwann Cell deleted mutant expressing a floxed *c-jun* allele and cre recombinase under the control of P0 promoter. These results show the integral role played by peripherally expressed c-Jun

This study illustrates the importance of *c-jun* as a mediator of trophic factor signalling in peripheral regeneration. As mentioned previously, axons in the PNS spontaneously regenerate whereas those in the CNS do not. However, retinal ganglion cells, medullary and pontine reticular neurons, as well as striatal, cerebellar and thalamic neurons, can extend axonal processes through a peripheral nerve graft (Campbell et al., 2005; Hüll et al., 1994; Schuetz et al., 2003; Tom et al., 2008; Houle et al., 2006; Zhang et al., 1995; Woolhead et al., 1998; Vaudano et al., 1995, 1998, 1996). This indicates that modulatory factors present in PNS and not CNS glia might play a key role in axonal regeneration and might also facilitate the functional recovery that is common with peripheral, but not central nerve injury. Furthermore, c-jun expression levels increase after nerve injury in both PNS and CNS tissue; however, they only show prolonged elevation in PNS injury models (Broude et al., 1997). This elevation corresponds closely to the period of regrowth exhibited by PNS neurons (Broude et al., 1997). Evidence from this study suggests that *c-*

jun – in particular, that expressed by Schwann Cells – plays a key role in this differential ability to regenerate.

5.4 Schwann cell c-Jun provides a Neuronal Survival Signal in Adulthood

Adult motoneurons ensheathed by c-Jun deficient Schwann cells exhibited a developmentally regulated, copy number dependent decrease in motoneuron survival following facial motor nerve axotomy. This suggests that c-Jun is an important signalling molecule in the Schwann Cell response to injury in adult animals. Studies investigating the molecular properties of c-Jun in Schwann cells indicate that it is an essential intermediate in Schwann Cell de-differentiation following injury; without it, Schwann cells were unable to de-differentiate from a myelinating to immature phenotype following injury and they also exhibited delayed demyelination in sciatic nerves after cut (Parkinson et al., 2008; Mirsky et al., 2008). Delayed demyelination results in increased myelin debris at the lesion site and inhibitory signalling molecules in myelin are known inhibitors of the successful regenerative response (Giger et al., 2008). This dysfunctional regulation of the regenerative response can contribute to decreased cell survival.

Interestingly, neonatal $Jun^{f/f}$ x P0::Cre mutant animals failed to develop the copy number dependent cell death visible in adult $Jun^{f/f}$ x P0::Cre motoneurons following facial nerve transection and instead, all showed similar, low levels of survival following cut. In general, neonates displayed only 50% survival 3 days following injury – whereas adult motor neurons generally show only around 20-40% cell death 30 days following facial nerve cut (Ferri et al., 1998a; Serpe et al., 2003b; Makwana et al., 2009). This indicates that nerve section generally has more severe effects on developing rather than adult motor nerves and that this is c-Jun independent in neonates.

5.5 The Role of c-Jun in Axotomy-Induced Monocyte and Non-neuronal Recruitment

5.5.1 Effect of Junf/f x P0::Cre Deletion in the Facial Motor Nucleus

The neuronal response to injury involves a series of precisely timed and monitored cellular events which are orchestrated by both neuronal and non-neuronal cells. T-cells invade from the vasculature and astrocytes become activated, hone to the site of injury, acquire antigen presenting properties and begin to secrete reactive oxygen intermediates like interleukin (IL)-1β, inducible nitric oxide (NO) synthase, the NO metabolite nitrite, superoxide (O2-) and the chemokine CX3CL1 (Tichauer et al., 2007; Ranaivo et al., 2009). Activated microglia contribute chemotactically to the injury response by expressing cell surface αM integrin subunit, MHC (either type I or II), as well as CD40, CD11b, Fc receptors I–III, complement receptors (CR1, 2, and 4), β2 integrins, the co stimulatory molecules CD80, CD86, and intercellular adhesion molecule-1 (ICAM-1, Matsumoto 1986, McGeer 1993, Hickey, 1988, Minagar 2002, Woodroofe 1991). At the site of injury, peripheral macrophages travel down a chemotactic gradient to participate in the regenerative response as phagocytes and professional antigen presenting cells (pAPCs).

Activated macrophages can also act as pro- or anti-inflammatory mediators, dependent on the means by which they are activated (DiPietro et al., 1998; Gallin et al., 1992) All monocytes share a common haematopoetic origin and studies show that microglia can develop from adult migratory peripheral macrophages (Priller et al., 2001; Flugel et al., 2001; Bechmann et al., 2005). Deletion of c-jun from Schwann cells results in an altered monocytic response, although lymphocyte infiltration and astroglial activation remained unchanged.

In the injured facial motor nucleus 14 days after axotomy, more phagocytic microglia were present in *Junf/f x P0::Cre* mutants than in *Junf/f* wild type animals. Increased phagocytic microglial infiltration was probably due to higher levels of motoneuron cell death and the increased need for phagocytic clearance of debris.

5.5.2 Junf/f x P0::Cre Ablates Monocyte Recruitment at the Site of Injury

Conversely, at the site of injury 4 days after facial motor nerve crush decreased levels of monocyte recruitment were present surrounding the injury site. As one progressed further from the site of injury, significantly fewer macrophages were present in Junf/f x P0::Cre transgenic knock outs compared to Junf/f wild type animals. This suggests that peripherally expressed c-Jun plays a role in creating a cellular cascade that results in the chemotactic gradient through which infiltrating non-neuronal cells are attracted to the injury site. Defects in Schwann cell expression of c-Jun led to impairments in their ability to attract pAPCs and phagocytic cells.

5.6 Impaired Target Reinnervation in Schwann cell c-Jun Deficient Mice

5.6.1 Copy Number-Dependent Decreases in Anatomical Reinnervation

To evaluate the role of glial *c-jun* in the periphery, functional recovery and target reinnervation were assessed in three ways – by using retrograde Fluorogold labelling, by observing whisker hair recovery and by gauging facial nerve regeneration four days after nerve crush. Retrograde labelling showed a strong failure to restore anatomical connectivity in *P0 x jun* $^{f/f}$ homozygote mice which was partially restored in heterozygote *P0 x jun* $^{f/WT}$ animals. However, full specific reinnervation, which is derived by dividing the

number of remaining Fluorogold positive neurons by the number of surviving neurons showed little difference between the two (null and wild type) groups. The observed decrease in anatomical reinnervation is thus likely due to the decreased motor neuron survival rather than deficits in regeneration in c-Jun deficient Schwann cell – associated neurons. Proportionally, surviving motoneurons were able to reconnect functionally, even in the absence of c-Jun, and were reduced by approximately 40%. However, due to substantial motoneuron cell death, there were much fewer surviving motoneurons remaining for regeneration, which primarily caused the dire reduction in reinnervation rate.

5.6.2 Copy Number Independent Impairments in Recovery of Whisker Vibrissae

Motor performance – as measured by whisker assessment – was also affected by c-Jun deletion in Schwann Cells. Mutant *P0 x jun* $^{f/f}$ animals showed more than three fold less increases in motor performance compared to their wild type counterparts. Anatomically, there was a linear correlation between number of copies of c-jun and extent of reinnervation. However, functional recovery did not show linearity and was affected by only complete excision of c-Jun. Thus, only one deleted copy of c-jun was necessary to affect survival and reinnervation but function was ablated only by homozygous deletion.

5.6.3 Decreased Regeneration 4 Days following Crush Injury

Lastly, axonal regeneration four days following facial nerve crush was severely affected in *P0 x jun* $^{f/f}$ mutants. Axon lengths of both CGRP and galanin immunoreactive sprouts decreased by almost 30 percent in *P0 x jun* $^{f/f}$ animals, compared to their *jun* $^{f/f}$ controls. This indicates that peripheral Schwann Cell c-jun is an important mediator of the cellular response that results in Schwann Cell-mediated increased tropism associated with successful functional recovery.

CHAPTER 6: JNK RESULTS: C-JUN ACTIVATION STATE IN NEURONAL REGENERATION AND REPAIR

As mentioned previously in this report, c-Jun protein presence is not the sole regulator of its function. Through N-terminal activation, by JNK phosphorylation of Serines 63 and 73 (ser63&73) and Threonines 91 and 93 (thr91&93), c-jun can exhibit differential regulatory effects (Raivich, 2008). Indeed, activation can alter binding activity (Boyle et al., 1991) in the absence of *de novo* protein synthesis (Angel et al., 1987) and JNK has been found to have neuroprotective effects in several different injury models (for a detailed review, see Haeusgen et al. 2009). This study aimed at elucidating the role, if any, played by the Jun-N-Terminal Kinases in facial nerve regeneration and repair following transection.

6.1 Generation of Mice Lacking Jun N-Terminal Kinase (JNK) function

To investigate the role of *c-jun* phosphorylation in regenerative response following facial nerve axotomy, two transgenic lines were investigated that ablated JNK function. The first, Jun AA, has been described previously (Behrens et al., 1999). Briefly, JNK function was inhibited by a substitution mutation of the c-jun N terminus. Serines 63 and 73 were replaced by Alanine residues, thereby preventing JNKs from interacting with and phosphorylating the active site. The second type of transgenic line that was investigated possessed global deletion of each of the major Jun N-Terminal Kinases, termed JNK1, 2 and 3. Like Jun AA, creation of these mutants and efficiency of this mutation has been described elsewhere (Yang et al., 1997; Kuan et al., 1999a, 2003; Dong et al., 1998; Brecht et al., 2005a).

Mice lacking the ability to phosphorylate *c-jun* (Jun AA, JNK1, JNK2 and JNK3) were born with Mendelian frequency and were viable and fertile.

6.2 Phosphorylation of c-jun Is Not Required During Axonal Regeneration and Sprouting

It is well known that transected peripheral nerves commonly react by initiating an extensive regenerative response. During axonal elongation and sprouting, molecules like CGRP and Galanin are upregulated in growth cones of regenerating axons (Makwana, Werner, et al., 2009). To observe the efficiency of axonal reinnervation in JunAA, JNK1, JNK2 and JNK3 mutants, whisker hair movement, an indicator of functional recovery, was scored by two observers unaware of the genotypes, on a scale of 0 (no movement) to 3 (strong, normal movement).

6.2.1 Functional Recovery

Twenty-eight days after facial nerve axotomy, there were no significant differences in functional recovery between wild types WTAA, WT1, WT2, and WT3 (1.3±0.2; N=17, 1.88±0.16; N=9, 1.2±0.1; N=17 and 1.38±0.16; N=12 respectively) and mutants JunAA (1.2±0.1; N=23), JNK1 (1.64±0.14; N=7), JNK2 (1.2±0.0; N=30) and JNK3 (1.39±0.12; N=18 (Figure 6-1). However, on average, JNK1 mutants exhibited delayed functional recovery (1.07±0.19; N=10, $p < 0.01$ in unpaired Student's T-test) compared to controls (1.35±0.16; N=11). All other JNK mutants showed no average variation from control animals (WTAA 9.9±0.7; N=17, WT2 8.7±0.8; N=20, WT3 10.92±0.1.26; N=13, JunAA 8.5±0.8; N=23, JNK2 8.4±0.3; N=30, and JNK3 9.39±0.91; N=18 and WT3 10.92±0.1.26; N=13).

6.2.2 Anatomical Reinnervation

Furthermore, at day 28 post axotomy, neuronal cell bodies were fluorescently labelled via Fluorogold implantation under the whisker pad (as described in Materials and Methods). Fluorogold implantation on the contralateral side served as intra-animal control. JNK knock-out and JunAA mutant animals had similar numbers of retrogradely labelled motoneurons on both the contralateral and ipsilateral sides compared to their wild-type counterparts (refer to Figure 6-1).

Per 20 µm section, WTAA control animals exhibited 68±6 (n=7) and 40±7 (n=7) on the control and injured side respectively, and JunAA mice had an average of 58±11 (n=7) Fluorogold positive neurons on the control side and 32±6 (n=7) on the axotomized side. WT1 control animals exhibited 51±8 (n=10) and 16±2 (n=10) on the control and injured side respectively, and JNK1 animals averaged 61±10 (n=9) Fluorogold positive neurons on the control side and 21±7 (n=9) on the axotomized side. WT2 control animals exhibited 42±4 (n=5) and 19±3 (n=5) on the control and injured side respectively and JNK2 animals averaged 53±7 (n=6) Fluorogold positive neurons on the control side and 25±5 (n=6) on the axotomized side. Finally, WT3 control animals exhibited 44±7 (n=9) and 16±4 (n=9) on the control and injured side respectively, and JNK3 animals averaged 51±7 (n=6) Fluorogold positive neurons on the control side and 20±3 (n=6) on the axotomized side.

Overall, the ratio of Fluorogold positive neurons on the axotomized vs. contralateral sides (ax/co ratio), as shown in Figure 6-1, was 57.5% ± 7.5% in WTAA and 55.6% ± 7.9% in JunAA. Ax/co ratio was 35.7% ± 3.9% in WT1 controls and 31.6% ± 5.3% in JNK1 mutants. Furthermore, WT2 mutants showed 45.0%±4.9%, and JNK2 mutants showed 46%±4.6% ax/co ratio. Lastly, ax/co ratio for WT3 was 34.0%±5.1%, and for JNK3 mutants was 38.3%±3.1%.

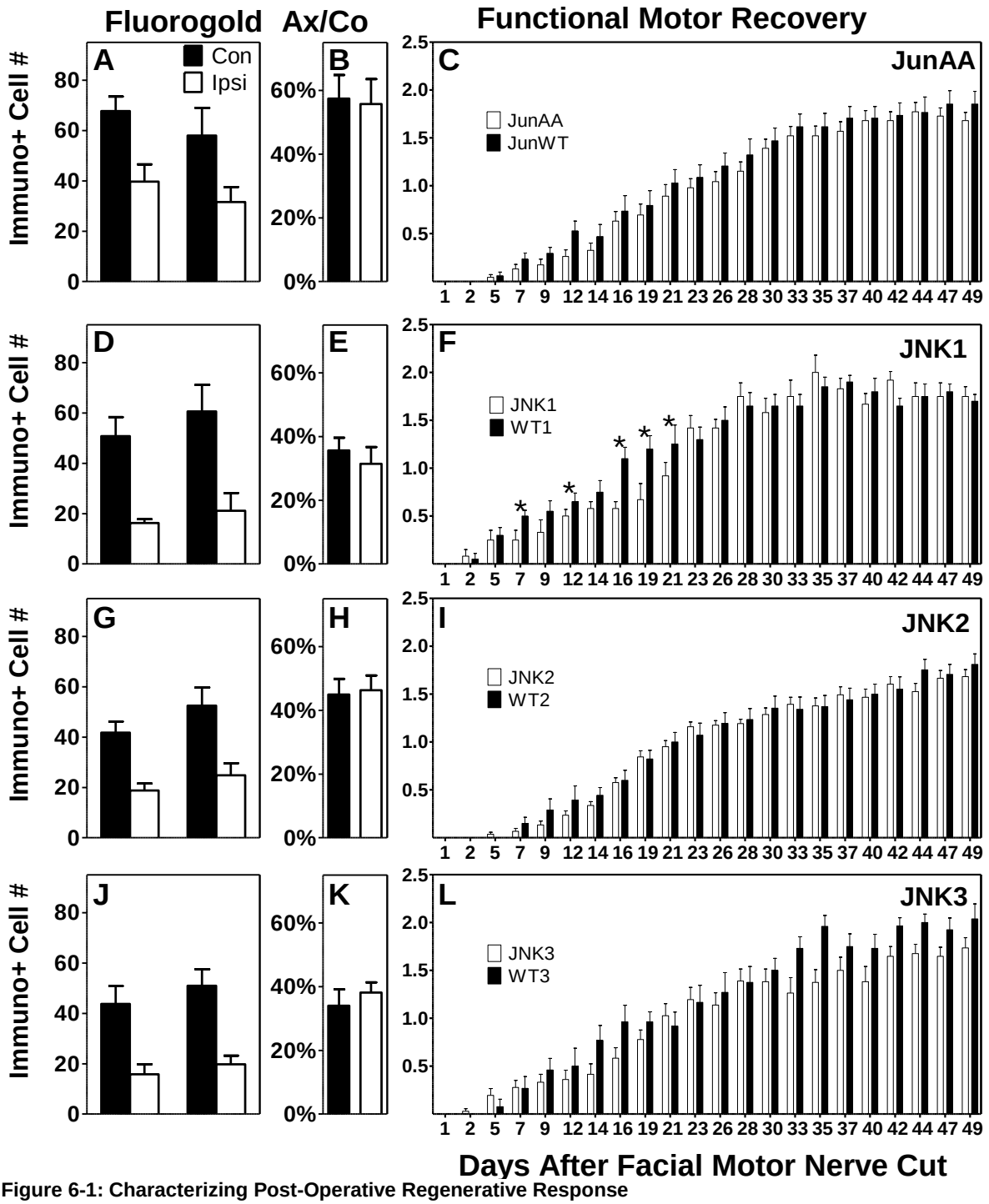

Figure 6-1: Characterizing Post-Operative Regenerative Response

c-Jun phosphorylation is Unnecessary for Functional and Anatomical Reinnervation. (A, D, G, J) Quantification of retrogradely labelled motoneurons in the facial motor nucleus of (A) JunAA (N=7) and WTAA (N=7) mice, (D) JNK1 (N=9) and WT1 (N=10) mice, (G) JNK2 (N=6) and WT2 (N=5) mice, and finally, (J) JNK3 (N=6) and WT3 (N=9), using FluoroGold, performed 28 days post-operatively. Contralateral side, white bars; ipsilateral side, black bars. *P<0.05 in uSTT between all groups of animals. (B, E, H, K) Ax/Co ratio of FluoroGold positive neurons is shown; (B) WTAA, (E) WT1, (H) WT2 and (K) WT3 mice, black bars; (B) JunAA, (E) JNK1, (H) JNK2 and (K) JNK3 animals, white bars. *p<0.05 in uSTT between all groups. (C, F, I, L) Posttraumatic whisker hair movement was measured 28 days after facial nerve transection, on a scale of 0 (no movement) to 3 (normal, strong movement - similar to that on the contralateral side); N = 23 for JunAA animals, N=17 for WTAA animals; N=7 for JNK1 animals, N=9 for WT1 animals; N=30 for JNK2 animals, N=17 for WT2 animals; N=18 for JNK3 animals and N=12 for WT3 animals. *p < 0.02 between JNK1 and WT1 groups only, in unpaired Student's t test (uSTT). Data collected in collaboration with N. Staak.

6.2.3 Facial Nerve Regeneration

Additionally, axonal sprouting was studied four days after facial nerve crush. Enhanced sprouting is a common result of peripheral nerve injury; during which time axons extend galanin and CGRP immunoreactive growth cones anterogradely toward the neuromuscular junction (Galiano et al., 2001; Werner et al., 2000, 2001b). This growth response is absent on the contralateral side. As shown in Figure 6-2, no difference in the central sprouting response was observed between JNK 1-3 or JunAA animals and their respective wild type littermates. Average CGRP positive growth cone lengths for wild types - WTAA, WT1, WT2 and WT3- were 5.3±0.2 (n=4), 5.9±0.1mm (n=4) WT2 6.1±0.1mm (n=3) WT3 5.5±0.3mm (n=5) respectively. The mutant counterparts JunAA, JNK1, JNK2 and JNK3 extended CGRP positive processes of 5.9±0.3mm (n=5), 5.8±0.2 (n=7), 5.9±0.1mm (n=2) and 5.9±0.2mm (n=5) respectively. Galanin positive growth cones were extended for WT1, WT2 and WT3 by 5.6±0.1mm by 5.7±0.3mm (n=4), 5.9±0.1mm (n=3) and 5.4±0.3mm (n=5) respectively. Mutants extended processes of JNK1 (n=6), 5.7±0.2mm by JNK2 mutants (n=2) and 5.5±0.2mm by JNK3 mutants (n=5).

Taken together, these data suggest that N-terminal phosphorylation state has little effect on anatomical and functional reinnervation. No differences were observed in anatomical reinnervation or sprouting. JNK1 deletion can delay functional recovery – suggesting it might play a small role in early regeneration. However, despite this overall delay in early reinnervation, JNK1 KO animals exhibit similar end-stage functional recovery as their wild type counterparts. Furthermore, JNK2-3 and JunAA mutants exhibit no difference in functional recovery compared to their wild type controls. This suggests that regeneration is not heavily influenced by the Jun phosphorylation state.

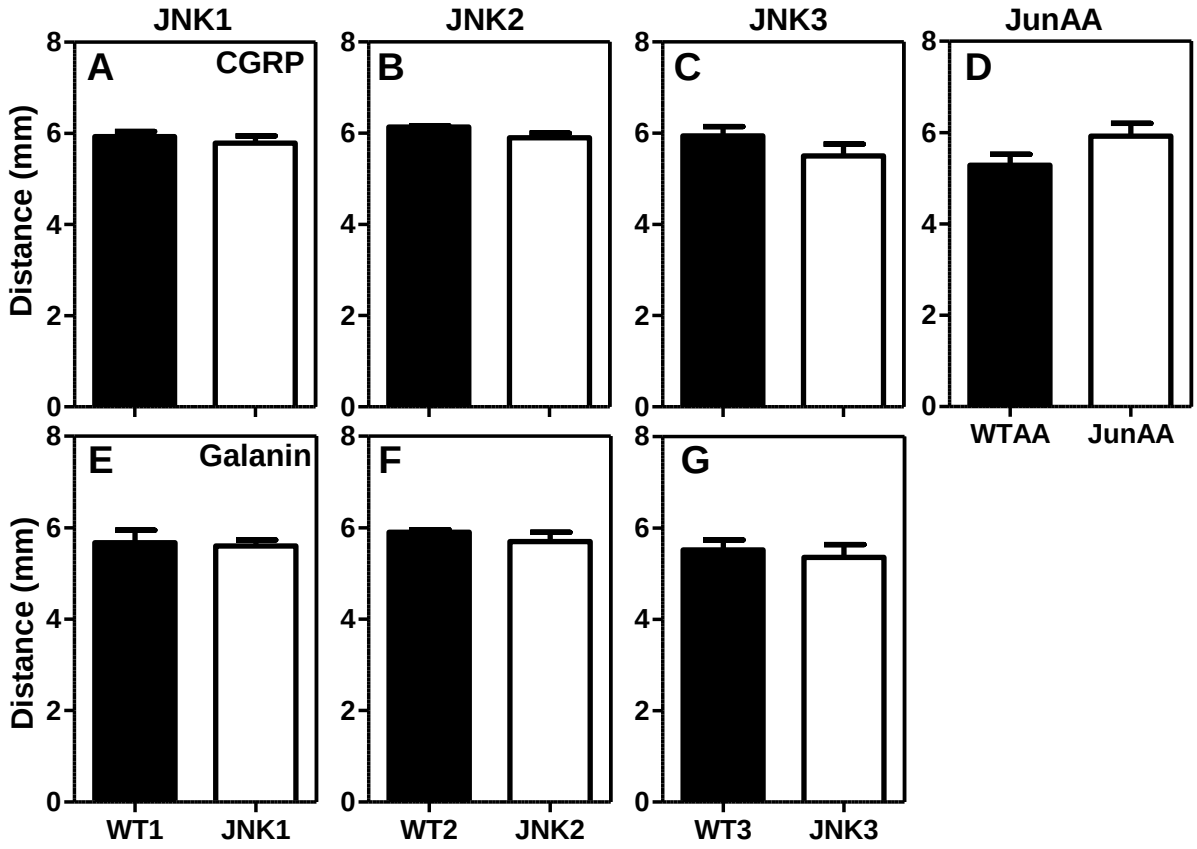

Figure 6-2: No Difference in 4 day post-axotomy Sprouting Response in JunAA, JNK1, JNK2 and JNK3 animals after Facial Nerve Axotomy.
(A-D) CGRP immunoreactive growth cone length on the axotomized side in JNK1 (A), JNK2 (B), JNK3 (C) and JunAA (D) animals (in mm). (E-G) Galanin immunoreactive growth cone length on the axotomized side in JNK1 (E), JNK2 (F) and JNK3 (G) animals (in mm). Black bars, mutants; white bars, control animals. N=17 for WTAA animals; N=7 for JNK1 animals, N=4 for WT1 animals; N=2 for JNK2 animals, N=3 for WT2 animals; N=5 for JNK3 animals and N=5 for WT3 animals.

6.3 Effect of c-jun Phosphorylation State on Neuronal Cell Death

After facial nerve axotomy, there is considerable neuronal cell death; some studies have observed generally 20 to 30 percent motoneuron cell death post –axotomy in the facial nerve model (Ferri et al., 1998a; Hottinger et al., 2000). Survival data has shown previously that JNK1-3 and JunAA mutations have no effect on facial motor neuron survival following axonal transection (Brecht et al., 2005a).

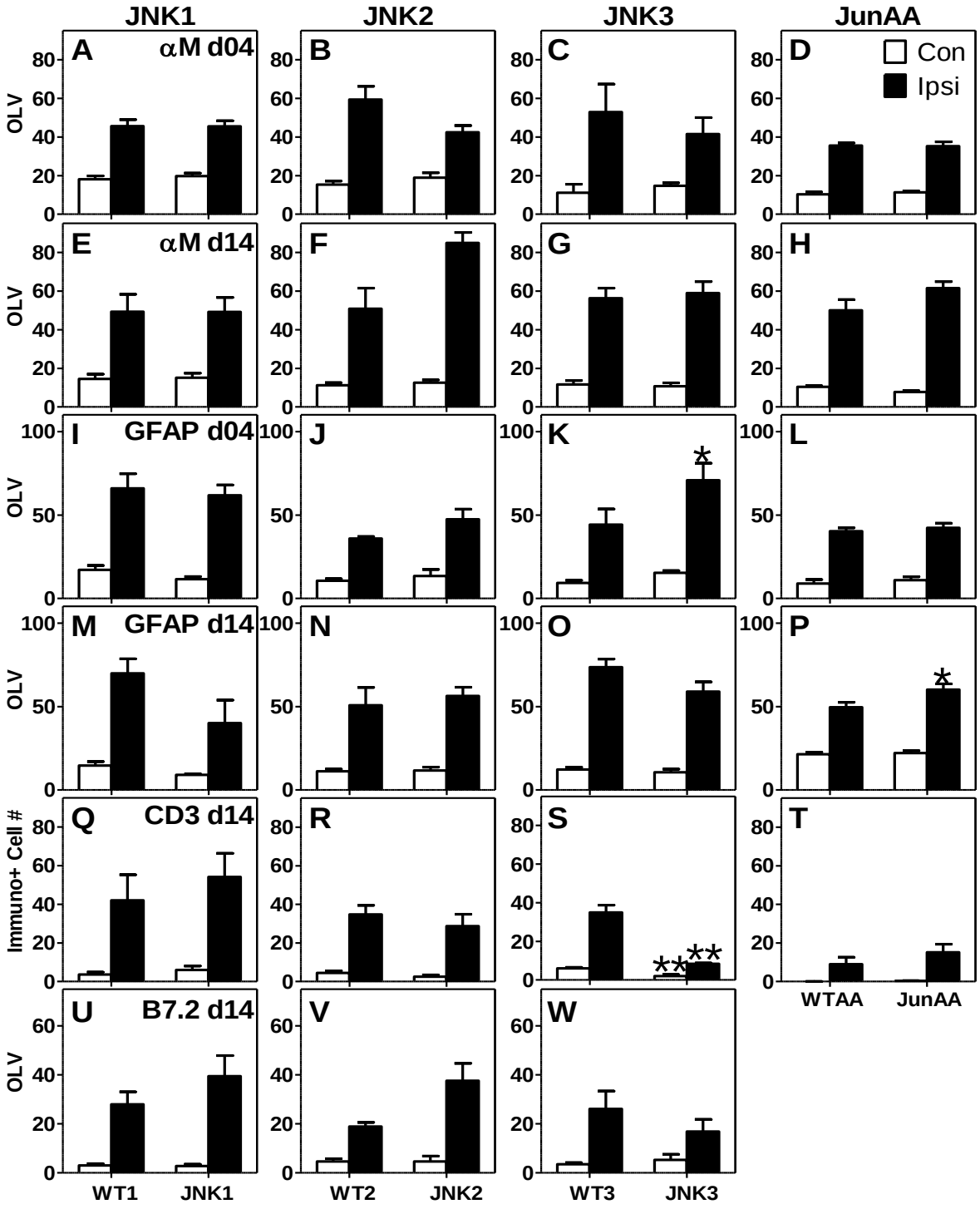

Figure 6-3: No Major Difference in Non-Neuronal Cell Reaction in JunAA, JNK1, JNK2 and JNK3 animals after Facial Nerve Axotomy.

(A-H) Quantification of microglial αM Immunoreactivity (IR) at day 4 (d04, A-D) and day 14 (d14, E-H) in JNK1 (A, E), JNK2 (B, F), JNK3 (C, G) and JunAA (D, H) animals after axotomy using the MEAN-SD algorithm (Moller et al., 1996). (I-P) Quantification of GFAP IR – an indicator of Activated Astroglia - at day 4 (d04, I-L) and day 14 (d14, M-P) in JNK1 (I, M), JNK2 (J, N), JNK3 (K, O) and JunAA (L, P) animals after axotomy. (Q-T) Quantification of CD3 T-Cell IR at day 14 in JNK1 (Q), JNK2 (R), JNK3 (S) and JunAA (T) animals after axotomy. (U-W) Quantification of microglial B7.2 IR at day 14 in JNK1 (U), JNK2 (W) and JNK3 (W) animals after facial nerve transection. White bars, contralateral side; black bars, axotomized side. *p< 0.05, **p< 0.01 in uSTT between KO and WT mice. N = 23 for JunAA animals, N=17 for WTAA animals; N=7 for JNK1 animals, N=9 for WT1 animals; N=30 for JNK2 animals, N=17 for WT2 animals; N=18 for JNK3 animals and N=12 for WT3 animals. JunAA data collected in collaboration with N. Staak.

6.4 Effects of inhibited Jun Phosphorylation on Non-Neuronal Cells

Nerve transection results in robust changes - not only to the neuron itself, but also to the local microenvironment. T-cells and other lymphocytes are recruited from the periphery. Also brain-resident non-neuronal cells such as astrocytes and microglia become activated; thereby releasing reactive intermediates to mediate the neuronal response to injury. Animals with global deletion of the JNK isoforms and also JunAA animals show very little variation in non-neuronal cell upregulation and activation from their wild-type counterparts

Figure 6-3. Early microglial activation, as measured by αM integrin subunit (also known as MAC-1) immunoreactivity, revealed no differences between WT and mutant animals. Please refer to Table 5 of the Appendix for a detailed summary of αM integrin subunit expression at 4 and 14 days post-axotomy in JNK1-3 and JunAA deficient animals. In addition to MAC-1, B7.2 – which is another microglial marker – was also used to further characterize the microglial response in c-Jun phosphorylation-deficient animals. Similarly to what was observed with MAC-1, there were no significant differences between any of the phosphorylation-deficient mutants and their wild-type counterparts (Table 8 of the Appendix,

Figure 6-3) at 14 days post-axotomy. Furthermore, GFAP is expressed by activated Astroglia in response to neuronal stress. For the most part, there is no difference between JNK 1-3 mutants and JunAA mutants and their wild-type counterparts in GFAP expression four and 14 days post-facial nerve transection. Small increases in astrogliosis are visible, however, at day four post-axotomy in JNK3-deficient mutants and also at day 14 in JunAA deficient mutants ($p<0.05$ in unpaired Student's T-test, refer to Table 6 of the Appendix and

Figure 6-3), which are not visible at their respective alternative timepoints. Please refer to Table 6 of the Appendix for detailed statistical data.

Moreover, CD3 is a marker for lymphocytes – in particular, it identifies infiltrating T-Cells. As revealed in

Figure 6-3, no major differences were observed between wild type animals and JNK1, JNK2 and JunAA mutants in CD3 positive T-Cell infiltration as a result of facial nerve axotomy. JNK3 mutants showed significantly lower baseline rates of CD3 positive T-Cell infiltration (Refer to Table 7 of the Appendix), as well as lower T-Cell presence in response to nerve transection (

Figure 6-3, $p<0.05$ in unpaired Student's T-test), but this difference after axotomy is probably due to reduced basal T-Cell levels rather than a result of the injury. Please refer to Table 7 of the Appendix for statistics.

6.5 Jun N-Terminal Phosphorylation is Not Necessary for the Cell Body Response to Injury

The cell body – or chromatolytic - response to injury involves the upregulation of various transcriptional factors and the initiation of a complex cellular cascade of events. Nuclear expression of various growth-related markers - such as neuropeptides CGRP and galanin, CD44 hyaluronic acid receptor and transcription factors c-Jun and ATF3 – is common in regenerating cell somas (Jones et al., 1997, 2000; Tsujino et al., 2000; Shadiack et al., 2001b). Such expression was characterized in JNK1-3 mutants and also in JunAA animals and their wild-type counterparts. As illustrated in Table 9 of the Appendix and Figure 6-4, CD44 expression shows no major differences between mutants and wild-type animals. A small decrease in immunoreactivity was seen at day four in JunAA animals and at day 14 in JNK3 animals compared to WT controls ($p<0.05$ in unpaired Student's T-test), but those differences were not repeated at alternative time points. For the most part, mutants with the inability to phosphorylate c-Jun show no difference in levels of CD44 expression.

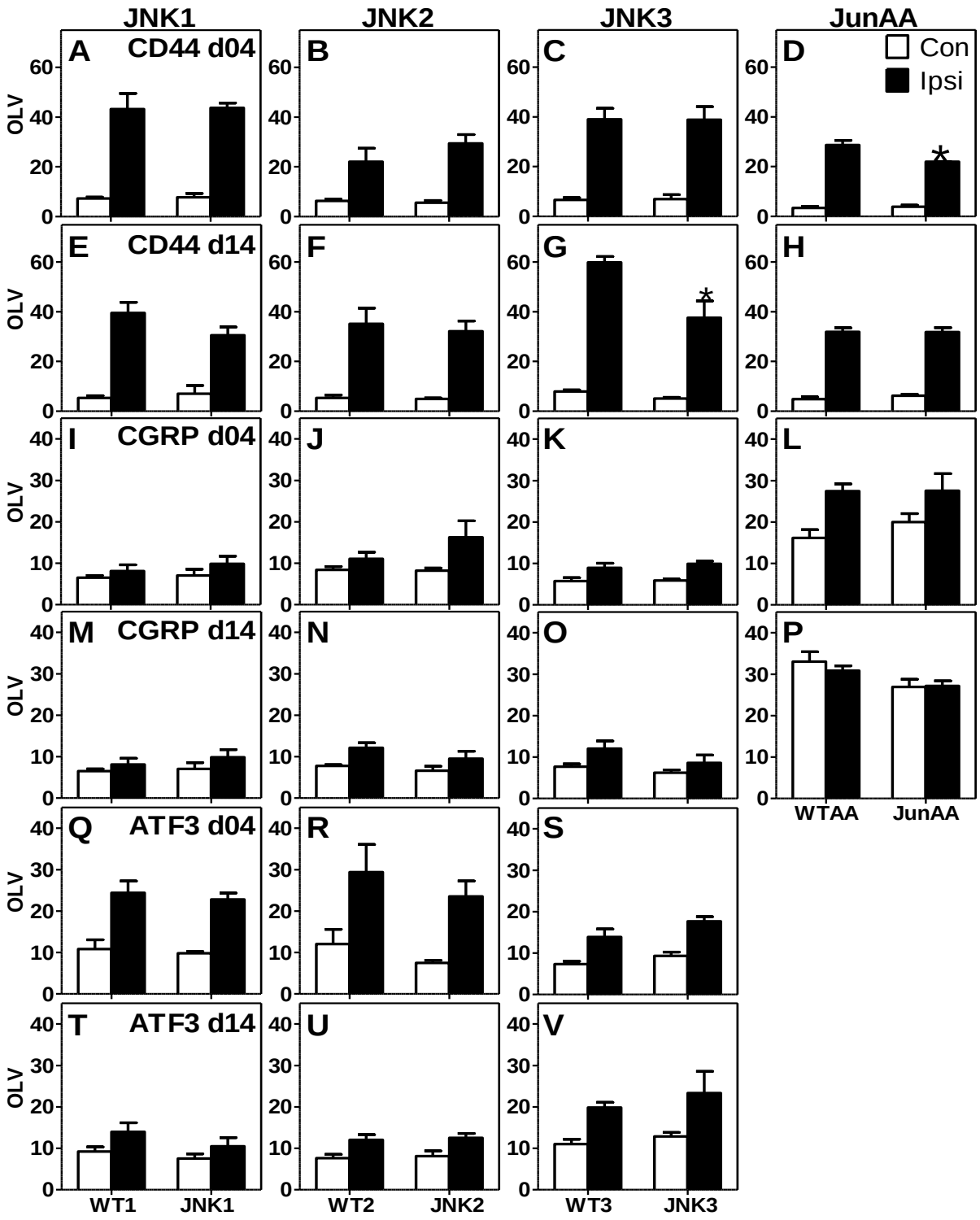

Figure 6-4: No Major Difference in Neuronal Cell Reaction in JunAA, JNK1, JNK2 and JNK3 animals after Facial Nerve Axotomy.

(A-H) Quantification of CD44 Hyaluronic Acid immunoreactivity (IR) at day 4 (d04, A-D) and day 14 (d14, E-H in JNK1 (A, E), JNK2 (B, F), JNK3 (C, G) and JunAA (D, H) animals after axotomy using the MEAN-SD algorithm (Moller et al., 1996). (I-P) Quantification of CGRP IR at day 4 (d04, I-L) and day 14 (d14, M-P) in JNK1 (I, M), JNK2 (J, N), JNK3 (K, O) and JunAA (L, P) animals after axotomy using the MEAN-SD algorithm. (Q-W) Quantification of ATF3 IR at day 4 (d04, Q-S) and day 14 (d14, U-W) in JNK1 (Q, U), JNK2 (R, V) and JNK3 (S, W) animals after axotomy using the MEAN-SD algorithm. White bars, contralateral side; black bars, axotomized side. *p< 0.05 in uSTT between WT and KO mice. N = 23 for JunAA animals, N=17 for WTAA animals; N=7 for JNK1 animals, N=9 for WT1 animals; N=30 for JNK2 animals, N=17 for WT2 animals; N=18 for JNK3 animals and N=12 for WT3 animals. JunAA data collected in collaboration with N. Staak.

Next, levels of CGRP expressed by regenerating facial motor neurons were compared. CGRP is produced in the cell body and transported into growth cones in the growing axonal tip (Makwana, Werner, et al., 2009). As shown in Table 10 of the Appendix and Figure 6-4, no differences were observed between JNK1-3 mutants and wild type animals either four or 14 days after facial nerve transection. Lastly, ATF3 expression was quantified in the nucleus. ATF3 belongs to the ATF family of AP1 transcription factors and commonly heterodimerizes with c-Jun in regenerating cells (Pearson et al., 2003b). However, ATF3 levels were unchanged at both four and 14 days post-axotomy in JNK1-3 and JunAA animals (Figure 6-4, Table 11 of the Appendix). This would indicate that phospho-Jun does not interact with ATF3 during its regenerative function.

JNK DISCUSSION: C-JUN N-TERMINAL PHOSPHORYLATION HAS NO MAJOR AFFECT ON FACIAL NERVE REGENERATION

C-jun is an immediate early gene that is consistently upregulated after neuronal injury; previous studies link it to both pro-regenerative and pro-apoptotic pathways (Herdegen et al., 1997). As described earlier in this report, its phosphorylation state can influence dimer stability and can affect its biological role in regeneration, both *in vivo* and *in vitro*. This study aimed to investigate whether ablation of JNK function, either through global deletion of JNK or through inactivation via substitution mutation, plays a role in the neuronal regenerative response. Based on data characterizing survival, regeneration and cellular response of JNK1, JNK2, JNK3 and JunAA mutants following facial nerve injury, it is evident that N-Terminal phosphorylation of c-jun does not play a major role in neuronal regeneration after facial nerve axotomy.

6.6 Non-Neuronal Reaction to Facial Nerve Injury in JNK1-3 and JunAA Mutants

Few differences were observed between animals deficient in Jun phosphorylation and their wild-type counterparts. This indicates that activated c-Jun is not essential for the peripheral response to facial nerve transection. Furthermore, c-Jun phosphorylation does not affect microglial infiltration to the site of injury, nor does it affect astrogliosis. Levels of CD3 reactive T-Lymphocytes were lower in JNK3 mutant facial motor nuclei following injury compared to wild type littermates; however, baseline expression of these non-neuronal cells was also lower – indicating that this decrease was not due to injury, but due to a JNK3 mutation-specific defect in T-Cell maturation or production. It seems that c-Jun, in its phosphorylated state, is not a major transcriptional regulator of the non-neuronal response to facial nerve injury.

6.7 Phospho-Jun is a non-essential regulator of the motor neuron injury response

It is known that a successful cellular response to injury – such as that seen peripherally - necessitates the expression and temporal synchronization of several growth-related transcription factors. These factors can be upregulated immediately after injury – as is the case with ATF3 (Tsujino et al., 2000)– or slightly later and the cellular response peaks around day 4 post-axotomy, while the inflammatory response in the facial motor nucleus reaches a maximum 14 days after injury (Makwana, Werner, et al., 2009; Raivich, 2008; Raivich et al., 2007). Expression levels of several of the most important of these factors were measured at two separate time points to characterize the neuronal response; data indicated that phosphorylation of c-Jun plays no role in successful upregulation of growth-related molecules CD44, CGRP and ATF3. Since all of these molecules are known to be upregulated in the successful regenerative response (Seijffers et al., 2007; Pearson et al., 2003b; Jones et al., 2000; Kalousa and Keast, 2009), this data shows that phospho-jun is not the major regulator of transcriptional events leading to and maintaining the cellular response.

6.8 Assessment of Target Reinnervation

Target reinnervation was assessed using three paradigms; for thirty days following injury, whisker hair performance assessed functional recovery and, at thirty days following facial nerve transection, Fluorogold retrograde labelling illustrated anatomical reinnervation. Peripheral axonal sprouting was quantified four days following facial nerve crush injury to quantify the length of neuropeptide-rich growth cones extending from the injured proximal axonal tip. Retrograde labelling showed no differences in anatomical reinnervation between JNK1-3 or JunAA mutants and their wild type counterparts. This was echoed by similar motor performance, except with JNK1 mutants – whose motor performance was

delayed. Whisker function was restored in a linear fashion in all cases except JNK1 – whose restoration of function was parabolic. This indicates that most anatomical and functional regeneration takes place via a phospho-jun independent mechanism. Phosphorylation by JNK1 plays a minor role in early functional regeneration, however its absence is eventually compensated for and JNK1 mutants reach wild type levels of functional recovery by day 30. 4 days following crush injury, there were again no differences between any JNK mutant and their wild type littermates in either CGRP or Galanin immunopositive axon length.

CHAPTER 7: ATMIN RESULTS: ATMIN'S ROLE IN THE NEURONAL CELL STRESS RESPONSE

Upregulation of growth-associated molecules is essential for an effective post-traumatic regenerative response; cells that are deficient in pro-regenerative transcription factors or neuropeptides consistently fail to enter into the regenerating phenotype that enables successful neuromuscular target reinnervation (Galiano et al., 2001). In particular, ATF3 and c-Jun are growth-related peptides that combine to form the AP1 transcription complex. Studies show that expression of both ATF3 and c-Jun are under ATM control (mice deficient in upstream ATM show increased AP-1 activation, Weizman et al. 2003) and that ATF3 over-expression in particular can negatively regulate cell cycle progression from G1 to S phase (Fan et al., 2002). ATF3 and c-jun co-expression have previously been associated in vivo with increased axonal sprouting (Campbell et al., 2005; Pearson et al., 2003a) and ATF3 upregulation, in particular, has been attributed to increased branching in Dorsal Root Ganglia (DRG) cells (Seijffers et al., 2006).

7.1 Generation of Mice Lacking ATMIN in the CNS

To examine and characterize the role of ATMIN in the axonal response to neuronal injury, transgenic mice expressing the nestin promoter-driven Cre recombinase (nestin::cre) were crossed with mice carrying a lox P tagged (floxed) ATMIN gene ($ATMIN^{F/F}$). The resulting F1 generation, $ATMIN^{\Delta N/WT}$, were again crossed with the $ATMIN^{F/F}$ animals, to produce a homozygous deletion of ATMIN in central neuroepithelium-derived cells, in the brain and spinal cord (Behrens et al. 2002 and Tronche et al. 1999). Previous studies demonstrate the efficiency and neuroepithelial specificity of the nestin-cre transgenic line (Gass et al. 2000; Knoepfler et al. 2002; Mantamadiotis et al. 2002 and Tronche et al. 1999). As shown in Figure 7-1, homozygous deletion of ATMIN led to the disappearance of ATMIN mRNA as well as most of the ATMIN protein immunoreactivity throughout the brain. These

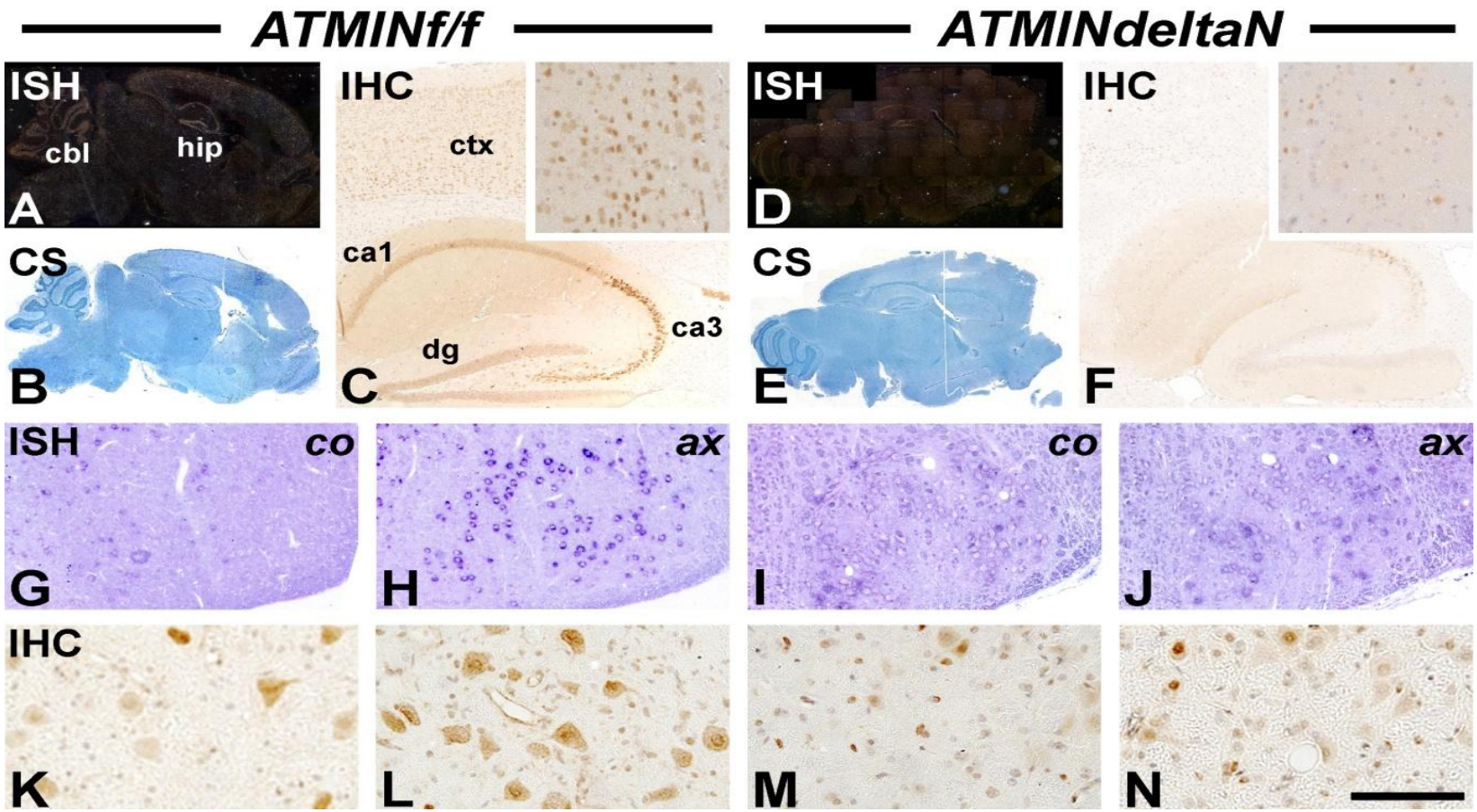

Figure 7-1: ATMIN mRNA and protein immunoreactivity is expressed throughout the brain
(A-F), increases in facial motoneurons following axotomy (G-N) and disappears in the ATMIN$^{\Delta N}$ mutants (D-F, I,J,M,N), compared with the ATMIN-competent, f/f control littermates (ATMIN$^{F/F}$) (A-C, G,H,K,L). **A-F:** Sagittal brain sections, **G-N:** Coronal sections of facial motor nucleus. **A,B,D,E, G-J:** Darkfield illuminated radioactive in situ hybridisation (ISH) for ATMIN mRNA (A,D), the respective bright-field counterstain for methylene blue (B,E), and non-radioactive in situ in the axotomized (ax) and contralateral (co, uninjured) facial motor nuclei, 14 days after facial nerve cut (G-J). **C,F,K-N:** Immunohistochemistry (IHC) for ATMIN specific JCro-antibody, in forebrain cerebral cortex and hippocampus (C,F), and facial motor nucleus (K-N). The inserts in C&F show higher magnification of cerebral cortex. Note the prominent ATMIN mRNA expression in cerebellum (cbl) and hippocampus (hip), and on the immunoreactivity level, particularly in the hippocampal CA3 region, as well as the 80-85% reduction in the number of ATMIN-immunoreactive neurons in the ATMIN$^{\Delta N}$ mutants, compared with the ATMIN-competent control littermates. Scale bar: A,B,D,E - 4mm (A,B,D,E), C,F - 0.6mm, E-H - 0.5mm, C,F inserts - 0.25mm, and I-L - 0.1mm. Data collected in collaboration with N.Kanu.

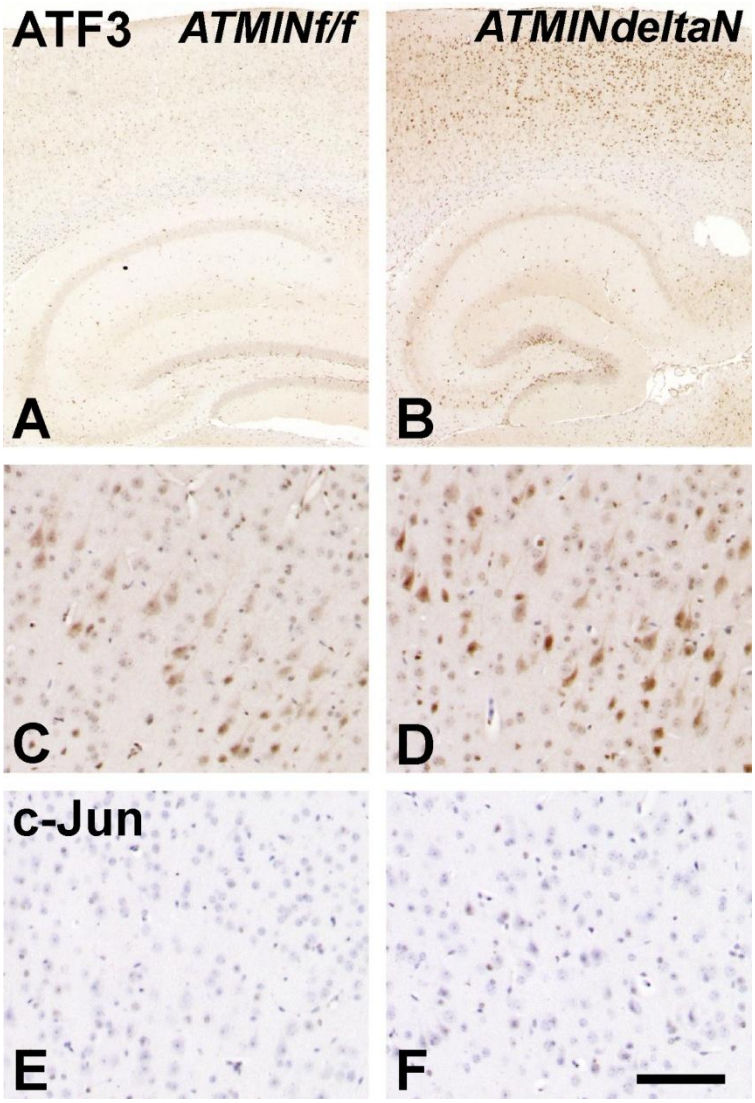

Figure 7-2: ATMIN deletion causes strong increase in neuronal ATF3 (A-D), but not c-Jun (E,F) immunoreactivity in the cerebral motor cortex.
A,C,E: ATMIN$^{F/F}$, **B,D,F:** ATMIN$^{\Delta N}$ mice, scale bar: A,B – 0.5mm, C-F – 80um. Figure produced in collaboration with N. Kanu.

ATMIN$^{\Delta N}$ animals were born with Mendelian frequency, although they were smaller in size than their wild-type counterparts.

Under higher magnification, normal, ATMIN$^{F/F}$ animals revealed moderate neuronal immunoreactivity throughout the cytoplasm, and slightly more in the nuclei, throughout the brain, including the cerebral cortex, hippocampus and cerebellum (Figure 7-1A-C). Particularly high levels were observed in the cerebellar granular layer and in the hippocampal CA3 region (Figure 7-1A-C); a strong increase in ATMIN mRNA and immunoreactivity was also observed in axotomized motoneurons, 14 days after facial nerve cut (Figure 7-1G,H,K,L). Homozygous, ATMIN$^{\Delta N}$ mutants showed an almost complete loss of immunoreactivity in the hippocampus (Figure 7-1-C), as well as an 80-85% reduction in the number of positive neurons in the cerebral cortex (compare Figure 7-1F and Figure 7-1C, inserts) and in the control as well as in the axotomized facial motor nuclei (Figure 7-1G-N). ATMIN's Role in the Neuronal Response to Nerve Injury

After transection, non-neuronal cells like microglia and astrocytes are recruited from the local micro-environment, become activated and – in the case of microglia – can act to phagocytose neuronal debris. T-cells invade from the periphery through the vasculature to the site of injury and help to orchestrate the damage response. Simultaneously, in the neuronal cell body, changes take place that result in upregulation of growth-associated molecules that are essential for cell survival and successful neuromuscular reinnervation. ATMIN's role in regeneration was explored after nerve transection using the facial nerve axotomy paradigm. Cellular response was explored at 14 days post-axotomy; cell survival was explored 30 days post-axotomy; functional and anatomical reinnervation was explored 30 days post-axotomy.

7.1.1 Effects of ATMIN deficiency on neuronal cells.

Since facial axotomy caused strong increase in the ATMIN mRNA expression and protein immunoreactivity, we first explored the effects of ATMIn deletion on neuronal response. Neuronal axotomy normally results in the upregulation of regeneration associated transcription factors (c-Jun, ATF3), adhesion molecules (e.g. CD44 hyaluronate receptor) and the neuropeptides Calcitonin Gene-Related Peptide (CGRP) and Galanin (Campbell et al., 2005; Makwana, Serchov, et al., 2009; Pearson et al., 2003a; Jones, Kreutzberg, et al., 1997; Jones et al., 2000; Werner et al., 2000; D. Wynick et al., 2001; Lin et al., 2003).

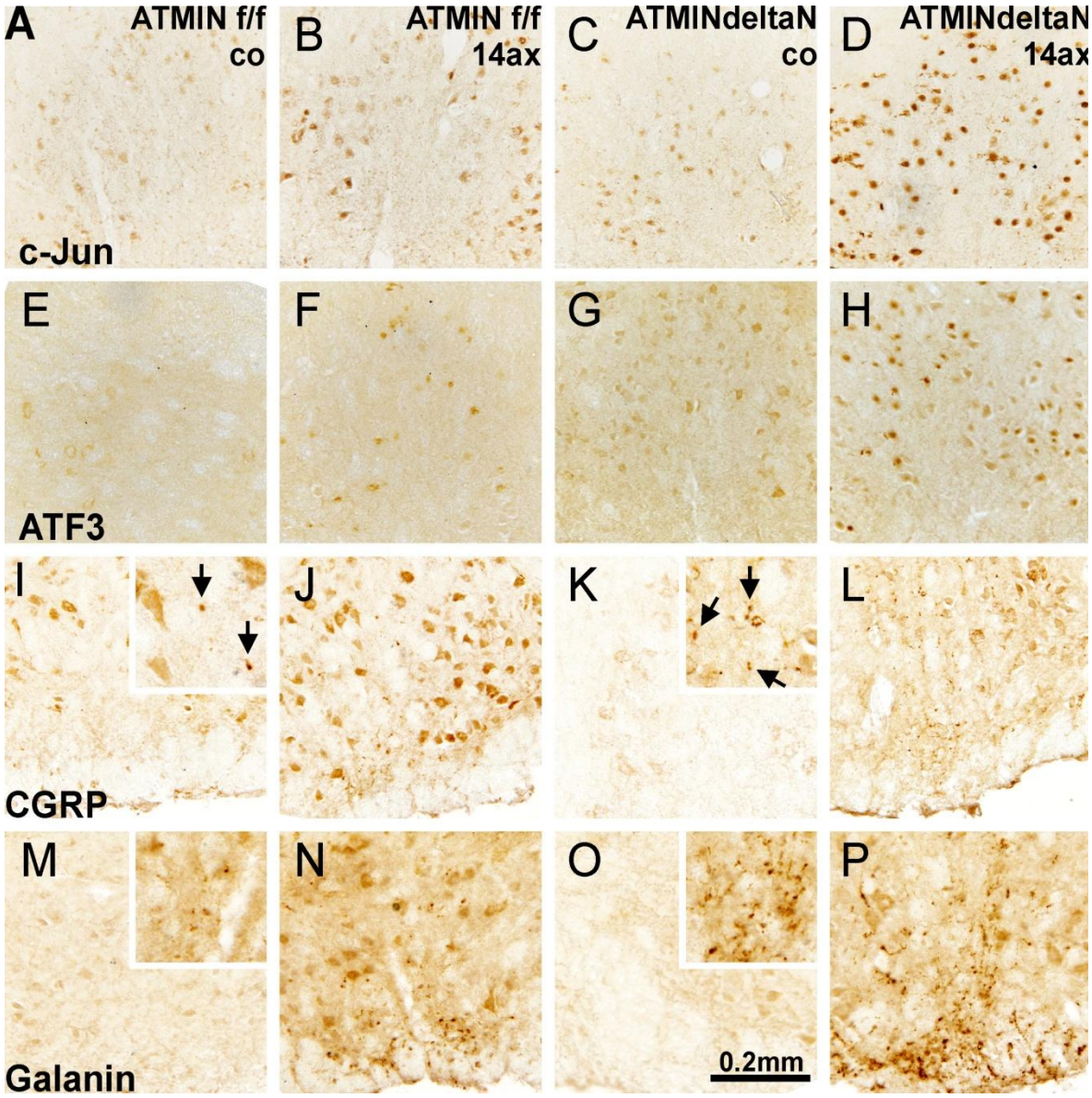

Figure 7-3: ATMIN$^{\Delta N}$ mutants reveal increased neuronal response to axotomy, compared with the ATMIN$^{F/F}$ littermate controls 14 days after nerve cut.
The facial motor nuclei from the ATMIN$^{F/F}$ littermate controls are shown in the 1st&2nd columns (A,B,E,F,I,J,M,N), those from the ATMIN$^{\Delta N}$ mutants are n the 3rd&4th column (C,D,G,H,K,L,O,P). Second and 4th columns are axotomized, 1st&3th columns, contralateral sides, respectively. **A-H:** Effects of ATMIN deletion on axotomy-induced increase in neuronal nuclear c-Jun (A-D) and ATF3 (E-H) immunoreactivity, with enhanced c-Jun staining in axotomized side, as well as a bilateral increase for ATF3 in the ATMIN$^{\Delta N}$ facial motoneurons. **I-P:** Axotomy-induced central sprouting of CGRP-immunoreactive (I-L) and galanin-immunoreactive (M-P) motor neurites. Note the absence of sprouts on the uninjured side and the increased sprouting density in ATMIN$^{\Delta N}$ mutants. The inserts in I, K, M and O show the sprouting response on the injured side at 5x fold higher magnification. Scale bar. 40um in the inserts and 0.2mm for all other micrographs.

Baseline and Injury-Induced ATF3 Upregulation

Deletion of ATMIN produced prominent changes in this neuronal response, with clearly enhanced ATF3 immunoreactivity on the uninjured as well as the axotomized side (Figure 7-4A, Figure 7-5A-D), and a significant increase in the number of ATF3+ motoneurons with strong cytoplasmic (Figure 7-4B) and nuclear (Figure 7-4C) immunostaining. Total ATF3 positive cells were 45.3±14.0 on the contralateral side of wild type animals, of which 44.2±13.7 cells expressed it solely in the cytoplasm and 1.1±0.9 cells expressed ATF3 nuclearly (N=7). In ATMIN null mutants, 52.4±16.2 facial motor neurons expressed ATF3 on average on the control side, of which 49.0±15.2 expressed it cytoplasmically and 3.4±2.6 expressed ATF3 in the nucleus (N=5). Average numbers of ATF3 positive cells in the injured facial motor nucleus of control animals were 66.4±6.4 (N=7) and were 108.7 ± 5.4 (N=5) for their mutant littermates ($p<0.01$ in unpaired Student's T-test). Of those cells, the quantity stained solely cytoplasmically – 10.4 ± 4.0 in wild type (N=7) and 27.3±5.5 in $ATMIN^{\Delta N}$ animals (N=5) - reveal a significant increase in cytoplasmic expression of ATF3 in mutant mice but not wild-type ($p<0.02$ in unpaired Student's T-test). Lastly, motoneurons expressing ATF3 in the nucleus only or in the nucleus and cytoplasm were more prevalent in mutant animals than in their wild type counterparts; wild type animals exhibited 56.0±4.9 (N=7) immunopositive cells and mutants displayed 81.4±6.3 (N=5) per facial motor nucleus ($p<0.05$ in unpaired Student's T-test). Luminosity revealed 0.3±0.1 units of OLV on the control side of wild type animals, with upregulation of ATF3 following injury to 7±1.2. Mutants, however, showed increased baseline measures of ATF3 immunoreactivity (2.6±0.9), with accompanying increases following injury to 13±1.2 units of optical luminosity value (OLV, N=5 for control and transgenic animals, $p<0.05$ in unpaired Student's T-test). Upregulation of ATF3, but not c-Jun, was also observed in other, uninjured parts of the brain of $ATMIN^{\Delta N}$ mutant mice, for example in cerebral motor cortex (see Figure 7-2A-F).

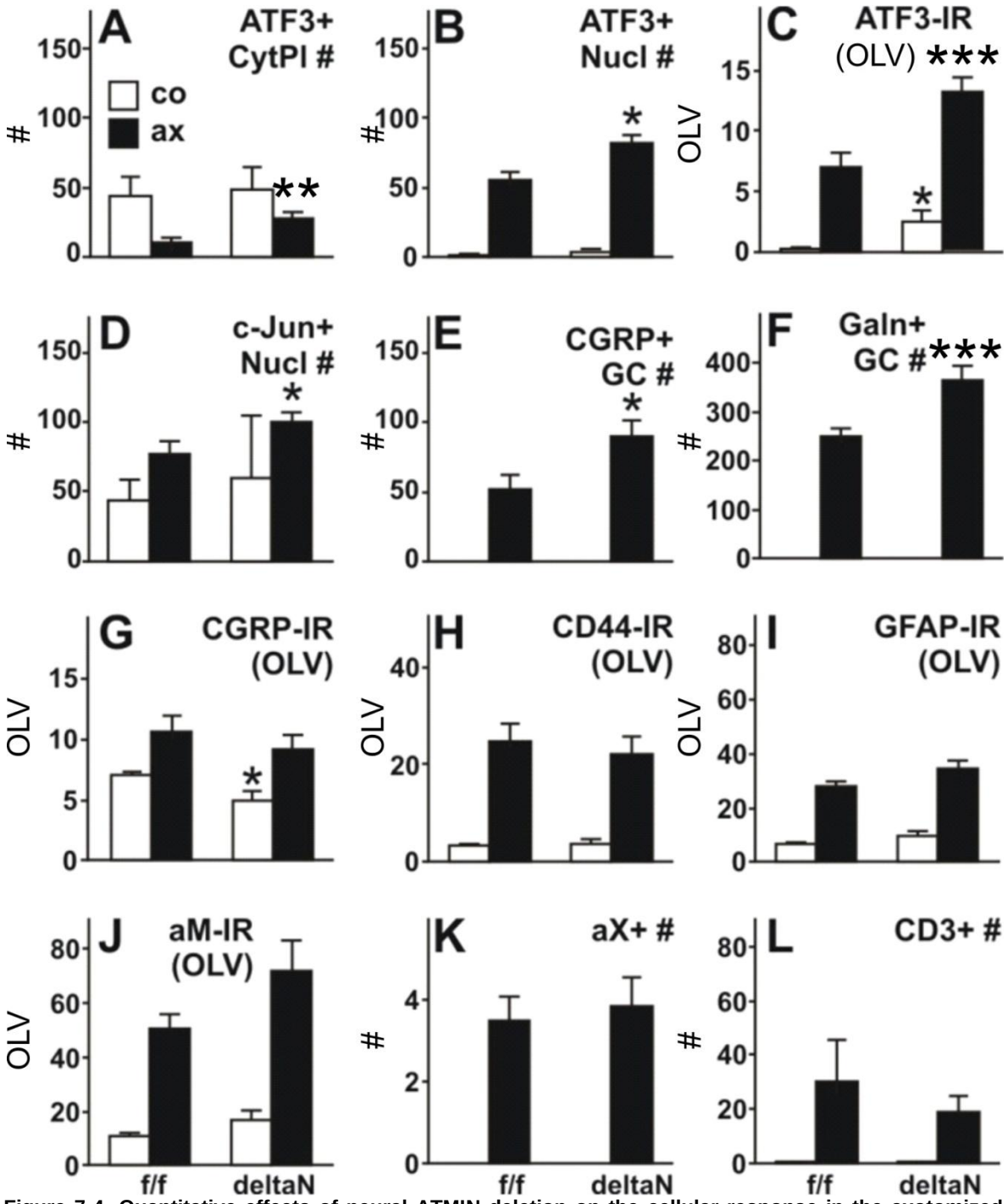

Figure 7-4: Quantitative effects of neural ATMIN deletion on the cellular response in the axotomized facial motor nucleus, 14 days after nerve cut.

A-C: ATF3 Immunoreactivity, showing increase in the number of cytoplasmic (A) and nuclear (B) ATF3+ profiles, and the overall, facial nucleus ATF3-immunoreactivity (C) in the ATMIN$^{\Delta N}$ mutants. A milder increase in the overall ATF3-immunostaining was also observed on the contralateral side. **D:** Increased number of c-Jun+ axotomized motoneurons. **E, F:** Total number of CGRP+ sprouts (E) and the overall nucleus immunoreactivity (F). **G:** Total number of Galanin+ sprouts. **H-J:** Neuronal CD44 (H), astrocyte GFAP (I) and microglial αM (J) immunoreactivity is strongly increased after axotomy, but not affected by ATMIN deletion. **K, L:** αX+ phagocytic microglial clusters (K) and newly recruited, CD3+ T-cells (L) are only observed on the axotomized side. Again, their numbers are not affected by neural deletion of ATMIN. Mean +/- standard error of the mean (SEM) in this and following graphs, n=5 animals per group, filled bar: axotomized$^{\Delta N}$, empty bar:

7.1.1.1 c-Jun upregulation following injury

Furthermore, the number of c-jun immunopositive cells post-injury was greater in ATMIN deficient animals than in their wild-type littermates ($p<0.05$ in unpaired Student's T-test, Figure 7-4D, Figure 7-5E-H). Although baseline expression levels were similar - control animals averaged 43.2±15.7 c-jun immunopositive neurons in the contralateral facial motor nucleus (N=5) and ATMIN null littermates showed 60.4±44.1 (N=5) – the number of c-jun immunoreactive neurons was increased in mutants compared to controls after injury. Wild type animals exhibited 76.6±9.5 c-Jun immunopositive motor neurons on the axotomized side (N=5). ATMIN mutants had 100.6±7.0 c-Jun immunopositive motor neurons on the axotomized side (N=5). These data, taken together, propose a regulatory role for ATMIN in neurite outgrowth, elongation and guidance.

7.1.1.2 No Injury-Induced Difference in Cell Neuropeptide or Adhesion Molecule Expression

With respect to general immunoreactivity, facial axotomy elicited a pronounced increase in the overall immunostaining density for CD44 (Figure 7-4E), CGRP (Figure 7-4F) and Galanin (not shown). However, compared to the $ATMIN^{F/F}$ controls, there was no $ATMIN^{\Delta N}$ induced, overall change for CD44 or galanin, and even a reduction in the constitutively present CGRP-immunoreactivity in the uninjured, facial motoneurons. In wild type animals, CGRP contralateral expression was 7.1±0.2 and ipsilateral expression was 10.6±1.3 OLV (N=7). Mutants showed contralateral expression of 4.9±0.9 and ipsilateral expression of 9.2±1.1 OLV (N=5). Galanin contralateral expression was 18.1±1.0 and ipsilateral expression 24.0±1.6 OLV for littermate controls (N=7) and transgenic contralateral expression was 16.7±3.6, with ipsilateral expression of 23.5±4.9 OLV (N=5). Lastly, CD44 levels were 3.5±0.3 on the contralateral side of wild type animals and 24.9±3.5 OLV

following facial nerve injury (N=7) and mutant baseline expression did not differ: contralateral expression was 3.8±0.7and ipsilateral expression was 22.0±3.8 OLV; (N=5).

7.1.1.3 Increased Central sprouting in ATMIN$^{\Delta N}$ Mutants

In addition to the enhancement of growth-related transcription factors, ATMIN$^{\Delta N}$ mutants presented increased levels of Galanin (Figure 7-4G, Figure 7-5I-L) and CGRP (Figure 7-4H, Figure 7-5M-P) immunoreactive sprouts following injury. The number of Galanin immunopositive central sprouts in injured ATMIN$^{F/F}$ facial motor nuclei was, 249±18. ATMIN$^{\Delta N}$ mutants showed an almost 70 percent increase, with 366± 29 in injured nuclei. Likewise, CGRP showed an almost twofold upregulation in ATMIN$^{\Delta N}$ mutants. Following injury, neurite number for ATMIN$^{F/F}$ was 51±11 and ATMIN$^{\Delta N}$ mutants averaged 90± 11 per nucleus.

7.1.2 Neuronal survival and functional recovery.

Since 20-40% of adult axotomized mouse facial motoneurons die within 4 weeks of nerve cut (Ferri et al., 1998b; Serpe et al., 2003a; Makwana, Serchov, et al., 2009), we next explored the effect of ATMIN deletion on neuronal survival by counting cresyl-violet stained motoneurons in 20um serial sections throughout the facial nuclei, 28 days after transection (Figure 7-6A,B). ATMIN$^{F/F}$ controls showed a 23+/-3% cell loss (n=13 mice, mean+/-standard error of mean/SEM here and in all following sets of data), with 2251+/-89 motoneurons in the facial nucleus on the uninjured, and 1716+/-77 on the axotomized side. Very similar numbers were also observed in the ATMIN$^{\Delta N}$ mice, with 21+/-2% cell loss, and with 2141+/-78 motoneurons on the uninjured and 1695+/-73 on the injured side.

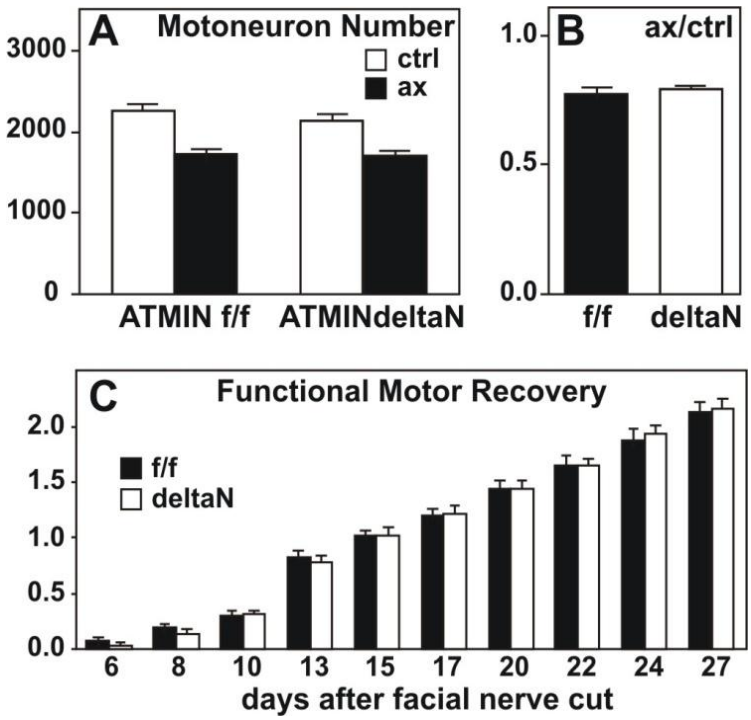

Figure 7-5: Neural deletion of ATMIN does not affect neuronal survival
(A, B) or functional recovery (C) following facial nerve cut. **A, B:** Number of facial motoneurons on the uninjured, contralateral and axotomized side (A) and axotomized/contralateral ratio (B), 30 days after facial nerve cut. **C:** Recovery of whisker hair movement, on a scale of 0 (no movement) to 3 (normal strong movement similar to that of contralateral side). N = 13 $ATMIN^{F/F}$ and 11 $ATMIN^{\Delta N}$ mice in A&B, and 12 and 12, respectively, in C.

As with neuronal survival, neural deletion of ATMIN did not affect functional recovery after facial nerve cut using the whisker hair test. Briefly, extent of whisker movement was scored by three observers unaware of the genotypes, on a scale of 0 (no movement) to 1 (barely observable), 2 (moderate) and 3 (strong, normal movement, as on the control side). As shown in Figure 7-6C, no differences were observed at any of the time points 6 to 27 days post axotomy. Twenty-six days after facial nerve transection, both control and mutant mice showed strong normal movement on the uninjured side (3.0). On the ipsilateral side, control animals had an average motor score of 2.13 ± 0.09 (n = 14). $ATMIN^{\Delta N}$ mice showed no significant difference in motor performance to their wild-type counterparts and exhibited an average motor score of 2.16 ± 0.09 (n=8).

7.1.3 Non-neuronal cell response.

The neuronal response is normally accompanied by glial and immune activation, with increased number of αM immunopositive microglia, de novo expression of GFAP-immunoreactivity in reactive astrocytes, and the influx of CD3 immunopositive T-cells into

the injured part of the central nervous system. In the presence of neuronal cell death, in the mouse facial motor nucleus this reaches its maximum 14 days after nerve cut (Moller et al., 1996), local microglia will transform into brain macrophages that remove neural debris and express high levels of phagocyte specific markers such as the αXβ2 integrin (Kloss et al., 1997; Kalla et al., 2001; Raivich et al., 1999; Schwaiger et al., 1998). As shown in Figure 7-4I-L, the deletion of neural ATMIN did not affect the increase in the immunoreactivity for astrocyte GFAP (Figure 7-4I) and microglial αM (Figure 7-4J), the influx of CD3 positive T-cells (Figure 7-4L) and the number of αX immunoreactive phagocytic microglial clusters (Figure 7-4K), 14 days post-axotomy, which corresponds with the lack of effect of ATMIN on neuronal survival. The average number of CD3 immunopositive T-cells on the contralateral side was 0.3±0.1 (N=7) for controls and 0.4±0.2 for mutants (N=5); on the ipsilateral side, wild types averaged 30.3±15.2 CD3 positive T-cells (N=7) and mutants exhibited 18.8±5.9 (N=5). Baseline astrocyte activation, as measured by GFAP immunoreactivity on the contralateral side, was 6.8±0.6 for wild type animals (N=5) and 9.8±1.7 for mutants (N=5); on the injured side, controls exhibited 28.2±1.4 average pixel values while ATMIN null mutants averaged 34.4±3.3. Activated microglial marker αM baseline activation was 10.7±1.2 in wild type animals (N=6) and 16.9±3.5 in mutants (N=5). After injury, there was no difference between wild type and mutant animals – controls showed 50.6±5.1 pixels and mutants showed upregulation to 71.7±11.4 pixels. Lastly, phagocytic microglial marker αX integrin showed no differences between ATMINF/F and ATMINΔN animals. While phagocytic microglia were not present in the uninjured facial motor nuclei of either wild type or mutant animals, 3.5±0.6 and 3.85±0.7 immunoreactive cells were present in the axotomized facial motor nucleus of ATMINF/F and ATMINΔN animals respectively.

7.2 The Role of ATMIN in Peripheral Target Reinnervation

Reinnervation of the peripheral target was determined by a 48 hour retrograde labelling of facial motoneurons with FluoroGold (FG) injected into the facial whisker pad 28 days after nerve cut. Retrograde FluoroGold labelling of intact motoneurons on the uninjured, contra-animal side served as an intra-animal control. Under normal conditions, using a 1/64x intensity filter, to observe just the brightly fluorescent, FluoroGold immunoreactive motoneurons (Figure 7-6B), facial nucleus sections from control $ATMIN^{F/F}$ animals revealed 159±13 FluoroGold motoneurons on the uninjured (contralateral) side and 101±16 on the ipsilateral, formerly axotomized side (n=12 mice). Relatively similar numbers were also observed for the $ATMIN^{\Delta N}$ mutants (n=12), with 170±9 retrogradely labelled motoneurons on the uninjured side and 130±15 following facial nerve cut (p= 49% and 20%, respectively, compared to $ATMIN^{F/F}$, unpaired Student's t-test).

A further 4-fold increase in fluorescence intensity using 1/16x filter to also allow detection of moderately and weakly fluorescent neurons did reveal ATMIN-specific differences. As shown in Figure 7-6C, $ATMIN^{F/F}$ controls displayed 186± 15 FluoroGold immunopositive motoneurons on the contralateral and 169±23 on the axotomized side; the $ATMIN^{\Delta N}$ mutants showed a similar number of 196±13 motoneurons on the uninjured side (p = 59%), but 251± 23 on the axotomized side (p=2%), an approx 50% increase compared with the control animals.

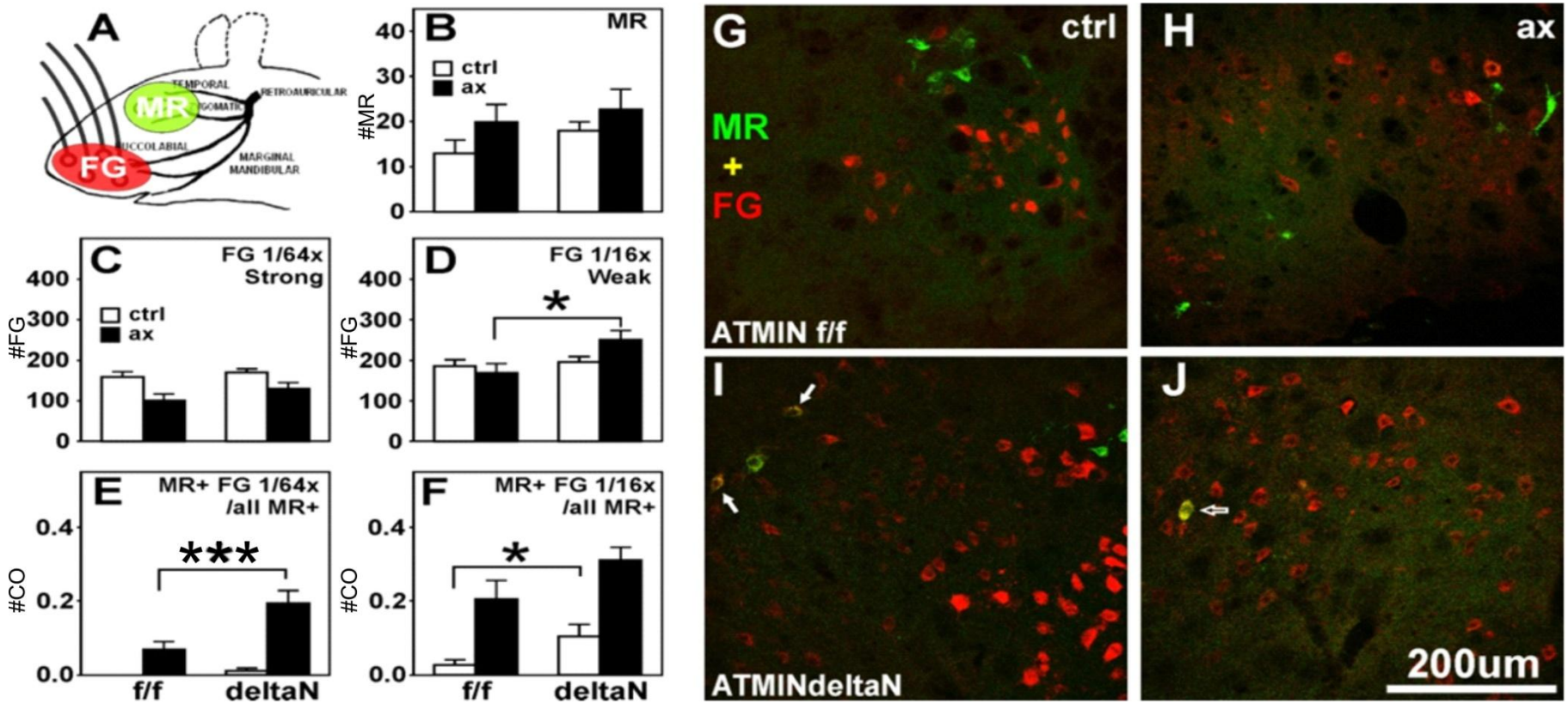

Figure 7-6: Deletion of ATMIN enhances the reconnection of weak and aberrant regenerating axons with their peripheral targets.

A-D: Number of retrogradely labelled facial motoneurons following application of MiniRuby (MR) into the eyelid (B) and FluoroGold (FG) into the whisker pad (C,D) 28 days after facial nerve cut, followed by 48 hours of retrograde transport. A shows a schematic summary of the procedure. Co-injection of retrograde tracers on the contralateral side was used to provide intra-animal uninjured control. ATMIN$^{\Delta N}$ mutants showed a slight trend towards higher numbers for Mini-Ruby labelled motoneurons (B), and the strongly FluoroGold labelled ones, observable with the 1/64x filter (C). However, there was a clear and significant increase in the number of faintly FG-labelled motoneurons, observable with the 1/16x filter, in ATMIN$^{\Delta N}$ mutant mice compared with the ATMIN$^{F/F}$ controls, following axotomy and ensuing regeneration. **E, F:** Number of the double-labelled FG+/MR+ motoneurons, with projections to the eyelid (MR) and whisker pad (FG) as a fraction of all MR+ motoneurons is increased in ATMIN$^{\Delta N}$ mice, for brightly FG+ labelled motoneurons on the axotomized (E), and for the faintly labelled ones on the uninjured side (F). In both cases, there was a similar trend on the contralateral side, but this did not reach statistical significance of 5%. C&D are the results of two separate experiments. *p<5% in unpaired Student t-test, n = 8 ATMIN$^{\Delta N}$ and 8 ATMIN$^{F/F}$ mice in B, E&F; n = 12 ATMIN$^{\Delta N}$ and 12 ATMIN$^{F/F}$ mice in C&D). **G-J:** Tracer Fluorescence for FluoroGold (FG – red pseudocolour) and MiniRuby (MR - green pseudocolour) on the uninjured (G, I) and previously axotomized (H, J) side. The arrows point to 2 faint to moderately double labelled neurons on the uninjured, and a brightly double labelled neuron on the previously axotomized side in the ATMIN$^{\Delta N}$ mutant mouse.

To investigate whether this increase in faint labelling was due to augmented branching of neurons before or following axonal injury, we next carried out a double labelling experiment where the axons innervating the eye muscles were labelled with MiniRuby (MR) and those for the whisker hair pad with FluoroGold. As shown in Figure 7-6A, total MiniRuby counts did not differ between wild type and mutant mice on the injured or contralateral side. However, ATMIN$^{\Delta N}$ animals exhibited a greater, overall number of FG+ MR+ double labelled motoneurons as a fraction of all MR+ neurons. This increase of the double labelled fraction reached statistical significance using unpaired t test on the ipsilateral side at 1/64X filter for the brightly fluorescent motoneurons (Figure 7-6D), and at 1/16x filter for the moderately/faintly labelled cell bodies on the contralateral side (Figure 7-6E). Similar, but borderline changes were also observed for the contralateral (uninjured), brightly fluorescent neurons (p=15%) and the ipsilateral (formerly axotomized) neurons with weak FG fluorescence (p=11%).

7.3 The Role of ATMIN in Central Regeneration

As shown in Figure 7-3, Figure 7-4, Figure 7-5 and Figure 7-6, deletion of ATMIN did not affect functional recovery following facial nerve cut, but it did produce a significant increase in peripheral branching as well as central post-traumatic sprouting. Since the facial motor nerve regenerates well (Werner et al., 2000; Makwana et al., 2009), we postulated that any small advantages conferred by the absence of ATMIN may be masked by the already robust peripheral response, and decided to investigate the deletion effects following spinal cord injury, a system without spontaneous axonal regeneration and very moderate functional recovery due to plasticity of surviving axonal connections.

7.3.1 Dorsal hemisection: Enhanced Number of Aberrant CST sprouts.

ATMIN$^{\Delta N}$ mice and their littermate ATMIN$^{F/F}$ controls underwent left dorsal spinal cord hemisection at the 5th cervical vertebra (C5) level, injected stereotactically with MiniRuby (MR) into the right motor cortex after 30 days, followed by anterograde transport in the corticospinal tract (CST) axons for further 12 days, perfusion fixation and embedding in OCT. Labelled CST axons were quantified in horizontally (longitudinally) cut spinal cord sections of 40um thickness, counting MiniRuby immunoreactive axons crossing a line perpendicular to the longitudinal axis, starting at 1.5mm Rostral to the lesion site and proceeding in 0.5mm increments throughout of the entire depth of the cord tissue, in every 5th consecutive section.

As shown in Figure 7-7, although overall, there was little difference between the ATMIN$^{\Delta N}$ and the ATMIN$^{F/F}$ groups in the total number of MiniRuby immunopositive axons in the ipsilateral CST above the lesion site (+1.5 to +0.5mm), the ATMIN$^{\Delta N}$ mice exhibited a 2-10 fold higher density in other parts of the spinal cord. When these numbers were corrected for the average number of MiniRuby immunoreactive axons in the ipsilateral CST +1.5 to +0.5mm for each individual animal, and then normalized using log (x+0.01) algorithm, statistical analysis using unpaired t-test revealed a significant change ($p<0.05$) in the contralateral CST at +1.5, +1.0 and +0.5mm, the contralateral grey matter (+1.5, +1.0) and even in the ipsilateral CST just above the lesion site (+0.5mm). Borderline changes with a p-value between 0.05 and 0.1 were also observed in the ipsilateral (+1.0) and contralateral (+0.5) lateral white matter, and in the ipsilateral dorsal horn and white matter immediately below the lesion site (-0.5). Results are summarized in Table 12 of the Appendix.

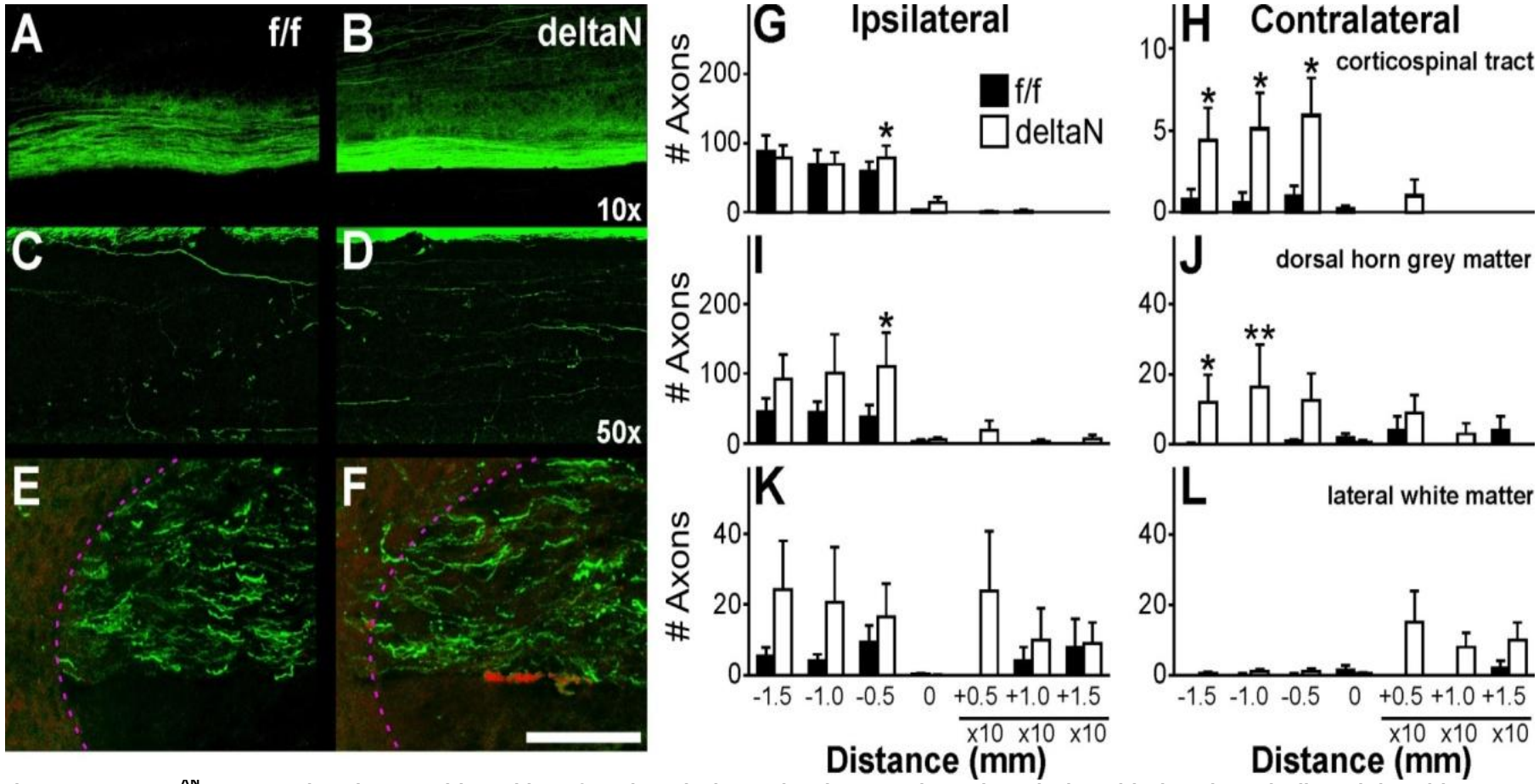

Figure 7-7: ATMIN$^{\Delta N}$ mutants show increased branching of corticospinal tract (CST) axons above the spinal cord lesion site to ipsilateral dorsal horn grey matter and contralateral spinal cord.

Effects following over-midline spinal cord hemisection at C5, transversing ipsilateral CST, dorsal funiculus and dorsal horn, but sparing lateral white matter. CST axons were anterogradely traced for 12 days by MiniRuby injection into contralateral motor cortex 30 days after hemisection. **A-F:** MiniRuby fluorescence in longitudinal (A-D) and transversal sections (E, F) of spinal cord above lesion site at low (A, B) and high (C-F) magnification. In E&F, autofluorescence, additionally shown in red and higher in grey matter tissue, is used to demarcate grey (dorsal horn) from white (dorsal funiculus) matter, the demarcation between the two is indicated by a stippled magenta line. Note the numerous CST fibers crossing into the ATMIN$^{\Delta N}$ grey matter. Scale bar (in F): A,B - 0.5mm, C,D - 0.1mm, E,F – 50um. **G-L:** Number of MR+ axons crossing a hairline, placed perpendicular to the longitudinal spinal axis, at 1.5mm above to 1.5mm below the lesion site, in the corticospinal tract in the dorsal funiculus (G,H), adjacent grey matter

As illustrated in Figure 7-2, like facial motor neurons, ATMIN$^{\Delta N}$ corticospinal neurons that show enhanced branching also exhibit increased levels of nuclear ATF3, without concomitant increases in baseline c-Jun expression, compared to wild-type littermates.

7.3.2 Poorer Fine Motor Performance following Dorsolateral Hemisection.

Since dorsal hemisection only severs the corticospinal tract and the ascending dorsal sensory fibres resulting in relatively moderate motor deficits, we next explored the effects of the C5 dorsolateral hemisection that also cuts the rubrospinal tract (Figure 7-8A), producing a major impairment in gross motor function as well as in the precision of their paw placement. As shown in Figure 7-8B, both ATMIN$^{\Delta N}$ and the ATMIN$^{F/F}$ mice revealed very similar loss of ipsilateral forepaw use in rearing in the cylinder rearing test directly after injury, followed by a moderate recovery in the gross motor function to 20-30% of normal values after 2-4 weeks. In contrast, deletion of ATMIN strongly affected fine motor coordination using paw placement while moving along a horizontally suspended wire grid. Compared with the ATMIN$^{F/F}$ controls, ATMIN$^{\Delta N}$ mutants revealed a significant increase in the number of forepaw footslips on the ipsilateral (Figure 7-8C) as well as on the contralateral (Figure 7-8D) side. Interestingly, deletion of ATMIN did not affect the precision of the hindpaw placement, on the injured or the contralateral side (Figure 7-8E, F). Results are summarized in Table 13 of the Appendix.

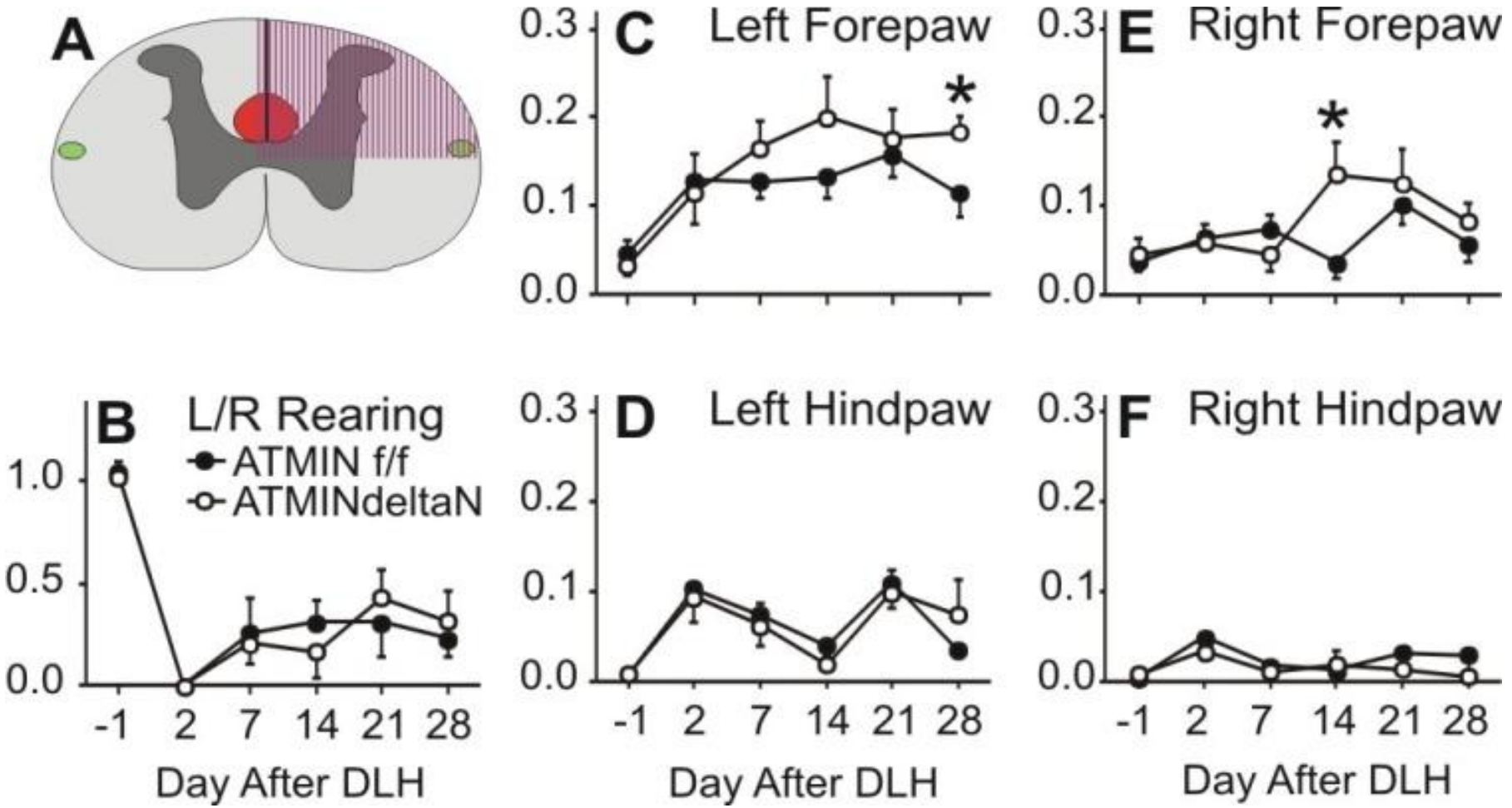

Figure 7-8: ATMIN deletion impairs coordinated functional motor behaviour following dorsolateral C5 hemisection.
A: Schematic summary of the surgical intervention, showing transversal section not only of the dorsal corticospinal tract, dorsal funiculus and dorsal horn, but also of the rubrospinal and lateral corticospinal tracts in the adjacent white matter. B: Forepaw usage in rearing on the injured side is not affected by ATMIN deletion. The Y axis shows fraction of ipsilateral usage as percentage of all rearing attempts. For each attempt, contralateral usage alone was given 0 points, bilateral usage 1 and ipsilateral usage alone 2 points. **C-F:** Incorrect foot placement (footslips) in wire grid test, as a fraction of all placements for the left (C) and right forepaw (D), and left (E) and right hindpaw (F). Dorsolateral hemisection was on the left side. *p<5% in unpaired Student t-test, n= 6 $ATMIN^{F/F}$ and 8 $ATMIN^{\Delta N}$ mice. Data collected 1 day prior (-1) to dorsolateral hemisection served as the pre-trauma control.

ATMIN DISCUSSION: ATMIN IN SPROUTING AND BRANCHING

The 88kD ATMIN protein is newly identified target of ataxia telangiectasia mutated kinase involved in response to stress induced by hypo-osmolarity, UV exposure or hydroxyurea, causing a halt to cell cycle progression, activating checkpoints and promoting cellular repair (Kanu and Behrens 2007; Kanu and Behrens 2008). In the current study, tissue-specific deletion of ATMIN in the nervous system using nestin-promoter driven cre recombinase strongly increases axonal sprouting and branching. These effects were observed in both central and peripheral nervous system, but were also associated with more errors in fine motor coordination, and aberrant multi-target innervation. Neural deletion of ATMIN did not affect speed of peripheral regeneration and gross functional recovery, neuronal cell survival, glial or immune reaction, or most components of the molecular response. However, mutant mice did show a strong neuronal expression of the c-Jun and ATF3 transcription factors that could contribute to the enhanced and frequently aberrant sprouting response, which is normally counteracted in the presence of ATMIN.

7.4 Axonal Projections and Functional Recovery

Neural deletion of ATMIN augmented axonal sprouting and branching in the periphery, as well as in the central part of the nervous system. Compared with the $ATMIN^{F/F}$ controls, mutant mice showed a clear increase in the number of just moderately or faintly retrogradely labelled motoneurons following application of FluoroGold into the whisker pad area 30 days following facial nerve cut and an increase in the number of CGRP-immunoreactive and galanin-immunoreactive motor axon sprouts in and around the axotomized facial motor nucleus, that are known to appear transiently 2 weeks after injury (Makwana, Werner, et al., 2009). ATMIN deletion did not reduce neuronal cell death or

augment neuropeptide expression. In fact, ATMIN$^{\Delta N}$ mutants even exhibited reduced overall CGRP immunoreactivity, suggesting that the increased number of sprouts was not due to the increases in survival or neuropeptide immunostaining, but enhanced branching. A similar, but even stronger, 2-10 fold increase was also observed for the anterogradely, MiniRuby-labelled corticospinal tract axons sprouting into the ipsilateral dorsal horn and projecting into the contralateral CST in the ventral part of the dorsal funiculus above the lesion site. This was accompanied by less retrograde retraction of CST neurites above the lesion site, as well as a trend ($5<p<10\%$) towards higher number of MiniRuby-positive axons, in the dorsal horn and lateral white matter just below the lesion.

Surprisingly, this augmented branching was not associated with improved functional performance. Recovery of gross motor function was unchanged, as illustrated by the more or less identical time course of whisker hair movement improvement in the ATMIN$^{\Delta N}$ mutant mice and their littermate controls following peripheral nerve injury (Figure 7-5C), or the use of affected forelimb in rearing following central injury after the dorsolateral C5 spinal cord hemisection (Figure 7-8B). However, mutant mice showed actual deterioration in forepaw footslips on both the injured and the contralateral side in the grid walking, a test used to assess fine motor coordination. It is possible that the overall motor function was not impeded because the threshold in absolute number of axons for gross function was reached in both control and mutant mice, or that that the higher ratio of improper/proper connections detracted from beneficial effects of enhanced neurite outgrowth.

Although improved sprouting in the CNS is normally associated with a much better functional recovery (Jiang et al., 2007; Karimi-Abdolrezaee et al., 2006; Tysseling-Mattiace et al., 2008; Xiao et al., 2007), the current study suggests that the generation of and failure to prune imprecise connections will impair fine motor performance and coordination. For example, conflicting signals from inappropriately projecting axons could be simultaneously

firing action potentials onto extensor and flexor muscles or onto muscles innervating opposite limbs, resulting in defects in co-ordinated behaviour. Here, the higher number of CST axons projecting into the anatomically inappropriate, contralateral dorsal funiculus could also contribute to the increased number of forepaw footslips on the uninjured side.

Precision defects were also observed in the peripheral, facial nerve projections of mutant mice. Peripheral nerve injury is known to increase number of axons projecting into inappropriate nerves (e.g. motor axons in cutaneous nerves) or the appearance of exuberant innervation of 2 or more disparate targets through the same motoneuron (Melle et al., 2009; Skouras et al., 2009; Suarez et al., 2006; Guntinas-Lichius et al., 2005; Streppel et al., 2002a). However, the multi-innervation of two disparate targets, in the current case, the eye lid and whisker hair projections, was significantly increased in the ATMIN$^{\Delta N}$ mutant mice, identifying ATMIN as a regulatory element that mediates the removal of some, even if not all of the exuberant and imprecise posttraumatic innervation. Interestingly, similar projection imprecision in mutants was also observed on a smaller scale on the contralateral side, which could suggest the involvement of ATMIN not only after injury but also in the initial axonal guidance and the postnatal “sharpening” of somatotopic projection maps in the peripheral nervous system.

7.5 Molecular Mechanisms

At present, the molecular mechanisms of ATMIN are just beginning to be understood. As shown in the present study, ATMIN did not affect neuronal survival, astrogliosis, microglial activation or T-cell recruitment. It also did not affect some prominent components of the molecular response of the injured neuron, for example the post-traumatic increase in CD44 and galanin. However, in addition to its enhanced and imprecise sprouting and worsened fine motor coordination, ATMIN$^{\Delta N}$ mutants did show increase in c-Jun and ATF3

transcription factors, with augmented expression of the former in the injured, and of the latter in both the axotomized and the contralateral, uninjured facial motoneurons. Both c-Jun and ATF3 are AP1 transcription factors that have been shown to mediate in vitro neurite outgrowth (Pearson et al., 2003a; Nakagomi et al., 2003; Campbell et al., 2005; Kiryu-Seo et al., 2008) and cellular response to stress (Chaum et al., 2009). In vivo, forced neuronal expression of ATF3 will strongly improve DRG neurite outgrowth in the injured spinal cord (Seijffers 2007). Neuronal deletion of c-Jun will also abolish post-axotomy neuronal cell death, and strongly reduce peripheral regeneration and central axonal sprouting (Raivich et al., 2004a; Makwana, Werner, et al., 2009). Although both transcription factors could be implicated in promoting sprouting, experiments so far only revealed increased ATF3, but not c-Jun expression in the cerebral motor cortex of $ATMIN^{\Delta N}$ mutant mice Figure 7-2); this pattern did not change following cervical transection of the corticospinal tract (data not shown).

Axonal regeneration in the adult CNS is normally very poor. However, it can be improved by increasing the robustness of neuronal injury response (Lu et al., 1991; Smith et al., 2009; Kalousa et al., 2009; Gordon et al., 2009), removal or neutralisation of extrinsic inhibitory signals including CSPG, NOGO, MAG or OMG (Shen et al., 1998, 2009; Tang et al., 1997; Bradbury et al., 2002; Galtrey et al., 2007; McGee et al., 2003; Robak et al., 2009; Hossain-Ibrahim et al., 2007), or blocking intracellular signals such as RhoA, involved in growth cone collapse following contact with chemorepellant cues (Dergham et al., 2002; Ellezam et al., 2002; Fournier et al., 2003; Wu et al., 2005, 2009). Any one or a combination of these pathways could be affected to produce a combination of more and imprecisely connected new neurite sprouts. However, it is interesting that those pathways, at least those under the control of ATMIN, apparently regulate the fidelity of axonal connections in the central, as well as in the peripheral system, possibly on a side by side

basis. Here, identifying these downstream targets of ATMIN involved in axonal guidance and pruning could help to improve functional recovery following nerve injury.

CHAPTER 8: SUMMARY OF RESULTS

The neuronal regenerative response relies on transcriptional regulation at several different levels. Interactions involving transcription factors, not only in the neuronal cell body, but also in local supporting cells, orchestrate the successful peripheral injury response. These data illustrate that neuronal c-Jun regulates the cellular response to damage; without it, neurons are unable to upregulate several key transcription factors, neuropeptides and adhesion molecules associated with successful regeneration. In addition, c-Jun deficient neurons are less able to recruit and activate non-neuronal cells such as CD3+ T cells, astrocytes and microglia, and also show decreased levels of cell death with accompanying neuronal atrophy of many surviving cells. Although N-terminal phosphorylation does not play a role in the neuronal response to facial motor nerve injury, c-Jun deletion targeted to peripheral Schwann Cells shows downstream opposite effects on survival, with neurons showing increased cell death without Jun-mediated Schwann Cell signals.

Jun is also involved in ATMIN regulation of sprouting and branching following nerve injury. ATMIN-deficient motor neurons display increases in growth-related transcription factors, such as c-Jun and ATF3, as well as increased central sprouting of CGRP and Galanin immunopositive neurites. Anatomically, ATMIN deletion causes increased branching of corticospinal and facial motor nerve axons, both during development and following injury. This increased branching leads to differences in fine, but not gross motor co-ordination.

CHAPTER 9: C-JUN CONCLUSIONS

9.1 Neuronally Expressed c-Jun Regulates the Cellular Response to Injury and is Essential for Cell Death

Neuronal c-Jun is an integral modulator of the peripheral response to Facial motor nerve injury. Genetic ablation of its expression in neurons led to a heavily impaired cellular response, lack of lymphocyte and phagocytic monocyte recruitment to the injured facial motor nucleus, virtually no astrocytic activation and very mild microglial activation following facial nerve section. Upregulation of all of these factors has been implicated in the successful response to peripheral nerve injury, (Butovsky et al., 2006; Jones, Banati, et al., 1997; Jones et al., 2000; Bramanti et al., 2010; Ha et al., 2008; Kloss et al., 1999; Werner et al., 2000; Vogelezang et al., 2001; Raivich et al., 2002; Ekstrom et al., 2003; Gschwendtner et al., 2003; Wallquist et al., 2004). Resultant regeneration was also impaired – both anatomically and functionally - as well as sprouting from the proximal portion of the axotomized nerve stump. Lack of regeneration is probably due to inadequate signalling from injured motoneurons during the cellular response, as well as poor trophic signalling from non-neuronal cells. Perhaps most importantly, despite the lack of cellular response and the vast cell damage resulting from axotomy, injured $Jun^{\Delta S}$ motor neurons were unable to die following facial nerve transection. In addition to increased survival following injury, there seems to also be enhanced survival of $Jun^{\Delta S}$ motor neurons during development – as indicated by a roughly 20% increase in baseline facial motor neuron number in $Jun^{\Delta S}$ mutants. This illustrates the integral regulatory role of jun in the neuronal death response and highlights its potential neuroprotective role in chronic degenerative disease models.

9.2 Schwann Cell c-Jun Is an Important Regulator of Peripheral Nerve Growth that is Necessary for Neuronal Survival

This research indicates that *c-jun* expressed in supporting glia plays an important role in post-traumatic axonal regeneration. The pro-regenerative peripheral cellular injury response is strongly ablated in its absence. In addition to its role in survival signalling to the neuron, Schwann cell c-Jun is an integral component of the chemotactic signalling gradient created after injury and macrophage recruitment is affected by Schwann cell-specific ablation of c-jun. This data describes how Jun-mediated retrograde signalling to the neuron is an import factor in motoneuron survival and that in the absence of a proliferative Schwann cell signal, injured motoneurons cannot survive.

Since regeneration and cell survival are so strongly affected by trophic withdrawal of c-jun, establishment and upregulation of an appropriate c-jun response in central supporting cells - oligodendroglia and astrocytes - might be a possible future treatment strategy for neuronal damage. This study illustrates that c-Jun expression by Schwann cells is essential for regulating cellular response to injury and establishing a successful regenerative system.

9.3 c-Jun N-Terminal Phosphorylation Plays no Role in Facial Nerve Regeneration

The pro-regenerative/pro-apoptotic role of c-jun has been heavily discussed in literature (Suh et al., 2005; Kuan et al., 2003; Raivich et al., 2002; Sun et al., 2006; Herdegen et al., 1991; Ham et al., 1995); however, the *in vivo* role of phospho-jun in the facial motor nerve regenerative response has been previously uncharacterized. Taken together, these data indicate that phosphorylated Jun is not the key c-Jun isoform that regulates its pro-regenerative or pro-apoptotic role after facial nerve transection. This begs the question as to what aspect of Jun facilitates its function in this particular faculty. As discussed earlier in

this report, activation of the c-Jun mediated transcriptional apparatus appears to be affected by interactions at 3 major sites: N-Terminal phosphorylation at Ser 63&73 and Thr 91&93 (Smeal et al., 1994; Morton et al., 2003), dephosphorylation of Thr239 (Morton et al., 2003) and C-terminal lysine acetylation near aa257-276 (Vries et al., 2001). This investigation eliminates the former of these three options as the interaction primarily responsible for c-Jun's role in the neuronal response to facial nerve axotomy. It is commonly said that when a door closes, a window opens; this evidence suggests that perhaps the window of opportunity for exploring the latter two alternative pathways has now opened a little wider. Future studies will characterize the role of alternative c-Jun activation in facial nerve regeneration.

9.4 Overall Implications of c-Jun in Neuronal Regeneration and Repair

C-Jun is an important regulator of the neuronal response to injury. Thus, c-junf/f, Synapsin::Cre animals exhibit defects in functional and anatomical reinnervation following facial nerve transection. Schwann cell *c-jun* deletion shows a copy number dependent decrease in specific reinnervation (ax/co) – each copy of deleted c-jun halves the number of anatomical connections made. Animals lacking neuronal c-Jun are resistant to neuronal cell death following injury and exhibit severely impaired non-neuronal cell recruitment and a much reduced molecular response compared to wild type controls. c-Jun in Schwann Cells shows reverse function in neuronal cell survival. Without Schwann cell c-Jun signalling, injured facial motoneurons had lower levels of survival. Although Schwann cell c-Jun has no affect on neuronal cellular response, it enhances successful target reinnervation. After injury, facial axons are less able to form functional connections in its absence. Evidence involving Nestin::Cre mediated neuroepithelial excision of *jun* in both Neurons and Schwann Cells (Raivich et al., 2004a) shows a phenotype similar to

Synapsin::Cre mediated neuronal excision – indicating that neuronal Jun signalling is upstream of Schwann cell mediated Jun survival signals. Interestingly, c-Jun phosphorylation state does not seem to play a major role in the regenerative response to facial motoneuron injury. There were no major differences in survival, cellular response or reinnervation after facial nerve axotomy between JNK1-3 and JunAA mutants and their wild type controls. Taken together, these data indicate that c-Jun is a powerful Transcriptional regulator, both in the periphery and the central nervous system, that controls trophic propensity in Schwann cells and upstream cellular response, regeneration and survival in neurons.

CHAPTER 10: ATMIN CONCLUSIONS

10.1 ATMIN is an Important Guidance Molecule in Neuronal Regeneration

Nestin::Cre targeted ATMIN deletion results in altered cell body response to neuronal injury and is associated with increased branching of previously intact, as well as regenerating, facial motoneurons. 14 days after FNA, ATMIN mutants upregulate c-Jun & ATF3 in the Facial motor nucleus– co-expression of these transcription factors has previously been associated with increased sprouting in vitro (Pearson et al., 2003a; Nakagomi et al., 2003; Campbell et al., 2005; Kiryu-Seo et al., 2008) and cellular response to stress (Chaum et al., 2009). Indeed, Furthermore, double labelling of distal temporal and zygomatic (with MiniRuby), and buccolabial (with Fluorogold) facial motor nerve branches results in increased numbers of facial motor nerve cell bodies expressing both MiniRuby and Fluorogold in mutant animals. Despite an increase in growth marker expression and anatomical reinnervation, 30 day functional recovery and motoneuron survival remained unaffected in PNS facial motor nerves. Further studies carried out in the CNS after Dorsal and Dorsolateral Spinal Cord Hemisection show increased anatomical cross-innervation (more axons in ipsilateral grey matter and contralateral white matter) in $ATMIN^{\Delta n}$ mutants compared to wild type controls. This correlates with an increased number of both contralateral and ipsilateral forepaw slips from these animals on a grid test. Despite deficits in fine motor placement, weight bearing and gross co-ordination of motor movement, as demonstrated by the cylinder rearing test, remain unaffected. This highlights the inhibitory role of ATMIN in axonal trafficking both after injury and during development.

CHAPTER 11: GENERAL CONCLUSIONS

Table 2: c-Jun in Regeneration following Injury, a Summary

	Survival	**Gross Motor Recovery**	**Fine Motor Recovery**	**Neuronal Response**	**Non-Neuronal Response**
c-Jun CNS deletion (Raivich et al., 2004)	↑ Atrophic	↓	↓	↓ to Absent	Astrocytes ↓ Phagocytes X Lymphocytes X
c-Jun Neuronal Deletion	↑ Atrophic	↓	↓	↓ to Absent	Astrocytes ↓ Phagocytes X Lymphocytes X
c-Jun Schwann Cell Deletion	↓	↓	↓	No Difference	No Difference (↑ phagocytes to clear up ↑ cell death)
c-Jun Phosphorylation Deficiency	No Difference	No Difference	No Difference	No Difference	No Difference
c-Jun upregulation (via ATMIN deletion)	No Difference	No Difference	↑ Sprouting, ↓ co-ordination	↑ Growth-Associated TFs and NPs (↑ C. Sprouting)	No Difference

This series of experiments shows the complex and multi-faceted role of c-Jun in the neuronal response to injury and stress. c-Jun is needed for neuronal cell death and lymphocyte influx following injury, as well as the neuronal signalling response to stress. These experiments show that, in particular, neuronal c-Jun is the most prominent or upstream orchestrator of this response, since Neuronal+Schwann Cell deletion (via the Nestin Promoter) shows the same injury phenotype as Neuronal deletion alone (via the Synapsin promoter). This phenotype is different from that displayed by Schwann Cell-specific deletion (via P0 promoter). Although Schwann Cell Jun has no effect on the neuronal cell response to stress, neuronal survival is decreased in its absence; contrastingly, neuronal survival is enhanced by Jun deletion in the Neuron. Phosphorylation state does not have an affect on c-Jun function in peripheral facial motoneuron regeneration. These experiments also show that c-Jun signalling – in both

neurons and Schwann cells - is necessary for functional axonal recovery following injury, as mutants show decreased reinnervation following facial nerve injury in both instances.

In agreement with c-Jun deletion data, upregulation of injury-induced c-Jun via neural deletion of ATMIN shows complementary results. ATMIN deficient animals showed upregulation of growth associated transcription factors and neuropeptides both baseline (ATF3) and following facial nerve injury (ATF3, c-Jun, CGRP and galanin), although non-neuronal cell recruitment and neuronal survival was normal. ATMIN deletion caused increased peripheral and central misrouting that did not interfere with gross motor performance when rearing, but impeded precise motor coordination and paw-placement, resulting in increased number of forepaw footslips in grid-walking tasks.

Taken together, these results highlight the dual and cell-specific role of c-Jun in neuronal regeneration and repair. Schwann cell c-Jun signalling during the de-differentiaton response to axotomy is essential for Schwann cell support of the injured neuron resulting in neuronal survival; conversely, Jun in the neuron is necessary for neuronal cell death and cellular response to axotomy-induced stress. Upregulation of it and ATF3 via ATMIN deletion leads to increased, albeit aberrant axonal sprouting. Novel understanding of this versatile and complex transcriptional regulator, gleaned through this study, will prove integral in the further translation of c-Jun-related treatment strategies for neuronal injury and will positively shape the future of regenerative medicine.

CHAPTER 12: APPENDIX

Table 3: Immunohistochemical Antibody Data for Cellular Response Trials.

ATF3	1:300	Rabbit (Rb)	Titration	Gift from Prof. PN Anderson	Goat Anti-Rabbit
CD3	1:1600	Rat (Rt)	Titration	Chemicon	Goat Anti-Rat
CD44	1:1000	Rat	Titration	Chemicon	Goat Anti-Rat
CGRP	1:800	Rabbit	Titration	Penninsula Lab ICH	Goat Anti-Rabbit
c-Jun	1:200	Rabbit	Titration	Santa Cruz	Goat Anti-Rabbit
GALANIN	1:400	Rabbit	Titration	Penninsula Lab ICH	Goat Anti-Rabbit
GFAP	1:6000	Rabbit	Stable	Zymed	Goat Anti-Rabbit
αM	1:5000	Rat	Stable	Serotec	Goat Anti-Rat
αX	1:200	Hamster (Hm)	Titration	Novus Molecular Inc	Goat Anti-Hamster
β1 Integrin	1:300	Rat	Titration	Chemicon	Goat Anti-Rat

Table 4: Impaired Cellular Response in c-Jun$^{\Delta S}$ animals.

			4 Days		14 Days	
			Contralateral	Ipsilateral	Contralateral	Ipsilateral
CGRP	**c-Jun$^{F/F}$**	**Average**	**46.3**	**62.2**	**41.3**	**54.6**
		SEM	**2.9**	**2.1**	**4.8**	**2.4**
		N	**5.0**	**5.0**	**9.0**	**9.0**
	c-Jun$^{\Delta S}$	Average	46.9	50.4	47.9	45.6
		SEM	3.3	3.4	2.4	1.7
		N	4.0	4.0	6.0	5.0
GALANIN	**c-Jun$^{F/F}$**	**Average**	**6.6**	**13.4**	**6.7**	**13.0**
		SEM	**1.2**	**3.3**	**0.9**	**1.4**
		N	**5.0**	**5.0**	**10.0**	**10.0**
	c-Jun$^{\Delta S}$	Average	4.9	5.6	9.8	8.1
		SEM	0.6	0.8	1.6	1.2
		N	5.0	5.0	6.0	6.0
CD44	**c-Jun$^{F/F}$**	**Average**	**9.3**	**51.7**	**7.5**	**45.2**
		SEM	**1.2**	**4.8**	**1.5**	**9.1**
		N	**5.0**	**5.0**	**10.0**	**10.0**
	c-Jun$^{\Delta S}$	Average	12.8	15.9	8.2	13.3
		SEM	1.8	1.8	2.5	4.2
		N	5.0	5.0	6.0	6.0
BETA 1	**c-Jun$^{F/F}$**	**Average**	**5.8**	**9.3**	**7.6**	**17.0**
		SEM	**0.4**	**0.7**	**1.1**	**1.8**
		N	**5.0**	**5.0**	**10.0**	**10.0**
	c-Jun$^{\Delta S}$	Average	6.7	6.0	5.3	6.5
		SEM	1.5	0.9	0.4	0.6
		N	5.0	5.0	6.0	6.0
ATF3	**c-Jun$^{F/F}$**	**Average**	**30.5**	**41.7**	**29.1**	**40.8**
		SEM	**3.0**	**1.2**	**1.9**	**2.7**
		N	**5.0**	**5.0**	**9.0**	**9.0**
	c-Jun$^{\Delta S}$	Average	26.8	27.8	28.3	30.9
		SEM	3.6	1.7	3.4	3.0
		N	5.0	5.0	6.0	6.0
Data Measured in OLV						

Table 5: Alpha M (MAC-1) Expression Day 4 and 14 After Facial Nerve Axotomy in JNK mutants

Alpha M	Day 4						Day 14				
	Contra		Ipsi				Contra		Ipsi		
	Mean	SEM	Mean	SEM	N		Mean	SEM	Mean	SEM	N
WT1	18.2	1.6	45.6	3.4	5		14.5	2.4	49.3	9.0	5
JNK1	19.8	1.6	45.5	2.9	3		15.2	2.3	49.2	7.5	5
WT2	15.4	1.8	59.4	6.9	3		11.2	1.3	50.9	10.6	3
JNK2	19.0	2.5	42.5	3.4	4		12.7	1.4	84.9	5.4	6
WT3	11.1	4.5	52.9	14.5	3		11.7	2.0	56.3	5.2	4
JNK3	14.7	1.5	41.5	8.5	3		10.7	1.8	58.9	6.0	3
WTAA	10.3	1.2	35.6	1.4	5		10.4	0.6	50.0	5.6	7
JunAA	11.4	0.7	35.3	2.2	5		7.7	0.7	61.5	3.4	7

Table 6: GFAP Expression Day 4 and 14 After Facial Nerve Axotomy in JNK mutants

GFAP	Day 4						Day 14				
	Contra		Ipsi				Contra		Ipsi		
	Mean	SEM	Mean	SEM	N		Mean	SEM	Mean	SEM	N
WT1	17.2	2.6	65.9	8.9	5		14.7	2.5	69.9	8.8	3
JNK1	11.6	1.6	61.8	6.3	4		9.1	0.6	40.1	13.7	2
WT2	10.7	1.0	36.0	1.2	3		11.2	1.3	50.9	10.6	3
JNK2	13.5	3.8	47.4	6.1	4		11.7	2.0	56.3	5.2	4
WT3	9.3	1.5	44.3	9.3	4		12.4	1.3	12.4	1.3	6
JNK3	15.3	1.4	70.9	10.1	4		10.7	1.8	58.9	6.0	3
WTAA	9.0	2.3	40.3	2.0	5		21.5	1.1	49.6	2.9	7
JunAA	11.0	1.9	42.3	2.9	5		22.1	1.5	60.2	3.4	7

Table 7: CD3 Expression Day 14 After Facial Nerve Axotomy in JNK mutants

CD3	Day 14				
	Contralateral		Ipsilateral		
	Mean	SEM	Mean	SEM	N
WT1	3.7	1.2	42.0	13.3	5
JNK1	6.0	2.1	54.1	12.3	5
WT2	4.5	1.0	34.8	4.6	3
JNK2	2.6	0.9	28.7	6.2	5
WT3	6.0	0.5	34.9	3.9	6
JNK3	2.0	0.8	8.4	0.4	4
WTAA	0.1	0.1	9.0	3.5	7
JunAA	0.4	0.2	15.1	4.2	7

Table 8: B 7.2 Expression Day 14 After Facial Nerve Axotomy in JNK mutants

B7.2	Day 14				
	Contralateral		Ipsilateral		
WT1	Mean	SEM	Mean	SEM	N
JNK1	3.0	0.8	28.0	5.1	6
WT2	2.8	0.8	39.5	8.4	8
JNK2	4.6	1.2	18.9	1.7	4
WT3	4.7	2.2	37.6	7.1	4
JNK3	3.5	0.7	26.1	7.3	4
WTAA	5.3	2.3	16.9	4.9	5

Table 9: CD44 Expression Day 4 and 14 After Facial Nerve Axotomy in JNK Animals

CD44	Day 4						Day 14				
	Contra		Ipsi				Contra		Ipsi		
	Mean	SEM	Mean	SEM	N		Mean	SEM	Mean	SEM	N
WT1	7.3	0.6	43.2	6.4	5		5.3	0.9	39.5	4.2	4
JNK1	7.8	1.6	43.7	1.9	5		7.0	3.4	30.6	3.3	5
WT2	6.3	0.8	22.1	5.4	3		5.3	1.2	35.2	6.3	4
JNK2	5.6	0.9	29.5	3.6	4		5.0	0.4	32.2	4.1	6
WT3	6.7	0.9	39.0	4.4	4		8.0	0.6	59.9	2.3	4
JNK3	7.0	1.8	38.9	5.3	3		5.1	0.5	37.6	6.8	3
WTAA	3.4	0.7	28.7	1.8	5		4.8	0.9	31.9	1.7	7
JunAA	3.9	0.7	22.0	0.1	5		6.2	0.6	31.9	1.8	7

Table 10: CGRP Expression Day 4 and 14 After Facial Nerve Axotomy in JNK Animals

CGRP	Day 4						Day 14				
	Contra		Ipsi				Contra		Ipsi		
	Mean	SEM	Mean	SEM	N		Mean	SEM	Mean	SEM	N
WT1	6.5	0.5	8.1	1.5	4		6.5	0.5	8.1	1.5	4
JNK1	7.1	1.5	9.9	1.8	5		7.1	1.5	9.9	1.8	5
WT2	8.4	0.8	11.1	1.6	3		7.8	0.3	12.1	1.2	2
JNK2	8.2	0.6	16.3	4.0	3		6.6	1.0	9.5	1.8	4
WT3	5.7	0.9	9.0	1.1	5		7.7	0.7	12.0	1.9	6
JNK3	5.9	0.3	9.9	0.6	4		6.2	0.7	8.6	1.9	4
WTAA	16.2	1.9	27.4	1.8	5		33.0	2.4	30.8	1.2	7
JunAA	20.0	2.1	27.6	4.1	5		26.9	1.8	27.2	1.2	7

Table 11: ATF3 Expression Day 4 and 14 After Facial Nerve Axotomy in JNK Animals

ATF3	Day 4						Day 14				
	Contra		Ipsi				Contra		Ipsi		
	Mean	SEM	Mean	SEM	N		Mean	SEM	Mean	SEM	N
WT1	10.8	2.2	24.4	2.9	4		9.2	1.1	14.0	2.2	3
JNK1	9.8	0.4	22.8	1.5	4		7.5	1.2	10.5	2.1	5
WT2	12.0	3.6	29.4	6.7	3		7.6	0.9	12.1	1.2	3
JNK2	7.5	0.7	23.5	3.7	4		8.1	1.3	12.5	1.1	5
WT3	7.3	0.7	13.9	1.9	5		11.0	1.2	19.9	1.2	6
JNK3	9.3	0.9	17.7	1.1	4		12.8	1.0	23.3	5.2	4

Table 12: Anatomical Recovery Following DH in ATMIN-null Mutants

Contralateral White		ATMIN +/+			ATMIN -/-		
Distance From Lesion		Mean	SEM	N	Mean	SEM	N
	-1.5	0.0	0.0	4	0.0	0.0	5
	-1	0.3	0.3	4	0.6	0.6	5
	-0.5	0.0	0.0	4	0.6	0.6	5
	0	1.8	1.8	4	0.0	0.0	5
	+05	0.0	0.0	4	6.0	6.0	5
	+1	0.0	0.0	4	2.0	2.0	5
	+1.5	0.0	0.0	4	6.0	6.0	5
Contralateral Grey		ATMIN +/+			ATMIN -/-		
Distance From Lesion		Mean	SEM	N	Mean	SEM	N
	-1.5	0.3	0.3	4	17.0	12.4	5
	-1	0.0	0.0	4	24.4	19.0	5
	-0.5	0.8	0.5	4	17.0	12.2	5
	0	1.0	0.7	4	1.0	1.0	5
	+05	5.0	5.0	4	6.0	6.0	5
	+1	0.0	0.0	4	4.0	4.0	5
	+1.5	5.0	5.0	4	0.0	0.0	5
Contralateral CST		ATMIN +/+			ATMIN -/-		
Distance From Lesion		Mean	SEM	N	Mean	SEM	N
	-1.5	0.3	0.3	4	5.8	3.0	5
	-1	0.0	0.0	4	6.4	3.2	5
	-0.5	0.5	0.5	4	7.6	3.4	5
	0	0.3	0.3	4	0.0	0.0	5
	+05	0.0	0.0	4	2.0	2.0	5
	+1	0.0	0.0	4	0.0	0.0	5
	+1.5	0.0	0.0	4	0.0	0.0	5
Ipsilateral CST		ATMIN +/+			ATMIN -/-		
Distance From Lesion		Mean	SEM	N	Mean	SEM	N
	-1.5	68.5	16.6	4	100.4	22.2	5
	-1	49.8	13.7	4	84.4	25.5	5
	-0.5	50.5	13.4	4	89.0	27.9	5
	0	3.5	1.3	4	13.6	10.7	5
	+05	0.0	0.0	4	2.0	2.0	5
	+1	2.5	2.5	4	0.0	0.0	5
	+1.5	0.0	0.0	4	0.0	0.0	5
Ipsilateral Grey		ATMIN +/+			ATMIN -/-		
Distance From Lesion		Mean	SEM	N	Mean	SEM	N
	-1.5	29.8	10.8	4	120.6	52.6	5
	-1	32.5	12.4	4	131.0	89.1	5
	-0.5	24.3	13.6	4	151.8	72.7	5
	0	3.5	3.5	4	7.6	4.8	5
	+05	0.0	0.0	4	30.0	21.4	5
	+1	0.0	0.0	4	4.0	4.0	5
	+1.5	0.0	0.0	4	10.0	10.0	5
Ipsilateral White		ATMIN +/+			ATMIN -/-		
From Distance Lesion		Mean	SEM	N	Mean	SEM	N
	-1.5	4.3	2.8	4	35.4	21.3	5
	-1	4.5	2.4	4	30.6	24.9	5
	-0.5	8.5	6.0	4	25.0	14.2	5
	0	0.3	0.3	4	0.2	0.2	5
	+05	0.0	0.0	4	38.0	25.8	5
	+1	5.0	5.0	4	16.0	13.6	5
	+1.5	10.0	10.0	4	14.0	9.8	5

Table 13: Functional Recovery after DLH in ATMIN-null Mutants

Left Forepaw		ATMIN +/+			ATMIN -/-		
Days After Injury		Average WT	SEM	N	Average MU	SEM	N
	-1	4.8	1.3	8	3.4	1.3	7
	2	13.0	3.0	8	11.7	3.8	7
	7	12.8	2.0	8	16.6	3.0	7
	14	13.3	2.3	6	20.0	4.6	5
	21	15.8	2.6	8	17.7	3.3	7
	28	11.5	2.6	8	18.3	1.7	7
Right Forepaw		ATMIN +/+			ATMIN -/-		
Days After Injury		Average WT	SEM	N	Average MU	SEM	N
	-1	3.8	1.1	8	4.6	1.7	7
	2	6.5	1.5	8	6.0	1.9	7
	7	7.5	1.7	8	4.6	1.9	7
	14	3.7	1.7	8	13.6	3.7	7
	21	10.3	2.2	8	12.6	3.8	7
	28	5.8	2.0	8	8.3	2.0	7
Left Hindpaw		ATMIN +/+			ATMIN -/-		
Days After Injury		Average WT	SEM	N	Average MU	SEM	N
	-1	0.8	0.4	8	0.9	0.4	7
	2	10.3	3.7	8	9.4	1.6	7
	7	7.5	3.5	8	6.3	2.5	7
	14	4.0	1.0	6	2.0	1.1	5
	21	11.0	2.9	8	10.0	2.5	7
	28	3.5	0.9	8	7.4	3.9	7
Right Hindpaw		ATMIN +/+			ATMIN -/-		
Days After Injury		Average WT	SEM	N	Average MU	SEM	N
	-1	0.5	0.3	8	0.9	0.4	7
	2	5.0	2.5	8	3.4	2.0	7
	7	1.8	0.8	8	1.1	0.6	7
	14	1.3	0.8	6	2.0	1.5	5
	21	3.3	1.4	8	1.4	0.6	7
	28	3.0	2.0	8	0.6	0.4	7

Rearing Left/Right		ATMIN +/+			ATMIN -/-		
Days After Injury		Average WT	SEM	N	Average MU	SEM	N
	-1	104.00	5.00	8	102.00	7.00	7
	2	0.00	0.00	8	0.00	0.00	7
	7	26.00	17.00	8	21.00	10.00	7
	14	31.00	11.00	8	17.00	13.00	7
	21	31.00	17.00	8	43.00	14.00	7
	28	23.00	9.00	8	32.00	14.00	7

REFERENCES

Abercrombie, M. (1946). Estimation of nuclear population from microtome sections. The Anatomical Record *94*, 239-247.

About, I., Laurent-Maquin, D., Lendahl, U., and Mitsiadis, T. A. (2000). Nestin Expression in Embryonic and Adult Human Teeth under Normal and Pathological Conditions. Am J Pathol *157*, 287-295.

Aepfelbacher, M., Essler, M., Huber, E., Sugai, M., and Weber, P. C. (1997). Bacterial toxins block endothelial wound repair. Evidence that Rho GTPases control cytoskeletal rearrangements in migrating endothelial cells. Arterioscler Thromb Vasc Biol *17*, 1623-9.

Akazawa, C., Nakamura, Y., Sango, K., Horie, H., and Kohsaka, S. (2004). Distribution of the galectin-1 mRNA in the rat nervous system: its transient upregulation in rat facial motor neurons after facial nerve axotomy. Neuroscience *125*, 171-8.

Alarcon-Vargas, D., and Ronai, Z. (2004). c-Jun-NH2 Kinase (JNK) Contributes to the Regulation of c-Myc Protein Stability. Journal of Biological Chemistry *279*, 5008-5016.

Aldskogius, H., Liu, L., and Svensson, M. (1999). Glial responses to synaptic damage and plasticity. J. Neurosci. Res *58*, 33-41.

Alnemri, E. S., Livingston, D. J., Nicholson, D. W., Salvesen, G., Thornberry, N. A., Wong, W. W., and Yuan, J. (1996). Human ICE/CED-3 protease nomenclature. Cell *87*, 171.

Aloisi, F. (2001). Immune function of microglia. Glia *36*, 165-179.

Amankulor, N. M., Hambardzumyan, D., Pyonteck, S. M., Becher, O. J., Joyce, J. A., and Holland, E. C. (2009). Sonic hedgehog pathway activation is induced by acute brain injury and regulated by injury-related inflammation. J. Neurosci *29*, 10299-10308.

Andersen, A. B., Finger, S., Andersen, C. S., and Hoagland, N. (1990). Sensorimotor cortical lesion effects and treatment with nimodipine. Physiol Behav *47*, 1045-52.

Angel, P., and Karin, M. (1992). Specific members of the Jun protein family regulate collagenase expression in response to various extracellular stimuli. Matrix Suppl *1*, 156-164.

Angel, P., and Karin, M. (1991). The role of Jun, Fos and the AP-1 complex in cell-proliferation and transformation. Biochim. Biophys. Acta *1072*, 129-157.

Angel, P., Hattori, K., Smeal, T., and Karin, M. (1988). The jun proto-oncogene is positively autoregulated by its product, Jun/AP-1. Cell *55*, 875-885.

Angel, P., Imagawa, M., Chiu, R., Stein, B., Imbra, R., Rahmsdorf, H., Jonat, C., Herrlich, P., and Karin, M. (1987). Phorbol ester-inducible genes contain a common cis element recognized by a TPA-modulated trans-acting factor. Cell *49*, 729-739.

Angeletti, P. U., Levi-Montalcini, R., and Calissano, P. (1968). The nerve growth factor (NGF): chemical properties and metabolic effects. Adv Enzymol Relat Areas Mol Biol *31*, 51-75.

Angelov, A., Dikranian, K., and Trosheva, M. (1996). Immunomorphological characteristics of pleomorphic adenoma of salivary glands. Bull Group Int Rech Sci Stomatol Odontol *39*, 67-75.

Anouar, Y., Lee, H. W., and Eiden, L. E. (1999). Both inducible and constitutive activator protein-1-like transcription factors are used for transcriptional activation of the galanin gene by different first and second messenger pathways. Mol. Pharmacol *56*, 162-169.

Anzi, S., Finkin, S., and Shaulian, E. (2008). Transcriptional repression of c-Jun's E3 ubiquitin ligases contributes to c-Jun induction by UV. Cellular Signalling *20*, 862-871.

Araki, T., and Milbrandt, J. (2000). Ninjurin2, a novel homophilic adhesion molecule, is expressed in mature sensory and enteric neurons and promotes neurite outgrowth. J Neurosci *20*, 187-95.

Archer, F. R., Doherty, P., Collins, D., and Bolsover, S. R. (1999). CAMs and FGF cause a local submembrane calcium signal promoting axon outgrowth without a rise in bulk calcium concentration. Eur J Neurosci *11*, 3565-73.

Asher, R. A., Morgenstern, D. A., Fidler, P. S., Adcock, K. H., Oohira, A., Braistead, J. E., Levine, J. M., Margolis, R. U., Rogers, J. H., and Fawcett, J. W. (2000). Neurocan is upregulated in injured brain and in cytokine-treated astrocytes. J Neurosci *20*, 2427-38.

Aspenstrom, P., Fransson, A., and Saras, J. (2004). Rho GTPases have diverse effects on the organization of the actin filament system. Biochem J *377*, 327-37.

Bar, P. R., Traber, J., Schuurman, T., and Gispen, W. H. (1990). CNS and PNS effects of nimodipine. J Neural Transm Suppl *31*, 55-71.

Bass, M. D., and Humphries, M. J. (2002). Cytoplasmic interactions of syndecan-4 orchestrate adhesion receptor and growth factor receptor signalling. Biochem J *368*, 1-15.

Bechmann, I., Goldmann, J., Kovac, A. D., Kwidzinski, E., Simburger, E., Naftolin, F., Dirnagl, U., Nitsch, R., and Priller, J. (2005). Circulating monocytic cells infiltrate layers of anterograde axonal degeneration where they transform into microglia. FASEB J., 04-2599fje.

Beggah, A. T., Dours-Zimmermann, M. T., Barras, F. M., Brosius, A., Zimmermann, D. R., and Zurn, A. D. (2005). Lesion-induced differential expression and cell association of Neurocan, Brevican, Versican V1 and V2 in the mouse dorsal root entry zone. Neuroscience *133*, 749-62.

Begum, R., Nur, E. K. M. S., and Zaman, M. A. (2004). The role of Rho GTPases in the regulation of the rearrangement of actin cytoskeleton and cell movement. Exp Mol

Med *36*, 358-66.

Behrens, A., Haigh, J., Mechta-Grigoriou, F., Nagy, A., Yaniv, M., and Wagner, E. F. (2003). Impaired intervertebral disc formation in the absence of Jun. Development *130*, 103-9.

Behrens, A., Sibilia, M., David, J. P., Mohle-Steinlein, U., Tronche, F., Schutz, G., and Wagner, E. F. (2002). Impaired postnatal hepatocyte proliferation and liver regeneration in mice lacking c-jun in the liver. Embo J *21*, 1782-90.

Behrens, A., Sibilia, M., and Wagner, E. F. (1999). Amino-terminal phosphorylation of c-Jun regulates stress-induced apoptosis and cellular proliferation. Nat Genet *21*, 326-9.

Bement, W. M., Yu, H. Y., Burkel, B. M., Vaughan, E. M., and Clark, A. G. (2007). Rehabilitation and the single cell. Curr Opin Cell Biol *19*, 95-100.

Benarroch, E. E. (2007). Rho GTPases: role in dendrite and axonal growth, mental retardation, and axonal regeneration. Neurology *68*, 1315-8.

Benbrook, D., and Jones, N. (1990). Heterodimer formation between CREB and JUN proteins. Oncogene *5*, 295-302.

Benes, F., and Lange, N. (2001). Two-dimensional versus three-dimensional cell counting: A practical perspective. Trends in Neurosciences *24*, 11-17.

Bhattacharyya, A., Frank, E., Ratner, N., and Brackenbury, R. (1991). P0 is an early marker of the Schwann cell lineage in chickens. Neuron *7*, 831–844.

Bishop, B. (1982). Neural plasticity: Part 3. Responses to lesions in the peripheral nervous system. Phys Ther *62*, 1275-1282.

Bishop, D. L., and Milton, R. L. (1998). Nimodipine suppresses preferential reinnervation of mouse soleus muscles by slow alpha-motoneurons. Exp Neurol *154*, 366-70.

Bixby, J. L., Lilien, J., and Reichardt, L. F. (1988). Identification of the major proteins that promote neuronal process outgrowth on Schwann cells in vitro. J Cell Biol *107*, 353-61.

Björkblom, B., Östman, N., Hongisto, V., Komarovski, V., Filén, J., Nyman, T., Kallunki, T., Courtney, M., and Coffey, E. (2005). Constitutively active cytoplasmic c-Jun N-terminal kinase 1 is a dominant regulator of dendritic architecture: Role of microtubule-associated protein 2 as an effector. Journal of Neuroscience *25*, 6350-6361.

Blinzinger, K., and Kreutzberg, G. (1968). Displacement of synaptic terminals from regenerating motoneurons by microglial cells. Z Zellforsch Mikrosk Anat *85*, 145-57.

Bogoyevitch, M., and Arthur, P. (2008). Inhibitors of c-Jun N-terminal kinases-JuNK no more? Biochimica et Biophysica Acta - Proteins and Proteomics *1784*, 76-93.

Bohatschek, M., Kloss, C. U., Kalla, R., and Raivich, G. (2001). In vitro model of microglial deramification: ramified microglia transform into amoeboid phagocytes following addition of brain cell membranes to microglia-astrocyte cocultures. J Neurosci Res *64*, 508-22.

Bohatschek, M., Kloss, C. U., Pfeffer, K., Bluethmann, H., and Raivich, G. (2004). B7.2 on activated and phagocytic microglia in the facial axotomy model: regulation by interleukin-1 receptor type 1, tumor necrosis factor receptors 1 and 2 and endotoxin. J Neuroimmunol *156*, 132-45.

Bomze, H. M., Bulsara, K. R., Iskandar, B. J., Caroni, P., and Skene, J. H. (2001). Spinal axon regeneration evoked by replacing two growth cone proteins in adult neurons. Nat Neurosci *4*, 38-43.

Borasio, G. D., Horstmann, S., Anneser, J. M., Neff, N. T., and Glicksman, M. A. (1998). CEP-1347/KT7515, a JNK pathway inhibitor, supports the in vitro survival of chick embryonic neurons. Neuroreport *9*, 1435-9.

Borsello, T., Clarke, P. G., Hirt, L., Vercelli, A., Repici, M., Schorderet, D. F., Bogousslavsky, J., and Bonny, C. (2003). A peptide inhibitor of c-Jun N-terminal kinase protects against excitotoxicity and cerebral ischemia. Nat Med *9*, 1180-6.

Borsello, T., and Forloni, G. (2007). JNK signalling: A possible target to prevent neurodegeneration. Current Pharmaceutical Design *13*, 1875-1886.

Bottcher, R. T., Pollet, N., Delius, H., and Niehrs, C. (2004). The transmembrane protein XFLRT3 forms a complex with FGF receptors and promotes FGF signalling. Nat Cell Biol *6*, 38-44.

Boyd, J. G., and Gordon, T. (2002). A dose-dependent facilitation and inhibition of peripheral nerve regeneration by brain-derived neurotrophic factor. Eur J Neurosci *15*, 613-26.

Boyd, J. G., and Gordon, T. (2003a). Glial cell line-derived neurotrophic factor and brain-derived neurotrophic factor sustain the axonal regeneration of chronically axotomized motoneurons in vivo. Exp Neurol *183*, 610-9.

Boyd, J., and Gordon, T. (2003b). Glial cell line-derived neurotrophic factor and brain-derived neurotrophic factor sustain the axonal regeneration of chronically axotomized motoneurons in vivo. Experimental Neurology *183*, 610-619.

Boyle, W., Smeal, T., Defize, L., Angel, P., Woodgett, J., Karin, M., and Hunter, T. (1991). Activation of protein kinase C decreases phosphorylation of c-Jun at sites that negatively regulate its DNA-binding activity. Cell *64*, 573-584.

Bradbury, E. J., Moon, L. D., Popat, R. J., King, V. R., Bennett, G. S., Patel, P. N., Fawcett, J. W., and McMahon, S. B. (2002). Chondroitinase ABC promotes functional recovery after spinal cord injury. Nature *416*, 636-40.

Bramanti, V., Tomassoni, D., Avitabile, M., Amenta, F., and Avola, R. (2010). Biomarkers of glial cell proliferation and differentiation in culture. Front Biosci (Schol Ed) *2*, 558-570.

Bravo, R., Neuberg, M., Burckhardt, J., Almendral, J., Wallich, R., and Müller, R. (1987). Involvement of common and cell type-specific pathways in c-fos gene control: Stable induction by cAMP in macrophages. Cell *48*, 251-260.

Brecht, S., Kirchhof, R., Chromik, A., Willesen, M., Nicolaus, T., Raivich, G., Wessig, J., Waetzig, V., Goetz, M., Claussen, M., et al. (2005a). Specific pathophysiological functions of JNK isoforms in the brain. Eur J Neurosci *21*, 363-77.

Brecht, S., Kirchhof, R., Chromik, A., Willesen, M., Nicolaus, T., Raivich, G., Wessig, J., Waetzig, V., Goetz, M., Claussen, M., et al. (2005b). Specific pathophysiological functions of JNK isoforms in the brain. European Journal of Neuroscience *21*, 363-377.

Broude, E., McAtee, M., Kelley, M. S., and Bregman, B. S. (1997). c-Jun expression in adult rat dorsal root ganglion neurons: differential response after central or peripheral axotomy. Exp. Neurol *148*, 367-377.

Broude, E., McAtee, M., Kelley, M. S., and Bregman, B. S. (1999). Fetal spinal cord transplants and exogenous neurotrophic support enhance c-Jun expression in mature axotomized neurons after spinal cord injury. Exp. Neurol *155*, 65-78.

Brushart, T. M. (1993). Motor axons preferentially reinnervate motor pathways. J Neurosci *13*, 2730-8.

Brushart, T. M. (1988). Preferential reinnervation of motor nerves by regenerating motor axons. J Neurosci *8*, 1026-31.

Brushart, T. M., and Seiler, W. A. T. (1987). Selective reinnervation of distal motor stumps by peripheral motor axons. Exp Neurol *97*, 289-300.

Brust, T. B., Cayabyab, F. S., and MacVicar, B. A. (2007). C-Jun N-terminal kinase regulates adenosine A1 receptor-mediated synaptic depression in the rat hippocampus. Neuropharmacology *53*, 906-917.

BUPA (2009). BUPA Fact Sheet.

Burroni, D., White, F. V., Ceccarini, C., Matthieu, J. M., and Costantino-Ceccarini, E. (1988). Expression of myelin components in mouse Schwann cells in culture. J. Neurochem *50*, 331-336.

Buscher, M., Rahmsdorf, H., Litfin, M., Karin, M., and Herrlich, P. (1988). Activation of the c-fos gene by UV and phorbol ester: different signal transduction pathways converge to the same enhancer element. Oncogene *3*, 301-311.

Buschmann, T., Martin-Villalba, A., Kocsis, J. D., Waxman, S. G., Zimmermann, M., and Herdegen, T. (1998). Expression of Jun, Fos, and ATF-2 proteins in axotomized explanted and cultured adult rat dorsal root ganglia. Neuroscience *84*, 163-76.

Buss, A., Pech, K., Kakulas, B. A., Martin, D., Schoenen, J., Noth, J., and Brook, G. A. (2009). NG2 and phosphacan are present in the astroglial scar after human traumatic spinal cord injury. BMC Neurol *9*, 32.

Butchi, N. B., Du, M., and Peterson, K. E. (2009). Interactions between TLR7 and TLR9 agonists and receptors regulate innate immune responses by astrocytes and microglia. Glia. Available at: http://www.ncbi.nlm.nih.gov/pubmed/19998480 [Accessed December 30, 2009].

Butovsky, O., Ziv, Y., Schwartz, A., Landa, G., Talpalar, A. E., Pluchino, S., Martino, G., and Schwartz, M. (2006). Microglia activated by IL-4 or IFN-gamma differentially induce neurogenesis and oligodendrogenesis from adult stem/progenitor cells. Mol. Cell. Neurosci *31*, 149-160.

Byram, S. C., Carson, M. J., DeBoy, C. A., Serpe, C. J., Sanders, V. M., and Jones, K. J. (2004). CD4-positive T cell-mediated neuroprotection requires dual compartment antigen presentation. J. Neurosci *24*, 4333-4339.

Cajal, S. R. Y. (1928). Estudios sobre la Degeneración y Regeneración del Sistema Nervioso (Degeneration and Regeneration of the Nervous System).

Campbell, G., Hutchins, K., Winterbottom, J., Grenningloh, G., Lieberman, A. R., and Anderson, P. N. (2005). Upregulation of activating transcription factor 3 (ATF3) by intrinsic CNS neurons regenerating axons into peripheral nerve grafts. Exp Neurol *192*, 340-7.

Canettieri, G., Coni, S., Della Guardia, M., Nocerino, V., Antonucci, L., Di Magno, L., Screaton, R., Screpanti, I., Giannini, G., and Gulino, A. (2009). The coactivator CRTC1 promotes cell proliferation and transformation via AP-1. Proc. Natl. Acad. Sci. U.S.A *106*, 1445-1450.

Caroni, P. (1997). Intrinsic neuronal determinants that promote axonal sprouting and elongation. Bioessays *19*, 767-75.

Caroni, P. (2001). New EMBO members' review: actin cytoskeleton regulation through modulation of PI(4,5)P(2) rafts. Embo J *20*, 4332-6.

Casaccia-Bonnefil, P. (2000). Cell death in the oligodendrocyte lineage: a molecular perspective of life/death decisions in development and disease. Glia *29*, 124-35.

Casaccia-Bonnefil, P., Pandozy, G., and Mastronardi, F. (2008). Evaluating epigenetic landmarks in the brain of multiple sclerosis patients: a contribution to the current debate on disease pathogenesis. Prog Neurobiol *86*, 368-78.

Castellazzi, M., Spyrou, G., La Vista, N., Dangy, J. P., Piu, F., Yaniv, M., and Brun, G. (1991). Overexpression of c-jun, junB, or junD affects cell growth differently. Proc Natl Acad Sci U S A *88*, 8890-4.

Cerretti, D. P., Kozlosky, C. J., Mosley, B., Nelson, N., Van Ness, K., Greenstreet, T. A., March, C. J., Kronheim, S. R., Druck, T., Cannizzaro, L. A., et al. (1992). Molecular cloning of the interleukin-1 beta converting enzyme. Science *256*, 97-100.

Chaisuksunt, V., Campbell, G., Zhang, Y., Schachner, M., Lieberman, A., and Anderson, P. (2003). Expression of regeneration-related molecules in injured and regenerating striatal and nigral neurons. Journal of Neurocytology *32*, 161-183.

Chan, Y. M., Yick, L. W., Yip, H. K., So, K. F., Oppenheim, R. W., and Wu, W. (2003). Inhibition of caspases promotes long-term survival and reinnervation by axotomized spinal motoneurons of denervated muscle in newborn rats. Exp Neurol *181*, 190-203.

Chang, F., Steelman, L., Lee, J., Shelton, J., Navolanic, P., Blalock, W., Franklin, R., and McCubrey, J. (2003). Signal transduction mediated by the Ras/Raf/MEK/ERK pathway from cytokine receptors to transcription factors: Potential targeting for therapeutic intervention. Leukemia *17*, 1263-1293.

Chang, L., Jones, Y., Ellisman, M., Goldstein, L., and Karin, M. (2003). JNK1 is required for maintenance of neuronal microtubules and controls phosphorylation of microtubule-associated proteins. Developmental Cell *4*, 521-533.

Chaudhry, V., Glass, J. D., and Griffin, J. W. (1992). Wallerian degeneration in peripheral nerve disease. Neurol Clin *10*, 613-627.

Chaum, E., Yin, J., Yang, H., Thomas, F., and Lang, J. C. (2009). Quantitative AP-1 gene regulation by oxidative stress in the human retinal pigment epithelium. J. Cell. Biochem *108*, 1280-1291.

Chen, C., Ng, J., Choo, P., Wu, W., and Porter, A. (2009). Mammalian Sterile 20-like kinase 3 (MST3) mediates oxidative stress-induced cell death by modulating JNK activation. Biosci. Rep. Available at: http://www.ncbi.nlm.nih.gov/pubmed/19604147 [Accessed August 17, 2009].

Chen, Z. L., Indyk, J. A., and Strickland, S. (2003). The hippocampal laminin matrix is dynamic and critical for neuronal survival. Mol Biol Cell *14*, 2665-76.

Chen, Z. L., and Strickland, S. (2003). Laminin gamma1 is critical for Schwann cell differentiation, axon myelination, and regeneration in the peripheral nerve. J Cell Biol *163*, 889-99.

Cheng, L., and Mudge, A. W. (1996). Cultured Schwann cells constitutively express the myelin protein P0. Neuron *16*, 309–320.

Chiu, R., Angel, P., and Karin, M. (1989). Jun-B differs in its biological properties from, and is a negative regulator of, c-Jun. Cell *59*, 979-986.

Chiu, R., Boyle, W., Meek, J., Smeal, T., Hunter, T., and Karin, M. (1988). The c-Fos protein interacts with c-Jun/AP-1 to stimulate transcription of AP-1 responsive genes. Cell *54*, 541-552.

Ciani, L., and Salinas, P. (2007). c-Jun N-terminal kinase (JNK) cooperates with Gsk3β to regulate Dishevelled-mediated microtubule stability. BMC Cell Biology *8*. Available at: http://www.scopus.com/inward/record.url?eid=2-s2.0-34547737016&partnerID=40 [Accessed December 7, 2009].

Coffey, E., Hongisto, V., Dickens, M., Davis, R., and Courtney, M. (2000). Dual roles for c-Jun N-terminal kinase in developmental and stress responses in cerebellar granule neurons. Journal of Neuroscience *20*, 7602-7613.

Coggeshall, R. E. (1992). A consideration of neural counting methods. Trends Neurosci *15*, 9-13.

Coisy-Quivy, M., Sanguesa-Ferrer, J., Weill, M., Johnson, D. S., Donnay, J. M., Hipskind, R., Fort, P., and Philips, A. (2006). Identification of Rho GTPases implicated in terminal differentiation of muscle cells in ascidia. Biol Cell *98*, 577-88.

Cooper, G. M., and Hausman, R. E. (2006). The Cell: A Molecular Approach, Fourth Edition 4th ed. (Sinauer Associates, Inc.).

Corness, J., and Hökfelt, T. (1998). Analysis of selected regulatory pathways for rat galanin gene transcription and their suitability as putative models for negative regulation by NGF. Ann. N. Y. Acad. Sci *863*, 14-21.

Corradi, A., Zanardi, A., Giacomini, C., Onofri, F., Valtorta, F., Zoli, M., and Benfenati, F. (2008). Synapsin-I- and synapsin-II-null mice display an increased age-dependent cognitive impairment. J Cell Sci *121*, 3042-3051.

Crocker, S. J., Lamba, W. R., Smith, P. D., Callaghan, S. M., Slack, R. S., Anisman, H., and Park, D. S. (2001). c-Jun mediates axotomy-induced dopamine neuron death in vivo. Proc. Natl. Acad. Sci. U.S.A *98*, 13385-13390.

Cuadrado, A., González, L., Suárez, Y., Martínez, T., and Muñoz, A. (2004). JNK activation is critical for Aplidin-induced apoptosis. Oncogene *23*, 4673-4680.

Curinga, G. M., Snow, D. M., Mashburn, C., Kohler, K., Thobaben, R., Caggiano, A. O., and Smith, G. M. (2007). Mammalian-produced chondroitinase AC mitigates axon inhibition by chondroitin sulfate proteoglycans. J Neurochem *102*, 275-88.

D. Wynick, S. W. T., and McMahon, S. B. (2001). The role of galanin as a multi-functional neuropeptide in the nervous system. Curr. Opin. Pharmacol. *1*, 73–77.

Dahlstrand, J., Lardelli, M., and Lendahl, U. (1995). Nestin mRNA expression correlates with the central nervous system progenitor cell state in many, but not all, regions of developing central nervous system. Brain Res. Dev. Brain Res *84*, 109-129.

Dahlstrand, J., Zimmerman, L. B., McKay, R. D., and Lendahl, U. (1992). Characterization of the human nestin gene reveals a close evolutionary relationship to neurofilaments. J. Cell. Sci *103 (Pt 2)*, 589-597.

Davies, J. E., Tang, X., Bournat, J. C., and Davies, S. J. (2006). Decorin promotes plasminogen/plasmin expression within acute spinal cord injuries and by adult microglia in vitro. J Neurotrauma *23*, 397-408.

De Camilli, P., Benfenati, F., Valtorta, F., and Greengard, P. (1990). The synapsins. Annu. Rev. Cell Biol *6*, 433-460.

Deboy, C. A., Xin, J., Byram, S. C., Serpe, C. J., Sanders, V. M., and Jones, K. J. (2006). Immune-mediated neuroprotection of axotomized mouse facial motoneurons is dependent on the IL-4/STAT6 signaling pathway in CD4(+) T cells. Exp. Neurol *201*, 212-224.

Demestre, M., Wells, G. M., Miller, K. M., Smith, K. J., Hughes, R. A., Gearing, A. J., and Gregson, N. A. (2004). Characterisation of matrix metalloproteinases and the effects of a broad-spectrum inhibitor (BB-1101) in peripheral nerve regeneration. Neuroscience *124*, 767-79.

Dergham, P., Ellezam, B., Essagian, C., Avedissian, H., Lubell, W. D., and McKerracher, L. (2002). Rho signaling pathway targeted to promote spinal cord repair. J Neurosci *22*, 6570-7.

Desbarats, J., Birge, R., Mimouni-Rongy, M., Weinstein, D., Palerme, J., and Newell, M. (2003). Fas engagement induces neurite growth through ERK activation and p35 upregulation. Nature Cell Biology *5*, 118-125.

Diamond, J., Coughlin, M., Macintyre, L., Holmes, M., and Visheau, B. (1987). Evidence that endogenous beta nerve growth factor is responsible for the collateral sprouting, but not the regeneration, of nociceptive axons in adult rats. Proc Natl Acad Sci U S A *84*, 6596-600.

Dickens, M., Rogers, J., Cavanagh, J., Raitano, A., Xia, Z., Halpern, J., Greenberg, M., Sawyers, C., and Davis, R. (1997). A cytoplasmic inhibitor of the JNK signal transduction pathway. Science *277*, 693-696.

DiPietro, L. A., Burdick, M., Low, Q. E., Kunkel, S. L., and Strieter, R. M. (1998). MIP-1alpha as a critical macrophage chemoattractant in murine wound repair. J. Clin. Invest *101*, 1693-1698.

Dobrea, G. M., Unnerstall, J. R., and Rao, M. S. (1992). The expression of CNTF message and immunoreactivity in the central and peripheral nervous system of the rat. Brain Res Dev Brain Res *66*, 209-19.

Dong, C., Yang, D. D., Wysk, M., Whitmarsh, A. J., Davis, R. J., and Flavell, R. A. (1998). Defective T cell differentiation in the absence of Jnk1. Science *282*, 2092-5.

Donovan, N., Becker, E., Konishi, Y., and Bonni, A. (2002). JNK phosphorylation and activation of bad couples the stress-activated signaling pathway to the cell death machinery. Journal of Biological Chemistry *277*, 40944-40949.

Dopp, J. M., Mackenzie-Graham, A., Otero, G. C., and Merrill, J. E. (1997). Differential expression, cytokine modulation, and specific functions of type-1 and type-2 tumor necrosis factor receptors in rat glia. Journal of Neuroimmunology *75*, 104-112.

Dunican, D. J., and Doherty, P. (2000). The generation of localized calcium rises mediated by cell adhesion molecules and their role in neuronal growth cone motility. Mol Cell Biol Res Commun *3*, 255-63.

Eckenstein, F., Woodward, W. R., and Nishi, R. (1991). Differential localization and possible functions of aFGF and bFGF in the central and peripheral nervous systems. Ann N Y Acad Sci *638*, 348-60.

Eilers, A., Whitfield, J., Shah, B., Spadoni, C., Desmond, H., and Ham, J. (2001). Direct inhibition of c-Jun N-terminal kinase in sympathetic neurones prevents c-jun

promoter activation and NGF withdrawal-induced death. J Neurochem *76*, 1439-54.

Ekblom, P., Lonai, P., and Talts, J. F. (2003). Expression and biological role of laminin-1. Matrix Biol *22*, 35-47.

Ekstrom, P. A., Mayer, U., Panjwani, A., Pountney, D., Pizzey, J., and Tonge, D. A. (2003). Involvement of alpha7beta1 integrin in the conditioning-lesion effect on sensory axon regeneration. Mol Cell Neurosci *22*, 383-95.

Eliasson, C., Sahlgren, C., Berthold, C., Stakeberg, J., Celis, J. E., Betsholtz, C., Eriksson, J. E., and Pekny, M. (1999). Intermediate Filament Protein Partnership in Astrocytes. Journal of Biological Chemistry *274*, 23996-24006.

Ellezam, B., Dubreuil, C., Winton, M., Loy, L., Dergham, P., Selles-Navarro, I., and McKerracher, L. (2002). Inactivation of intracellular Rho to stimulate axon growth and regeneration. Prog Brain Res *137*, 371-80.

Eminel, S., Roemer, L., Waetzig, V., and Herdegen, T. (2008). c-Jun N-terminal kinases trigger both degeneration and neurite outgrowth in primary hippocampal and cortical neurons. Journal of Neurochemistry *104*, 957-969.

Eriksson, J. E., Brautigan, D. L., Vallee, R., Olmsted, J., Fujiki, H., and Goldman, R. D. (1992). Cytoskeletal integrity in interphase cells requires protein phosphatase activity. Proc. Natl. Acad. Sci. U.S.A *89*, 11093-11097.

Esser, L., Wang, C. R., Hosaka, M., Smagula, C. S., Südhof, T. C., and Deisenhofer, J. (1998). Synapsin I is structurally similar to ATP-utilizing enzymes. EMBO J *17*, 977-984.

Falck, J., Coates, J., and Jackson, S. P. (2005). Conserved modes of recruitment of ATM, ATR and DNA-PKcs to sites of DNA damage. Nature *434*, 605-11.

Fan, F., Jin, S., Amundson, S. A., Tong, T., Fan, W., Zhao, H., Zhu, X., Mazzacurati, L., Li, X., Petrik, K. L., et al. (2002). ATF3 induction following DNA damage is regulated by distinct signaling pathways and over-expression of ATF3 protein suppresses cells growth. Oncogene *21*, 7488-7496.

Farina, C., Aloisi, F., and Meinl, E. (2007). Astrocytes are active players in cerebral innate immunity. Trends Immunol *28*, 138-145.

Feltri, M. L., D'Antonio, M., Previtali, S., Fasolini, M., Messing, A., and Wrabetz, L. (1999). P0-Cre transgenic mice for inactivation of adhesion molecules in Schwann cells. Ann N Y Acad Sci *883*, 116-23.

Ferguson, C., Hardy, S. L., Werner, D. F., Hileman, S. M., Delorey, T. M., and Homanics, G. E. (2007). New insight into the role of the beta3 subunit of the GABAA-R in development, behavior, body weight regulation, and anesthesia revealed by conditional gene knockout. BMC Neurosci *8*, 85.

Fernandes, A., Vaz, A. R., Falcao, A. S., Silva, R. F., Brito, M. A., and Brites, D. (2007). Glycoursodeoxycholic acid and interleukin-10 modulate the reactivity of rat cortical astrocytes to unconjugated bilirubin. J Neuropathol Exp Neurol *66*, 789-98.

Ferri, C. C., Moore, F. A., and Bisby, M. A. (1998a). Effects of facial nerve injury on mouse motoneurons lacking the p75 low-affinity neurotrophin receptor. J Neurobiol *34*, 1-9.

Ferri, C., Moore, F., and Bisby, M. (1998b). Effects of facial nerve injury on mouse motoneurons lacking the p75 low- affinity neurotrophin receptor. Journal of Neurobiology *34*, 1-9.

Filbin, M. T. (2003). Myelin-associated inhibitors of axonal regeneration in the adult mammalian CNS. Nat Rev Neurosci *4*, 703-13.

Flugel, A., Bradl, M., Kreutzberg, G. W., and Graeber, M. B. (2001). Transformation of donor-derived bone marrow precursors into host microglia during autoimmune CNS inflammation and during the retrograde response to axotomy. Journal of Neuroscience Research *66*, 74–82.

Forte, G., Minieri, M., Cossa, P., Antenucci, D., Sala, M., Gnocchi, V., Fiaccavento, R., Carotenuto, F., De Vito, P., Baldini, P. M., et al. (2006). Hepatocyte growth factor effects on mesenchymal stem cells: proliferation, migration, and differentiation. Stem Cells *24*, 23-33.

Fournier, A., Takizawa, B., and Strittmatter, S. (2003). Rho kinase inhibition enhances axonal regeneration in the injured CNS. Journal of Neuroscience *23*, 1416-1423.

Frey, D., Laux, T., Xu, L., Schneider, C., and Caroni, P. (2000). Shared and unique roles of CAP23 and GAP43 in actin regulation, neurite outgrowth, and anatomical plasticity. J Cell Biol *149*, 1443-54.

Fröjdman, K., Pelliniemi, L. J., Lendahl, U., Virtanen, I., and Eriksson, J. E. (1997). The intermediate filament protein nestin occurs transiently in differentiating testis of rat and mouse. Differentiation *61*, 243-249.

Fugleholm, K., Schmalbruch, H., and Krarup, C. (1994). Early peripheral nerve regeneration after crushing, sectioning, and freeze studied by implanted electrodes in the cat. J Neurosci *14*, 2659-73.

Fujitani, M., Yamagishi, S., Che, Y. H., Hata, K., Kubo, T., Ino, H., Tohyama, M., and Yamashita, T. (2004). P311 accelerates nerve regeneration of the axotomized facial nerve. J Neurochem *91*, 737-44.

Funakoshi, H., Frisen, J., Barbany, G., Timmusk, T., Zachrisson, O., Verge, V. M., and Persson, H. (1993). Differential expression of mRNAs for neurotrophins and their receptors after axotomy of the sciatic nerve. J Cell Biol *123*, 455-65.

Galiano, M., Liu, Z. Q., Kalla, R., Bohatschek, M., Koppius, A., Gschwendtner, A., Xu, S., Werner, A., Kloss, C. U., Jones, L. L., et al. (2001). Interleukin-6 (IL6) and cellular response to facial nerve injury: effects on lymphocyte recruitment, early microglial activation and axonal outgrowth in IL6-deficient mice. Eur J Neurosci *14*, 327-41.

Gallin, J. I., and Goldstein, I. M. (1992). Inflammation: Basic Principles and Clinical Correlates 2nd ed. (Lippincott Williams & Wilkins).

Galtrey, C. M., Asher, R. A., Nothias, F., and Fawcett, J. W. (2007). Promoting plasticity in the spinal cord with chondroitinase improves functional recovery after peripheral nerve repair. Brain *130*, 926-39.

Garcia-Alias, G., Barkhuysen, S., Buckle, M., and Fawcett, J. W. (2009). Chondroitinase ABC treatment opens a window of opportunity for task-specific rehabilitation. Nat Neurosci *12*, 1145-1151.

Gentz, R., Rauscher III, F., Abate, C., and Curran, T. (1989). Parallel association of Fos and Jun leucine zippers juxtaposes DNA binding domains. Science *243*, 1695-1699.

Gerendasy, D. D., Herron, S. R., Jennings, P. A., and Sutcliffe, J. G. (1995). Calmodulin stabilizes an amphiphilic alpha-helix within RC3/neurogranin and GAP-43/neuromodulin only when Ca2+ is absent. J Biol Chem *270*, 6741-50.

Ghabriel, M. N., and Allt, G. (1979a). The role of Schmidt-Lanterman incisures in Wallerian degeneration. I. A quantitative teased fibre study. Acta Neuropathol *48*, 93-93.

Ghabriel, M. N., and Allt, G. (1979b). The role of Schmidt-Lanterman incisures in Wallerian degeneration. II. An electron microscopic study. Acta Neuropathol *48*, 95-103.

Ghislain, J., and Charnay, P. (2006). Control of myelination in Schwann cells: a Krox20 cis-regulatory element integrates Oct6, Brn2 and Sox10 activities. EMBO Rep *7*, 52-58.

Giese, K. P., Martini, R., Lemke, G., Soriano, P., and Schachner, M. (1992). Mouse P0 gene disruption leads to hypomyelination, abnormal expression of recognition molecules, and degeneration of myelin and axons. Cell *71*, 565-576.

Giger, R. J., Venkatesh, K., Chivatakarn, O., Raiker, S. J., Robak, L., Hofer, T., Lee, H., and Rader, C. (2008). Mechanisms of CNS myelin inhibition: evidence for distinct and neuronal cell type specific receptor systems. Restor Neurol Neurosci *26*, 97-115.

Gillingwater, T. H., and Ribchester, R. R. (2003). The relationship of neuromuscular synapse elimination to synaptic degeneration and pathology: insights from WldS and other mutant mice. J. Neurocytol *32*, 863-881.

Glazner, G. W., Lupien, S., Miller, J. A., and Ishii, D. N. (1993). Insulin-like growth factor II increases the rate of sciatic nerve regeneration in rats. Neuroscience *54*, 791-7.

Goerdt, S., and Orfanos, C. E. (1999). Other functions, other genes: alternative activation of antigen-presenting cells. Immunity *10*, 137-142.

Gold, B. G. (1997). FK506 and the role of immunophilins in nerve regeneration. Mol Neurobiol *15*, 285-306.

Gold, B. G., Storm-Dickerson, T., and Austin, D. R. (1993). Regulation of the transcription factor c-JUN by nerve growth factor in adult sensory neurons. Neurosci Lett *154*, 129-33.

Goldshmit, Y., Lythgo, N., Galea, M. P., and Turnley, A. M. (2008). Treadmill training after spinal cord hemisection in mice promotes axonal sprouting and synapse formation and improves motor recovery. J. Neurotrauma *25*, 449-465.

Golub, T., and Caroni, P. (2005). PI(4,5)P2-dependent microdomain assemblies capture microtubules to promote and control leading edge motility. J Cell Biol *169*, 151-65.

Gordon, T., Chan, K. M., Sulaiman, O. A. R., Udina, E., Amirjani, N., and Brushart, T. M. (2009). Accelerating axon growth to overcome limitations in functional recovery after peripheral nerve injury. Neurosurgery *65*, 132-144.

Graeber, M., and Kreutzberg, G. (1986). Astrocytes increase in glial fibrillary acidic protein during retrograde changes of facial motor neurons. Journal of Neurocytology *15*, 363-373.

Graeber, M., Tetzlaff, W., Streit, W., and Kreutzberg, G. (1988). Microglial cells but not astrocytes undergo mitosis following rat facial nerve axotomy. Neuroscience Letters *85*, 317-321.

Graham, L., Cooper, P. R., Cassidy, N., Nor, J. E., Sloan, A. J., and Smith, A. J. (2006). The effect of calcium hydroxide on solubilisation of bio-active dentine matrix components. Biomaterials *27*, 2865-2873.

Griffin, J. W., George, E. B., and Chaudhry, V. (1996). Wallerian degeneration in peripheral nerve disease. Baillieres Clin Neurol *5*, 65-75.

Griffin, J. W., and Thompson, W. J. (2008). Biology and pathology of nonmyelinating Schwann cells. Glia *56*, 1518-1531.

Grimm, C., Wenzel, A., Behrens, A., Hafezi, F., Wagner, E. F., and Remé, C. E. (2001). AP-1 mediated retinal photoreceptor apoptosis is independent of N-terminal phosphorylation of c-Jun. Cell Death Differ *8*, 859-867.

Gschwendtner, A., Liu, Z., Hucho, T., Bohatschek, M., Kalla, R., Dechant, G., and Raivich, G. (2003). Regulation, cellular localization, and function of the p75 neurotrophin receptor (p75NTR) during the regeneration of facial motoneurons. Mol Cell Neurosci *24*, 307-22.

Guntinas-Lichius, O., Irintchev, A., Streppel, M., Lenzen, M., Grosheva, M., Wewetzer, K., Neiss, W. F., and Angelov, D. N. (2005). Factors limiting motor recovery after facial nerve transection in the rat: combined structural and functional analyses. Eur. J. Neurosci *21*, 391-402.

Guo, C., and Whitmarsh, A. (2008). The β-arrestin-2 scaffold protein promotes c-Jun N-terminal kinase-3 activation by binding to its nonconserved N terminus. Journal of Biological Chemistry *283*, 15903-15911.

Gupta, S., Barrett, T., Whitmarsh, A., Cavanagh, J., Sluss, H., Dérijard, B., and Davis, R. (1996). Selective interaction of JNK protein kinase isoforms with transcription factors. EMBO Journal *15*, 2760-2770.

Guseva, D., Angelov, D. N., Irintchev, A., and Schachner, M. (2009). Ablation of adhesion molecule L1 in mice favours Schwann cell proliferation and functional recovery after peripheral nerve injury. Brain *132*, 2180-2195.

Ha, G. K., Huang, Z., Streit, W. J., and Petitto, J. M. (2006). Endogenous T lymphocytes and microglial reactivity in the axotomized facial motor nucleus of mice: effect of genetic background and the RAG2 gene. J. Neuroimmunol *172*, 1-8.

Ha, G. K., Parikh, S., Huang, Z., and Petitto, J. M. (2008). Influence of injury severity on the rate and magnitude of the T lymphocyte and neuronal response to facial nerve axotomy. J. Neuroimmunol *199*, 18-23.

Hadlock, T. A., Heaton, J., Cheney, M., and Mackinnon, S. E. (2005). Functional Recovery After Facial and Sciatic Nerve Crush Injury in the Rat. Arch Facial Plast Surg *7*, 17-20.

Haeusgen, W., Boehm, R., Zhao, Y., Herdegen, T., and Waetzig, V. (2009). Specific activities of individual c-Jun N-terminal kinases in the brain. Neuroscience *161*, 951-959.

Halazonetis, T., Georgopoulos, K., Greenberg, M., and Leder, P. (1988). C-Jun dimerizes with itself and with c-Fos, forming complexes of different DNA binding affinities. Cell *55*, 917-924.

Ham, J., Babij, C., Whitfield, J., Pfarr, C., Lallemand, D., Yaniv, M., and Rubin, L. (1995). A c-Jun dominant negative mutant protects sympathetic neurons against programmed cell death. Neuron *14*, 927-939.

Hammarberg, H., Piehl, F., Risling, M., and Cullheim, S. (2000). Differential regulation of trophic factor receptor mRNAs in spinal motoneurons after sciatic nerve transection and ventral root avulsion in the rat. J Comp Neurol *426*, 587-601.

Han, T. H., Lamph, W. W., and Prywes, R. (1992). Mapping of epidermal growth factor-, serum-, and phorbol ester-responsive sequence elements in the c-jun promoter. Mol. Cell. Biol *12*, 4472-4477.

Hanada, R., Leibbrandt, A., Hanada, T., Kitaoka, S., Furuyashiki, T., Fujihara, H., Trichereau, J., Paolino, M., Qadri, F., Plehm, R., et al. (2009). Central control of fever and female body temperature by RANKL/RANK. Nature *462*, 505-509.

Hasue, F., Kuwaki, T., Kisanuki, Y., Yanagisawa, M., Moriya, H., Fukuda, Y., and Shimoyama, M. (2005). Increased sensitivity to acute and persistent pain in neuron-specific endothelin-1 knockout mice. Neuroscience *130*, 349-358.

Hattori, K., Angel, P., Le Beau, M., and Karin, M. (1988). Structure and chromosomal localization of the functional intronless human JUN protooncogene. Proceedings of the National Academy of Sciences of the United States of America *85*, 9148-9152.

He, X., Kotloski, R., Nef, S., Luikart, B. W., Parada, L. F., and McNamara, J. O. (2004). Conditional deletion of TrkB but not BDNF prevents epileptogenesis in the kindling model. Neuron *43*, 31-42.

Heffron, D. S., Landreth, G. E., Samuels, I. S., and Mandell, J. W. (2009). Brain-specific deletion of extracellular signal-regulated kinase 2 mitogen-activated protein kinase leads to aberrant cortical collagen deposition. Am. J. Pathol *175*, 2586-2599.

Hendry, I. A. (1976). A method to correct adequately for the change in neuronal size when estimating neuronal numbers after nerve growth factor treatment. J. Neurocytol *5*, 337-349.

Henley, J., and Poo, M. M. (2004). Guiding neuronal growth cones using Ca2+ signals. Trends Cell Biol *14*, 320-30.

Henley, J. R., Huang, K. H., Wang, D., and Poo, M. M. (2004). Calcium mediates bidirectional growth cone turning induced by myelin-associated glycoprotein. Neuron *44*, 909-16.

Heo, Y., Kim, S., Seo, C., Kim, Y., Sung, B., Lee, H., Lee, J., Park, S., Kim, J., Hwang, K., et al. (2004). Structural basis for the selective inhibition of JNK1 by the scaffolding protein JIP1 and SP600125. EMBO Journal *23*, 2185-2195.

Herdegen, T., Blume, A., Buschmann, T., Georgakopoulos, E., Winter, C., Schmid, W., Hsieh, T., Zimmermann, M., and Gass, P. (1997). Expression of activating transcription factor-2, serum response factor and camp/ca response element binding protein in the adult rat brain following generalized seizures, nerve fibre lesion and ultraviolet irradiation. Neuroscience *81*, 199-212.

Herdegen, T., Kummer, W., Fiallos, C., Leah, J., and Bravo, R. (1991). Expression of c-JUN, JUN B and JUN D proteins in rat nervous system following transection of vagus nerve and cervical sympathetic trunk. Neuroscience *45*, 413-422.

Herdegen, T., and Zimmermann, M. (1994). Expression of c-Jun and JunD transcription factors represent specific changes in neuronal gene expression following axotomy. Prog Brain Res *103*, 153-71.

Hernández-Benítez, R., Pasantes-Morales, H., Saldaña, I. T., and Ramos-Mandujano, G. (2009). Taurine stimulates proliferation of mice embryonic cultured neural progenitor cells. J Neurosci Res. Available at: http://www.ncbi.nlm.nih.gov/pubmed/20029963 [Accessed January 2, 2010].

Herrmann, H., and Aebi, U. (2000). Intermediate filaments and their associates: multi-talented structural elements specifying cytoarchitecture and cytodynamics. Curr. Opin. Cell Biol *12*, 79-90.

Hess, J., Angel, P., and Schorpp-Kistner, M. (2004). AP-1 subunits: quarrel and harmony among siblings. J. Cell. Sci *117*, 5965-5973.

Hickey, W. F., and Kimura, H. (1988). Perivascular microglial cells of the CNS are bone marrow-derived and present antigen in vivo. Science *239*, 290-292.

Hilfiker, S., Pieribone, V. A., Czernik, A. J., Kao, H. T., Augustine, G. J., and Greengard, P. (1999). Synapsins as regulators of neurotransmitter release. Philos. Trans. R. Soc. Lond., B, Biol. Sci *354*, 269-279.

Hirata, A., Masaki, T., Motoyoshi, K., and Kamakura, K. (2002). Intrathecal administration of nerve growth factor delays GAP 43 expression and early phase regeneration of adult rat peripheral nerve. Brain Res *944*, 146-56.

Hiroi, S., Tsukamoto, Y., Sasaki, F., Miki, N., and Taira, E. (2003). Involvement of gicerin, a cell adhesion molecule, in development and regeneration of chick sciatic nerve. FEBS Lett *554*, 311-4.

Hirota, H., Kiyama, H., Kishimoto, T., and Taga, T. (1996). Accelerated Nerve Regeneration in Mice by upregulated expression of interleukin (IL) 6 and IL-6 receptor after trauma. J Exp Med *183*, 2627-34.

Hisanaga, S., and Hirokawa, N. (1988). Structure of the peripheral domains of neurofilaments revealed by low angle rotary shadowing. J. Mol. Biol *202*, 297-305.

Ho, M. F., Bähler, M., Czernik, A. J., Schiebler, W., Kézdy, F. J., Kaiser, E. T., and Greengard, P. (1991). Synapsin I is a highly surface-active molecule. J. Biol. Chem *266*, 5600-5607.

Hockfield, S., and McKay, R. D. (1985). Identification of major cell classes in the developing mammalian nervous system. J. Neurosci *5*, 3310-3328.

Hoesche, C., Sauerwald, A., Veh, R. W., Krippl, B., and Kilimann, M. W. (1993). The 5'-flanking region of the rat synapsin I gene directs neuron-specific and developmentally regulated reporter gene expression in transgenic mice. J. Biol. Chem *268*, 26494-26502.

Hoffman, P. N. (1989). Expression of GAP-43, a rapidly transported growth-associated protein, and class II beta tubulin, a slowly transported cytoskeletal protein, are coordinated in regenerating neurons. J Neurosci *9*, 893-7.

Hong, K., Nishiyama, M., Henley, J., Tessier-Lavigne, M., and Poo, M. (2000). Calcium signalling in the guidance of nerve growth by netrin-1. Nature *403*, 93-8.

Horie, H., and Kadoya, T. (2000). Identification of oxidized galectin-1 as an initial repair regulatory factor after axotomy in peripheral nerves. Neurosci Res *38*, 131-7.

Hosaka, M., and Südhof, T. C. (1998a). Synapsin III, a novel synapsin with an unusual regulation by Ca2+. J. Biol. Chem *273*, 13371-13374.

Hosaka, M., and Südhof, T. C. (1998b). Synapsins I and II are ATP-binding proteins with differential Ca2+ regulation. J. Biol. Chem *273*, 1425-1429.

Hossain-Ibrahim, M. K., Rezajooi, K., Stallcup, W. B., Lieberman, A. R., and Anderson, P. N. (2007). Analysis of axonal regeneration in the central and peripheral nervous systems of the NG2-deficient mouse. BMC Neurosci *8*, 80.

Hottinger, A. F., Azzouz, M., Deglon, N., Aebischer, P., and Zurn, A. D. (2000). Complete and long-term rescue of lesioned adult motoneurons by lentiviral-mediated expression of glial cell line-derived neurotrophic factor in the facial nucleus. J Neurosci *20*, 5587-93.

Houle, J. D., Tom, V. J., Mayes, D., Wagoner, G., Phillips, N., and Silver, J. (2006). Combining an Autologous Peripheral Nervous System "Bridge" and Matrix Modification by Chondroitinase Allows Robust, Functional Regeneration beyond a Hemisection Lesion of the Adult Rat Spinal Cord. J. Neurosci. *26*, 7405-7415.

Hristova, M., Cuthill, D., Zbarsky, V., Acosta-Saltos, A., Wallace, A., Blight, K., Buckley, S. M., Peebles, D., Heuer, H., Waddington, S. N., et al. (2009). Activation and deactivation of periventricular white matter phagocytes during postnatal mouse development. Glia. Available at: http://www.ncbi.nlm.nih.gov/entrez/query.fcgi?cmd=Retrieve&db=PubMed&dopt=Citation&list_uids=19544386.

Hsu, J. C., McKeon, R., Goussev, S., Werb, Z., Lee, J., Trivedi, A., and Noble-Haeusslein, L. J. (2006). Matrix metalloproteinase-2 facilitates wound healing events that promote functional recovery after spinal cord injury. J. Neurosci *26*, 9841-9850.

Huang, Z., Yan, D., and Ge, B. (2008). JNK regulates cell migration through promotion of tyrosine phosphorylation of paxillin. Cellular Signalling *20*, 2002-2012.

Hüll, M., and Bähr, M. (1994). Regulation of immediate-early gene expression in rat retinal ganglion cells after axotomy and during regeneration through a peripheral nerve graft. J. Neurobiol *25*, 92-105.

Huizar, P., Kuno, M., Kudo, N., and Miyata, Y. (1977). Reaction of intact spinal motoneurones to partial denervation of the muscle. J. Physiol. (Lond.) *265*, 175-191.

Huppenbauer, C. B., Tanzer, L., DonCarlos, L. L., and Jones, K. J. (2005). Gonadal Steroid Attenuation of Developing Hamster Facial Motoneuron Loss by Axotomy: Equal Efficacy of Testosterone, Dihydrotestosterone, and 17-{beta} Estradiol. J. Neurosci. *25*, 4004-4013.

Huttner, W. B., Schiebler, W., Greengard, P., and De Camilli, P. (1983). Synapsin I (protein I), a nerve terminal-specific phosphoprotein. III. Its association with synaptic vesicles studied in a highly purified synaptic vesicle preparation. J. Cell Biol *96*, 1374-1388.

Hydman, J., Remahl, S., Bjorck, G., Svensson, M., and Mattsson, P. (2007). Nimodipine improves reinnervation and neuromuscular function after injury to the recurrent laryngeal nerve in the rat. Ann Otol Rhinol Laryngol *116*, 623-30.

Ikegami, T., Nakamura, M., Yamane, J., Katoh, H., Okada, S., Iwanami, A., Watanabe, K., Ishii, K., Kato, F., Fujita, H., et al. (2005). Chondroitinase ABC combined with neural stem/progenitor cell transplantation enhances graft cell migration and outgrowth of growth-associated protein-43-positive fibers after rat spinal cord injury. Eur J Neurosci *22*, 3036-46.

Ito, Y., Sasaki, Y., Horimoto, M., Wada, S., Tanaka, Y., Kasahara, A., Ueki, T., Hirano, T., Yamamoto, H., Fujimoto, J., et al. (1998). Activation of mitogen-activated protein kinases/extracellular signal-regulated kinases in human hepatocellular carcinoma. Hepatology *27*, 951-8.

Jaegle, M., Ghazvini, M., Mandemakers, W., Piirsoo, M., Driegen, S., Levavasseur, F., Raghoenath, S., Grosveld, F., and Meijer, D. (2003). The POU proteins Brn-2 and Oct-6 share important functions in Schwann cell development. Genes Dev *17*, 1380-1391.

Jana, M., Dasgupta, S., Liu, X., and Pahan, K. (2002). Interleukin-12 P40 induces the expression of TNF-α in microglia and macrophages. Journal of Neurochemistry *81*, 52-53.

Jessen, K. R. (2004). Glial cells. The International Journal of Biochemistry & Cell Biology *36*, 1861-1867.

Jiang, S., Bendjelloul, F., Ballerini, P., D'Alimonte, I., Nargi, E., Jiang, C., Huang, X., and Rathbone, M. P. (2007). Guanosine reduces apoptosis and inflammation associated with restoration of function in rats with acute spinal cord injury. Purinergic Signal *3*, 411-421.

Johnson, G., and Nakamura, K. (2007). The c-jun kinase/stress-activated pathway: Regulation, function and role in human disease. Biochimica et Biophysica Acta - Molecular Cell Research *1773*, 1341-1348.

Jones, L. L., Banati, R. B., Graeber, M. B., Bonfanti, L., Raivich, G., and Kreutzberg, G. W. (1997). Population control of microglia: does apoptosis play a role? J Neurocytol *26*, 755-70.

Jones, L. L., Kreutzberg, G. W., and Raivich, G. (1997). Regulation of CD44 in the regenerating mouse facial motor nucleus. Eur J Neurosci *9*, 1854-63.

Jones, L. L., Liu, Z., Shen, J., Werner, A., Kreutzberg, G. W., and Raivich, G. (2000). Regulation of the cell adhesion molecule CD44 after nerve transection and direct trauma to the mouse brain. J Comp Neurol *426*, 468-92.

Jones, L., Kreutzberg, G., and Raivich, G. (1997). Regulation of CD44 in the regenerating mouse facial motor nucleus. European Journal of Neuroscience *9*, 1854-1863.

Jones, L., Liu, Z., Shen, J., Werner, A., Kreutzberg, G., and Raivich, G. (2000). Regulation of the cell adhesion molecule CD44 after nerve transection and direct trauma to the mouse brain. Journal of Comparative Neurology *426*, 468-492.

Jurewicz, A., Matysiak, M., Tybor, K., and Selmaj, K. (2003). TNF-induced death of adult human oligodendrocytes is mediated by c-jun NH2-terminal kinase-3. Brain *126*, 1358-70.

K. A. Street, G. Xu, K. L. Hall, G. W. Intano, J. R. McCarrey, D. C. Herbert, M. W. Kilimann, and C. A. Walter (2005). Rat Synapsin 1 Promoter Mediated Transgene Expression in Testicular Cell Types. Available at: http://www.liebertonline.com/doi/abs/10.1089%2Fdna.2005.24.133 [Accessed August 28, 2009].

Kalla, R., Liu, Z., Xu, S., Koppius, A., Imai, Y., Kloss, C. U., Kohsaka, S., Gschwendtner, A., Moller, J. C., Werner, A., et al. (2001). Microglia and the early phase of immune surveillance in the axotomized facial motor nucleus: impaired microglial activation

and lymphocyte recruitment but no effect on neuronal survival or axonal regeneration in macrophage-colony stimulating factor-deficient mice. J Comp Neurol *436*, 182-201.

Kalousa, A., and Keast, J. R. (2009). Conditioning lesions enhance growth state only in sensory neurons lacking calcitonin gene-related peptide and Bandeiraea simplicifolia I-isolectin B4-binding. Neuroscience. Available at: http://www.ncbi.nlm.nih.gov/pubmed/20006678 [Accessed December 26, 2009].

Kanje, M., Skottner, A., Sjoberg, J., and Lundborg, G. (1989). Insulin-like growth factor I (IGF-I) stimulates regeneration of the rat sciatic nerve. Brain Res *486*, 396-8.

Kanu (2010). Characterizing the transcription factor ATMIN.

Kanu, N., and Behrens, A. (2007). ATMIN defines an NBS1-independent pathway of ATM signalling. Embo J *26*, 2933-41.

Kanu, N., and Behrens, A. (2008). ATMINistrating ATM signalling: regulation of ATM by ATMIN. Cell Cycle *7*, 3483-6.

Kao, H. T., Porton, B., Czernik, A. J., Feng, J., Yiu, G., Häring, M., Benfenati, F., and Greengard, P. (1998). A third member of the synapsin gene family. Proc. Natl. Acad. Sci. U.S.A *95*, 4667-4672.

Karimi-Abdolrezaee, S., Eftekharpour, E., Wang, J., Morshead, C. M., and Fehlings, M. G. (2006). Delayed Transplantation of Adult Neural Precursor Cells Promotes Remyelination and Functional Neurological Recovery after Spinal Cord Injury. J. Neurosci. *26*, 3377-3389.

Kenney, A. M., and Kocsis, J. D. (1998). Peripheral axotomy induces long-term c-Jun amino-terminal kinase-1 activation and activator protein-1 binding activity by c-Jun and junD in adult rat dorsal root ganglia In vivo. J Neurosci *18*, 1318-28.

Kerschensteiner, M., Schwab, M. E., Lichtman, J. W., and Misgeld, T. (2005). In vivo imaging of axonal degeneration and regeneration in the injured spinal cord. Nat. Med *11*, 572-577.

Kim, S. J., Lafyatis, R., Kim, K. Y., Angel, P., Fujiki, H., Karin, M., Sporn, M. B., and Roberts, A. B. (1990). Regulation of collagenase gene expression by okadaic acid, an inhibitor of protein phosphatases. Cell Regul *1*, 269-278.

Kim, S. T., Lim, D. S., Canman, C. E., and Kastan, M. B. (1999). Substrate specificities and identification of putative substrates of ATM kinase family members. J. Biol. Chem *274*, 37538-37543.

Kiryu, S., Morita, N., Ohno, K., Maeno, H., and Kiyama, H. (1995). Regulation of mRNA expression involved in Ras and PKA signal pathways during rat hypoglossal nerve regeneration. Brain Res Mol Brain Res *29*, 147-56.

Kiryu-Seo, S., Kato, R., Ogawa, T., Nakagomi, S., Nagata, K., and Kiyama, H. (2008). Neuronal injury-inducible gene is synergistically regulated by ATF3, c-Jun, and STAT3 through the interaction with Sp1 in damaged neurons. J Biol Chem *283*,

6988-96.

Kloss, C. U., Bohatschek, M., Kreutzberg, G. W., and Raivich, G. (2001). Effect of lipopolysaccharide on the morphology and integrin immunoreactivity of ramified microglia in the mouse brain and in cell culture. Exp Neurol *168*, 32-46.

Kloss, C. U., Kreutzberg, G. W., and Raivich, G. (1997). Proliferation of ramified microglia on an astrocyte monolayer: characterization of stimulatory and inhibitory cytokines. J Neurosci Res *49*, 248-54.

Kloss, C. U., Werner, A., Klein, M. A., Shen, J., Menuz, K., Probst, J. C., Kreutzberg, G. W., and Raivich, G. (1999). Integrin family of cell adhesion molecules in the injured brain: regulation and cellular localization in the normal and regenerating mouse facial motor nucleus. J Comp Neurol *411*, 162-78.

Kobayashi, S., Kimura, F., Ikeda, T., Osawa, Y., Torikai, H., Kobayashi, A., Sato, K., and Motoyoshi, K. (2009). BCR-ABL promotes neutrophil differentiation in the chronic phase of chronic myeloid leukemia by downregulating c-Jun expression. Leukemia *23*, 1622-1627.

Kohno, H., Sakai, T., and Kitahara, K. (2006). Induction of nestin, Ki-67, and cyclin D1 expression in Müller cells after laser injury in adult rat retina. Graefe's Archive for Clinical and Experimental Ophthalmology *244*, 90-95.

Kolch, W. (2000). Meaningful relationships: the regulation of the Ras/Raf/MEK/ERK pathway by protein interactions. Biochem J *351 Pt 2*, 289-305.

Kouzarides, T., and Ziff, E. (1988). The role of the leucine zipper in the fos-jun interaction. Nature *336*, 646-651.

Kozubenko, N., Turnovcova, K., Kapcalova, M., Butenko, O., Anderova, M., Rusnakova, V., Kubista, M., Hampl, A., Jendelova, P., and Sykova, E. (2009). Analysis of in vitro and in vivo characteristics of human embryonic stem cell-derived neural precursors. Cell Transplant. Available at: http://www.ncbi.nlm.nih.gov/pubmed/20021734 [Accessed January 2, 2010].

Kraft, A. D., McPherson, C. A., and Harry, G. J. (2009). Heterogeneity of microglia and TNF signaling as determinants for neuronal death or survival. NeuroToxicology *30*, 785-793.

Krause, T. L., Fishman, H. M., Ballinger, M. L., and Bittner, G. D. (1994). Extent and mechanism of sealing in transected giant axons of squid and earthworms. J. Neurosci *14*, 6638-6651.

Kuan, C. Y., Yang, D. D., Samanta Roy, D. R., Davis, R. J., Rakic, P., and Flavell, R. A. (1999a). The Jnk1 and Jnk2 protein kinases are required for regional specific apoptosis during early brain development. Neuron *22*, 667-76.

Kuan, C., Yang, D., Samanta Roy, D., Davis, R., Rakic, P., and Flavell, R. (1999b). The Jnk1 and Jnk2 protein kinases are required for regional specific apoptosis during early brain development. Neuron *22*, 667-676.

Kuan, C., Whitmarsh, A. J., Yang, D. D., Liao, G., Schloemer, A. J., Dong, C., Bao, J., Banasiak, K. J., Haddad, G. G., Flavell, R. A., et al. (2003). A critical role of neural-specific JNK3 for ischemic apoptosis. Proc. Natl. Acad. Sci. U.S.A *100*, 15184-15189.

Kuecherer-Ehret, A., Graeber, M. B., Edgar, D., Thoenen, H., and Kreutzberg, G. W. (1990). Immunoelectron microscopic localization of laminin in normal and regenerating mouse sciatic nerve. J Neurocytol *19*, 101-9.

Kügler, S., Kilic, E., and Bähr, M. (2003). Human synapsin 1 gene promoter confers highly neuron-specific long-term transgene expression from an adenoviral vector in the adult rat brain depending on the transduced area. Gene Ther *10*, 337-347.

Kügler, S., Meyn, L., Holzmüller, H., Gerhardt, E., Isenmann, S., Schulz, J. B., and Bähr, M. (2001). Neuron-specific expression of therapeutic proteins: evaluation of different cellular promoters in recombinant adenoviral vectors. Mol. Cell. Neurosci *17*, 78-96.

Kuhn, R., Pravtcheva, D., Ruddle, F., and Lemke, G. (1990). The gene encoding peripheral myelin protein zero is located on mouse chromosome 1. J. Neurosci *10*, 205-209.

Ladiwala, U., Li, H., Antel, J. P., and Nalbantoglu, J. (1999). p53 induction by tumor necrosis factor-alpha and involvement of p53 in cell death of human oligodendrocytes. J Neurochem *73*, 605-11.

Laux, T., Fukami, K., Thelen, M., Golub, T., Frey, D., and Caroni, P. (2000). GAP43, MARCKS, and CAP23 modulate PI(4,5)P(2) at plasmalemmal rafts, and regulate cell cortex actin dynamics through a common mechanism. J Cell Biol *149*, 1455-72.

Lavin, M. F., and Shiloh, Y. (1997). The genetic defect in ataxia-telangiectasia. Annu Rev Immunol *15*, 177-202.

Le, N., Nagarajan, R., Wang, J. Y. T., Svaren, J., LaPash, C., Araki, T., Schmidt, R. E., and Milbrandt, J. (2005). Nab proteins are essential for peripheral nervous system myelination. Nat. Neurosci *8*, 932-940.

Lee, H., Yuan, C., Hammet, A., Mahajan, A., Chen, E. S., Wu, M., Su, M., Heierhorst, J., and Tsai, M. (2008). Diphosphothreonine-specific interaction between an SQ/TQ cluster and an FHA domain in the Rad53-Dun1 kinase cascade. Mol. Cell *30*, 767-778.

Lee, M., Brennan, A., Blanchard, A., Zoidl, G., Dong, Z., Tabernero, A., Zoidl, C., Dent, M. A., Jessen, K. R., and Mirsky, R. (1997). P0 is constitutively expressed in the rat neural crest and embryonic nerves and is negatively and positively regulated by axons to generate non-myelin-forming and myelin-forming Schwann cells, respectively. Mol. Cell. Neurosci *8*, 336-350.

Lee, M. J., Calle, E., Brennan, A., Ahmed, S., Sviderskaya, E., Jessen, K. R., and Mirsky, R. (2001). In early development of the rat mRNA for the major myelin protein P(0) is expressed in nonsensory areas of the embryonic inner ear, notochord, enteric nervous system, and olfactory ensheathing cells. Dev. Dyn *222*, 40-51.

Lee, S. C., Liu, W., Brosnan, C. F., and Dickson, D. W. (1994). GM-CSF promotes proliferation of human fetal and adult microglia in primary cultures. Glia *12*, 309-318.

Lee, S. O., Lou, W., Qureshi, K. M., Mehraein-Ghomi, F., Trump, D. L., and Gao, A. C. (2004). RNA interference targeting Stat3 inhibits growth and induces apoptosis of human prostate cancer cells. Prostate *60*, 303-9.

Lee, S. I., Kim, B. G., Hwang, D. H., Kim, H. M., and Kim, S. U. (2009). Overexpression of Bcl-XL in human neural stem cells promotes graft survival and functional recovery following transplantation in spinal cord injury. J. Neurosci. Res *87*, 3186-3197.

Lee, T. H., Klampfer, L., Shows, T. B., and Vilcek, J. (1993). Transcriptional regulation of TSG6, a tumor necrosis factor- and interleukin-1-inducible primary response gene coding for a secreted hyaluronan-binding protein. J. Biol. Chem *268*, 6154-6160.

Lemke, G., and Axel, R. (1985). Isolation and sequence of a cDNA encoding the major structural protein of peripheral myelin. Cell *40*, 501-508.

Lendahl, U., Zimmerman, L. B., and McKay, R. D. (1990). CNS stem cells express a new class of intermediate filament protein. Cell *60*, 585-595.

Li, L., Chin, L. S., Shupliakov, O., Brodin, L., Sihra, T. S., Hvalby, O., Jensen, V., Zheng, D., McNamara, J. O., and Greengard, P. (1995). Impairment of synaptic vesicle clustering and of synaptic transmission, and increased seizure propensity, in synapsin I-deficient mice. Proceedings of the National Academy of Sciences of the United States of America *92*, 9235-9239.

Li, Y., and Chopp, M. (1999). Temporal profile of nestin expression after focal cerebral ischemia in adult rat. Brain Res *838*, 1-10.

Lin, L., and Chan, S. O. (2003). Perturbation of CD44 function affects chiasmatic routing of retinal axons in brain slice preparations of the mouse retinofugal pathway. Eur J Neurosci *17*, 2299-312.

Lin, L., Rao, Y., and Isacson, O. (2005). Netrin-1 and slit-2 regulate and direct neurite growth of ventral midbrain dopaminergic neurons. Mol Cell Neurosci *28*, 547-55.

Lindholm, D., Heumann, R., Meyer, M., and Thoenen, H. (1987). Interleukin-1 regulates synthesis of nerve growth factor in non-neuronal cells of rat sciatic nerve. Nature *330*, 658-9.

Lindwall, C., Dahlin, L., Lundborg, G., and Kanje, M. (2004). Inhibition of c-Jun phosphorylation reduces axonal outgrowth of adult rat nodose ganglia and dorsal root ganglia sensory neurons. Mol Cell Neurosci *27*, 267-79.

Lindwall, C., and Kanje, M. (2005a). The Janus role of c-Jun: Cell death versus survival and regeneration of neonatal sympathetic and sensory neurons. Experimental Neurology *196*, 184-194.

Lindwall, C., and Kanje, M. (2005b). The Janus role of c-Jun: Cell death versus survival

and regeneration of neonatal sympathetic and sensory neurons. Experimental Neurology *196*, 184-194.

Liu, C., Chen, B., Zhu, J., Zhang, R., Yao, F., Jin, F., Xu, H., and Lu, P. (2009). Clinical implications for nestin protein expression in breast cancer. Cancer Sci. Available at: http://www.ncbi.nlm.nih.gov/pubmed/20028381 [Accessed January 2, 2010].

Liu, J., Minemoto, Y., and Lin, A. (2004). c-Jun N-terminal protein kinase 1 (JNK1), but not JNK2, is essential for tumor necrosis factor alpha-induced c-Jun kinase activation and apoptosis. Molecular and Cellular Biology *24*, 10844-10856.

Liu, R. Y., and Snider, W. D. (2001). Different signaling pathways mediate regenerative versus developmental sensory axon growth. J Neurosci *21*, RC164.

Liu, W., Brosnan, C. F., Dickson, D. W., and Lee, S. C. (1994). Macrophage colony-stimulating factor mediates astrocyte-induced microglial ramification in human fetal central nervous system culture. Am. J. Pathol *145*, 48-53.

Lonart, G., and Simsek-Duran, F. (2006). Deletion of synapsins I and II genes alters the size of vesicular pools and rabphilin phosphorylation. Brain Res *1107*, 42-51.

Lothian, C., and Lendahl, U. (1997). An evolutionarily conserved region in the second intron of the human nestin gene directs gene expression to CNS progenitor cells and to early neural crest cells. Eur. J. Neurosci *9*, 452-462.

Lu, X., and Richardson, P. M. (1991). Inflammation near the nerve cell body enhances axonal regeneration. J Neurosci *11*, 972-8.

Macgregor, P., Abate, C., and Curran, T. (1990). Direct cloning of leucine zipper proteins: Jun binds cooperatively to the CRE with CRE-BP1. Oncogene *5*, 451-458.

Madison, R., Archibald, S., and Brushart, T. (1996). Reinnervation accuracy of the rat femoral nerve by motor and sensory neurons. Journal of Neuroscience *16*, 5698-5703.

Madura, T., Yamashita, T., Kubo, T., Tsuji, L., Hosokawa, K., and Tohyama, M. (2004). Changes in mRNA of Slit-Robo GTPase-activating protein 2 following facial nerve transection. Brain Res Mol Brain Res *123*, 76-80.

Makwana, M., Serchov, T., Hristova, M., Bohatschek, M., Gschwendtner, A., Kalla, R., Liu, Z., Heumann, R., and Raivich, G. (2009). Regulation and function of neuronal GTP-Ras in facial motor nerve regeneration. J Neurochem *108*, 1453-63.

Makwana, M., Jones, L. L., Cuthill, D., Heuer, H., Bohatschek, M., Hristova, M., Friedrichsen, S., Ormsby, I., Bueringer, D., Koppius, A., et al. (2007). Endogenous transforming growth factor beta 1 suppresses inflammation and promotes survival in adult CNS. J. Neurosci *27*, 11201-11213.

Makwana, M., Serchov, T., Hristova, M., Bohatschek, M., Gschwendtner, A., Kalla, R., Liu, Z., Heumann, R., and Raivich, G. (2009). Regulation and function of neuronal GTP-Ras in facial motor nerve regeneration. J. Neurochem *108*, 1453-1463.

Makwana, M., Werner, A., et al. (2009). Peripheral facial nerve axotomy in mice causes sprouting of motor axons into perineuronal central white matter: Time course and molecular characterization. J Comp Neurol *518*, 699-721.

Malnou, C., Salem, T., Brockly, F., Wodrich, H., Piechaczyk, M., and Jariel-Encontre, I. (2007). Heterodimerization with Jun family members regulates c-Fos nucleocytoplasmic traffic. Journal of Biological Chemistry *282*, 31046-31059.

Manthorpe, M., Engvall, E., Ruoslahti, E., Longo, F. M., Davis, G. E., and Varon, S. (1983). Laminin promotes neuritic regeneration from cultured peripheral and central neurons. J Cell Biol *97*, 1882-90.

Maroney, A. C., Finn, J. P., Bozyczko-Coyne, D., O'Kane, T. M., Neff, N. T., Tolkovsky, A. M., Park, D. S., Yan, C. Y., Troy, C. M., and Greene, L. A. (1999). CEP-1347 (KT7515), an inhibitor of JNK activation, rescues sympathetic neurons and neuronally differentiated PC12 cells from death evoked by three distinct insults. J Neurochem *73*, 1901-12.

Maroney, A. C., Glicksman, M. A., Basma, A. N., Walton, K. M., Knight, E., Murphy, C. A., Bartlett, B. A., Finn, J. P., Angeles, T., Matsuda, Y., et al. (1998). Motoneuron apoptosis is blocked by CEP-1347 (KT 7515), a novel inhibitor of the JNK signaling pathway. J Neurosci *18*, 104-11.

Martin, L. J., Pardo, C. A., Cork, L. C., and Price, D. L. (1994). Synaptic pathology and glial responses to neuronal injury precede the formation of senile plaques and amyloid deposits in the aging cerebral cortex. Am. J. Pathol *145*, 1358-1381.

Martini, R., Schachner, M., and Brushart, T. M. (1994). The L2/HNK-1 carbohydrate is preferentially expressed by previously motor axon-associated Schwann cells in reinnervated peripheral nerves. J Neurosci *14*, 7180-91.

Martini, R., Schachner, M., and Faissner, A. (1990). Enhanced expression of the extracellular matrix molecule J1/tenascin in the regenerating adult mouse sciatic nerve. J Neurocytol *19*, 601-16.

Marvin, M. J., Dahlstrand, J., Lendahl, U., and McKay, R. D. (1998). A rod end deletion in the intermediate filament protein nestin alters its subcellular localization in neuroepithelial cells of transgenic mice. J. Cell. Sci *111 (Pt 14)*, 1951-1961.

Mason, M., Lieberman, A., and Anderson, P. (2003). Corticospinal neurons up-regulate a range of growth-associated genes following intracortical, but not spinal, axotomy. European Journal of Neuroscience *18*, 789-802.

Mathiasen, J. R., McKenna, B. A., Saporito, M. S., Ghadge, G. D., Roos, R. P., Holskin, B. P., Wu, Z. L., Trusko, S. P., Connors, T. C., Maroney, A. C., et al. (2004). Inhibition of mixed lineage kinase 3 attenuates MPP+-induced neurotoxicity in SH-SY5Y cells. Brain Res *1003*, 86-97.

Matsumoto, Y., Hara, N., Tanaka, R., and Fujiwara, M. (1986). Immunohistochemical analysis of the rat central nervous system during experimental allergic encephalomyelitis, with special reference to Ia-positive cells with dendritic morphology. J. Immunol *136*, 3668-3676.

Mattsson, P., Bjorck, G., Remahl, S., Backdahl, M., Hamberger, B., Hydman, J., and Svensson, M. (2005). Nimodipine and microsurgery induced recovery of the vocal cord after recurrent laryngeal nerve resection. Laryngoscope *115*, 1863-5.

Mattsson, P., Janson, A. M., Aldskogius, H., and Svensson, M. (2001). Nimodipine promotes regeneration and functional recovery after intracranial facial nerve crush. J Comp Neurol *437*, 106-17.

May, P., Rohlmann, A., Bock, H. H., Zurhove, K., Marth, J. D., Schomburg, E. D., Noebels, J. L., Beffert, U., Sweatt, J. D., Weeber, E. J., et al. (2004). Neuronal LRP1 Functionally Associates with Postsynaptic Proteins and Is Required for Normal Motor Function in Mice. Mol. Cell. Biol. *24*, 8872-8883.

McGee, A. W., and Strittmatter, S. M. (2003). The Nogo-66 receptor: focusing myelin inhibition of axon regeneration. Trends Neurosci *26*, 193-8.

McGeer, P. L., Kawamata, T., Walker, D. G., Akiyama, H., Tooyama, I., and McGeer, E. G. (1993). Microglia in degenerative neurological disease. Glia *7*, 84-92.

McGraw, J., McPhail, L. T., Oschipok, L. W., Horie, H., Poirier, F., Steeves, J. D., Ramer, M. S., and Tetzlaff, W. (2004). Galectin-1 in regenerating motoneurons. Eur J Neurosci *20*, 2872-80.

McGraw, J., Oschipok, L. W., Liu, J., Hiebert, G. W., Mak, C. F., Horie, H., Kadoya, T., Steeves, J. D., Ramer, M. S., and Tetzlaff, W. (2004). Galectin-1 expression correlates with the regenerative potential of rubrospinal and spinal motoneurons. Neuroscience *128*, 713-9.

McNamara, R. K., Vasquez, P. A., Mathe, A. A., and Lenox, R. H. (2003). Differential expression and regulation of myristoylated alanine-rich C kinase substrate (MARCKS) in the hippocampus of C57/BL6J and DBA/2J mice. J Neurochem *85*, 462-8.

McNees, C. J., Conlan, L. A., Tenis, N., and Heierhorst, J. (2005). ASCIZ regulates lesion-specific Rad51 focus formation and apoptosis after methylating DNA damage. EMBO J *24*, 2447-57.

Mears, S., Schachner, M., and Brushart, T. M. (2003). Antibodies to myelin-associated glycoprotein accelerate preferential motor reinnervation. J Peripher Nerv Syst *8*, 91-9.

Mechta-Grigoriou, F., Gerald, D., and Yaniv, M. (2001). The mammalian Jun proteins: redundancy and specificity. Oncogene *20*, 2378-2389.

Medina, R. J., Kataoka, K., Takaishi, M., Miyazaki, M., and Huh, N. (2006). Isolation of epithelial stem cells from dermis by a three-dimensional culture system. J. Cell. Biochem *98*, 174-184.

Mei, Y., Yuan, Z., Song, B., Li, D., Ma, C., Hu, C., Ching, Y., and Li, M. (2008a). Activating transcription factor 3 up-regulated by c-Jun NH(2)-terminal kinase/c-Jun contributes to apoptosis induced by potassium deprivation in cerebellar granule

neurons. Neuroscience *151*, 771-779.

Mei, Y., Yuan, Z., Song, B., Li, D., Ma, C., Hu, C., Ching, Y. P., and Li, M. (2008b). Activating transcription factor 3 up-regulated by c-Jun NH(2)-terminal kinase/c-Jun contributes to apoptosis induced by potassium deprivation in cerebellar granule neurons. Neuroscience *151*, 771-9.

Melle, C., Ernst, G., Grosheva, M., Angelov, D. N., Irintchev, A., Guntinas-Lichius, O., and von Eggeling, F. (2009). Proteomic analysis of microdissected facial nuclei of the rat following facial nerve injury. J. Neurosci. Methods. Available at: http://www.ncbi.nlm.nih.gov/pubmed/19748522 [Accessed October 1, 2009].

Melli, G., and Höke, A. (2007). Canadian Association of Neurosciences review: regulation of myelination by trophic factors and neuron-glial signaling. Can J Neurol Sci *34*, 288-295.

Meyer, M., Matsuoka, I., Wetmore, C., Olson, L., and Thoenen, H. (1992). Enhanced synthesis of brain-derived neurotrophic factor in the lesioned peripheral nerve: Different mechanisms are responsible for the regulation of BDNF and NGF mRNA. Journal of Cell Biology *119*, 45-54.

Michalczyk, K., and Ziman, M. (2005a). Nestin structure and predicted function in cellular cytoskeletal organisation. Histol. Histopathol *20*, 665-671.

Michalczyk, K., and Ziman, M. (2005b). Nestin structure and predicted function in cellular cytoskeletal organisation. Histol. Histopathol *20*, 665-671.

Micro Bright Field Bioscience (2010). Stereo Investigator. Available at: www.mbfbioscience.com.

Mills, C., Makwana, M., Wallace, A., Benn, S., Schmidt, H., Tegeder, I., Costigan, M., Brown, R. H., Raivich, G., and Woolf, C. J. (2008). Ro5-4864 promotes neonatal motor neuron survival and nerve regeneration in adult rats. Eur J Neurosci *27*, 937-46.

Minagar, A., Shapshak, P., Fujimura, R., Ownby, R., Heyes, M., and Eisdorfer, C. (2002). The role of macrophage/microglia and astrocytes in the pathogenesis of three neurologic disorders: HIV-associated dementia, Alzheimer disease, and multiple sclerosis. J. Neurol. Sci *202*, 13-23.

Minovi, A., Witt, M., Prescher, A., Gudziol, V., Dazert, S., Hatt, H., and Benecke, H. (2010). Expression and distribution of the intermediate filament protein nestin and other stem cell related molecules in the human olfactory epithelium. Histol. Histopathol *25*, 177-187.

Mirsky, R., Woodhoo, A., Parkinson, D. B., Arthur-Farraj, P., Bhaskaran, A., and Jessen, K. R. (2008). Novel signals controlling embryonic Schwann cell development, myelination and dedifferentiation. Journal of the Peripheral Nervous System *13*, 122-135.

Miskimins, R., Srinivasan, R., Marin-Husstege, M., Miskimins, W. K., and Casaccia-Bonnefil, P. (2002). p27(Kip1) enhances myelin basic protein gene promoter

activity. J Neurosci Res *67*, 100-5.

Miyauchi, A., Kanje, M., Danielsen, N., and Dahlin, L. B. (1997). Role of macrophages in the stimulation and regeneration of sensory nerves by transposed granulation tissue and temporal aspects of the response. Scand J Plast Reconstr Surg Hand Surg *31*, 17-23.

Mohiuddin, L., Delcroix, J. D., Fernyhough, P., and Tomlinson, D. R. (1999). Focally administered nerve growth factor suppresses molecular regenerative responses of axotomized peripheral afferents in rats. Neuroscience *91*, 265-71.

Moller, J. C., Klein, M. A., Haas, S., Jones, L. L., Kreutzberg, G. W., and Raivich, G. (1996). Regulation of thrombospondin in the regenerating mouse facial motor nucleus. Glia *17*, 121-32.

Morrison, S., Mitchell, L. S., Ecob-Prince, M. S., Griffiths, I. R., Thomson, C. E., Barrie, J. A., and Kirkham, D. (1991). P0 gene expression in cultured Schwann cells. J. Neurocytol *20*, 769-780.

Morton, S., Davis, R. J., McLaren, A., and Cohen, P. (2003). A reinvestigation of the multisite phosphorylation of the transcription factor c-Jun. EMBO J *22*, 3876-86.

Murashov, A. K., Ul Haq, I., Hill, C., Park, E., Smith, M., Wang, X., Goldberg, D. J., and Wolgemuth, D. J. (2001). Crosstalk between p38, Hsp25 and Akt in spinal motor neurons after sciatic nerve injury. Brain Res Mol Brain Res *93*, 199-208.

Murphy, G. A., Solski, P. A., Jillian, S. A., Perez de la Ossa, P., D'Eustachio, P., Der, C. J., and Rush, M. G. (1999). Cellular functions of TC10, a Rho family GTPase: regulation of morphology, signal transduction and cell growth. Oncogene *18*, 3831-45.

MURRAY, H. W. (1988). Interferon-Gamma, the Activated Macrophage, and Host Defense Against Microbial Challenge. Annals of Internal Medicine *108*, 595-608.

Musti, A., Treier, M., and Bohmann, D. (1997). Reduced ubiquitin-dependent degradation of c-Jun after phosphorylation by map kinases. Science *275*, 400-402.

Nah, S., Saya, D., and Vogel, Z. (1993). Long-Term Opiate Exposure Leads to Increase in Synapsin I in Rat Spinal Cord–Dorsal Root Ganglion Cocultures. Journal of Neurochemistry *60*, 1147-1150.

Nakabeppu, Y., Ryder, K., and Nathans, D. (1988). DNA binding activities of three murine Jun proteins: Stimulation by Fos. Cell *55*, 907-915.

Nakagomi, S., Suzuki, Y., Namikawa, K., Kiryu-Seo, S., and Kiyama, H. (2003). Expression of the activating transcription factor 3 prevents c-Jun N-terminal kinase-induced neuronal death by promoting heat shock protein 27 expression and Akt activation. J Neurosci *23*, 5187-96.

Nakamae, T., Tanaka, N., Nakanishi, K., Kamei, N., Sasaki, H., Hamasaki, T., Yamada, K., Yamamoto, R., Mochizuki, Y., and Ochi, M. (2009). Chondroitinase ABC promotes corticospinal axon growth in organotypic cocultures. Spinal Cord *47*, 161-

5.

Namikawa, K., Honma, M., Abe, K., Takeda, M., Mansur, K., Obata, T., Miwa, A., Okado, H., and Kiyama, H. (2000). Akt/protein kinase B prevents injury-induced motoneuron death and accelerates axonal regeneration. J Neurosci *20*, 2875-86.

Nathan, D. G., and Sieff, C. A. (1987). The biological activities and uses of recombinant granulocyte-macrophage and multi-colony stimulating factors. Prog Hematol *15*, 1-18.

Nickols, J. C., Valentine, W., Kanwal, S., and Carter, B. D. (2003). Activation of the transcription factor NF-kappaB in Schwann cells is required for peripheral myelin formation. Nat. Neurosci *6*, 161-167.

Nieke, J., and Schachner, M. (1985a). Expression of the neural cell adhesion molecules L1 and N-CAM and their common carbohydrate epitope L2/HNK-1 during development and after transection of the mouse sciatic nerve. Differentiation *30*, 141-151.

Nieke, J., and Schachner, M. (1985b). Expression of the neural cell adhesion molecules L1 and N-CAM and their common carbohydrate epitope L2/HNK-1 during development and after transection of the mouse sciatic nerve. Differentiation *30*, 141-51.

Nishida, K., Kitazawa, R., Mizuno, K., Maeda, S., and Kitazawa, S. (1997). Identification of regulatory elements of human alpha 6 integrin subunit gene. Biochem. Biophys. Res. Commun *241*, 258-263.

Nishiyama, M., Hoshino, A., Tsai, L., Henley, J. R., Goshima, Y., Tessier-Lavigne, M., Poo, M. M., and Hong, K. (2003). Cyclic AMP/GMP-dependent modulation of Ca2+ channels sets the polarity of nerve growth-cone turning. Nature *423*, 990-5.

Niwa-Kawakita, M., Abramowski, V., Kalamarides, M., Thomas, G., and Giovannini, M. (2000). Targeted expression of Cre recombinase to myelinating cells of the central nervous system in transgenic mice. genesis *26*, 127-129.

Nixon, R. A., Saito, K. I., Grynspan, F., Griffin, W. R., Katayama, S., Honda, T., Mohan, P. S., Shea, T. B., and Beermann, M. (1994). Calcium-activated neutral proteinase (calpain) system in aging and Alzheimer's disease. Ann. N. Y. Acad. Sci *747*, 77-91.

Nolin, W. B., Emmetsberger, J., Bukhari, N., Zhang, Y., Levine, J. M., and Tsirka, S. E. (2008). tPA-mediated generation of plasmin is catalyzed by the proteoglycan NG2. Glia *56*, 177-89.

North, R. J. (1978). The concept of the activated macrophage. J. Immunol *121*, 806-809.

Oka, H., Sakai, W., Sonoda, E., Nakamura, J., Asagoshi, K., Wilson, S. H., Kobayashi, M., Yamamoto, K., Heierhorst, J., Takeda, S., et al. (2008). DNA damage response protein ASCIZ links base excision repair with immunoglobulin gene conversion. Biochem. Biophys. Res. Commun *371*, 225-229.

Okada, S., Nakamura, M., Mikami, Y., Shimazaki, T., Mihara, M., Ohsugi, Y., Iwamoto, Y., Yoshizaki, K., Kishimoto, T., Toyama, Y., et al. (2004). Blockade of interleukin-6 receptor suppresses reactive astrogliosis and ameliorates functional recovery in experimental spinal cord injury. J Neurosci Res *76*, 265-76.

Okuno, K., Ohta, S., Kato, H., Taga, T., Sugita, K., and Takeuchi, Y. (2010). Expression of neural stem cell markers in malignant rhabdoid tumor cell lines. Oncol. Rep *23*, 485-492.

Oliveira, A. L., Thams, S., Lidman, O., Piehl, F., Hokfelt, T., Karre, K., Linda, H., and Cullheim, S. (2004). A role for MHC class I molecules in synaptic plasticity and regeneration of neurons after axotomy. Proc Natl Acad Sci U S A *101*, 17843-8.

Ooashi, N., Futatsugi, A., Yoshihara, F., Mikoshiba, K., and Kamiguchi, H. (2005). Cell adhesion molecules regulate Ca2+-mediated steering of growth cones via cyclic AMP and ryanodine receptor type 3. J Cell Biol *170*, 1159-67.

Ovanesov, M. V., Ayhan, Y., Wolbert, C., Moldovan, K., Sauder, C., and Pletnikov, M. V. (2008). Astrocytes play a key role in activation of microglia by persistent Borna disease virus infection. J Neuroinflammation *5*, 50.

Owada, Y., Utsunomiya, A., Yoshimoto, T., and Kondo, H. (1997). Expression of mRNA for Akt, serine-threonine protein kinase, in the brain during development and its transient enhancement following axotomy of hypoglossal nerve. J Mol Neurosci *9*, 27-33.

Palmada, M., Kanwal, S., Rutkoski, N., Gufstafson-Brown, C., Johnson, R., Wisdom, R., and Carter, B. (2002). c-jun is essential for sympathetic neuronal death induced by NGF withdrawal but not by p75 activation. Journal of Cell Biology *158*, 453-461.

Pandita, T. K. (2003). A multifaceted role for ATM in genome maintenance. Expert Rev Mol Med *5*, 1-21.

Parkinson, D. B., Bhaskaran, A., Arthur-Farraj, P., Noon, L. A., Woodhoo, A., Lloyd, A. C., Feltri, M. L., Wrabetz, L., Behrens, A., Mirsky, R., et al. (2008). c-Jun is a negative regulator of myelination. J Cell Biol *181*, 625-37.

Parkinson, D. B., Bhaskaran, A., Droggiti, A., Dickinson, S., D'Antonio, M., Mirsky, R., and Jessen, K. R. (2004). Krox-20 inhibits Jun-NH2-terminal kinase/c-Jun to control Schwann cell proliferation and death. J Cell Biol. *164*, 385–394.

Pearson, A. G., Gray, C. W., Pearson, J. F., Greenwood, J. M., During, M. J., and Dragunow, M. (2003a). ATF3 enhances c-Jun-mediated neurite sprouting. Brain Res Mol Brain Res *120*, 38-45.

Pearson, A., Gray, C., Pearson, J., Greenwood, J., During, M., and Dragunow, M. (2003b). ATF3 enhances c-Jun-mediated neurite sprouting. Molecular Brain Research *120*, 38-45.

Pennypacker, K. (1997). Transcription factors in brain injury. Histol Histopathol *12*, 1125-33.

Pieribone, V. A., Shupliakov, O., Brodin, L., Hilfiker-Rothenfluh, S., Czernik, A. J., and Greengard, P. (1995). Distinct pools of synaptic vesicles in neurotransmitter release. Nature *375*, 493-497.

Pifarré, P., Prado, J., Giralt, M., Molinero, A., Hidalgo, J., and Garcia, A. (2009). CYCLIC GMP PHOSPHODIESTERASE INHIBITION ALTERS THE GLIAL INFLAMMATORY RESPONSE, REDUCES OXIDATIVE STRESS AND CELL DEATH AND INCREASES ANGIOGENESIS FOLLOWING FOCAL BRAIN INJURY. J Neurochem. Available at: http://www.ncbi.nlm.nih.gov/pubmed/20002517 [Accessed December 30, 2009].

Pilkington, G. J. (2005). Cancer stem cells in the mammalian central nervous system. Cell Prolif *38*, 423-433.

Pirvola, U., Xing-Qun, L., Virkkala, J., Saarma, M., Murakata, C., Camoratto, A. M., Walton, K. M., and Ylikoski, J. (2000). Rescue of hearing, auditory hair cells, and neurons by CEP-1347/KT7515, an inhibitor of c-Jun N-terminal kinase activation. J Neurosci *20*, 43-50.

Popratiloff, A. S., Neiss, W. F., Skouras, E., Streppel, M., Guntinas-Lichius, O., and Angelov, D. N. (2001). Evaluation of muscle re-innervation employing pre- and post-axotomy injections of fluorescent retrograde tracers. Brain Res. Bull *54*, 115-123.

Powell, S. K., and Kleinman, H. K. (1997). Neuronal laminins and their cellular receptors. Int J Biochem Cell Biol *29*, 401-14.

Priller, J., Flügel, A., Wehner, T., Boentert, M., Haas, C. A., Prinz, M., Fernández-Klett, F., Prass, K., Bechmann, I., de Boer, B. A., et al. (2001). Targeting gene-modified hematopoietic cells to the central nervous system: use of green fluorescent protein uncovers microglial engraftment. Nat. Med *7*, 1356-1361.

Properzi, F., Asher, R. A., and Fawcett, J. W. (2003). Chondroitin sulphate proteoglycans in the central nervous system: changes and synthesis after injury. Biochem Soc Trans *31*, 335-6.

Qin, H., Roberts, K. L., Niyongere, S. A., Cong, Y., Elson, C. O., and Benveniste, E. N. (2007). Molecular mechanism of lipopolysaccharide-induced SOCS-3 gene expression in macrophages and microglia. J. Immunol *179*, 5966-5976.

Radler-Pohl, A., Sachsenmaier, C., Gebel, S., Auer, H. P., Bruder, J. T., Rapp, U., Angel, P., Rahmsdorf, H. J., and Herrlich, P. (1993). UV-induced activation of AP-1 involves obligatory extranuclear steps including Raf-1 kinase. Embo J *12*, 1005-12.

Raivich, G. (2008). c-Jun expression, activation and function in neural cell death, inflammation and repair. J Neurochem *107*, 898-906.

Raivich, G., and Behrens, A. (2006). Role of the AP-1 transcription factor c-Jun in developing, adult and injured brain. Progress in Neurobiology *78*, 347-363.

Raivich, G., Bohatschek, M., Da Costa, C., Iwata, O., Galiano, M., Hristova, M., Nateri, A. S., Makwana, M., Riera-Sans, L., Wolfer, D. P., et al. (2004a). The AP-1

transcription factor c-Jun is required for efficient axonal regeneration. Neuron *43*, 57-67.

Raivich, G., Bohatschek, M., Da Costa, C., Iwata, O., Galiano, M., Hristova, M., Nateri, A., Makwana, M., Riera-Sans, L., Wolfer, D., et al. (2004b). The AP-1 transcription factor c-Jun is required for efficient axonal regeneration. Neuron *43*, 57-67.

Raivich, G., Bohatschek, M., Kloss, C. U., Werner, A., Jones, L. L., and Kreutzberg, G. W. (1999). Neuroglial activation repertoire in the injured brain: graded response, molecular mechanisms and cues to physiological function. Brain Res Brain Res Rev *30*, 77-105.

Raivich, G., Gehrmann, J., and Kreutzberg, G. W. (1991). Increase of macrophage colony-stimulating factor and granulocyte-macrophage colony-stimulating factor receptors in the regenerating rat facial nucleus. J Neurosci Res *30*, 682-6.

Raivich, G., Hellweg, R., and Kreutzberg, G. W. (1991). NGF receptor-mediated reduction in axonal NGF uptake and retrograde transport following sciatic nerve injury and during regeneration. Neuron *7*, 151-64.

Raivich, G., Jones, L. L., Werner, A., Bluthmann, H., Doetschmann, T., and Kreutzberg, G. W. (1999). Molecular signals for glial activation: pro- and anti-inflammatory cytokines in the injured brain. Acta Neurochir Suppl *73*, 21-30.

Raivich, G., and Kreutzberg, G. W. (1987a). Expression of growth factor receptors in injured nervous tissue. II. Induction of specific platelet-derived growth factor binding in the injured PNS is associated with a breakdown in the blood-nerve barrier and endoneurial interstitial oedema. J Neurocytol *16*, 701-11.

Raivich, G., and Kreutzberg, G. W. (1987b). The localization and distribution of high affinity beta-nerve growth factor binding sites in the central nervous system of the adult rat. A light microscopic autoradiographic study using [125I]beta-nerve growth factor. Neuroscience *20*, 23-36.

Raivich, G., Liu, Z. Q., Kloss, C. U., Labow, M., Bluethmann, H., and Bohatschek, M. (2002). Cytotoxic potential of proinflammatory cytokines: combined deletion of TNF receptors TNFR1 and TNFR2 prevents motoneuron cell death after facial axotomy in adult mouse. Exp Neurol *178*, 186-93.

Raivich, G., and Makwana, M. (2007). The making of successful axonal regeneration: genes, molecules and signal transduction pathways. Brain Res Rev *53*, 287-311.

Ranaivo, H. R., and Wainwright, M. S. (2009). Albumin activates astrocytes and microglia through mitogen-activated protein kinase pathways. Brain Res. Available at: http://www.ncbi.nlm.nih.gov/pubmed/19961838 [Accessed December 30, 2009].

Ransone, L., Visvader, J., Sassone-Corsi, P., and Verma, I. (1989). Fos-Jun interaction: mutational analysis of the leucine zipper domain of both proteins. Genes & development *3*, 770-781.

Rao, M. S. (1999). Multipotent and restricted precursors in the central nervous system. Anat Rec *257*, 137-48.

Read, D. J., Li, Y., Chao, M. V., Cavanagh, J. B., and Glynn, P. (2009). Neuropathy target esterase is required for adult vertebrate axon maintenance. J. Neurosci *29*, 11594-11600.

Rempe, D., Vangeison, G., Hamilton, J., Li, Y., Jepson, M., and Federoff, H. J. (2006). Synapsin I Cre transgene expression in male mice produces germline recombination in progeny. Genesis *44*, 44-49.

Rende, M., Muir, D., Ruoslahti, E., Hagg, T., Varon, S., and Manthorpe, M. (1992). Immunolocalization of ciliary neuronotrophic factor in adult rat sciatic nerve. Glia *5*, 25-32.

Rezajooi, K., Pavlides, M., Winterbottom, J., Stallcup, W. B., Hamlyn, P. J., Lieberman, A. R., and Anderson, P. N. (2004). NG2 proteoglycan expression in the peripheral nervous system: upregulation following injury and comparison with CNS lesions. Mol Cell Neurosci *25*, 572-84.

Riese, U., Ziegler, E., and Hamburger, M. (2004). Militarinone A induces differentiation in PC12 cells via MAP and Akt kinase signal transduction pathways. FEBS Letters *577*, 455-459.

Robak, L. A., Venkatesh, K., Lee, H., Raiker, S. J., Duan, Y., Lee-Osbourne, J., Hofer, T., Mage, R. G., Rader, C., and Giger, R. J. (2009). Molecular basis of the interactions of the Nogo-66 receptor and its homolog NgR2 with myelin-associated glycoprotein: development of NgROMNI-Fc, a novel antagonist of CNS myelin inhibition. J. Neurosci *29*, 5768-5783.

Robinson, G. A., and Madison, R. D. (2004). Motor neurons can preferentially reinnervate cutaneous pathways. Experimental Neurology *190*, 407-413.

Robinson, M., Parsons Perez, M. C., Tebar, L., Palmer, J., Patel, A., Marks, D., Sheasby, A., De Felipe, C., Coffin, R., Livesey, F. J., et al. (2004). FLRT3 is expressed in sensory neurons after peripheral nerve injury and regulates neurite outgrowth. Mol Cell Neurosci *27*, 202-14.

Rolls, A., Shechter, R., London, A., Segev, Y., Jacob-Hirsch, J., Amariglio, N., Rechavi, G., and Schwartz, M. (2008). Two faces of chondroitin sulfate proteoglycan in spinal cord repair: a role in microglia/macrophage activation. PLoS Med *5*, e171.

Rosahl, T., Spillane, D., Missler, M., Herz, J., Selig, D., Wolff, J., Hammer, R., Malenka, R., and Sudhof, T. (1995). Essential functions of synapsins I and II in synaptic vesicle regulation. Nature *375*, 488-493.

Rosahl, T. W., Geppert, M., Spillane, D., Herz, J., Hammer, R. E., Malenka, R. C., and Südhof, T. C. (1993). Short-term synaptic plasticity is altered in mice lacking synapsin I. Cell *75*, 661-670.

Rosso, S., Sussman, D., Wynshaw-Boris, A., and Salinas, P. (2005). Wnt signaling through Dishevelled, Rac and JNK regulates dendritic development. Nature Neuroscience *8*, 34-42.

Rovira, M., Scott, S., Liss, A. S., Jensen, J., Thayer, S. P., and Leach, S. D. (2009). Isolation and characterization of centroacinar/terminal ductal progenitor cells in adult mouse pancreas. Proc Natl Acad Sci U S A. Available at: http://www.ncbi.nlm.nih.gov/pubmed/20018761 [Accessed January 2, 2010].

Sahenk, Z., Serrano-Munuera, C., Chen, L., Kakabadze, I., and Najagara, H. N. (2003). Evidence for impaired axonal regeneration in PMP22 duplication: studies in nerve xenografts. J Peripher Nerv Syst *8*, 116-27.

Sahlgren, C. M., Mikhailov, A., Hellman, J., Chou, Y. H., Lendahl, U., Goldman, R. D., and Eriksson, J. E. (2001). Mitotic reorganization of the intermediate filament protein nestin involves phosphorylation by cdc2 kinase. J. Biol. Chem *276*, 16456-16463.

Saito, S., Suzuki, A., Nozawa-Inoue, K., Kawano, Y., Hoshino, M., Saito, C., and Maeda, T. (2009). Immunohistochemical detection of nestin in the periodontal Ruffini endings of the rat incisor. Neurosci Lett *449*, 195-200.

Salonen, V., Aho, H., Roytta, M., and Peltonen, J. (1988). Quantitation of Schwann cells and endoneurial fibroblast-like cells after experimental nerve trauma. Acta Neuropathol *75*, 331-6.

Sanders, V. M., and Jones, K. J. (2006). Role of immunity in recovery from a peripheral nerve injury. J Neuroimmune Pharmacol *1*, 11-19.

Sandvig, A., Berry, M., Barrett, L. B., Butt, A., and Logan, A. (2004). Myelin-, reactive glia-, and scar-derived CNS axon growth inhibitors: expression, receptor signaling, and correlation with axon regeneration. Glia *46*, 225-51.

Saporito, M. S., Brown, E. M., Miller, M. S., and Carswell, S. (1999). CEP-1347/KT-7515, an inhibitor of c-jun N-terminal kinase activation, attenuates the 1-methyl-4-phenyl tetrahydropyridine-mediated loss of nigrostriatal dopaminergic neurons In vivo. J Pharmacol Exp Ther *288*, 421-7.

Saporito, M. S., Hudkins, R. L., and Maroney, A. C. (2002). Discovery of CEP-1347/KT-7515, an inhibitor of the JNK/SAPK pathway for the treatment of neurodegenerative diseases. Prog Med Chem *40*, 23-62.

Saporito, M. S., Thomas, B. A., and Scott, R. W. (2000). MPTP activates c-Jun NH(2)-terminal kinase (JNK) and its upstream regulatory kinase MKK4 in nigrostriatal neurons in vivo. J Neurochem *75*, 1200-8.

Sassone-Corsi, P., Lamph, W., Kamps, M., and Verma, I. (1988). Fos-associated cellular p39 is related to nuclear transcription factor AP-1. Cell *54*, 553-560.

Sassone-Corsi, P., Sisson, J., and Verma, I. (1988). Transcriptional autoregulation of the proto-oncogene fos. Nature *334*, 314-319.

Sato, Y., and Endo, T. (2000). Alterations with age of the neurons expressing P(0) in the rat spinal cord. Neurosci. Lett *281*, 41-44.

Sato, Y., Kimura, M., Yasuda, C., Nakano, Y., Tomita, M., Kobata, A., and Endo, T. (1999). Evidence for the presence of major peripheral myelin glycoprotein P0 in

mammalian spinal cord and a change of its glycosylation state during aging. Glycobiology *9*, 655-660.

Savitsky, K., Sfez, S., Tagle, D. A., Ziv, Y., Sartiel, A., Collins, F. S., Shiloh, Y., and Rotman, G. (1995). The complete sequence of the coding region of the ATM gene reveals similarity to cell cycle regulators in different species. Hum Mol Genet *4*, 2025-32.

Schiebler, W., Jahn, R., Doucet, J. P., Rothlein, J., and Greengard, P. (1986). Characterization of synapsin I binding to small synaptic vesicles. J. Biol. Chem *261*, 8383-8390.

Schlaepfer, W. W., and Hasler, M. B. (1979). Characterization of the calcium-induced disruption of neurofilaments in rat peripheral nerve. Brain Res *168*, 299-309.

Schoch, S., Cibelli, G., and Thiel, G. (1996). Neuron-specific gene expression of synapsin I. Major role of a negative regulatory mechanism. J. Biol. Chem *271*, 3317-3323.

Schonthal, A., Buscher, M., Angel, P., Rahmsdorf, H., Ponta, H., Hattori, K., Chiu, R., Karin, M., and Herrlich, P. (1989). The Fos and Jun/AP-1 proteins are involved in the downregulation of Fos transcription. Oncogene *4*, 629-636.

Schonthal, A., Gebel, S., Stein, B., Ponta, H., Rahmsdorf, H., and Herrlich, P. (1988). Nuclear oncoproteins determine the genetic program in response to external stimuli. Cold Spring Harbor Symposia on Quantitative Biology *53*, 779-787.

Schuetz, E., Rose, K., and Thanos, S. (2003). Regeneration of ganglion cell axons into a peripheral nerve graft alters retinal expression of glial markers and decreases vulnerability to re-axotomy. Restor. Neurol. Neurosci *21*, 11-18.

Schutte, J., Viallet, J., Nau, M., Segal, S., Fedorko, J., and Minna, J. (1989). jun-B inhibits and c-fos stimulates the transforming and trans-activating activities of c-jun. Cell *59*, 987-997.

Schutze, S., Tchikov, V., and Schneider-Brachert, W. (2008). Regulation of TNFR1 and CD95 signalling by receptor compartmentalization. Nat Rev Mol Cell Biol *9*, 655-62.

Schwab, M. E. (2004). Nogo and axon regeneration. Curr Opin Neurobiol *14*, 118-24.

Schwaiger, F. W., Hager, G., Raivich, G., and Kreutzberg, G. W. (1998). Cellular activation in neuroregeneration. Prog Brain Res *117*, 197-210.

Schweizer, U., Gunnersen, J., Karch, C., Wiese, S., Holtmann, B., Takeda, K., Akira, S., and Sendtner, M. (2002). Conditional gene ablation of Stat3 reveals differential signaling requirements for survival of motoneurons during development and after nerve injury in the adult. J Cell Biol *156*, 287-97.

Seijffers, R., Allchorne, A. J., and Woolf, C. J. (2006). The transcription factor ATF-3 promotes neurite outgrowth. Mol Cell Neurosci *32*, 143-54.

Seijffers, R., Mills, C. D., and Woolf, C. J. (2007). ATF3 increases the intrinsic growth state of DRG neurons to enhance peripheral nerve regeneration. J Neurosci *27*, 7911-

20.

Selak, S., and Fritzler, M. J. (2004). Altered neurological function in mice immunized with early endosome antigen 1. BMC Neurosci *5*, 2.

Sendtner, M., Dittrich, F., Hughes, R. A., and Thoenen, H. (1994a). Actions of CNTF and neurotrophins on degenerating motoneurons: preclinical studies and clinical implications. J Neurol Sci *124 Suppl*, 77-83.

Sendtner, M., Dittrich, F., Hughes, R., and Thoenen, H. (1994b). Actions of CNTF and neurotrophins on degenerating motoneurons: Preclinical studies and clinical implications. Journal of the Neurological Sciences *124*, 77-83.

Senger, D. L., Tudan, C., Guiot, M. C., Mazzoni, I. E., Molenkamp, G., LeBlanc, R., Antel, J., Olivier, A., Snipes, G. J., and Kaplan, D. R. (2002). Suppression of Rac activity induces apoptosis of human glioma cells but not normal human astrocytes. Cancer Res *62*, 2131-40.

Serpe, C. J., Kohm, A. P., Huppenbauer, C. B., Sanders, V. M., and Jones, K. J. (1999). Exacerbation of facial motoneuron loss after facial nerve transection in severe combined immunodeficient (scid) mice. J. Neurosci *19*, RC7.

Serpe, C., Sanders, V., and Jones, K. (2000). Kinetics of facial motoneuron loss following facial nerve transection in severe combined immunodeficient mice. Journal of Neuroscience Research *62*, 273-278.

Serpe, C., Tetzlaff, J., Coers, S., Sanders, V., and Jones, K. (2002). Functional recovery after facial nerve crush is delayed in severe combined immunodeficient mice. Brain, Behavior, and Immunity *16*, 808-812.

Serpe, C. J., Byram, S. C., Sanders, V. M., and Jones, K. J. (2005). Brain-derived neurotrophic factor supports facial motoneuron survival after facial nerve transection in immunodeficient mice. Brain Behav. Immun *19*, 173-180.

Serpe, C. J., Coers, S., Sanders, V. M., and Jones, K. J. (2003a). CD4+ T, but not CD8+ or B, lymphocytes mediate facial motoneuron survival after facial nerve transection. Brain Behav. Immun *17*, 393-402.

Serpe, C. J., Coers, S., Sanders, V. M., and Jones, K. J. (2003b). CD4+ T, but not CD8+ or B, lymphocytes mediate facial motoneuron survival after facial nerve transection. Brain Behav. Immun *17*, 393-402.

Sesaki, H., and Jensen, R. E. (2001). UGO1 encodes an outer membrane protein required for mitochondrial fusion. J Cell Biol *152*, 1123-34.

Shadiack, A. M., Sun, Y., and Zigmond, R. E. (2001a). Nerve growth factor antiserum induces axotomy-like changes in neuropeptide expression in intact sympathetic and sensory neurons. J Neurosci *21*, 363-71.

Shadiack, A., Sun, Y., and Zigmond, R. (2001b). Nerve growth factor antiserum induces axotomy-like changes in neuropeptide expression in intact sympathetic and sensory neurons. Journal of Neuroscience *21*, 363-371.

Shaulian, E., and Karin, M. (2001). AP-1 in cell proliferation and survival. Oncogene *20*, 2390-2400.

Shaw, D., Wang, S., Villaseñor, A., Tsing, S., Walter, D., Browner, M., Barnett, J., and Kuglstatter, A. (2008). The Crystal Structure of JNK2 Reveals Conformational Flexibility in the MAP Kinase Insert and Indicates Its Involvement in the Regulation of Catalytic Activity. Journal of Molecular Biology *383*, 885-893.

Shechter, R., London, A., Varol, C., Raposo, C., Cusimano, M., Yovel, G., Rolls, A., Mack, M., Pluchino, S., Martino, G., et al. (2009). Infiltrating Blood-Derived Macrophages Are Vital Cells Playing an Anti-inflammatory Role in Recovery from Spinal Cord Injury in Mice. PLoS Med *6*, e1000113.

Shen, A., Yan, J., Ding, F., Gu, X., Zhu, D., and Gu, J. (2003). Overexpression of beta-1,4-galactosyltransferase I in rat Schwann cells promotes the growth of co-cultured dorsal root ganglia. Neurosci Lett *342*, 159-62.

Shen, Y. J., DeBellard, M. E., Salzer, J. L., Roder, J., and Filbin, M. T. (1998). Myelin-associated glycoprotein in myelin and expressed by Schwann cells inhibits axonal regeneration and branching. Mol. Cell. Neurosci *12*, 79-91.

Shen, Y., Tenney, A. P., Busch, S. A., Horn, K. P., Cuascut, F. X., Liu, K., He, Z., Silver, J., and Flanagan, J. G. (2009). PTPsigma is a receptor for chondroitin sulfate proteoglycan, an inhibitor of neural regeneration. Science *326*, 592-596.

Shi, Y. (2002). Mechanisms of caspase activation and inhibition during apoptosis. Mol Cell *9*, 459-70.

Shiloh, Y. (2003). ATM and related protein kinases: safeguarding genome integrity. Nat. Rev. Cancer *3*, 155-168.

Shoemaker, S. E., Sachs, H. H., Vaccariello, S. A., and Zigmond, R. E. (2006). Reduction in nerve growth factor availability leads to a conditioning lesion-like effect in sympathetic neurons. J. Neurobiol *66*, 1322-1337.

Sims, K., Ahmed, Z., Gonzalez, A. M., Read, M. L., Cooper-Charles, L., Berry, M., and Logan$, A. (2008). Targeting adenoviral transgene expression to neurons. Molecular and Cellular Neuroscience *39*, 411-417.

Skalli, O., Chou, Y. H., and Goldman, R. D. (1992). Intermediate filaments: not so tough after all. Trends Cell Biol *2*, 308-312.

Skouras, E., Merkel, D., Grosheva, M., Angelova, S. K., Schiffer, G., Thelen, U., Kaidoglou, K., Sinis, N., Igelmund, P., Dunlop, S. A., et al. (2009). Manual stimulation, but not acute electrical stimulation prior to reconstructive surgery, improves functional recovery after facial nerve injury in rats. Restor. Neurol. Neurosci *27*, 237-251.

Smeal, T., Angel, P., Meek, J., and Karin, M. (1989). Different requirements for formation of Jun: Jun and Jun: Fos complexes. Genes Dev *3*, 2091-2100.

Smeal, T., Hibi, M., and Karin, M. (1994). Altering the specificity of signal transduction cascades: positive regulation of c-Jun transcriptional activity by protein kinase A. Embo J *13*, 6006-10.

Smith, P. D., Sun, F., Park, K. K., Cai, B., Wang, C., Kuwako, K., Martinez-Carrasco, I., Connolly, L., and He, Z. (2009). SOCS3 deletion promotes optic nerve regeneration in vivo. Neuron *64*, 617-623.

Sommer, L., and Suter, U. (1998). The glycoprotein P0 in peripheral gliogenesis. Cell and Tissue Research *292*, 11-16.

Spencer T, F. M. (2004). A role for cAMP in regeneration of the adult mammalian CNS. J. Anat *204*, 49-55.

Starkey, M. L., Barritt, A. W., Yip, P. K., Davies, M., Hamers, F. P. T., McMahon, S. B., and Bradbury, E. J. (2005). Assessing behavioural function following a pyramidotomy lesion of the corticospinal tract in adult mice. Exp. Neurol *195*, 524-539.

Stolz, B., Erulkar, S. D., and Kuffler, D. P. (1991). Macrophages direct process elongation from adult frog motorneurons in culture. Proc Biol Sci *244*, 227-31.

Streit, W., and Kreutzberg, G. (1988). Response of endogenous glial cells to motor neuron degeneration induced by toxic ricin. Journal of Comparative Neurology *268*, 248-263.

Streppel, M., Azzolin, N., Dohm, S., Guntinas-Lichius, O., Haas, C., Grothe, C., Wevers, A., Neiss, W. F., and Angelov, D. N. (2002a). Focal application of neutralizing antibodies to soluble neurotrophic factors reduces collateral axonal branching after peripheral nerve lesion. Eur. J. Neurosci *15*, 1327-1342.

Streppel, M., Azzolin, N., Dohm, S., Guntinas-Lichius, O., Haas, C., Grothe, C., Wevers, A., Neiss, W. F., and Angelov, D. N. (2002b). Focal application of neutralizing antibodies to soluble neurotrophic factors reduces collateral axonal branching after peripheral nerve lesion. Eur J Neurosci *15*, 1327-42.

Suarez, V., Guntinas-Lichius, O., Streppel, M., Ingorokva, S., Grosheva, M., Neiss, W. F., Angelov, D. N., and Klimaschewski, L. (2006). The axotomy-induced neuropeptides galanin and pituitary adenylate cyclase-activating peptide promote axonal sprouting of primary afferent and cranial motor neurones. Eur. J. Neurosci *24*, 1555-1564.

Suckfuell, M., Canis, M., Strieth, S., Scherer, H., and Haisch, A. (2007). Intratympanic treatment of acute acoustic trauma with a cell-permeable JNK ligand: A prospective randomized phase I/II study. Acta Oto-Laryngologica *127*, 938-942.

Suh, H., Kim, M., and Lee, S. C. (2005). Inhibition of Granulocyte-Macrophage Colony-Stimulating Factor Signaling and Microglial Proliferation by Anti-CD45RO: Role of Hck Tyrosine Kinase and Phosphatidylinositol 3-Kinase/Akt. J Immunol *174*, 2712-2719.

Sun, D. S., and Chang, H. H. (2003). Differential regulation of JNK in caspase-3-mediated apoptosis of MPP(+)-treated primary cortical neurons. Cell Biol Int *27*, 769-77.

Sun, J., Bronk, P., Liu, X., Han, W., and Südhof, T. C. (2006). Synapsins regulate use-dependent synaptic plasticity in the calyx of Held by a Ca2+/calmodulin-dependent pathway. Proc. Natl. Acad. Sci. U.S.A *103*, 2880-2885.

Sun, W., and Oppenheim, R. W. (2003). Response of motoneurons to neonatal sciatic nerve axotomy in Bax-knockout mice. Mol Cell Neurosci *24*, 875-86.

Sun, Y., Shi, J., Fu, S. L., Lu, P. H., and Xu, X. M. (2003). [Effects of embryonic neural stem cells and glial cell line-derived neurotrophic factor in the repair of spinal cord injury]. Sheng Li Xue Bao *55*, 349-54.

Sunderland, S. (1951). A classification of peripheral nerve injuries producing loss of function. Brain *74*, 491-516.

Taira, E., Takaha, N., Taniura, H., Kim, C. H., and Miki, N. (1994). Molecular cloning and functional expression of gicerin, a novel cell adhesion molecule that binds to neurite outgrowth factor. Neuron *12*, 861-72.

Takahashi, M., and Osumi, N. (2005). Identification of a novel type II classical cadherin: rat cadherin19 is expressed in the cranial ganglia and Schwann cell precursors during development. Dev. Dyn *232*, 200-208.

Takatori, A., Geh, E., Chen, L., Zhang, L., Meller, J., and Xia, Y. (2008). Differential transmission of MEKK1 morphogenetic signals by JNK1 and JNK2. Development *135*, 23-32.

Tamai, K., Toyoshima, M., Tanaka, N., Yamamoto, N., Owada, Y., Kiyonari, H., Murata, K., Ueno, Y., Ono, M., Shimosegawa, T., et al. (2008). Loss of hrs in the central nervous system causes accumulation of ubiquitinated proteins and neurodegeneration. Am. J. Pathol *173*, 1806-1817.

Tanabe, K., Tachibana, T., Yamashita, T., Che, Y. H., Yoneda, Y., Ochi, T., Tohyama, M., Yoshikawa, H., and Kiyama, H. (2000). The small GTP-binding protein TC10 promotes nerve elongation in neuronal cells, and its expression is induced during nerve regeneration in rats. J Neurosci *20*, 4138-44.

Tanaka, H., Yamashita, T., Asada, M., Mizutani, S., Yoshikawa, H., and Tohyama, M. (2002). Cytoplasmic p21(Cip1/WAF1) regulates neurite remodeling by inhibiting Rho-kinase activity. J Cell Biol *158*, 321-9.

Tang, S., Shen, Y. J., DeBellard, M. E., Mukhopadhyay, G., Salzer, J. L., Crocker, P. R., and Filbin, M. T. (1997). Myelin-associated glycoprotein interacts with neurons via a sialic acid binding site at ARG118 and a distinct neurite inhibition site. J. Cell Biol *138*, 1355-1366.

Tararuk, T., Östman, N., Li, W., Björkblom, B., Padzik, A., Zdrojewska, J., Hongisto, V., Herdegen, T., Konopka, W., Courtney, M., et al. (2006). JNK1 phosphorylation of SCG10 determines microtubule dynamics and axodendritic length. Journal of Cell Biology *173*, 265-277.

Tebar, L. A., Geranton, S. M., et al. (2008). Deletion of the mouse RegIIIbeta (Reg2) gene

disrupts ciliary neurotrophic factor signaling and delays myelination of mouse cranial motor neurons. Proc Natl Acad Sci U S A *105*, 11400-5.

Tebar, L. A., Géranton, S. M., et al. (2008). Deletion of the mouse RegIIIβ (Reg2) gene disrupts ciliary neurotrophic factor signaling and delays myelination of mouse cranial motor neurons. Proceedings of the National Academy of Sciences *105*, 11400-11405.

Terenghi, G. (1999). Peripheral nerve regeneration and neurotrophic factors. Journal of Anatomy *194*, 1-14.

Terrado, J., Monnier, D., Perrelet, D., Vesin, D., Jemelin, S., Buurman, W., Mattenberger, L., King, B., Kato, A., and Garcia, I. (2000). Soluble TNF receptors partially protect injured motoneurons in the postnatal CNS. European Journal of Neuroscience *12*, 3443-3447.

Thornberry, N. A., Bull, H. G., Calaycay, J. R., Chapman, K. T., Howard, A. D., Kostura, M. J., Miller, D. K., Molineaux, S. M., Weidner, J. R., Aunins, J., et al. (1992). A novel heterodimeric cysteine protease is required for interleukin-1 beta processing in monocytes. Nature *356*, 768-74.

Tichauer, J., Saud, K., and von Bernhardi, R. (2007). Modulation by astrocytes of microglial cell-mediated neuroinflammation: effect on the activation of microglial signaling pathways. Neuroimmunomodulation *14*, 168-174.

Tom, V. J., and Houle, J. D. (2008). Intraspinal microinjection of chondroitinase ABC following injury promotes axonal regeneration out of a peripheral nerve graft bridge. Exp Neurol *211*, 315-9.

Topilko, P., Schneider-Maunoury, S., Levi, G., Baron-Van Evercooren, A., Chennoufi, A. B., Seitanidou, T., Babinet, C., and Charnay, P. (1994). Krox-20 controls myelination in the peripheral nervous system. Nature *371*, 796-799.

Toti, P., Regoli, M., Nesi, G., Occhini, R., Bartolommei, S., Fonzi, L., and Bertelli, E. (2005). Nestin expression in normal adrenal gland and adrenocortical tumors. Histol. Histopathol *20*, 1115-1120.

Trapp, B. D., Hauer, P., and Lemke, G. (1988). Axonal regulation of myelin protein mRNA levels in actively myelinating Schwann cells. J. Neurosci *8*, 3515-3521.

Trapp, B. D., Wujek, J. R., Criste, G. A., Jalabi, W., Yin, X., Kidd, G. J., Stohlman, S., and Ransohoff, R. (2007). Evidence for synaptic stripping by cortical microglia. Glia *55*, 360-368.

Traven, A., and Heierhorst, J. (2005). SQ/TQ cluster domains: concentrated ATM/ATR kinase phosphorylation site regions in DNA-damage-response proteins. Bioessays *27*, 397-407.

Tronche, F., Kellendonk, C., Kretz, O., Gass, P., Anlag, K., Orban, P. C., Bock, R., Klein, R., and Schutz, G. (1999). Disruption of the glucocorticoid receptor gene in the nervous system results in reduced anxiety. Nat Genet *23*, 99-103.

Tsujino, H., Kondo, E., Fukuoka, T., Dai, Y., Tokunaga, A., Miki, K., Yonenobu, K., Ochi, T., and Noguchi, K. (2000). Activating transcription factor 3 (ATF3) induction by axotomy in sensory and motoneurons: A novel neuronal marker of nerve injury. Mol. Cell. Neurosci *15*, 170-182.

Turner, R., and Tjian, R. (1989). Leucine repeats and an adjacent DNA binding domain mediate the formation of functional cFos-cJun heterodimers. Science *243*, 1689-1694.

Tysseling-Mattiace, V. M., Sahni, V., Niece, K. L., Birch, D., Czeisler, C., Fehlings, M. G., Stupp, S. I., and Kessler, J. A. (2008). Self-assembling nanofibers inhibit glial scar formation and promote axon elongation after spinal cord injury. J. Neurosci *28*, 3814-3823.

Ueno, H., Yamada, Y., Watanabe, R., Mukai, E., Hosokawa, M., Takahashi, A., Hamasaki, A., Fujiwara, H., Toyokuni, S., Yamaguchi, M., et al. (2005). Nestin-positive cells in adult pancreas express amylase and endocrine precursor Cells. Pancreas *31*, 126-131.

Ugolini, G., Raoul, C., Ferri, A., Haenggeli, C., Yamamoto, Y., Salaun, D., Henderson, C. E., Kato, A. C., Pettmann, B., and Hueber, A. O. (2003). Fas/tumor necrosis factor receptor death signaling is required for axotomy-induced death of motoneurons in vivo. J Neurosci *23*, 8526-31.

Unlap, T., Franklin, C. C., Wagner, F., and Kraft, A. S. (1992). Upstream regions of the c-jun promoter regulate phorbol ester-induced transcription in U937 leukemic cells. Nucleic Acids Res *20*, 897-902.

Usukura, J., and Yamada, E. (1987). Ultrastructure of the synaptic ribbons in photoreceptor cells of Rana catesbeiana revealed by freeze-etching and freeze-substitution. Cell Tissue Res *247*, 483-488.

Utikal, J., Polo, J. M., Stadtfeld, M., Maherali, N., Kulalert, W., Walsh, R. M., Khalil, A., Rheinwald, J. G., and Hochedlinger, K. (2009). Immortalization eliminates a roadblock during cellular reprogramming into iPS cells. Nature *advance online publication*. Available at: http://dx.doi.org/10.1038/nature08285 [Accessed August 12, 2009].

Vargas, M. E., and Barres, B. A. (2007). Why is Wallerian degeneration in the CNS so slow? Annu. Rev. Neurosci *30*, 153-179.

Varona-Santos, J., Pileggi, A., Molano, R., Sanabria, N., Ijaz, A., Atsushi, M., Ichii, H., Pastori, R., Inverardi, L., Ricordi, C., et al. (2008). c-Jun N-terminal kinase 1 is deleterious to the function and survival of murine pancreatic islets. Diabetologia *51*, 2271-2280.

Vaudano, E., Campbell, G., Anderson, P. N., Davies, A. P., Woolhead, C., Schreyer, D. J., and Lieberman, A. R. (1995). The effects of a lesion or a peripheral nerve graft on GAP-43 upregulation in the adult rat brain: an in situ hybridization and immunocytochemical study. J. Neurosci *15*, 3594-3611.

Vaudano, E., Campbell, G., and Hunt, S. P. (1996). Change in the molecular phenotype of

Schwann cells upon transplantation into the central nervous system: down-regulation of c-jun. Neuroscience *74*, 553-565.

Vaudano, E., Campbell, G., Hunt, S. P., and Lieberman, A. R. (1998). Axonal injury and peripheral nerve grafting in the thalamus and cerebellum of the adult rat: upregulation of c-jun and correlation with regenerative potential. Eur. J. Neurosci *10*, 2644-2656.

Vaudano, E., Campbell, G., Anderson, P. N., Davies, A. P., Woolhead, C., Schreyer, D. J., and Lieberman, A. R. (1995). The effects of a lesion or a peripheral nerve graft on GAP-43 upregulation in the adult rat brain: an in situ hybridization and immunocytochemical study. J Neurosci *15*, 3594-611.

Verge, V. M., Richardson, P. M., Wiesenfeld-Hallin, Z., and Hokfelt, T. (1995). Differential influence of nerve growth factor on neuropeptide expression in vivo: a novel role in peptide suppression in adult sensory neurons. J Neurosci *15*, 2081-96.

Verge, V. M., Riopelle, R. J., and Richardson, P. M. (1989). Nerve growth factor receptors on normal and injured sensory neurons. J Neurosci *9*, 914-22.

Verhey, K. J. (2007). Motor proteins: trafficking and signaling collide. Curr Biol *17*, R804-6.

Verhey, K. J., and Rapoport, T. A. (2001). Kinesin carries the signal. Trends Biochem. Sci. *26*, 545–550.

Vogelezang, M. G., Liu, Z., Relvas, J. B., Raivich, G., Scherer, S. S., and ffrench-Constant, C. (2001). Alpha4 integrin is expressed during peripheral nerve regeneration and enhances neurite outgrowth. J Neurosci *21*, 6732-44.

Vollgraf, U., Wegner, M., and Richter-Landsberg, C. (1999). Activation of AP-1 and nuclear factor-kappaB transcription factors is involved in hydrogen peroxide-induced apoptotic cell death of oligodendrocytes. J Neurochem *73*, 2501-9.

Vooijs, M., Jonkers, J., and Berns, A. (2001). A highly efficient ligand-regulated Cre recombinase mouse line shows that LoxP recombination is position dependent. EMBO Rep *2*, 292-297.

Vries, R. G., Prudenziati, M., Zwartjes, C., Verlaan, M., Kalkhoven, E., and Zantema, A. (2001). A specific lysine in c-Jun is required for transcriptional repression by E1A and is acetylated by p300. EMBO J *20*, 6095-103.

Vukojevic, K., Petrovic, D., and Saraga-Babic, M. (2009). Nestin expression in glial and neuronal progenitors of the developing human spinal ganglia. Gene Expr Patterns. Available at: http://www.ncbi.nlm.nih.gov/pubmed/20044038 [Accessed January 2, 2010].

Waetzig, V., and Herdegen, T. (2005). Context-specific inhibition of JNKs: Overcoming the dilemma of protection and damage. Trends in Pharmacological Sciences *26*, 455-461.

Waetzig, V., and Herdegen, T. (2003). The concerted signaling of ERK1/2 and JNKs is essential for PC12 cell neuritogenesis and converges at the level of target proteins.

Molecular and Cellular Neuroscience *24*, 238-249.

Waetzig, V., Zhao, Y., and Herdegen, T. (2006). The bright side of JNKs-Multitalented mediators in neuronal sprouting, brain development and nerve fiber regeneration. Prog. Neurobiol *80*, 84-97.

Wainwright, D. A., Xin, J., Mesnard, N. A., Beahrs, T. R., Politis, C. M., Sanders, V. M., and Jones, K. J. (2009). Exacerbation of facial motoneuron loss after facial nerve axotomy in CCR3-deficient mice. ASN Neuro. Available at: http://www.ncbi.nlm.nih.gov/pubmed/19922414 [Accessed January 5, 2010].

Waller, A. (1850). Experiments on the Section of the Glossopharyngeal and Hypoglossal Nerves of the Frog, and Observations of the Alterations Produced Thereby in the Structure of Their Primitive Fibres. Philosophical Transactions of the Royal Society of London *140*, 423-429.

Wallquist, W., Plantman, S., Thams, S., Thyboll, J., Kortesmaa, J., Lannergren, J., Domogatskaya, A., Ogren, S. O., Risling, M., Hammarberg, H., et al. (2005). Impeded interaction between Schwann cells and axons in the absence of laminin alpha4. J Neurosci *25*, 3692-700.

Wallquist, W., Zelano, J., Plantman, S., Kaufman, S. J., Cullheim, S., and Hammarberg, H. (2004). Dorsal root ganglion neurons up-regulate the expression of laminin-associated integrins after peripheral but not central axotomy. J Comp Neurol *480*, 162-9.

Wang, L. H., and Johnson, E. M. (2008). Mixed lineage kinase inhibitor CEP-1347 fails to delay disability in early Parkinson disease. Neurology *71*, 462; author reply 462-3.

Wang, X., Destrument, A., and Tournier, C. (2007). Physiological roles of MKK4 and MKK7: Insights from animal models. Biochimica et Biophysica Acta - Molecular Cell Research *1773*, 1349-1357.

Wang, Y., Zhang, Y., Wei, Z., Li, H., Zhou, H., Zhang, Z., and Zhang, Z. (2009). JNK inhibitor protects dopaminergic neurons by reducing COX-2 expression in the MPTP mouse model of subacute Parkinson's disease. J. Neurol. Sci. Available at: http://www.ncbi.nlm.nih.gov/pubmed/19604516 [Accessed September 9, 2009].

Weizman, N., Shiloh, Y., and Barzilai, A. (2003). Contribution of the Atm protein to maintaining cellular homeostasis evidenced by continuous activation of the AP-1 pathway in Atm-deficient brains. J. Biol. Chem *278*, 6741-6747.

Werner, A., Willem, M., Jones, L. L., Kreutzberg, G. W., Mayer, U., and Raivich, G. (2000). Impaired axonal regeneration in alpha7 integrin-deficient mice. J. Neurosci *20*, 1822-1830.

Werner, A., Martin, S., Gutierrez-Ramos, J., and Raivich, G. (2001a). Leukocyte recruitment and neuroglial activation during facial nerve regeneration in ICAM-1-deficient mice: Effects of breeding strategy. Cell and Tissue Research *305*, 25-41.

Werner, A., Martin, S., Gutierrez-Ramos, J. C., and Raivich, G. (2001b). Leukocyte recruitment and neuroglial activation during facial nerve regeneration in ICAM-1-

deficient mice: effects of breeding strategy. Cell Tissue Res *305*, 25-41.

Werner, A., Willem, M., Jones, L. L., Kreutzberg, G. W., Mayer, U., and Raivich, G. (2000). Impaired axonal regeneration in alpha7 integrin-deficient mice. J Neurosci *20*, 1822-30.

Weston, C., and Davis, R. (2007). The JNK signal transduction pathway. Current Opinion in Cell Biology *19*, 142-149.

White, F. V., Toews, A. D., Goodrum, J. F., Novicki, D. L., Bouldin, T. W., and Morell, P. (1989). Lipid metabolism during early stages of Wallerian degeneration in the rat sciatic nerve. J. Neurochem *52*, 1085-1092.

Whitmarsh, A. (2006). The JIP family of MAPK scaffold proteins. Biochemical Society Transactions *34*, 828-832.

Widmann, C., Gibson, S., Jarpe, M., and Johnson, G. (1999). Mitogen-activated protein kinase: Conservation of a three-kinase module from yeast to human. Physiological Reviews *79*, 143-180.

Wiederkehr, A., Staple, J., and Caroni, P. (1997). The motility-associated proteins GAP-43, MARCKS, and CAP-23 share unique targeting and surface activity-inducing properties. Exp Cell Res *236*, 103-16.

Wiklund, P., Ekstrom, P. A., and Edstrom, A. (2002). Mitogen-activated protein kinase inhibition reveals differences in signalling pathways activated by neurotrophin-3 and other growth-stimulating conditions of adult mouse dorsal root ganglia neurons. J Neurosci Res *67*, 62-8.

Willard, M., Simon, C., Baitinger, C., Levine, J., and Skene, P. (1980). Association of an axonally transported polypeptide (H) with 100-A filaments. Use of immunoaffinity electron microscope grids. J Cell Biol *85*, 587-96.

Williams, P. L., and Hall, S. M. (1971a). Chronic Wallerian degeneration--an in vivo and ultrastructural study. J. Anat *109*, 487-503.

Williams, P. L., and Hall, S. M. (1971b). Prolonged in vivo observations of normal peripheral nerve fibres and their acute reactions to crush and deliberate trauma. J. Anat *108*, 397-408.

Wislet-Gendebien, S., Hans, G., Leprince, P., Rigo, J., Moonen, G., and Rogister, B. (2005). Plasticity of cultured mesenchymal stem cells: switch from nestin-positive to excitable neuron-like phenotype. Stem Cells *23*, 392-402.

Woo, M., Jang, P., Park, J., Kim, W., Joh, T. H., and Kim, H. (2003). Selective modulation of lipopolysaccharide-stimulated cytokine expression and mitogen-activated protein kinase pathways by dibutyryl-cAMP in BV2 microglial cells. Brain Res. Mol. Brain Res *113*, 86-96.

Woodroofe, M. N., Sarna, G. S., Wadhwa, M., Hayes, G. M., Loughlin, A. J., Tinker, A., and Cuzner, M. L. (1991). Detection of interleukin-1 and interleukin-6 in adult rat brain, following mechanical injury, by in vivo microdialysis: evidence of a role for

microglia in cytokine production. J. Neuroimmunol *33*, 227-236.

Woolhead, C. L., Zhang, Y., Lieberman, A. R., Schachner, M., Emson, P. C., and Anderson, P. N. (1998). Differential effects of autologous peripheral nerve grafts to the corpus striatum of adult rats on the regeneration of axons of striatal and nigral neurons and on the expression of GAP-43 and the cell adhesion molecules N-CAM and L1. J. Comp. Neurol *391*, 259-273.

Wu, D., Yang, P., Zhang, X., Luo, J., Haque, M. E., Yeh, J., Richardson, P. M., Zhang, Y., and Bo, X. (2009). Targeting a dominant negative rho kinase to neurons promotes axonal outgrowth and partial functional recovery after rat rubrospinal tract lesion. Mol. Ther *17*, 2020-2030.

Wu, K., Hengst, U., Cox, L., Macosko, E., Jeromin, A., Urquhart, E., and Jaffrey, S. (2005). Local translation of RhoA regulates growth cone collapse. Nature *436*, 1020-1024.

Xia, C., Roberts, E. A., Her, L., Liu, X., Williams, D. S., Cleveland, D. W., and Goldstein, L. S. B. (2003). Abnormal neurofilament transport caused by targeted disruption of neuronal kinesin heavy chain KIF5A. J. Cell Biol *161*, 55-66.

Xiao, M., Klueber, K. M., Zhou, J., Guo, Z., Lu, C., Wang, H., and Roisen, F. J. (2007). Human adult olfactory neural progenitors promote axotomized rubrospinal tract axonal reinnervation and locomotor recovery. Neurobiol. Dis *26*, 363-374.

Xie, X., Gu, Y., Fox, T., Coll, J., Fleming, M., Markland, W., Caron, P., Wilson, K., and Su, M. (1998). Crystal structure of JNK3: A kinase implicated in neuronal apoptosis. Structure *6*, 983-991.

Xin, J., Wainwright, D. A., Serpe, C. J., Sanders, V. M., and Jones, K. J. (2008). Phenotype of CD4+ T cell subsets that develop following mouse facial nerve axotomy. Brain Behav. Immun *22*, 528-537.

Xu, W., Manichella, D., Jiang, H., Vallat, J., Lilien, J., Baron, P., Scarlato, G., Kamholz, J., and Shy, M. E. (2000). Absence of P0 leads to the dysregulation of myelin gene expression and myelin morphogenesis. Journal of Neuroscience Research *60*, 714-724.

Xue, D., Shaham, S., and Horvitz, H. R. (1996). The Caenorhabditis elegans cell-death protein CED-3 is a cysteine protease with substrate specificities similar to those of the human CPP32 protease. Genes Dev *10*, 1073-83.

Yamauchi, Y., Abe, K., Mantani, A., Hitoshi, Y., Suzuki, M., Osuzu, F., Kuratani, S., and Yamamura, K. (1999). A novel transgenic technique that allows specific marking of the neural crest cell lineage in mice. Developmental Biology *212*, 191–203.

Yang, D. D., Kuan, C. Y., Whitmarsh, A. J., Rincon, M., Zheng, T. S., Davis, R. J., Rakic, P., and Flavell, R. A. (1997). Absence of excitotoxicity-induced apoptosis in the hippocampus of mice lacking the Jnk3 gene. Nature *389*, 865-70.

Yang, J., Moulin, N., van Bemmelen, M., Dubuis, G., Tawadros, T., Haefliger, J., Waeber, G., and Widmann, C. (2007). Splice variant-specific stabilization of JNKs by IB1/JIP1. Cellular Signalling *19*, 2201-2207.

Yang, X., Khosravi-Far, R., Chang, H. Y., and Baltimore, D. (1997). Daxx, a novel Fas-binding protein that activates JNK and apoptosis. Cell *89*, 1067-76.

Yick, L. W., Cheung, P. T., So, K. F., and Wu, W. (2003). Axonal regeneration of Clarke's neurons beyond the spinal cord injury scar after treatment with chondroitinase ABC. Exp Neurol *182*, 160-8.

Yoon, C., Korade, Z., and Carter, B. D. (2008). Protein kinase A-induced phosphorylation of the p65 subunit of nuclear factor-kappaB promotes Schwann cell differentiation into a myelinating phenotype. J. Neurosci *28*, 3738-3746.

Yuan, J., and Horvitz, H. R. (2004). A first insight into the molecular mechanisms of apoptosis. Cell *116*, S53-6, 1 p following S59.

Yuan, J., Shaham, S., Ledoux, S., Ellis, H. M., and Horvitz, H. R. (1993). The C. elegans cell death gene ced-3 encodes a protein similar to mammalian interleukin-1 beta-converting enzyme. Cell *75*, 641-52.

Zhang, Y., Campbell, G., Anderson, P. N., Martini, R., Schachner, M., and Lieberman, A. R. (1995). Molecular basis of interactions between regenerating adult rat thalamic axons and Schwann cells in peripheral nerve grafts. II. Tenascin-C. J. Comp. Neurol *361*, 210-224.

Zhou, F., Walzer, M. A., and Snider, W. D. (2004). Turning on the machine: genetic control of axon regeneration by c-Jun. Neuron *43*, 1-2.

Zhou, Q., Lam, P., Han, D., and Cadenas, E. (2008). c-Jun N-terminal kinase regulates mitochondrial bioenergetics by modulating pyruvate dehydrogenase activity in primary cortical neurons. Journal of Neurochemistry *104*, 325-335.

Zhu, Y., Romero, M. I., Ghosh, P., Ye, Z., Charnay, P., Rushing, E. J., Marth, J. D., and Parada, L. F. (2001). Ablation of NF1 function in neurons induces abnormal development of cerebral cortex and reactive gliosis in the brain. Genes Dev *15*, 859-876.

Zhuang, Z. Y., Wen, Y. R., Zhang, D. R., Borsello, T., Bonny, C., Strichartz, G. R., Decosterd, I., and Ji, R. R. (2006). A peptide c-Jun N-terminal kinase (JNK) inhibitor blocks mechanical allodynia after spinal nerve ligation: respective roles of JNK activation in primary sensory neurons and spinal astrocytes for neuropathic pain development and maintenance. J Neurosci *26*, 3551-60.

Zimmerman, L., Parr, B., Lendahl, U., Cunningham, M., McKay, R., Gavin, B., Mann, J., Vassileva, G., and McMahon, A. (1994). Independent regulatory elements in the nestin gene direct transgene expression to neural stem cells or muscle precursors. Neuron *12*, 11-24.

Zou, J., Yaoita, E., Watanabe, Y., Yoshida, Y., Nameta, M., Li, H., Qu, Z., and Yamamoto, T. (2006). Upregulation of nestin, vimentin, and desmin in rat podocytes in response to injury. Virchows Archiv *448*, 485-492.

PUBLICATIONS

Deletion of the mouse RegIIIβ (Reg2) gene disrupts ciliary neurotrophic factor signaling and delays myelination of mouse cranial motor neurons

L. A. Tebar*, S. M. Géranton†, C. Parsons-Perez†, A. S. Fisher†, R. Bayne‡, A. J. H. Smith‡, M. Turmaine†, S. Perez-Luz§, A. Sheasby†, C. De Felipe¶, C. Ruff‖, G. Raivich‖, and S. P. Hunt†**

*National Centre for Cancer Research, Melchor Fernández Almagro, 3. E-28029 Madrid, Spain; †Department of Anatomy and Developmental Biology, University College London, Medawar Building, Gower Street, WC1E 6BT London, United Kingdom; ‡Gene Targeting Laboratory, Institute for Stem Cell Research, University of Edinburgh, The King's Buildings, West Mains Road, Edinburgh EH9 3JQ, Scotland; §Department of Molecular Biology, Universidad Autonoma de Madrid Cantoblanco, 28049 Madrid, Spain; ¶Consejo Superior de Investigaciones Científicas, Universidad Miguel Hernandez, Campus de San Juan, Sant Joan d'Alacanti. Nacional 33203550, Alicante, Spain; and ‖Perinatal Brain Repair Group, Departments of Obstetrics and Gynaecology and Anatomy, University College London, 86-96 Chenies Mews, London WC1E 6HX, United Kingdom

Edited by Tomas Hökfelt, Karolinska Institutet, Stockholm, Sweden, and approved June 16, 2008 (received for review January 2, 2008)

A large number of cytokines and growth factors support the development and subsequent maintenance of postnatal motor neurons. RegIIIβ, also known as Reg2 in rat and HIP/PAP1 in humans, is a member of a family of growth factors found in many areas of the body and previously shown to play an important role in both the development and regeneration of subsets of motor neurons. It has been suggested that RegIIIβ expressed by motor neurons is both an obligatory intermediate in the downstream signaling of the leukemia inhibitory factor/ciliary neurotrophic factor (CNTF) family of cytokines, maintaining the integrity of motor neurons during development, as well as a powerful influence on Schwann cell growth during regeneration of the peripheral nerve. Here we report that in mice with a deletion of the RegIIIβ gene, motor neuron survival was unaffected up to 28 weeks after birth. However, there was no CNTF-mediated rescue of neonatal facial motor neurons after axotomy in KO animals when compared with wild-type. In mice, RegIIIβ positive motor neurons are concentrated in cranial motor nuclei that are involved in the patterning of swallowing and suckling. We found that suckling was impaired in RegIIIβ KO mice and correlated this with a significant delay in myelination of the hypoglossal nerve. In summary, we propose that RegIIIβ has an important role to play in the developmental fine-tuning of neonatal motor behaviors mediating the response to peripherally derived cytokines and growth factors and regulating the myelination of motor axons.

Schwann cells | suckling | hypoglossal nerve | LIF

A large number of neurotrophic factors and cytokines have been shown to sustain developing motor neurons and to encourage the survival of postnatal motor neurons after damage (1–6). Rat Reg2 [also known as RegIIIβ in mouse and HIP/PAP1 in humans (7)] has been reported to play an important role in both the support of motor neurons during development and in the process of axon regeneration through axon–Schwann cell signaling in the adult peripheral nervous system (8, 9). *Reg2* is a member of a large family of over 17 related genes divided into four subtypes (types I, II, III, and IV) based on the primary structures of the encoded proteins of the genes (10–13). *Reg2* is the equivalent of mouse *RegIIIβ* gene, which share 90% homology at both the nucleotide and protein level. First identified as a transcript up-regulated in pancreatitis, Reg2, a secreted protein (relative M_r 16,000) found in many sites throughout the body, was shown to have an anti-apoptotic action on pancreatic cell lines (14). Reg2 also promotes the growth of epithelial intestinal cells, whereas loss of Reg2/RegIIIβ delayed liver regeneration (10, 15–18).

Two roles have been proposed for Reg2 in the nervous system. First, *in vivo* studies have suggested that Reg2 is released from damaged motor and sensory neurons and has a proregenerative function (9, 19, 20). Secondly, *in vitro* data have cast Reg2 as a neurotrophic factor for motor neurons acting as an obligatory intermediate for the ciliary neurotrophic factor (CNTF)/leukemia inhibitory factor (LIF) family of cytokines (8). In the adult rat, Reg2 is massively up-regulated in motor neurons and some sensory neurons after nerve crush (19) and is rapidly transported to the lesion site, where it is thought to be secreted and act on Schwann cells. *In vitro*, Reg2 has a mitogenic effect on Schwann cells and inhibition of Reg2 with a neutralizing antibody retards the progress of regeneration. Taken together, it seemed likely that the Schwann cell response at the point of axotomy was potentiated by release of Reg2 from damaged axons (9).

Here, we describe the effects of targeted ablation of the *RegIIIβ* gene in mice and show a developmental role of RegIIIβ in axon–Schwann cell signaling. We also report that RegIIIβ is required to promote the response of subsets of motor neurons to CNTF but not for motor neuron survival.

Results

Generation of RegIIIβ-Deficient Mice. KO mice were homozygous for a targeted disruption of the *RegIIIβ* gene locus created in ES cells, in which a region from exons 2 to 5 was deleted and replaced by an IRES-*Tau-LacZ-loxP*/MC1*neo*pA/*loxP* reporter/selection cassette, thus resulting in a null allele. Mice homozygous for the *RegIIIβ*-null allele were phenotypically indistinguishable from wild-type or heterozygous littermates. No embryonic lethality or significant developmental defects were observed in *RegIII$\beta^{-/-}$* animals. Adult *RegIII$\beta^{-/-}$* mice of both sexes were fertile, and litter size was normal. We compared the expression of RegIIIβ between wild-type and KO animals by using quantitative RT-PCR (RT-qPCR) and found that, as expected, the expression of RegIIIβ mRNA dropped from 100 ± 25.2% (wild type) to 0.08 ± 0.02% (KO) (n = 6 per group). Immunohistochemistry also showed a complete lack of RegIIIβ protein-like immunoreactivity in postnatal KO mice (Fig. 1). To check for potential compensatory up-regulation, we also mea-

Author contributions: A.J.H.S., C.D.F., and S.P.H. designed research; L.A.T., S.M.G., C.P.-P., A.S.F., R.B., A.J.H.S., M.T., S.P.-L., A.S., C.D.F., C.R., G.R., and S.P.H. performed research; L.A.T., S.M.G., C.P.-P., A.S.F., A.J.H.S., S.P.-L., and S.P.H. analyzed data; and S.M.G. and S.P.H. wrote the paper.

The authors declare no conflict of interest.

This article is a PNAS Direct Submission.

**To whom correspondence should be addressed. E-mail: hunt@ucl.ac.uk.

This article contains supporting information online at www.pnas.org/cgi/content/full/0711978105/DCSupplemental.

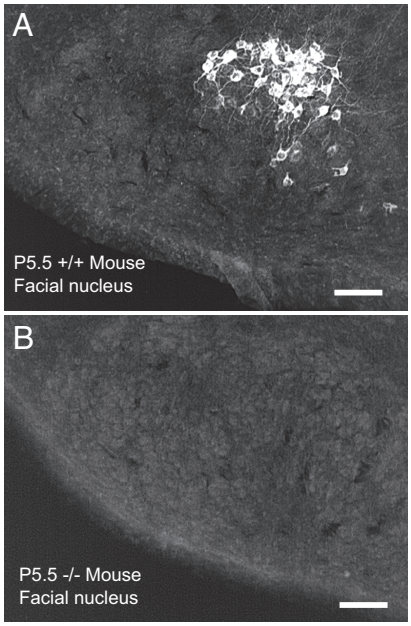

Fig. 1. RegIIIβ immunoreactivity is found in subsets of facial motor neurons in P5 wild-type mice but was not found in the postnatal KO mouse central nervous system. (*A*) Facial motor nucleus (P5) of a wild-type mouse. (*B*) Absence of staining in KO facial nucleus. (Scale bar, 120 μm.)

sured the expression of *RegIII*α and *RegIII*γ: There was no difference in *RegIII*γ expression (100 ± 67% in wild type vs. 62 ± 43% in KO), but we found a substantial elevation of *RegIII*α in the brainstem of KO mice (100 ± 26% in wild type vs. 667 ± 181% in KO).

RegIIIβ Labeling of Neuronal Populations Is Restricted and Developmentally Regulated. In wild-type embryos, RegIIIβ proteins are first detected in subsets of motor neurons at embryonic day (E)13–E14 in cervical spinal cord, as previously described in rat (8), with expression peaking at E18.5 (2). Within the brainstem at postnatal day (P)1–P5, subsets of neurons along the medial half of the motor nucleus of the trigeminal and in the dorsal and medial regions of the facial nucleus were immunoreactive for RegIIIβ (Fig. 2). The heaviest concentrations of RegIIIβ positive neurons (up to 50% at P1) were found throughout the caudal half of the hypoglossal nucleus (XII) and nucleus ambiguus notably at day 1, but staining intensity reached maximal levels by

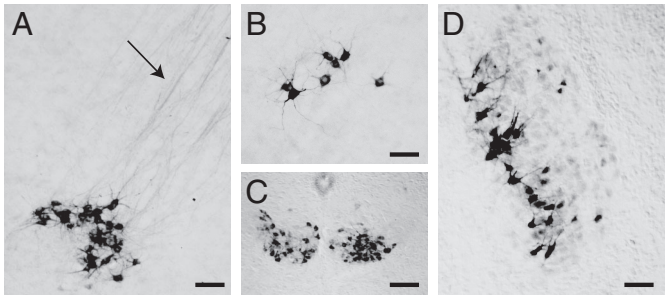

Fig. 2. RegIIIβ immunoreactivity is found in subsets of cranial and spinal motor nuclei up to P12. (*A*) Facial motor nucleus with labeled axons (arrow) streaming into the facial nerve. (*B–D*) RegIIIβ-positive neurons within the nucleus ambiguus (*B*), the hypoglossal nuclei (*C*), and the motor nucleus of the trigeminal (*D*). All specimens were from P5 mice. [Scale bars: 100 μm (*A*, *B*, and *D*); 150 μm (*C*).]

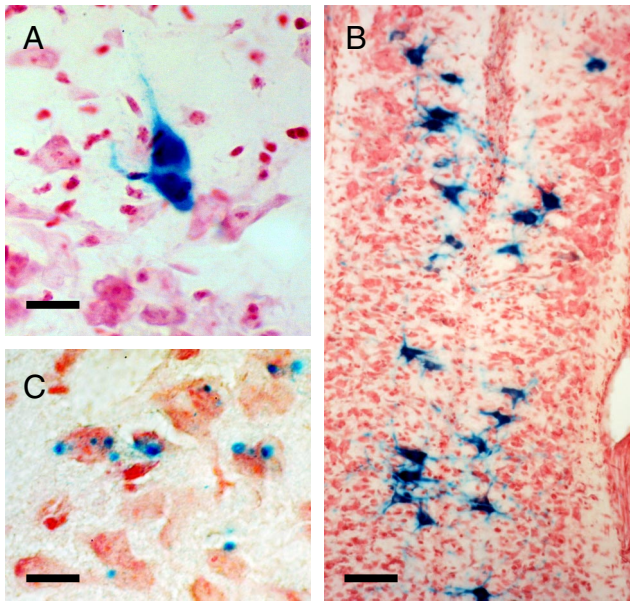

Fig. 3. β-Galactosidase activity is present postnatally in subsets of motor neurons in the RegIIIβ KO mouse. (*A*) Motor neuron in the facial motor nucleus at P3. (*B*) Sacral motor neurons at P1. (*C*) Punctate β-galactosidase staining in the facial motor nucleus at P5. [Scale bars: 20 μm (*A*); 60 μm (*B*); 40 μm (*C*).]

P4. By P11, RegIIIβ staining had been lost from all areas of the brain and spinal cord.

Motor Neurons Are Not Lost After RegIIIβ Deletion. Two lines of evidence imply that motor neuron survival is not compromised by loss of RegIIIβ. First, in KO mice, β-galactosidase staining is still visible in motor neurons similar in position to those that show RegIIIβ expression in wild-type mice (Fig. 3). The tau–lac-Z strategy designed to transport β-galactosidase into axons met with limited success because the reaction product was only obviously visualized in motor neuron cell bodies and dendrites. These motor neurons included the spinal motor neurons and trigeminal, facial, hypoglossal, and nucleus ambiguus motor neurons up to P10. Postnatally, sacral motor neurons stained positively for β-galactosidase (Fig. 3*B*), but brainstem expression was restricted to small foci within the cytoplasm of motor neurons (Fig. 3*C*) or the occasional heavily stained motor neuron (Fig. 3*A*). In the spinal cord, β-galactosidase reaction product was found in only the medial column of neurons comparable in position to RegIIIβ immunoreactive neurons seen in wild-type mice (Fig. 3*B*). β-Galactosidase expression was not present beyond P10. Second, the total number of motor neurones in the facial motor nucleus of P5.5–P10.5 mice or mice 24 weeks old were not significantly different between wild-type and KO mice implying that no motor neuron cell death had resulted from the loss of RegIIIβ [see supporting information (SI) Fig. S1].

Lack of Effect of CNTF on Facial Motor Neuron Survival in RegIIIβ KO Mice. CNTF applied to the cut end of the facial nerve delays the axotomy provoked death of neonatal rat facial motor neurons (21). To examine the effects of CNTF in RegIIIβ KO mice, we cut the facial motor nerve unilaterally at P3.5 and then immediately applied CNTF or saline to the cut end of the nerve. Mice were then allowed to survive for 3 days. The loss of facial motor neurons after facial nerve lesion (FNL) was comparable between wild-type and KO mice (45% and 49% loss when compared with contralateral side in wild-type and KO, respectively) (Fig. 4). There was a significant effect of CNTF on wild-type mice when

NEUROSCIENCE

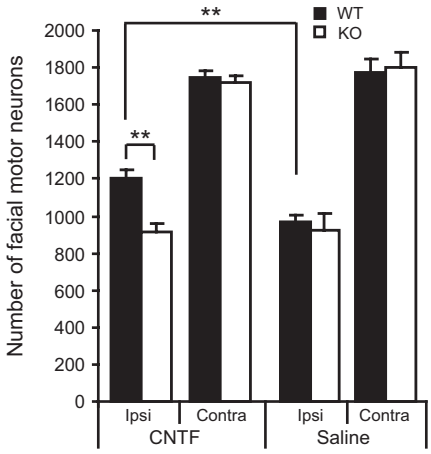

Fig. 4. Application of CNTF to the cut facial nerve results in increased survival of facial motor neurons in wild-type but not KO mice counted 3 days after nerve section. The data show means ± SEM (n = 4-5 in each group). **, $P < 0.001$.

compared with both CNTF-treated KO and saline-treated wild-type mice (24% and 32% savings respectively, $P < 0.001$ for both) (Fig. 4). When mice were allowed to survive for four days after FNL, cell loss was considerable but CNTF produced significant savings in the numbers of dying neurons in wild-type mice when compared with KO mice (Fig. S2).

We have previously shown (9) that section of the sciatic nerve results in down-regulation of Reg2/RegIIIβ in motor neurons in rat pups and up-regulation in adult rats. However, in mouse pups with facial nerve axotomy at P3.5 and perfused 2 days later, we did not detect any change in numbers of RegIIIβ-positive neurons in the facial motor nucleus. However, application of CNTF after facial nerve section at P3.5 in mouse pups significantly increased the number of RegIIIβ-positive neurons seen 2 days later to 148% compared with the contralateral side ($P < 0.0001$) (Fig. 5 and Fig. S3). Finally, whereas in adult rats, Reg2 is expressed by all facial motor neurons within 24h of axotomy, in adult mice, RegIIIβ is not reexpressed in facial motor neurons 1–7 days after axotomy (Fig. S4).

Loss of RegIIIβ Impairs Suckling Behavior. In newborn mouse pups, we noted that neurons immunoreactive for RegIIIβ were found

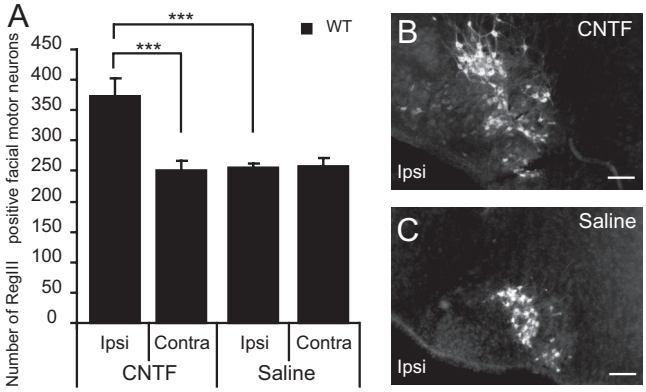

Fig. 5. CNTF increases the number of RegIIIβ positive neurons. (*A*) Application of CNTF to the cut facial nerve results in increased numbers of RegIIIβ-positive facial motor neurons in wild-type mice 2 days after nerve section. The data show means ± SEM (n = 7 in each group). ***, $P < 0.0001$. (*B* and *C*) RegIIIβ-positive neurons in wild-type mice after facial nerve cut and CNTF (*B*) or saline (*C*) application. The arrow indicates the increased number of RegIIIβ-positive neurons induced by CNTF. [Scale bar, 150 μm (*B* and *C*).]

to be concentrated in cranial motor neurons that have been associated with suckling and swallowing, such as the hypoglossal nucleus and nucleus ambiguus. We therefore examined the ability of RegIIIβ KO mice to ingest milk during a 1-h period of suckling after a 2-h period of isolation from the mother. Compared with wild-type pups, we found a significant reduction in milk/colostrum ingestion: percentage weight increase in wild-type mice, 3.1 ± 0.2%; and in KO mice, 0.45 ± 0.2 ($P < 0.01$).

Loss of RegIIIβ Delays Myelination of the Hypoglossal Nerve. Because of the influence of Reg2 on Schwann cells (9) and the reduced efficiency of suckling described above, we used electron microscopy to analyze myelination in the hypoglossal nerve at P5 in wild-type and KO mice. Oculomotor neurons never express RegIIIβ, and we, therefore, used the P5 oculomotor nerve as a control. We found a significant increase in the numbers of unmyelinated nerve fibres in both the medial and lateral hypoglossal nerves in KO mice at P5 (Fig. 6 *A–C*). One-way ANOVA revealed a significant effect of genotype on axon type in both the medial ($F_{1,14} = 24.8$; $P < 0.01$) and lateral hypoglossal nerves ($F_{1,13} = 21.5$; $P < 0.01$) There were no differences in the numbers of unmyelinated axons in the oculomotor nerves in P5 wild-type and KO mice. In the lateral hypoglossal nerve, the total numbers of axons in the RegIIIβ KO mice exceeded that in the wild-type animals (Fig. 6*C*). We therefore counted the total number of myelinated axons in the lateral and medial hypoglossal nerves at P21. We found that there were no differences between the two groups (wild type: lateral, 352.3 ± 25.8; medial, 980.3 ± 9.5; KO: lateral, 360.0 ± 16.5; medial, 950.3 ± 41.9 KO; n = 3 in each group). We concluded that excess collateralization of hypoglossal axons occurs because of delayed myelination during the early postnatal period in KO mice and is lost later by selective pruning of excess axonal branches (22, 23).

The impaired suckling phenotype, thus, may result from a disruption of myelination in mutant mice. We also examined the hypoglossal innervation of tongue musculature in wild-type and KO mice by using protein gene product (PGP) as a marker for nerve fibers and α-bungarotoxin for muscle end plates. We found no evidence of changes in innervation density or size of muscle end plates (data not shown).

Discussion

Previous research has suggested that *in vitro* rat Reg2 is a motor neuron survival factor essential for the actions of CNTF-like cytokines and a powerful Schwann cell mitogen that potentiates axonal repair and regeneration *in vivo* (8, 9). However, we show here that in mice with a genetic deletion of the RegIIIβ gene (the equivalent gene to Reg2 in rats), there is no increased motor neuron cell death during development. Nevertheless, we report that the efficacy of CNTF in reducing neuronal cell death was diminished in RegIIIβ KO mice indicating that RegIIIβ is important for the survival functions of CNTF. Finally, we found that myelination was delayed in subsets of hypoglossal motor neurones in KO animals and the efficiency of milk ingestion reduced.

RegIIIβ Is an Intermediate in the CNTF Survival Pathway. The suggestion that Reg2/RegIIIβ was a motor neuron neurotrophic factor and a signaling intermediary in the CNTF survival pathway stems from elegant *in vitro* studies demonstrating that purified Reg2 can act as a paracrine/autocrine neurotrophic factor for a subset of motor neurons (8). Furthermore, it has been shown that CNTF, as well as the related factors LIF, cardiotrophin 1, and oncostatin-M, rapidly induces Reg2 mRNA in some motor neurons and that released Reg2 acts in a paracrine/autocrine fashion to support motor neurons (8, 9). The CNTF/LIF family of cytokines signal through a receptor complex that includes the LIF receptor (LIFR) subunit, and it has been

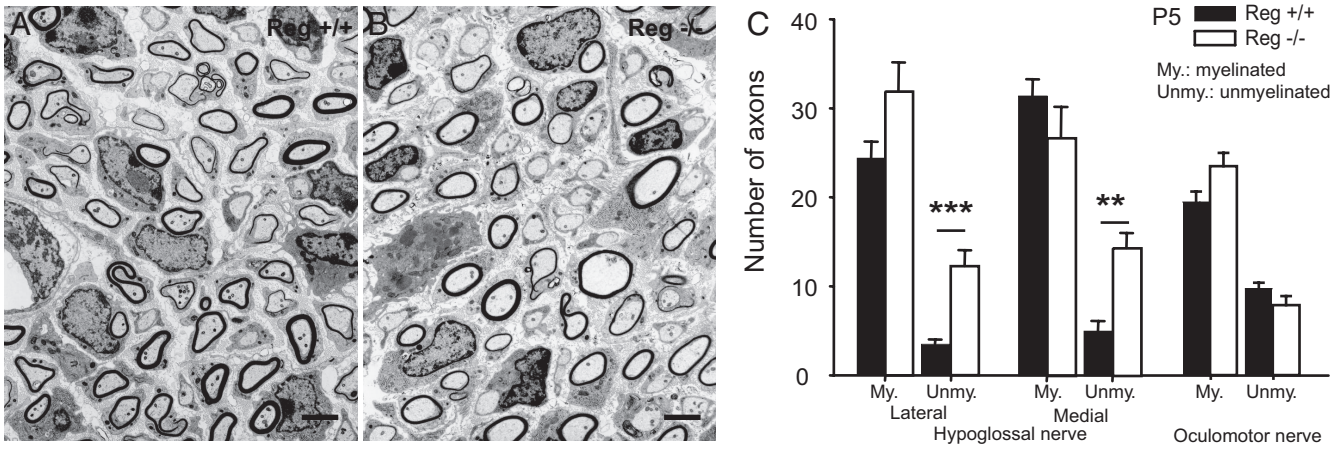

Fig. 6. Increased number of unmyelinated axons in RegIIIβ KO mice. Electron micrograph of the medial hypoglossal nerve of RegIIIβ wild-type (*A*) or RegIIIβ KO (*B*) mice. There is an increase in the number of unmyelinated fibers in the lateral and medial hypoglossal motor nerve of RegIIIβ KO mice ($n = 8$ in each group). (*C*) No differences were observed in the oculomotor nerve ($n = 3$ in each group). The data show means ± SEM. **, $P < 0.001$; ***, $P < 0.0001$. All nerves were studied at P5. [Scale bar, 2 μm (*A* and *B*).]

shown previously that in LIFR KO mice, there is no expression of Reg2/RegIIIβ during development (9). Thus, Reg2/RegIIIβ expression in some developing motor (and sensory) neurons depends on cytokines of the LIF family acting through a receptor complex containing LIFR.

The absence of motor neuron cell death in KO mice, therefore, is puzzling, especially given that RegIIIβ is essential for the *in vitro* neuronal survival effects of CNTF to be manifest. The evidence for a lack of effect on motor neuron survival comes from the presence of β-galactosidase reaction product in postnatal neurons up to P10 and the normal numbers of facial motor neurons in KO mice. However, in CNTF KO mice, there is similarly no increased loss of motor neurons during the first weeks of life (24, 25). This, perhaps, is not surprising, given that levels of CNTF are low during development and, although Schwann cells are the richest source of CNTF in the adult peripheral nervous system, levels only rise during the first postnatal week (26–28). Knockout of the CNTF gene did result in motor neuron loss 28 weeks after birth (24); however, RegIIIβ mice did not show motor neuron loss in later adult stages.

Previous studies suggest that CNTF itself is not the key ligand acting at the CNTF/LIF receptor complex. Nishimune *et al.* (8) found that RegIIIβ expression was unimpaired or delayed in a range of KOs including *cntf*, *ct1*, and *cntf/lif* double mutants, leading them to suggest that a factor as yet unknown was key to driving the expression of RegIIIβ in motor neurons.

That CNTF-like factors are as important *in vivo* as *in vitro* and require ReIIIβ expression is implied by the observation that RegIIIβ expression increases in axotomized neurons only when CNTF is applied to the nerve stump and that CNTF has no survival effect on motor neurons in RegIIIβ KO mice. We also show that the number of RegIIIβ neurons increased in wild-type mice when CNTF was applied to the cut nerve. This implies that many motor neurons have the capacity to express RegIIIβ, but this number is restricted by availability of CNTF-like factors during development. Nevertheless, RegIIIβ may not be the only intermediary involved in CNTF-like factor signaling as only ≈15–20% of facial motor neurons express RegIIIβ, and CNTF has previously been shown to rescue ≈75% of rat facial motor neurons from cell death when axotomized soon after birth (24). However, the substantially larger concentration of CNTF used in these experiments (5 μg vs. 250 ng used in the present study) may well have driven the expression of RegIIIβ in many more axotomized facial motor neurons than seen here and resulted in greater levels of survival (24). Also the dynamics of Reg2 expression in rat are different from that of RegIIIβ in mice. RegIIIβ never reappeared in the adult mouse after section of the facial nerve (Fig. S4) or sciatic nerve (data not shown) and did not noticeably decrease 24 h after axotomy, as was observed after sciatic transection in neonatal rats. Presumably other factors may play a similar role to RegIIIβ in adult mouse motor neurons, although it is unlikely to be RegIIIα, which although up-regulated in the KO mouse, did not potentiate CNTF-mediated survival.

Growth Factors and Myelination. We show here that myelination of a subset of hypoglossal motor neuron axons is delayed in RegIIIβ KO mice at P5.5 but normal by P21. This seems likely to be attributable to the loss of RegIIIβ because myelination of oculomotor axons in KO mice was normal and oculomotor motor neurons did not express RegIIIβ at any stages of development. This delayed myelination would be expected to disrupt the transmission of signals along the axon and may account for the reduced efficiency of suckling behavior. Delayed myelination did not, however, result in any reduction in the size or number of motor neuron end plates in target muscles of the hypoglossal such as the glossohyoid (unpublished data). However, how then does RegIIIβ promote myelination in discrete populations of motor neuron axons, and why is there such a restricted pattern of RegIIIβ expression?

Axons regulate Schwann cells during development of the peripheral nervous system (29–33). The axon signals for regulating Schwann cell differentiation are known to include both proteins encoded by the neuregulin gene (NRG) signaling through the erbB family of receptors, adhesion molecules such as L1 and N-cadherin and neurotrophic factors such as brain-derived neurotrophic factor (BDNF) (34–37). It has been suggested that cell adhesion molecules on the axon surface as well as signals from the extracellular matrix and neurotrophins are also required for myelination to proceed efficiently and accurately. For example, BDNF supports postnatal facial motor neurones after axotomy and acts through p75 NTR to inhibit Schwann cell migration and promote myelination (35, 36, 38). It seems likely that RegIIIβ released from subsets of motor neuron axons is playing much the same role as BDNF in driving the process of myelination. As with NRG1 type III, it has been shown that RegIIIβ signals through the PI3-kinase pathway (8, 17), and this may represent a common pathway for axonally released RegIIIβ to influence Schwann cells. Why RegIIIβ expression is restricted to motor neurons concerned with the suckling and swallowing is unclear, but we suggest that the patterning of this

critical function in neonatal mice may be plastic and regulated by release of factors from target musculature concerned with suckling in an activity-dependent fashion (8).

Materials and Methods

All procedures complied with the United Kingdom Animals (Scientific Procedures) Act 1986.

Generation of the RegIIIβ-Deficient Mice by Gene Targeting. The generation of these mice has been described elsewhere (18). Complete knockout of the gene was confirmed in nervous tissue with immunocytochemistry by using antibodies generated against rat Reg2 protein, and absence of *RegIII*β mRNA was confirmed by using real-time PCR in brain, pancreas, and regenerating liver (16, 18).

Real-Time RT-qPCR Assay. Tissue preparation and RNA extraction were as described previously (39). RNA samples were treated with DNase I (Qiagen). Equal amounts (3 μg) of total RNA were reversed transcribed by using random nonamers (Sigma) and SuperScript TM III RT (Invitrogen) for 1 h at 50°C in a total reaction volume of 20 μl. cDNAs were immediately quantified by real-time PCR or kept at −20°C until further experiments. Real-time PCRs were performed with a DNA Engine (Bio-Rad) by using SYBR Green Jump Start RT-PCR master mix (Sigma) with each gene-specific primer (*RegIII*β forward, 5′-AAGAATATACCCTCCGCACGC-3′; *RegIII*β reverse, 5′-CAGACATAGGGCAACTTCACC-3′; *RegIII*α forward, 5′-GAAGTGCCCTCTCCACGTACC-3′; *RegIII*α reverse, 5′-ACAAATGGTAATGTCCCATCG-3′; *RegIII*γ forward, 5′-GCTCCTATTGCTATGCCTTGTTTAG-3′; *RegIII*γ reverse 5′-CATGGAGGACAGGAAGGAAGC-3′; β-actin forward, 5′-CAACGAGCGGTTCCGATG-3′; β-actin reverse, 5′-GCCACAGGATTCCATACCCA-3′). One microliter of cDNA was amplified in a three-step cycling program in a final reaction volume of 25 μl. Control cDNA samples (obtained without transcriptase) were always included, as well as samples without any cDNA template. Reactions were performed in triplicate for five to six biological replicates, and threshold cycle values were normalized to β-actin gene expression. The specificity of the products was determined by melting curve analysis. The ratio of the relative expression of target genes to β-actin was calculated by using the $2^{\Delta CT}$ formula.

Facial Nerve Section. Pups were cooled on wet ice (4°C), and the extent of anesthesia was determined by assessing reflex responses to tail pinch. Adult mice were anesthetized with Fluothane. The right facial nerve was transected at the stylomastoid foramen. One to 10 days later, mice were deeply anesthetized with Euthatal i.p. and transcardially perfused with 4% paraformaldehyde (PFA) in 0.1 M sodium phosphate buffer (PB) (pH 7.4) preceded by a brief wash with heparinized saline. After a 2 h postfix in PFA, tissue was moved to sucrose (30%) PB solution in preparation for freeze sectioning. In some pups, 5 μl of CNTF (250 ng) applied to a piece of Gelfoam in 5 μl saline, or saline alone, was applied to the cut end of the facial nerve at the time of section. Animals received only one treatment: either CNTF or saline.

Detection of β-Galactosidase Staining by X-Gal Staining. PFA-fixed tissue was washed in PBT (PBS/0.1% Tween-20) several times. After a rinse in X-Gal staining solution [5 mM $K_3Fe(CN)_6$, 5 mM $K_4Fe(CN)_6$, 1 mM $MgCl_2$, 0.01% sodium deoxycholate, 0.02% Triton plus X-Gal (4-chloro,5-bromo,3-indolyl-β-galactosidase) at 1 mg/ml, suspended in PBS (pH 7.2)], tissue was transferred to fresh staining solution. Tissue was incubated at 37°C in the dark overnight. Sections were washed several times with PBT.

Cell Counting. Sections (40 μm) were cut through the facial nucleus and all sections (the facial nucleus is ≈700 μm in length in the anterior–posterior direction) were mounted and stained with neutral red. All neuronal profiles in every section were counted and total counts corrected by using the Abercrombie correction (40).

Immunohistochemistry. Mice were deeply anesthetized with pentobarbitone (60 mg/kg, i.p.) and transcardially perfused with 4% PFA in 0.1 M sodium phosphate buffer (PB) (pH 7.4) preceded by a brief wash with heparinized saline. Tissue was dissected and postfixed for 2 h at 4°C and then transferred to 30% (wt/vol) sucrose in 0.1 M PB containing 0.02% (wt/vol) sodium azide. 40 μm free-floating tissue sections were processed as previously described but for detection of RegIIIβ (9, 39). Hypoglossal innervation of tongue musculature in wild-type and KO mice was assessed with PGP, a marker for nerve fibres, and α-bungarotoxin, a marker for muscle end plates.

Electron Microscopy. Mouse pups or adult mice (P21) were deeply anesthetized with Nembutal and perfused with 10 ml heparinized saline followed by 20 ml 4% PFA plus 0.5% gluteraldehyde. Tissue was fixed overnight before dissection of the caudal tongue and attached hypoglossal nerves and the oculomotor nerve still attached to the optic nerve and eyecup. After being osmicated (30 min in 1% OsO_4 in 0.1 M PB), the sections were stained for 15 min in 0.1% uranyl acetate in sodium acetate buffer at 4°C, dehydrated in ethanols, cleared in propylene oxide, and embedded in Araldite. Semithin sections were cut with glass knives and stained with toluidine blue adjacent to thin sections cut with a diamond knife on an Ultracut ultramicrotome (Reichert). The sections were collected on mesh grids coated with a thin Formavar film, counterstained with lead citrate, and viewed in a JEOL 1010 electron microscope. Counts were made from four photographs of the lateral and medial nerves for each animal taken at ×4,000 magnification. Total counts of myelinated fibers at P21 were made from photomicrographs of the lateral and medial hypoglossal nerves at ×1,000 magnification.

Measurement of Milk/Colostrum Intake. The procedure described by Fujita and colleagues (41, 42) was followed. Briefly, pups were separated from the dam for 2 h and kept in a warm, dark chamber. The pups were then weighed and placed back with the mothers for 1 h before reweighing. Thirty to 40 pups of each genotype were used for the measurement of milk intake.

Statistical Analysis. The data are expressed as means ± SEM. The data were analyzed by general linear model univariate or multivariate test, as appropriate, followed by Bonferroni post hoc tests or Student's *t* test, as appropriate. For all statistical analysis, statistical significance was set at $P < 0.05$.

ACKNOWLEDGMENTS. We thank Austin Smith for support and advice during the early stages of this project and Rhona Mirsky for discussion. This work was supported by the Motor Neuron Disease Society (United Kingdom) and the Medical Research Council (United Kingdom).

1. Bruijn LI, Miller TM, Cleveland DW (2004) Unraveling the mechanisms involved in motor neuron degeneration in ALS. *Annu Rev Neurosci* 27:723–749.
2. Henderson CE, *et al.* (1998) Role of neurotrophic factors in motoneuron development. *J Physiol Paris* 92:279–281.
3. Oppenheim RW (1996) Neurotrophic survival molecules for motoneurons: An embarrassment of riches. *Neuron* 17:195–197.
4. Sendtner M, Holtmann B, Hughes RA (1996) The response of motoneurons to neurotrophins. *Neurochem Res* 21:831–841.
5. Thoenen H, Hughes RA, Sendtner M (1993) Trophic support of motoneurons: Physiological, pathophysiological, and therapeutic implications. *Exp Neurol* 124:47–55.
6. Wiese S, Beck M, Karch C, Sendtner M (2004) Signalling mechanisms for survival of lesioned motoneurons. *Acta Neurochir Suppl* 89:21–35.
7. Narushima Y, *et al.* (1997) Structure, chromosomal localization and expression of mouse genes encoding type III Reg, RegIII alpha, RegIII beta, RegIII gamma. *Gene* 185:159–168.
8. Nishimune H, *et al.* (2000) Reg-2 is a motoneuron neurotrophic factor and a signalling intermediate in the CNTF survival pathway. *Nat Cell Biol* 2:906–914.
9. Livesey FJ, *et al.* (1997) A Schwann cell mitogen accompanying regeneration of motor neurons. *Nature* 390:614–618.
10. Iovanna JL, Dagorn JC (2005) The multifunctional family of secreted proteins containing a C-type lectin-like domain linked to a short N-terminal peptide. *Biochim Biophys Acta* 1723:8–18.
11. Okamoto H (1999) The Reg gene family and Reg proteins: With special attention to the regeneration of pancreatic beta-cells. *J Hepatobiliary Pancreat Surg* 6:254–262.
12. Okamoto H, Takasawa S (2002) Recent advances in the Okamoto model: The CD38-cyclic ADP-ribose signal system and the regenerating gene protein (Reg)-Reg receptor system in beta-cells. *Diabetes 51 Suppl* 3:S462–S473.
13. Zhang YW, Ding LS, Lai MD (2003) Reg gene family and human diseases. *World J Gastroenterol* 9:2635–2641.
14. Malka D, *et al.* (2000) Tumor necrosis factor alpha triggers antiapoptotic mechanisms in rat pancreatic cells through pancreatitis-associated protein I activation. *Gastroenterology* 119:816–828.
15. Christa L, *et al.* (1999) Hepatocarcinoma-intestine-pancreas/pancreatic associated protein (HIP/PAP) is expressed and secreted by proliferating ductules as well as by hepatocarcinoma and cholangiocarcinoma cells. *Am J Pathol* 155:1525–1533.
16. Gironella M, *et al.* (2007) Experimental acute pancreatitis in PAP/HIP knock-out mice. *Gut* 56:1091–1097.
17. Lieu HT, *et al.* (2005) HIP/PAP accelerates liver regeneration and protects against acetaminophen injury in mice. *Hepatology* 42:618–626.
18. Lieu HT, *et al.* (2006) Reg2 inactivation increases sensitivity to Fas hepatotoxicity and delays liver regeneration post-hepatectomy in mice *Hepatology* 44:1452–1464.
19. Averill S, Davis DR, Shortland PJ, Priestley JV, Hunt SP (2002) Dynamic pattern of reg-2 expression in rat sensory neurons after peripheral nerve injury. *J Neurosci* 22:7493–7501.
20. Tam J, Rosenberg L, Maysinger D (2004) INGAP peptide improves nerve function and enhances regeneration in streptozotocin-induced diabetic C57BL/6 mice. *FASEB J* 18:1767–1769.

21. Sendtner M, *et al.* (1992) Ciliary neurotrophic factor prevents degeneration of motor neurons in mouse mutant progressive motor neuronopathy. *Nature* 358:502–504.
22. Bishop DL, Misgeld T, Walsh MK, Gan WB, Lichtman JW (2004) Axon branch removal at developing synapses by axosome shedding. *Neuron* 44:651–661.
23. Yamamoto M, Ueda R, Takahashi K, Saigo K, Uemura T (2006) Control of axonal sprouting and dendrite branching by the Nrg-Ank complex at the neuron-glia interface. *Curr Biol* 16:1678–1683.
24. Masu Y, *et al.* (1993) Disruption of the CNTF gene results in motor neuron degeneration. *Nature* 365:27–32.
25. Sendtner M, Arakawa Y, Stockli KA, Kreutzberg GW, Thoenen H (1991) Effect of ciliary neurotrophic factor (CNTF) on motoneuron survival. *J Cell Sci Suppl* 15:103–109.
26. Holtmann B, *et al.* (2005) Triple knock-out of CNTF, LIF, and CT-1 defines cooperative and distinct roles of these neurotrophic factors for motoneuron maintenance and function. *J Neurosci* 25:1778–1787.
27. Schweizer U, *et al.* (2002) Conditional gene ablation of Stat3 reveals differential signaling requirements for survival of motoneurons during development and after nerve injury in the adult. *J Cell Biol* 156:287–297.
28. Stockli KA, *et al.* (1991) Regional distribution, developmental changes, and cellular localization of CNTF-mRNA and protein in the rat brain. *J Cell Biol* 115:447–459.
29. ffrench-Constant C, Colognato H, Franklin RJ (2004) Neuroscience. The mysteries of myelin unwrapped. *Science* 304:688–689.
30. Jessen KR, Mirsky R (2002) Signals that determine Schwann cell identity. *J Anat* 200:367–376.
31. Jessen KR, Mirsky R (2005) The origin and development of glial cells in peripheral nerves. *Nat Rev Neurosci* 6:671–682.
32. Taveggia C, *et al.* (2005) Neuregulin-1 type III determines the ensheathment fate of axons. *Neuron* 47:681–694.
33. Taveggia C, Salzer JL (2007) PARsing the events of myelination. *Nat Neurosci* 10:17–18.
34. Bunge RP, Bunge MB, Eldridge CF (1986) Linkage between axonal ensheathment and basal lamina production by Schwann cells. *Annu Rev Neurosci* 9:305–328.
35. Chan JR, Cosgaya JM, Wu YJ, Shooter EM (2001) Neurotrophins are key mediators of the myelination program in the peripheral nervous system. *Proc Natl Acad Sci USA* 98:14661–14668.
36. Tolwani RJ, *et al.* (2004) BDNF overexpression produces a long-term increase in myelin formation in the peripheral nervous system. *J Neurosci Res* 77:662–669.
37. Zhang JY, Luo XG, Xian CJ, Liu ZH, Zhou XF (2000) Endogenous BDNF is required for myelination and regeneration of injured sciatic nerve in rodents. *Eur J Neurosci* 12:4171–4180.
38. Yan Q, Elliott J, Snider WD (1992) Brain-derived neurotrophic factor rescues spinal motor neurons from axotomy-induced cell death. *Nature* 360:753–755.
39. Geranton SM, Morenilla-Palao C, Hunt SP (2007) A role for transcriptional repressor methyl-CpG-binding protein 2 and plasticity-related gene serum- and glucocorticoid-inducible kinase 1 in the induction of inflammatory pain states. *J Neurosci* 27:6163–6173.
40. Vogelezang MG, *et al.* (2001) Alpha4 integrin is expressed during peripheral nerve regeneration and enhances neurite outgrowth. *J Neurosci* 21:6732–6744.
41. Fujita K, *et al.* (2006) Effects of hypoglossal and facial nerve injuries on milk-suckling. *Int J Dev Neurosci* 24:29–34.
42. Fukuyama T, *et al.* (2006) Differential effects of hypoglossal and facial nerve injuries on survival and growth of rats at different developmental stages. *Int J Dev Neurosci* 24:307–317.

Peripheral Facial Nerve Axotomy in Mice Causes Sprouting of Motor Axons Into Perineuronal Central White Matter: Time Course and Molecular Characterization

Milan Makwana,[1] Alexander Werner,[2,3] Alejandro Acosta-Saltos,[1] Roman Gonitel,[1,4] Abirami Pararajasingham,[1] Crystal Ruff,[1] Prakasham Rumajogee,[1] Dan Cuthill,[1] Mathias Galiano,[1,2] Marion Bohatschek,[1] Adam S. Wallace,[1] Patrick N. Anderson,[5] Ulrike Mayer,[6] Axel Behrens,[7] and Gennadij Raivich[1,2,5]*

[1]Perinatal Brain Repair Group, Department of Obstetrics and Gynaecology, EGA Institute for Women's Health, University College London, London WC1E 6HX, United Kingdom
[2]Department of Neuromorphology, Max-Planck Institute for Neurobiology, 82152 Martinsried, Germany
[3]Aurigon Co., D-82327 Tutzing, Germany
[4]Molecular Immunology Unit, Institute of Child Health, University College London, London WC1E 6HX, United Kingdom
[5]Department of Anatomy and Developmental Biology, University College London, London WC1E 6HX, United Kingdom
[6]Biomedical Research Centre, University of East Anglia, Norwich NR4 7, United Kingdom
[7]Cancer Research UK, London Research Institute, London WC2A 3PX, United Kingdom

ABSTRACT

Generation of new axonal sprouts plays an important role in neural repair. In the current study, we examined the appearance, composition and effects of gene deletions on intrabrainstem sprouts following peripheral facial nerve axotomy. Axotomy was followed by the appearance of galanin$^+$ and calcitonin gene-related peptide (CGRP)$^+$ sprouts peaking at day 14, matching both large, neuropeptide$^+$ subpopulations of axotomized facial motoneurons, but with CGRP$^+$ sprouts considerably rarer. Strong immunoreactivity for vesicular acetylcholine transporter (VAChT) and retrogradely transported MiniRuby following its application on freshly cut proximal facial nerve stump confirmed their axotomized motoneuron origin; the sprouts expressed CD44 and alpha7beta1 integrin adhesion molecules and grew apparently unhindered along neighboring central white matter tracts. Quantification of the galanin$^+$ sprouts revealed a stronger response following cut compared with crush (day 7–14) as well as enhanced sprouting after recut (day 8 + 6 vs. 14; 14 + 8 vs. 22), arguing against delayed appearance of sprouting being the result of the initial phase of reinnervation. Sprouting was strongly diminished in brain Jun-deficient mice but enhanced in alpha7 null animals that showed apparently compensatory up-regulation in beta1, suggesting important regulatory roles for transcription factors and the sprout-associated adhesion molecules. Analysis of inflammatory stimuli revealed a 50% reduction 12–48 hours following systemic endotoxin associated with neural inflammation and a tendency toward more sprouts in TNFR1/2 null mutants (P = 10%) with a reduced inflammatory response, indicating detrimental effects of excessive inflammation. Moreover, the study points to the usefulness of the facial axotomy model in exploring physiological and molecular stimuli regulating central sprouting. J. Comp. Neurol. 518:699–721, 2010.

INDEXING TERMS: growth cones; regeneration; central sprouting; adhesion molecules; transcription factors; inflammation

Additional Supporting Information may be found in the online version of this article.

The first three authors contributed equally to this work.

Grant sponsor: International Spinal Research Trust Natalie-Rose-Barr Fellowship (to M.M., G.R.); Grant sponsor: Motor Neuron Disease (MND) Association; Grant number: 06/6220 (to A.A.-S., G.R.); Grant sponsor: Biotechnology and Biological Sciences Research Council; Grant number: 31/S20299 (to G.R.); Grant number: BB/D009537/1 (to G.R.).

*CORRESPONDENCE TO: Gennadij Raivich, MD, PhD, Perinatal Brain Repair Group, Department of Obstetrics and Gynaecology and Department of Anatomy and Developmental Biology, University College London, 86-96 Chenies Mews, London WC1E 6HX, United Kingdom. E-mail: g.raivich@ucl.ac.uk

Received 2 June 2008; Revised 18 June 2009; Accepted 2 October 2009.
DOI 10.1002/cne.22240
Published online October 13, 2009 in Wiley InterScience (www.interscience.wiley.com).

Generation of new axonal sprouts and the process of axonal elongation play a vital role in the neural repair program following injury to the nervous system. In the classical case of axonal regeneration in the injured peripheral nerve, the tip of the proximal axon still connected to the neuronal cell body is gradually transformed into a motile and sprouting growth cone that moves across the gap between the proximal and nerve stump, enters neural tubes in the distal part, and uses them as a scaffold on its way to the peripheral target (Witzel et al., 2005). Supernumerary axonal sprouts can also develop more proximally, at the nodes of Ranvier (Ramon y Cajal, 1928; Friede and Bischausen, 1980; McQuarrie, 1985; Ide and Kato, 1990), from distal dendrites (Fenrich et al., 2007), and occasionally even at the level of the injured neuronal cell body (Linda et al., 1985).

In addition to outright regeneration, nerve injury can also elicit sprouting from uninjured axons. This includes collateral sprouting from functionally appropriate or inappropriate adjacent intact axons into the deafferented part of the central nervous system (Cotman et al., 1990) or peripheral tissues, including skin (Diamond et al., 1987), muscle (Mehta et al., 1993; Nguyen et al., 2002), and nerve (Ide and Kato, 1990; Tanigawa et al., 2005). Peripheral axotomy can also induce the sprouting of central sensory processes of the affected dorsal root ganglia (DRG) neurons in the spinal cord (Woolf et al., 1992) as well as the appearance of perineuronal neurite baskets in the DRGs themselves (McLachlan et al., 1993; McLachlan and Hu, 1998; Li and Zhou, 2001; Liu et al., 2005). Both processes have been indcated to contribute to posttraumatic neuropathic pain (Woolf et al., 1992; Liu et al., 2005). Despite the variability in origin, regulation, and dynamics, in most cases these different forms of posttraumatic neurite outgrowth appear to start within the first few days after injury or to represent a very late response that may be associated with frustrated regeneration.

Transection of the adult facial nerve is a well-established model system for studying the axonal response and neuronal regeneration (Moran and Graeber, 2004). Moreover, experimental work in gene-deficient and-overexpressing mice has begun to provide insight into molecular signals—transcription factors, cell adhesion molecules, cytokines, and neurotrophins—that determine axonal regeneration as well as posttraumatic neuronal survival and cell death and different aspects of the neural inflammatory response (Werner et al., 2000; Kalla et al., 2001; Heumann et al., 2001; Raivich et al., 2004; for review see Raivich and Makwana, 2007). However, these studies also suggested a de novo appearance of neuropeptide-immunoreactive sprouts in and around the axotomized facial motor nucleus, during the midphase of axonal regeneration after facial nerve cut (Kloss et al., 1999; Werner et al., 2000; Galiano et al., 2001).

The aim of the current study was to determine the precise neuronal origin of these sprouting neurites and define their time course, neuroanatomical distribution, and molecular characteristics. We show that these axons originate from injured and regenerating neurons, are capable of growing for more than 0.5 mm into different white matter tracts surrounding the lesioned facial motor nucleus, and express high levels of cell adhesion molecules such as CD44 and alpha7beta1 integrin. Surprisingly, deletion of the alpha7 integrin subunit led to a further increase in the number and extent of neuropeptide-immunoreactive neurite growth cones, suggesting an inhibitory role of alpha7 in this form of posttraumatic central axonal sprouting.

MATERIALS AND METHODS

Animals, surgical procedures, and tissue treatment

Normal, wild-type, C57Bl/6 mice were generated at our animal facilities at Max-Planck Institute of Neurobiology, Martinsried, and then at the Biological Services Unit, UCL. Transgenic, TNFR1/2−/− mice and wild-type controls (+/+) were obtained from BRL (Basel, Switzerland) and were on a mixed B6 × 129 background. In the TNFR1 transgenic strain, TNFR1 gene exons II and III, flanked by the Nhe I and Bgl II restriction sites were replaced by ortho-oriented pgk-neomycin resistance cassette, abolishing specific tumor necrosis factor-α (TNFα) binding in TNFR1−/− thymocytes (Rothe et al., 1993). In the TNFR2 strain, the pgk-neomycin resistance cassette was inserted into the BstB II site of the second TNFR2 exon, just downstream of the sequence encoding the signal peptide, resulting in a complete lack of TNFR2 protein (Erickson et al., 1994). Both strains were crossed together, to obtain double heterozygotes (TFR1+/−TNFR2+/−), then crossed again for the TNFR1&2−/− and controls.

Brain c-Jun-deficient animals were generated by crossing mice carrying a floxed *jun* allele encoding c-Jun, jun^{f}, with the loxP sequences at the XbaI restriction sites surrounding the exon carrying the entire c-Jun open reading frame (Behrens et al., 2002), with those expressing cre recombinase under the control of nestin promoter nes::cre. In the nes::cre transgene, the cre gene is placed immediately downstream of the 5-kb large 5′-promoter, followed by the human growth hormone polyadenylation signal and the second nestin intron, which contains a neuroepithelium-specific enhancer (Tronche et al., 1999). The resulting $jun^{f/wt}$ × nestin::cre animals were then crossed again with $jun^{f/f}$, to generate the $jun^{f/f}$ × nestin::cre mutant mice, in which both *jun* alleles are inactivated in cells derived from embryonic neuroepithelium

($jun^{\Delta n}$). Compound $jun^{\Delta n}$ mice were on a mixed 129Ola/C57BL6/FVBN genetic background. Sibling animals lacking the cre transgene, with functional, unrecombined homozygous jun^{f} ($jun^{f/f}$), served as controls. The homozygous alpha7−/−and littermate controls on the 129/Sv background used in this study were obtained from heterozygous crossing of alpha7+/−mice generated by Mayer et al. (1997). In that transgenic strain, a 1-kb stretch of the alpha7 genomic sequence flanked by the NcoI restriction sites including part of exon 1 and the following intron and encoding the entire signal sequence plus 107 bases coding for the start part of the mature protein is replaced by a reverse-oriented neomycin resistance cassette (Mayer et al., 1997).

To study the effects of enhanced neural inflammation, *Escherichia coli* lipopolysaccharide (O55:B5 serotype, 1 mg; Sigma, Deisenhofen, Germany) was dissolved in phosphate-buffered saline (PBS: 10 mM Na_2HPO_4, 0.85% NaCl, pH 7.4), and injected intraperitoneally into C57 black 6 mice (8 weeks old, 25–30 g weight; n = 3 per group) 12–96 hours prior to the 14-day time point. Control groups of animals were left alone or were injected with saline and allowed to survive for 24 hours.

All surgical techniques were performed with animals under anesthesia with 2,2,2-tribromethanol (Avertin; Sigma, Deisenhofen, Germany), 0.4 mg/g body weight, on 3–6-month-old mice. All animals belonging to the same experimental group (day 1 group, day 2 group, day 4 group, etc.) were also operated upon on the same day, inside a narrow time window of 1–3 hours. Animal experiments and care protocols were approved by the Regierung von Oberbayern (AZ 211-2531-10/93 and AZ 211-2531-37/97) in Germany and the Home Office (Scientific Procedures Act) in the United Kingdom.

The right facial nerve (including the retroauricular branch) was cut or crushed at its exit from the stylomastoid foramen. For the reaxotomy experiments, the cut was made 1 mm distal to the original injury, and the retroauricular branch was not recut. Animals were euthanized after survival times of 1–42 days and perfusion fixed with 200 ml PBS (10 mM Na_2HPO_4, 0.85% NaCl, pH 7.4), followed by 200 ml of 4% paraformaldehyde in PBS (PFA/PBS), then by a 2-hour immersion of the brainstem in 1% PFA/PBS at 4°C on a rotator (8 rpm), with an overnight rotating immersion in a phosphate-buffered sucrose solution (PB: 10 mM Na_2HPO_4, pH 7.4, 4°C; 30% sucrose), and frozen on dry ice.

Immunofluorescence, double labeling, and confocal scanning microscopy

Frozen brainstems were cut at the level of the facial nucleus, and 20-μm sections were collected on warm, 0.5% gelatin-coated slides (Merck, Darmstadt, Germany), refrozen on dry ice, and stored at −80°C until further use. Axonal growth cones in and around the facial motor nuclei were quantified by using immunofluorescence against CGRP or galanin, the neuropeptides expressed in axotomized facial motoneurons. For standard immunofluorescence, the sections were thawed, rehydrated and spread in distilled water, fixed in 4% formaldehyde in 0.1 M PB, defatted in acetone, and pretreated with 5% goat serum (Vector, Wiesbaden, Germany) in phosphate buffer/PB as described by Möller et al. (1996). Briefly, the sections were incubated overnight at 4°C with 1:100 diluted, primary rabbit antibodies against CGRP or galanin (Table 1), washed in PB, and incubated with a biotinylated goat anti-rabbit antibody (1:100; Vector) and Texas red streptavidin (Jackson Laboratories). The sections were then covered with VectaShield (Vector) and stored in the dark at 4°C for confocal scanning and quantification.

For immunofluorescence, fixed sections were preincubated as in brightfield immunohistochemistry. Both primary antibodies were applied overnight at 4°C, washed, incubated with two appropriate secondary antibodies (biotin-conjugated donkey anti-rabbit Ig and FITC-conjugated goat anti-rat Ig; 1:100; Dianova, Hamburg, Germany), washed again, and then incubated with a tertiary FITC-conjugated donkey anti-goat antibody (1:100; Sigma) and Cy3-avidin (1:1,000; Dianova). In the case of colocalization with the goat anti-VAChT, only the donkey anti-goat antibody was used. Omission of the primary antibody or replacement with nonspecific immunoglobulin from the same species (rat, rabbit, or hamster) at the same dilution led to the disappearance of specific labeling.

Digital micrographs of FITC and Cy3 or Texas red fluorescence were taken with a Leica TCS confocal laser microscope with a ×10 objective for quantification and a ×100 objective for illustrations in eight-bit gray-scale, 1,024 × 1,024 pixel format as described in previous studies (Raivich et al., 1998; Kloss et al., 1999). Twelve consecutive equidistant levels with 30-μm spacing with a ×10 objective or 20 levels with 0.5-μm spacing at ×100 objective were recorded and condensed onto a single bitmap by using the MaxIntense algorithm.

Antibody characterization

A summary of primary, secondary, and tertiary antibodies used to characterize the facial sprouts by double labeling with antibodies for galanin, CGRP, or vesicular acetylcholine transporter (VAChT) 14 days after facial nerve cut are listed in Table 1. The specificity of alpha7, alphaM, CD44, CGRP, and galanin was confirmed by using the appropriate knockouts, compared with the wild-type controls. Homozygous deletion of the alpha7 gene caused the disappearance of neuronal and terminal alpha7 immunoreactivity in facial motoneurons as well as throughout the

TABLE 1.
Summary of Antibodies[1]

Detected antigen	Immunization with	Primary antibody (code, type)	Dilution	Application	Source
Alpha4 integrin (CD49d)	Mouse spontaneous T-lymphoma line TK1 (AKR Cum strain)	R1-2, 01271D, RtM, IgG2b, κ	1:1,000	DIF	Pharmingen, United Kingdom catalog No. 553154 lot No. 38618
Alpha5 integrin (CD49e)	Mouse mast cell line MC/9	5H10-27 (MFR5) RtM, IgG2a, κ	1:200	DIF	Pharmingen, United Kingdom catalog No. 553319 lot No. C510514
Alpha6 integrin (CD49f)	Mouse mammary tumour (balb/C)	GoH3, RtM, IgG2a	1:3,000	DIF	Serotec, United Kingdom catalog No. MCA699GA
Alpha7 integrin (CD49g)	Synthetic peptide (aa 1117-1136) coupled to maleimide-activated key limphole hemocyanin (KLH), Pierce, Rockford, IL	Anti-alpha7, RbP	1:5,000	IHC, DIF	Ulrike Meyer, U East Anglia Norwich, United Kingdom
AlphaM integrin (CD11b)	T-cell-enriched B10 mouse spleen cells	5C6, RtM	1:6,000	DIF	Serotec, United Kingdom catalog No. MCA 711
Beta1 integrin (CD29)	Raised against the beta1 integrin (von Ballestrem et al., 1996)	MB1.2, RtM, IgG2a, κ	1:3,000	IHC, DIF	Chemicon, United Kingdom catalog No. MAB1997 lot No. 0507004326
CD44	Purified human blood lymphocyte CD44 lacking v1–v10 exons	MAB2137, RtM, IgG2b	1:5,000	DIF	Chemicon, United Kingdom catalog No. MAB2137
CGRP	Calcitonin gene-related peptide (Bachem)[2]	anti-CGRP, RbP	1:400	IHC, DIF	Bachem, United Kingdom T-4032.0050
Galanin	Galanin peptide (Bachem)[3]	Antigalanin, RbP	1:400	IHC, DIF	Bachem, United Kingdom T-4334.0050
MAP2	Purified rat brain microtubule-associated protein (MAP2)	Anti-MAP2, RbP, AB5622	1:3,000	DIF	Chemicon, United Kingdom P11137 AB5622
NF-H	Rat NFH fusion protein containing 37 KSP repeats	anti-NFH, RbP AB1991	1:200	DIF	Chemicon, United Kingdom catalog No. AB1991 lot No. 23080338
VaChT	Synthetic peptide (aa 511-530) from the cloned rat VAChT	G4481, GtP AB1588	1:6,000	DIF	Chemicon, United Kingdom AB1588
Secondary and tertiary					
Goat Ig	Goat immunoglobulin	FITC-cj α-Gt Ig, DkP	1:100	DIF	Dianova, United Kingdom
Hamster Ig	Hamster immunoglobulin	FITC-cj α-Hm Ig, GtP	1:100	DIF	Dianova, United Kingdom
Rat Ig	Rat immunoglobulin	Biot. α-Rt Ig, GtP	1:100	IHC	Vector, United Kingdom
Rat Ig	Rat immunoglobulin	FITC-cj α-Rt Ig, GtP	1:100	DIF	Dianova, United Kingdom
Rabbit Ig	Rabbit immunoglobulin	Biot α-Rb Ig, GtP	1:100	IHC	Vector, United Kingdom
Rabbit Ig	Rabbit immunoglobulin	Biot α-Rb Ig, DkP	1:100	DIF	Dianova, United Kingdom

[1]Antigens: CD44, cluster of differentiation 44; CGRP, calcitonin gene-related peptide; MAP2, microtubule-associated protein 2; NFHm, neurofilament heavy isoform; VaChT, vesicular acetylcholine transporter. Antibodies: RtM, rat monoclonal; HmM, hamster monoclonal; RbP, rabbit polyclonal; GtP, goat polyclonal; DkP, donkey polyclonal; FITC-cj fluorescein isothiocyanate conjugated. Applications: DIF, double immunofluorescence; IHC, immunohistochemistry (light microscopy).

[2]CGRP peptide sequence: H-Ser-Cys-Asn-Thr-Ala-Thr-Cys-Val-Thr-His-Arg-Leu-Ala-Gly-Leu-Leu-Ser-Arg-Ser-Gly-Gly-Val-Val-Lys-Asp-Asn-Phe-Val-Pro-Thr-Asn-Val-Gly-Ser-Glu-Ala-Phe-NH2, Cys1-Cys2 disulfide bond.

[3]Galanin peptide sequence: H-Gly-Trp-Thr-Leu-Asn-Ser-Ala-Gly-Tyr-Leu-Leu-Gly-Pro-His-Ala-Ile-Asp-Asn-His-Arg-Ser-Phe-Ser-Asp-Lys-His-Gly-Leu-Thr-NH2.

brain and peripheral nerve described in a previous study (Werner et al., 2000). Homozygous alphaM null mice and littermate controls (Hu et al., 2000), obtained through collaboration with Dr Tanya Mayadas Norton (Boston, MA), showed the disappearance of all microglial alphaM immunoreactivity throughout the brain of the alphaM null mice as well as in the axotomized facial motor nucleus. Similar absence of neuronal immunoreactivity for galanin was observed in galanin gene-deficient mice, obtained through collaboration with Dr David Wynick (Holmes et al., 2000); for CGRP in facial motoneurons of the alpha CGRP-deficient mice, through collaboration with Dr Jean-Pierre Changeux (Salmon et al., 2001); and for CD44 in CD44 null mice, provided through collaboration with Dr Rudolf Schmits (Schmits et al., 1997). In all cases, the wild-type littermate controls showed normal, specific immunoreactivity. The null mutants showed very little, diffuse staining throughout the brain.

In addition, antibody specificity for cell adhesion, neuropeptide, and cholinergic markers was further confirmed by Western blotting with unfractionated tissue homogenates from trigeminal ganglia, brainstem, spleen, and

heart muscle. The monoclonal R1-2 antibody against the alpha4 integrin subunit detected a prominent band that migrates at ~80 kDa and a faint band that migrates at ~65 kDa. Although the predicted molecular weight of alpha4 is 115 kDa (UniProt, Q00651), experimentally it has been demonstrated that the molecule is cleaved into fragments of 80 and 66 kDa upon T-cell activation (Blue et al., 1992). The monoclonal 5H10-27 (MFR5) antibody against the alpha5 integrin subunit detected a band at 90 kDa corresponding to the heavy chain. The full predicted molecular weight is 115 kDa; however, it is cleaved into heavy (~90 kDa) and light (~16 kDa) chains, (UniProt, P11688). Cleavage had also been reported experimentally (Teixido et al., 1992) with the products migrating at 80 and 70 kDa under nonreducing conditions. Under reducing conditions, migration of bands might be altered. The monoclonal GoH3 antibody to alpha6 detected a band at 87 kDa corresponding to the heavy chain predicted at 88 kDa (UniProt, Q61739) and a smaller band that migrates at 60 kDa. Cleavage has been previously reported for this molecule with the product migrating at ~70 kDa under nonreducing conditions (King et al., 2008). The polyclonal antibody against alpha7 detected a unique band at 129 kDa corresponding to the full-sized molecule (UniProt, Q61738; Echtermeyer et al., 1996); the monoclonal 5C6 antibody against alphaM detected a single band at 127 kDa corresponding to the full-size molecule (UniProt, P05555). The monoclonal MB1.2 antibody against beta1 detected a band at 88 kDa consistent with the predicted weight (UniProt, P09055) and two smaller bands at 70 and 53 kDa consistent with previously reported cleavage products (Menon et al., 2006). As a general trend, the literature associates proteolytic cleavage of integrins with more active cells. Antibody to CD44 detected a unique band at 63 kDa consistent with the common hematopoetic isoform 6 (UniProt, P15379-5). The polyclonal VAChT antibody detected a single band at 57 kDa as previously reported (UniProt, O35304, http://www.millipore.com/catalogue/item/ab1588). The antibody reveals strong staining on cholinergic terminals surrounding the brainstem and spinal motor neurons as well as comparatively week labeling of the cholinergic neuronal cell body itself (Gilmor et al., 1996). Both features were also confirmed in the current study (see Fig. 5AI–AIK). Galanin antibody detected a single band at 13 kDa consistent with its predicted size (UniProt, P47212). CGRP antibody detected a band at 14 kDa consistent with the signalling peptide (Uniprot, Q99JA0). The Western blots for alpha4, alpha6, alpha7, and beta1 integrin subunits and CD44 in trigeminal ganglion are shown in Supporting Information Figure 3.

The antibodies against microtubule-associated protein 2 (MAP2) and heavy neurofilament isoform (NF-H) were used as previously well-established cellular/subcellular markers. For the anti-MAP2 polyclonal antibody (http://www.millipore.com/catalogue/item/ab5622#), Western blotting with adult rat brain soluble extract detected a strong and specific band for the 280–300-kDa dimer, in our current study, appropriately diluted antibody also resulted in strong dendritic staining, in line with many previous publications (see, e.g., Sigurjonsson et al., 2005; Nateri et al., 2007). For the antineurofilament H (heavy, 200 kDa NFH) polyclonal antibody (http://www.millipore.com/catalogue/item/ab1991#), raised against the rat NFH fusion protein containing 37 lysine-serine-proline (KSP) domain repeats, the manufacturer's data sheet describes strong reactivity to this major neurofilament protein. Insofar as the middle neurofilament protein (160 kDa NFM) also contains a few lysine-serine-proline sequences, there is generally some NFM cross-reactivity, but not with the light 70-kD neurofilament, NFL (Harris et al., 1991). The NFL staining is generally restricted to neurofilaments in the white matter axons (see, e.g., Fig. 5J–L) as well as dendritic and perikaryal neurofilaments in the gray matter.

In the case of rat monoclonal antibodies raised against alpha4 (CD49d), alpha5 (CD49e), alpha6 (CD49f), and beta1 (CD29) integrins, previous studies have also detailed a massive up-regulation of encoding mRNA species following axotomy in the mouse facial motor nucleus, corresponding to a strong increase in the appropriate immunoreactivity (Kloss et al., 1999; Werner et al., 2000). All four monoclonal antibodies are well defined, with long-established functional characterization for alpha4 (Holzmann and Weissman, 1989), alpha5 (Uhlenkott et al., 1996), alpha6 (Hemler et al., 1988), and beta1 (von Ballestrem et al., 1996) integrin subunits. In the mouse, immunoreactivities for all four subunits were colocalized on blood vessel endothelia as well as on activated microglial cells (Hristova et al., 2009), but only the beta1 was also present in axotomized and regenerating motoneurons (Kloss et al., 1999; Raivich et al., 2004). This pattern of just vascular and microglial, and not neuronal (or sprout), immunoreactivity for alpha4, alpha5, and alpha6 immunoreactivity was also reproduced in the current study. The cranial motoneuron expression of the alpha7 and beta1 integrin subunits was also confirmed by Pinkstaff et al. (1999) for trigeminal, facial, and hypoglossal motoneurons.

Quantification of central axonal sprouting

Quantification of growth cones was performed on four sections per facial nucleus, with an interval of 200 μm between each section. Briefly, the sections were scanned in a TCS 4D confocal laser microscope (Leica, Nussloch, Germany) with a ×10 objective using Cy5 settings (ex wavelength 647 nm, LP665, pinhole 30). Fourteen consec-

utive, equidistant levels were recorded and condensed with the MaxIntense projection.

Small, strongly fluorescent growth cones were differentiated from the large neuronal cell bodies with the Sobel filter and a three-step Growth Cone Detection (GCD) algorithm in Optimas 6.2 software (Media Cybernetics, United Kingdom). In the first step, the mean value of the overall luminosity (MEANcor) and the standard deviation (SDcor) of the corrected images (normal image) was recorded. This procedure was repeated following Sobel filter treatment (MEANsob, SDsob, sobel image), which calculates the direction-independent local intensity gradient in a 3×3 pixel kernel. The threshold for neuropeptide-immunofluorescent growth cones in the Sobel image was set with the formula: Threshold = MEANsob + $11 \times$ SDcor. Areas at and above threshold were filtered with the Object Classes function using two additional criteria in the normal image: Area size $>$ 10 pixel and MEANarea –SDarea $>$ $1.4 \times$ MEANcor, with MEANarea being the mean intensity and SDarea the standard deviation for each individual area profile. The remaining areas matched with the profiles of the neuropeptide-immunofluorescent neuronal growth cones and served as a measure for their total area in the tissue section.

In addition, the number of sprouts in and around facial motor nucleus was visually counted by a blinded observer, with the identifying marking on the glass slide covered by an opaque adhesive sticker carrying a code. In this case, two sections per facial nucleus, 320 μm apart, were used to assess the number of sprouts per animal.

Immunohistochemistry for light and electron microscopy

Immunohistochemistry for light microscopy was performed by using the same procedure as for immunofluorescence up to the secondary antibody, followed by incubation with the ABC reagent (Vector), visualization with diaminobenzidine/H_2O_2 (DAB; Sigma, Deisenhofen, Germany), dehydration in alcohol and xylene, and then mounting with Depex (BDH, Poole, United Kingdom). For electron microscopy, 80-μm-thick vibratome sections cut at the facial nucleus level were stained for alpha7 integrin subunit, galanin, or VAChT with a slightly modified protocol (Werner et al., 2000). The vibratome sections were floated; treatment with acetone was omitted; preincubation with goat serum (or donkey serum in case of VAChT) was extended to 4 hours at RT; the rabbit anti-mouse alpha7 antibody was applied at a concentration of 1:500, galanin antibody at 1:400, or VAChT antibody at 1.1,000, overnight; the biotinylated goat anti-rabbít or donkey anti-goat secondary antibody (Vector, Jackson) was applied for 8 hours (4°C); and the incubation with the ABC reagent was performed overnight (4°C).

For the DAB staining, vibratome sections were first preincubated in DAB (without H_2O_2) for 20 minutes, followed by a 15-minute DAB/H_2O_2 reaction at RT, with Co/Ni enhancement (see above). The sections were then fixed for 7 days in 2% glutaraldehyde in PBS, osmicated, dehydrated, and embedded in araldite (Fluka, Basel, Switzerland). Semithin sections were counterstained with toluidine blue for light microscopy, and ultrathin 100-nm sections were counterstained with uranyl acetate and lead citrate and examined in a Zeiss EM 10 and EM 109 electron microscope.

Quantification of light microscopic immunohistochemistry

A Sony AVT-Horn 3CCD color video camera was used to obtain eight-bit digital images based on a 0–255 (eight-bit) scale of optical luminosity values. Images of both control and axotomized nuclei and for the glass were captured at $\times$10 magnification on a light microscope with 0.06 Neutralfilter. Captured images were run through an algorithm to obtain mean and SD values for optical luminosity. SD was subtracted from the mean for each image (mean-SD algorithm), and the resulting values for axotomized and control sides were each subtracted from the mean optical luminosity values of the glass as described previously (Möller et al., 1996).

Statistical analysis

Statistical analysis for growth cone areas in two group comparisons was performed by using a standard, two-tailed Student's *t*-test or with ANOVA followed by post hoc Tukey in cases of more than two groups.

RESULTS

Facial axotomy causes delayed central axonal sprouting: distribution and orientation

In view of previous reports of neuropeptide-immunoreactive sprout-like structures in the axotomized facial motor nucleus 2 weeks after facial nerve cut (Galiano et al., 2001; Werner et al., 2001; Makwana et al., 2007), our first aim was to provide a detailed mapping of their neuroanatomical distribution. As shown in Figure 1A, facial axotomy after nerve transection at the styloid foramen was associated with the appearance of sprout-like, galanin-immunoreactive (galanin$^+$) neurites inside the brainstem in and around the lesioned facial motor nucleus. A high number of galanin$^+$ sprouts with a 4–10-μm large terminal bulb was observed in the white matter surrounding the lesioned facial motor nucleus, in the ventral corticobasal tract, in the ascending as well as descending part of the intracerebral portion of the facial motor nerve (Fig. 1A,F),

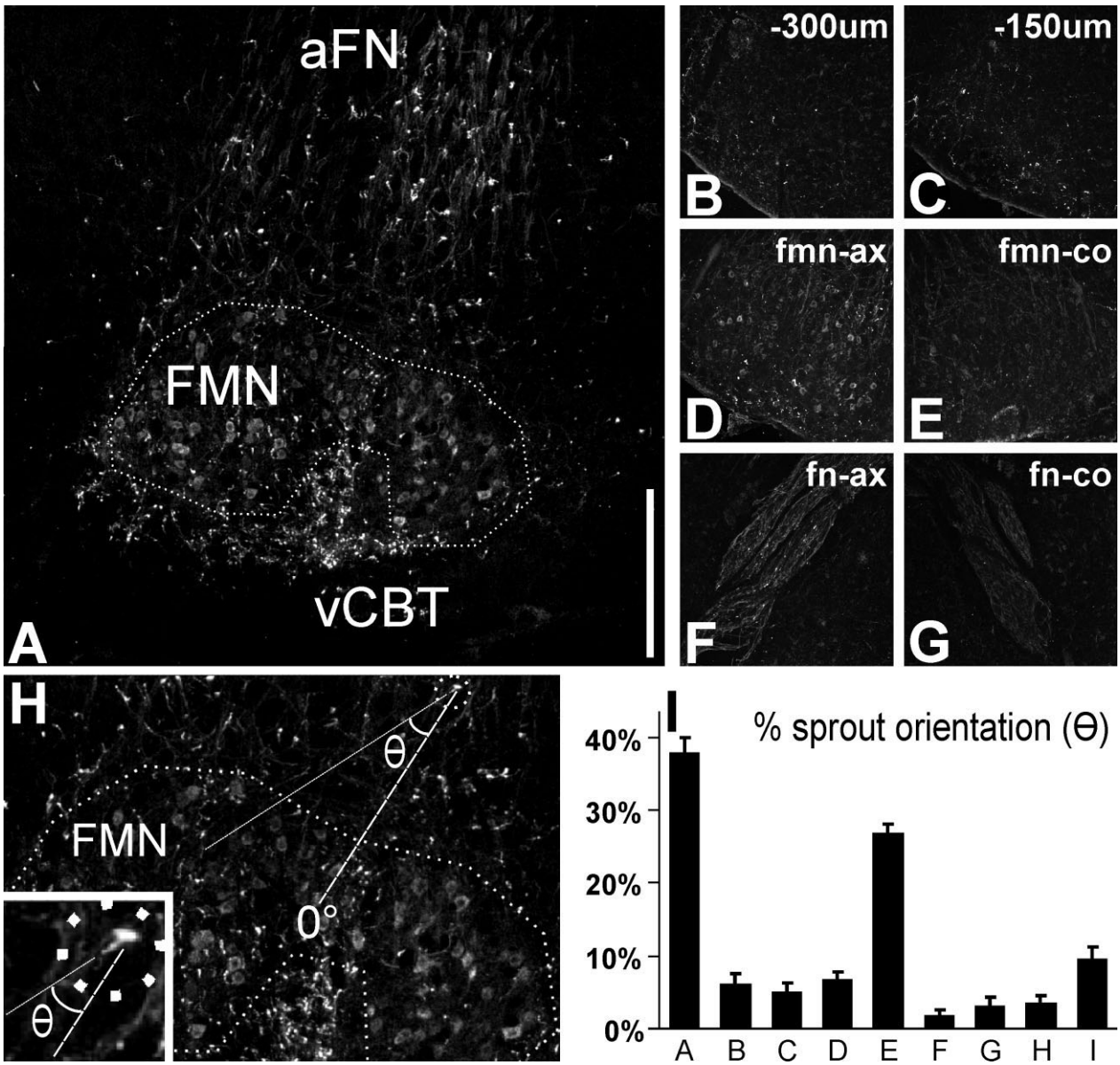

Figure 1. Distribution of galanin-immunoreactive sprouts in and around the facial motor nucleus (FMN), 14 days following facial nerve cut. **A:** Composite of the facial nucleus and surrounding areas; the nucleus outline is indicated by the dotted line. Note the numerous immunoreactive sprouts in the white matter surrounding the lesioned facial motor nucleus, particularly in the ventral corticobasal tract (vCBT) but also in the ascending part of the intracerebral portion of the facial nerve (aFN), and to the medial and lateral of the facial nucleus. **B–G:** Sprout distribution in the rostral direction, from the same ventrolateral brainstem position but 300 μm (B) and 150 μm (C) caudal to the axotomized facial nucleus, the axotomized nucleus (D), and the descending part of the intracerebral facial nerve (F). Note the paucity of strongly stained neurites in the contralateral, uninjured facial nucleus (E) and nerve (G). **H:** The orientation of central sprouts was determined by drawing two lines, one from the center of the terminal bulb to that of the nucleus (dashed line, 0°) and the second from the bulb center to that of the farthest visible part of the stalk and extending it farther into the image (dotted line) and then measuring the angle between the two lines as shown in H. The **inset** in H shows the terminal bulb, the attached stalk, and the orientation of the two lines at higher magnification. **I:** Distribution of the orientation angles for the galanin-immunoreactive sprouts outside the axotomized facial motor nucleus with respect to the nucleus. Percentage of the total number of sprouts, with orientation angles of 0–20°(A), 20–40°(B), 40–60°(C), etc., with 0° pointing directly away from and 180° pointing directly toward the nucleus. Mean ± SEM, n = 4 mice. Note that the most common orientation is the one facing away (A), with the second largest running approximately parallel to the facial nucleus (E). Scale bar = 0.5 mm in A; 0.8 mm for B–G; 0.36 mm for H; 0.1 mm for inset.

and in the medial and lateral parts of the facial nucleus. Some neurites were located as far as 0.5–1.0 mm away from the border of the facial nucleus in the dorsal (Fig. 1A), and 0.3 mm in the caudal (Fig. 1B,C) direction, with the stalk attached to a bulb, usually pointing away from the nucleus (Fig. 1H,I).

Sprouting neurites were also present inside the facial motor nucleus itself, but they were less dense in the horseshoe form of the facial nucleus gray matter, containing the axotomized motoneurons, than in its white matter-like ventral cleavage (Fig. 1H). A similar distribution was also observed for the CGRP$^+$ sprouts, but their density was considerably lower compared with that of the galanin$^+$ fibers. Although individual galanin$^+$ and CGRP$^+$ neurites were observed in the contralateral facial nucleus (Figs. 1E, 2H), these neurites lacked the typical appearance of sprouts with the engorged terminal bulb. These sprouts were also absent in the intracerebral part of the contralateral nerve (Fig. 1G); the ipsi-and contralateral pyramidal tract (Fig. 2H); the dense neurite network in the dorsal part of the spinal nucleus of the trigeminal nerve (Fig. 2G); or in other brainstem, cerebellar, or cortical white matterstructures (not shown). CGRP and galanin immunoreactivities were also present in adjacent axotomized motoneurons, each labeling approximately 40–45% of the total facial motoneuron pool (Moore, 1989; Raivich et al., 1995), but the intensity of the cell body labeling was weaker than that observed in the sprouts.

To explore the overall orientation of these central sprouts, we next examined the orientation angle of galanin$^+$ sprouts outside the facial nucleus on brainstem sections containing the axotomized nucleus. The orientation was determined as the angle between the line from the facial nucleus center to the center of the axonal bulb and a second line from the bulb center to the farthest visible part of the attached axonal stalk, as shown in Figure 2H and H, inset. The angles were determined at $\times$10 magnification, using confocal images from brainstems of four control C57Bl/6 mice, 14 days after facial nerve cut, and for each animal subgrouped into one of the nine categories A–I, from 0 ° to 20 ° (pointing outward, A), to 160–180° (pointing to the center of the facial nucleus, I). Angles greater than 180° (second line to the left of the central line, instead of to the right), were entered by subtracting 180°, i.e., 265° was entered as 95°. As shown in Figure 1, sprout angle distribution was very nonuniform, with the frequency in three groups (A, E, and I) rising above that in the directly adjacent groups. In total, these three groups were responsible for approximately 70% of the sprouts. The A group with sprouts facing away from the nucleus was the largest (39% $\pm$ 3%, mean $\pm$ SEM), followed by groups E, which contained sprouts oriented approximately parallel to the nucleus (24% $\pm$ 1%), and I, with the sprouts directly or almost directly facing toward the nucleus (8.5% $\pm$ 2.2%). The number of sprouts in the adjacent and intermediate categories was underrepresented. Although the number of sprouts in B was slightly higher (8.7% $\pm$ 0.6%) than in I, these two groups were not adjacent. In comparisons with the directly adjacent groups (A vs. B, E vs. D or F, and I vs. G) the frequency in A, E, and I was each time both significantly and very clearly higher ($P < 5\%$, one-way ANOVA followed by post hoc Tukey test). Although the numbers were considerably lower, the frequencies in the two segments directly adjacent to each of the three peaks, A, E and I, again showed similar proportions of approximately 3:2:1 for the outward pointing (B,C, 15.2%), to roughly perpendicular (D,F, 8.3%), to inward pointing (G,H, 4.5%) groups.

Motoneuron origin of central axonal sprouts

To determine whether the bulb-carrying neurites originated from the lesioned motoneurons, axotomized neurons were retrogradely labeled with a 1% solution of the dual, anterograde and retrograde, tracer Mini-Ruby (Fig. 2A). As shown in the composite of the ventral brainstem in Figure 2H, application of the tracer on the proximal nerve stump surface immediately after facial nerve cut led to a highly selective labeling of neuronal cell bodies and their proximal branches in the ipsilateral facial motor nucleus.

Double labeling with galanin immunoreactivity demonstrated clear Mini-Ruby fluorescence inside a fraction of galanin$^+$ sprouts around the axotomized facial motor nucleus (Fig. 2B,H, insets). Similar double labeling was also present inside the intracerebral part of the ipsilateral facial nerve (Fig. 2F, insets). Finally, this colocalization was also observed with the CGRP$^+$ sprouts (Fig. 2C). Compared with the neuropeptide immunoreactivity, Mini-Ruby fluorescence was more concentrated to the central parts of the axonal bulb, with weaker and more fragmented labeling of the neighboring axonal stalk.

Quantification of the double-labeled sprouts directly outside the facial motor nucleus, shown in Table 2, demonstrated clear Mini-Ruby fluorescence in 19% $\pm$ 3% of the galanin$^+$ and 42% $\pm$ 9% of the CGRP$^+$ sprouts and, in addition, 39% + 1% of the VAChT$^+$ sprouts in adjacent, galanin-, CGRP-, and VAChT antibody-stained brainstem sections ($P < 5\%$ ANOVA followed by Tukey post hoc test, for differences vs. the galanin$^+$ sprouts; n = 4 C57Bl/6 mice, three sections per animal). In the reverse experiment, quantification of the neuropeptide immunoreactivity showed that 64% $\pm$ 3% of the identified, Mini-Ruby fluorescent sprouts also exhibited galanin, 44% $\pm$ 10% CGRP, and 44% $\pm$ 2% VAChT immunoreactivity (not significant). This double labeling, Mini-Ruby/CGRP, Mini-Ruby/VAChT, or Mini-Ruby/galanin, was not observed outside the main areas of central axonal sprouts. Thus the ipsilateral spinal nuclei of the trigeminal nerve (Fig. 2G), contralateral facial nerve (Fig. 2F), or contralateral facial nucleus (Fig. 2H, right side) were all devoid of axonal Mini-Ruby fluorescence.

However, in addition to sprouts, Min-Ruby fluorescence was also occasionally present in large and ellipsoid

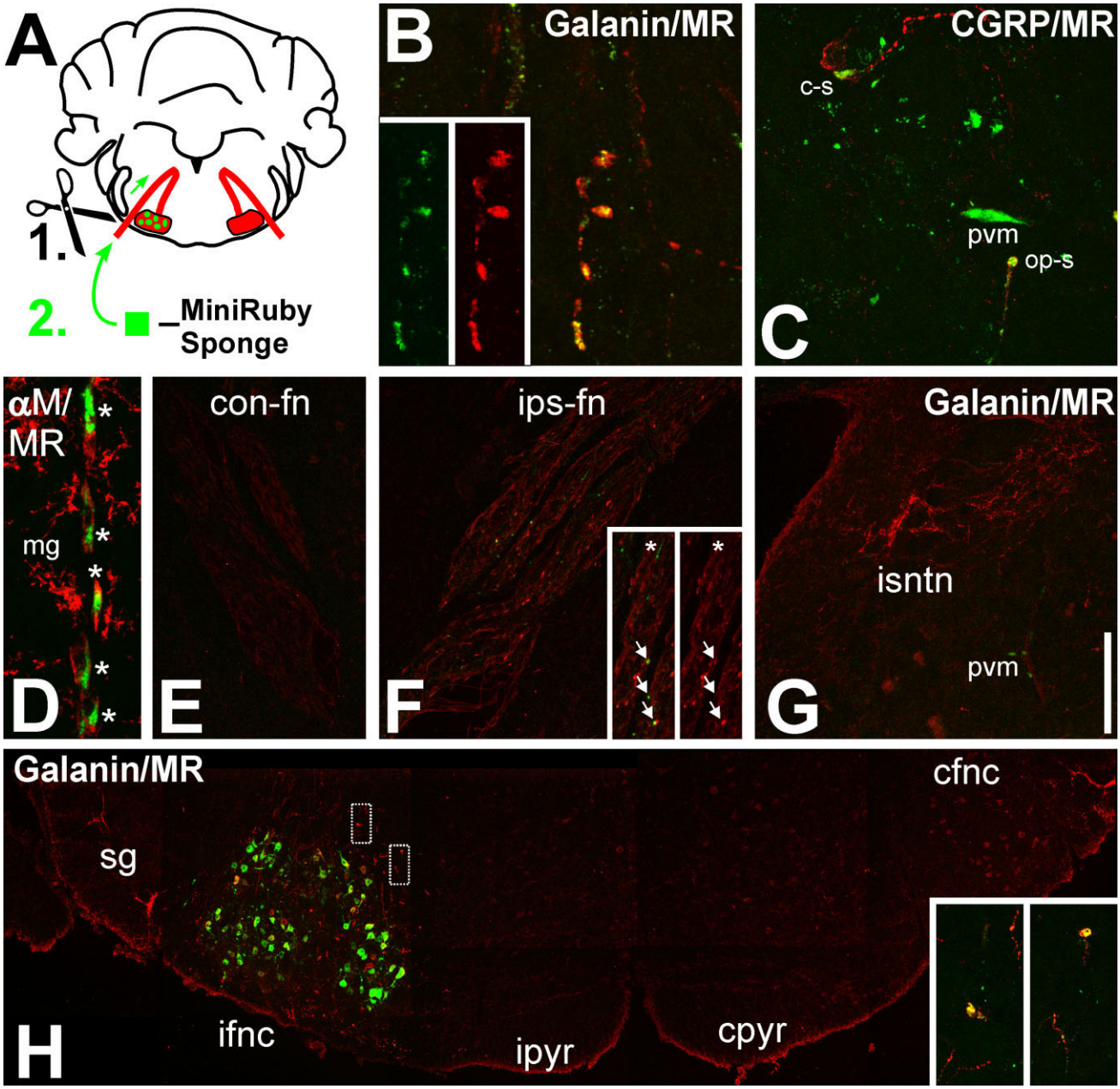

Figure 2. Demonstration of central axonal sprout origin using Mini-Ruby, a dual anterograde/retrograde tracer. **A:** Schematic summary. A gelfoam sponge soaked in 1% Mini-Ruby solution was applied onto the fresh, proximal cut end of the facial nerve, followed by retrograde transport to axotomized motoneurons and a 14-day survival. **B,C:** High magnification of Mini-Ruby (green) colocalization with the immunoreactivity (IR) for the neuropeptides galanin (B) and CGRP (C) (red) in axonal sprouts just outside the axotomized facial motor nucleus. The double-labeled sprout in B and the bottom sprout in C are outward pointing (op-s); the top sprout in C is oriented in parallel to the center of the nucleus ("cruising," c-s). The **insets** in B show the individual red and green fluorescence channels. In C, Mini-Ruby is also incorporated by perivascular macrophages (pvm). **D:** Mini-Ruby uptake in a string of alphaMbeta2 integrin (aM)-positive (red) perivascular macrophages (*) lining a cerebral blood vessel. The neighboring aM-positive and ramified microglia (mg) are devoid of Mini-Ruby. **E–G:** Double fluorescence for Mini-Ruby and galanin-IR in the descending intracerebral part of the contralateral facial nerve (E); the axotomized, ipsilateral facial nerve (F); and the ipsilateral spinal nucleus of trigeminal nerve (G, isntn). The **insets** in F show a higher magnification of the facial nerve (left, red and green; right, red only fluorescence). Note the double-labeled sprouts in the axotomized nerve (arrows) and their absence in the neighboring trigeminal nerve nucleus and contralateral nerve. The asterisk points to a Mini-Ruby^{+} but galanin^{-} sprout. As in C, Mini-Ruby is frequently present in the populations of perivascular macrophages associated with larger blood vessels (D, pvm). The micrographs in E and F show the same galanin labeling motif as in Figure 1E,F but combine it with the Mini-Ruby fluorescence. **H:** Composite of Mini-Ruby and galanin-IR fluorescence in the ventral brainstem across the ipsilateral substantia gelatinosa, the ipsilateral and contralateral facial motor nuclei (ifnc, left; cfnc, right, respectively), and the ipsilateral and contralateral pyramidal tracts (ipyr and cpyr). Mini-Ruby neuronal cell body labeling is strictly limited to the axotomized facial motor nucleus, with a high density of galanin-positive sprouts in the surrounding tissue. Note the absence of both in the pyramidal tracts and the contralateral facial nucleus. The **insets** show higher magnifications for galanin/Mini-Ruby double labeling (yellow) of two sprouts just dorsal of the axotomized facial nucleus; their positions in the composite are indicated by the rectangles in H. A magenta/green version of Figure 2 is available as Supporting Information Figure 1. Scale bar = 10 μm in B, 45 μm in C and D, 270 μm in E–G; 350 μm in F insets.

TABLE 2.
Colocalization of Mini-Ruby (MR) With Galanin and CGRP-Positive Growth Cones (n = 4 Animals, Three Facial Nucleus Sections per Animal; Mean ± SEM)

Growth cone neurochemical marker (NCM)	MR^+NCM^+/NCM^+ (%)	MR^+NCM^+/MR^+ (%)
Galanin	19 ± 3	64 ± 3
CGRP	42 ± 9[1]	44 ± 10
VAChT	39 ± 1[1]	44 ± 2

[1] $P < 5\%$, one-way ANOVA, followed by Tukey post hoc test for differences in the frequency to $MR^+/galanin^+$ growth cones. The percentages are derived from, on average, approximately 50-60 double-labelled growth cones per animal and axotomized facial motor nucleus.

perivascular macrophages (Fig. 2C,G). As shown in Figure 2D, this Mini-Ruby labeling colocalized with the alphaM-beta2 immunoreactivity in the perivascular macrophages and was easy to differentiate from the smaller Mini-Ruby-fluorescent axonal bulbs inside the neural parenchyma. The alphaMbeta2$^+$ parenchymal microglia were uniformly Mini-Ruby$^-$.

Time course after injury and effects of reinnervation and recut

Comparison of the galanin-and CGRP-immunostained, axotomized facial motor nuclei 1–42 days after facial nerve cut with unoperated controls (day 0) revealed a transient sprouting pattern, shown in Figure 3A–AF. No sprouts were observed in the unoperated facial nuclei or 1–4 days after nerve cut. A moderate number of galanin$^+$ and CGRP$^+$ sprouting neurites was observed at day 7; these became much more common at day 14, decreased in number at day 21, and disappeared by 42 days after nerve injury and the ensuing regeneration (Fig. 3A–F,AG,AI).

As shown in Figure 3AH, automatic quantification of the intensely neuropeptide-immunofluorescent end-bulbs in and around the facial motor nucleus using confocal scanning and the GCD algorithm (see Materials and Methods) reproduced this time course for galanin, with a peak density at day 14, with 5,200 parts per million (ppm) or 0.52% of the total area of the 1 mm × 1 mm region with the facial nucleus at its center covered with galanin$^+$ end-bulb structures. However, the GCD algortihm was associated with a low-level "noise" of 200–600 ppm on the contralateral side throughout the time course, or approximately 4–12% of the peak signal levels at day 14.

Direct visual counting of the CGRP$^+$ growth cones (Fig. 3AI) showed a time course with a shape similar to that with galanin (Fig. 3AG). Maximal levels were observed at day 14, with 24 ± 5 CGRP$^+$ sprouts per 20-μm section, approximately 3–4-fold less than with galanin in the directly adjacent sections (89 ± 8). Unlike the case with galanin, quantification of the CGRP$^+$ end-bulbs with the GCD algorithm revealed a comparatively broader and statistically significant elevation of detected structures on days 4–21 compared with the contralateral side (Fig. 3AJI). However, the overall levels (200–260 ppm) were much lower, and the more granular (Nissl-shoal) appearance of the CGRP immunoreactivity in neuronal cell bodies could have made automatic growth cone detection more complicated. For this reason, both quantitation methods, visual counting and GCD algorithm, were used side by side in the following experiments.

Because the time course of sprouting, with a peak at day 14, occurred at roughly the same time as the morphological reinnervation and functional recovery in the facial axotomy model (Gilad et al., 1996; Werner et al., 2000; Raivich et al., 2004), we next sought to determine whether the appearance of sprouts is due to target reinnervation. Reinnervation is known to occur earlier, more promptly, and with less error after crush than after cut (Nguyen et al., 2002; Witzel et al., 2005), so we first examined the differential effects of the facial nerve crush vs. cut on galanin$^+$ growth cone profiles at days 7, 10, and 14. Here, facial nerve crush induced the appearance of galanin$^+$ spouts that peaked at day 10, with 800 ppm of the total area (Fig. 4A). Compared with crush, nerve transection produced a more robust sprouting response, with a slight but not significant increase at days 7 and 10 and an almost 10-fold increase at day 14 ($P < 5\%$, Student's *t*-test). As shown in Figure 4A,C, automatic quantification with the GCD algorithm (Fig. 4A) and visual counting (Fig. 4C) revealed very similar changes in the timing of sprouting changes and

Figure 3. **A–AJ:** Time course of the appearance (A–AF) and quantification (AG–AJ) of galanin- and CGRP-immunoreactive sprouts in the facial motor nucleus, 1–42 days after facial nerve axotomy; day 0 are uninjured controls. A–AF show the immunofluorescence in injured facial nucleus at low magnification (A,E,I,M,Q,U,Y,AC for galanin, and C,G,K,O,S,W,AA,AE for CGRP) and at ×4 or ×8 higher magnification for galanin (B,F,J,N,R,V,Z,AD) and CGRP (D,H,L,P,T,X,AB,AF). Note the massive increase in the neuropeptide-labeled sprouts (arrows) at days 7–21; arrowheads point to neighboring motoneuron cell bodies. AG–AJ: The graphs at right show the total number of galanin-and CGRP-immunoreactive sprouts per section (AG and AI, respectively) and the quantification of the area taken by the galanin-and CGRP-immunoreactive sprouts (AH, AJ) in parts per million (ppm). Mean ± SEM, n = 3 animals per group in AG and AI, n = 4 in AH and AJ). *$P < 0.05$, Student's *t*-test compared with the unoperated, contralateral side. In the case of galanin, both parameters, number (AG) and area (AH), show a sharp peak at day 14. The same also holds true for the CGRP$^+$ sprout number (AI), but the CGRP$^+$ area recognized by the Optimas GCD algorithm (AJ) shows a broader, elevated plateau between day 4 and day 21. Scale bar = 250 μm in first and third columns; 0.063 μm in the second column; 0.032 μm in fourth column.

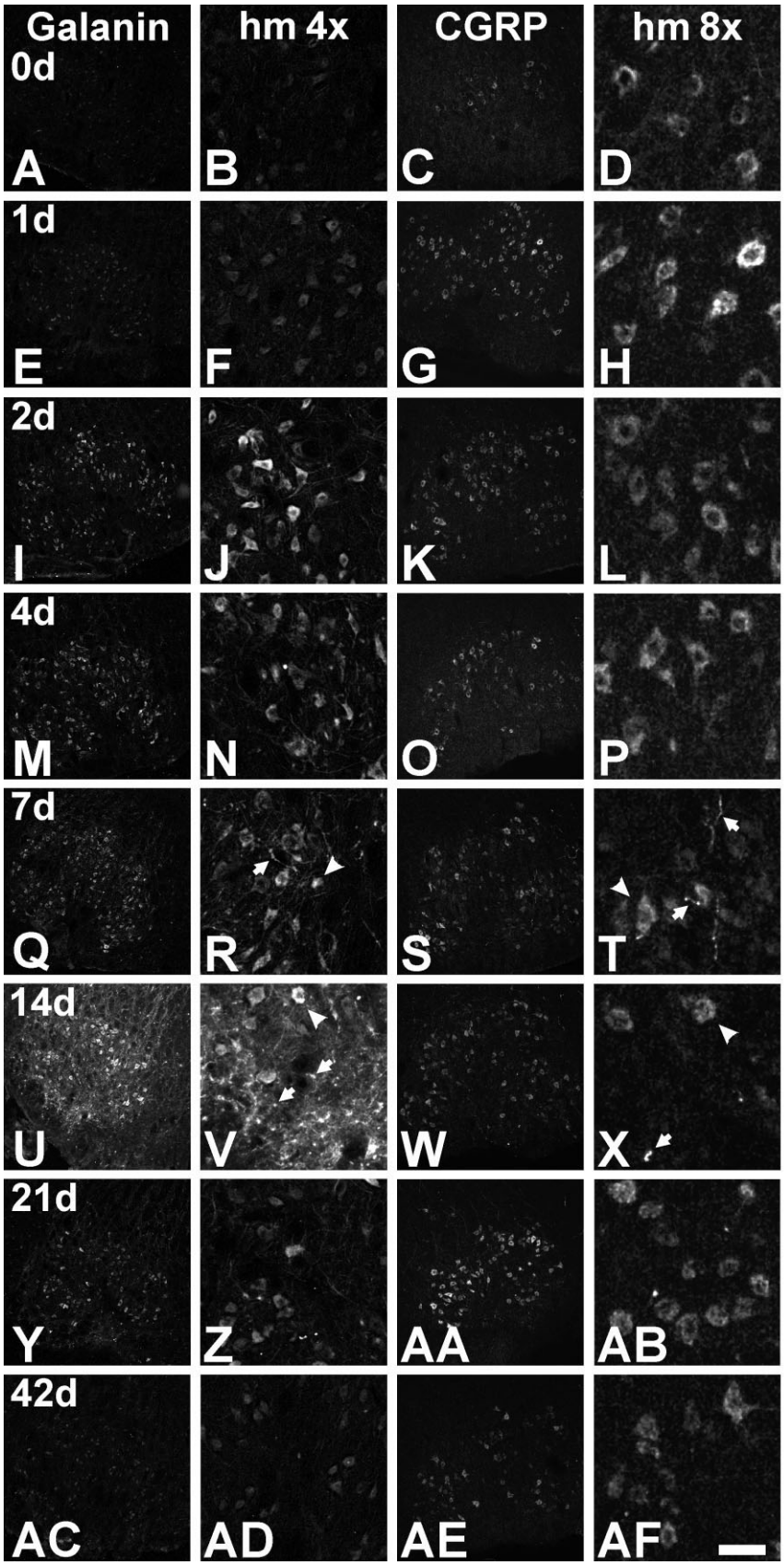
Galanin
hm 4x
CGRP
hm 8x
0d
A
B
C
D
1d
E
F
G
H
2d
I
J
K
L
4d
M
N
O
P
7d
Q
R
S
T
14d
U
V
W
X
21d
Y
Z
AA
AB
42d
AC
AD
AE
AF

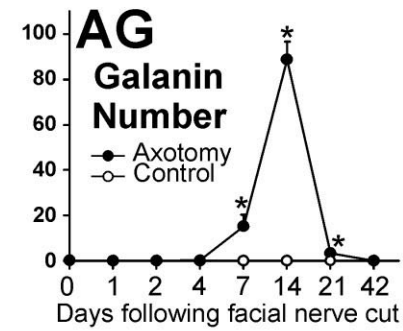
AG
Galanin
Number
Axotomy
Control
100
80
60
40
20
0
0 1 2 4 7 14 21 42
Days following facial nerve cut

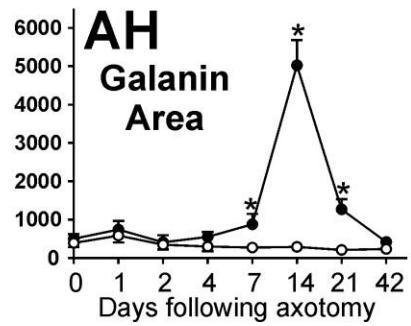
AH
Galanin
Area
6000
5000
4000
3000
2000
1000
0
0 1 2 4 7 14 21 42
Days following axotomy

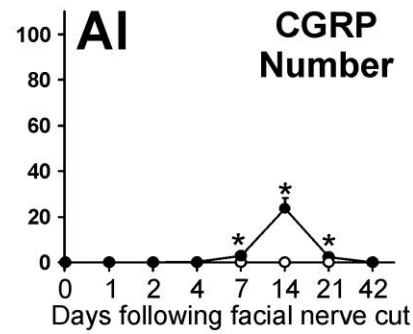
AI
CGRP
Number
100
80
60
40
20
0
0 1 2 4 7 14 21 42
Days following facial nerve cut

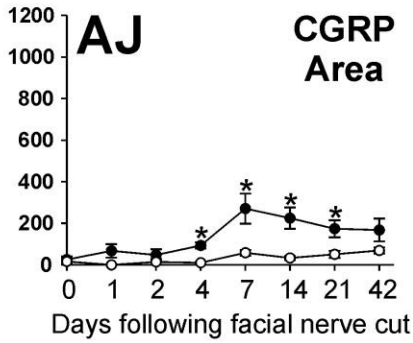
AJ
CGRP
Area
1200
1000
800
600
400
200
0
0 1 2 4 7 14 21 42
Days following facial nerve cut

Figure 3

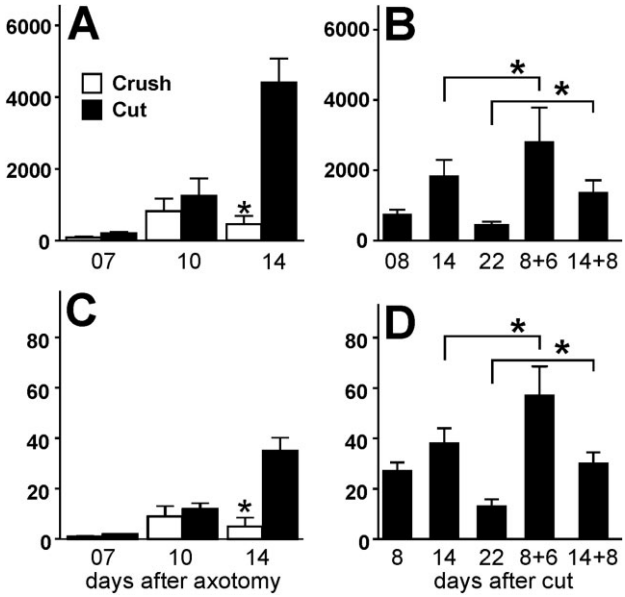

Figure 4. A–D: Central axonal sprouting depends on the mode of injury. A,C: After facial nerve crush, the sprout area in ppm (A) and the number of sprouts per section (C) reach a moderate peak at day 10 and after cut a much higher peak at day 14. *$P < 0.05$, Student's *t*-test for crush vs. cut (n = 3 animals per group, mean ± SEM). B,D: Additional injury exacerbates central axonal sprouting following facial nerve cut—both in total area (B) and in the number of sprouts (D)—compared with the same total cut period (8 + 6 vs. 14 days, 14 + 8 vs. 22 days). *$P < 0.05$, one-way ANOVA and post-hoc Tukey, n = 4–5 animals per group.

differences in the response to crush vs. cut response, confirming the cross-validity of both techniques for the galanin$^+$ sprouts.

To determine further whether the appearance of growth cones was due to the onset in reinnervation of peripheral targets occurring 8–14 days after injury, we next examined the effects of single facial nerve cut vs. a second transection. The facial nerve was recut 1 mm below the initial lesion (n = 5 animals per group) on day 8 with survival to day 14 or was recut on day 14 with survival to day 22 and compared with normal animals 8, 14, and 22 days after facial nerve cut, which served as controls (Fig. 4B,D). Surprisingly, the growth cones were not abrogated; in fact, the area under growth cone profiles was 1.5–2-fold greater than in control day 14 or day 22 postcut brainstems ($P <$ 2%, ANOVA). As in Figure 4A,C, very similar quantitative effects were observed with the GCD algorithm (Fig. 4B) and visual counting (Fig. 4D).

Preliminary studies with shorter recut times (1, 2, and 4 days) and total transection time of 14 days revealed that the growth cone profiles were more numerous than after a simple day 14 cut, but the effects were less pronounced than in 8 + 6 vs. 14, or 14 + 8 vs. 22 (data not shown). Finally, retrograde tracing experiments with application of MiniRuby to the ipsilateral whiskerpad, the principal peripheral target of the facial nerve maxillary and zygomatic branches on day 12, showed some motoneuron cell body labeling but failed to be incorporated into the facial growth cones at day 14 (data not shown), unlike the Mini-Ruby labeling applied on the freshly cut facial nerve stump, shown in Figure 2B,C,E and the inset in Figure 2H.

Molecular markers and ultrastructure

To define the molecular markers of axotomy-induced sprouts, we next examined the presence of VAChT, microtubule-associated protein 2 (MAP2), synaptophysin, and NFH as cholinergic, dendrite, presynaptic, and panneurite markers, respectively (Fig. 5, three left columns) as well as the CD44 hyaluronic acid receptor and the alpha4, alpha5, alpha6, alpha 7, and beta1 subunits of the beta1 integrin family (Fig. 5, three right columns), using double immunofluorescence with galanin, CGRP, or VAChT (Fig. 5G–I,S–Y). Markers labeled with rabbit polyclonal antibodies (MAP2, NFH, alpha7) were double stained with guinea pig antibodies against VAChT, and those labeled with rat monoclonal antibodies (alpha4–6, beta1, CD44) were double stained with galanin or CGRP.

The CGRP$^+$ (Fig. 5A–C) and galanin$^+$ (Fig. 5D–F) sprouts colocalized with VAChT immunoreactivity, confirming their cholinergic phenotype. They were also positive for CD44 (Fig. 5V–Y) and beta1 (Fig. 5S–U) but not for alpha4, alpha5 or alpha6 (not shown). Most VAChT sprouts were also positive for synaptophysin (Fig. 5P–R), and many were alpha7$^+$, even though some large and distended alpha7$^+$ sprout end-bulbs were VAChT$^-$ (Fig. 5G–I). VAChT$^+$ sprouts did not colocalize with NFH (Fig. 5G–I) or MAP2 (Fig. 5M–O) immunoreactivity, suggesting that most sprouts are derived from cholinergic neurons, that they do not colocalize with typical components of dendritic (McDermid et al., 2004) or axonal shaft cytoskeleton, and that they express regeneration-associated CD44 and alpha7beta1 integrin cell adhesion molecules (Werner et al., 2000; Raivich et al., 2004). Similarly pronounced, regeneration-associated immunoreactivity was also observed on the Mini-Ruby-labeled axonal sprouts, shown in Figure 5Z–AB for the alpha7, in Figure 5AC–AE for beta1, in Figure 5AF–AH for CD44, and in Figure 5AI–AK for VAChT, reconfirming the facial motoneuron origin of these neurochemically tagged structures.

Many alpha7$^+$, galanin$^+$, and VAChT$^+$ sprout end-bulbs were particularly pronounced in the basal white matter located ventrally of the axotomized facial motor nuclei, so we next explored their utrastructural morphology by transmission electron microscopy (EM), 14 days after facial nerve cut (Fig. 6A,B). Starting with alpha7, immunolabeling against the intracellular part of the alpha7 integrin subunit revealed strong cytoplasmic staining surrounding numer-

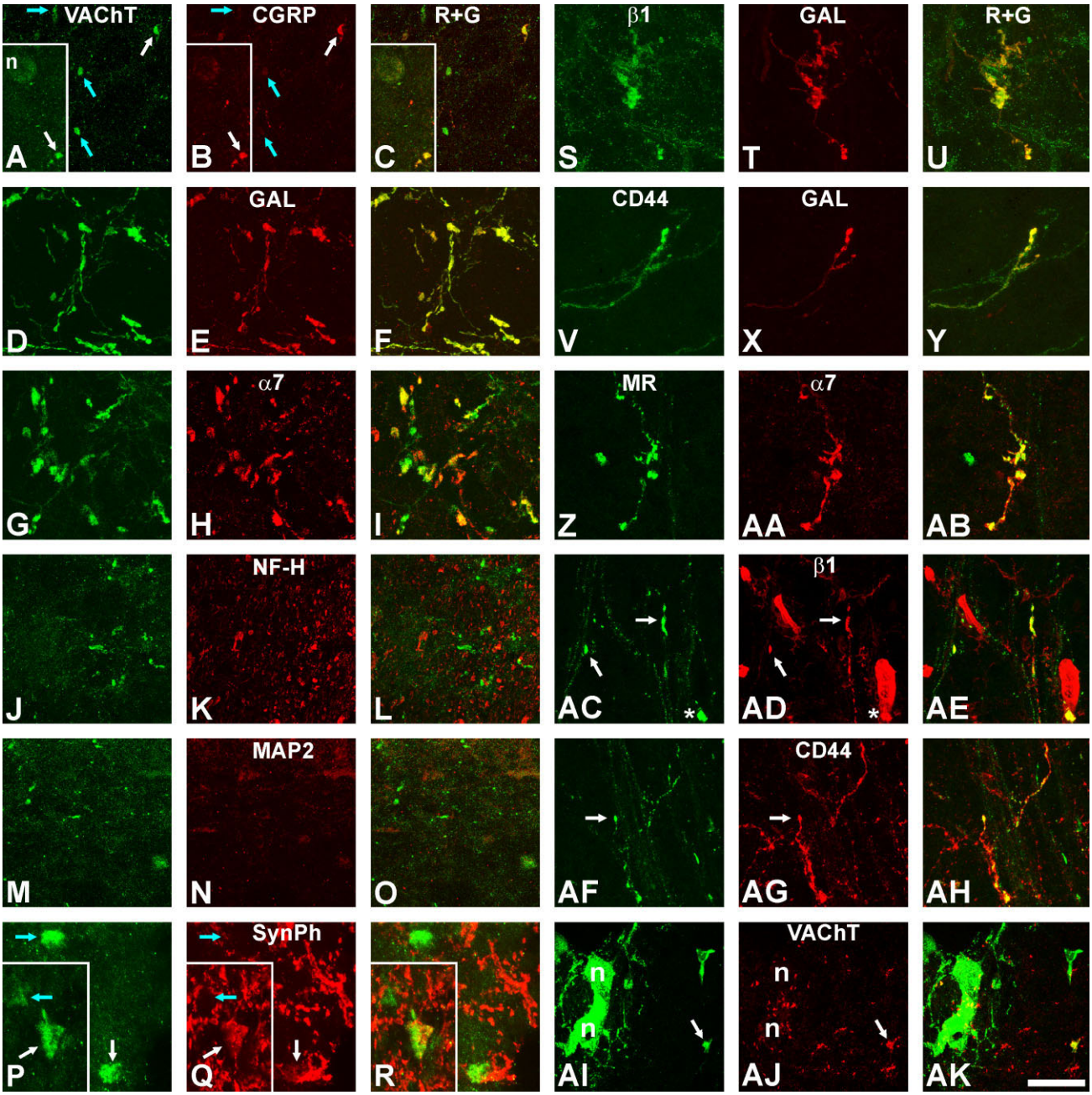

Figure 5. Molecular characterization of growth cones in the facial nucleus 14 days following facial nerve cut. **A–R:** Immunoreactivity for vesicular acetylcholine transporter (VAChT), double labeling with CGRP (A–C), galanin (D–F), alpha7 integrin subunit (G–I), neurofilament heavy (NFH) isoform (J–L), microtubule-associated protein-2/MAP2 (M–O), and synaptophysin/SynPh (P–R) immunoreactivities. VAChT$^+$ sprouts were very frequently positive for galanin, frequently also for alpha 7 and synaptophysin, and more rarely for CGRP immunoreactivity (white arrows in A–C, blue arrows mark single-labeled VAChT$^+$ sprouts). Note the absence of double labeling for NFH and MAP2. A–C and P–R are inside the facial motor nucleus, D–L in the adjacent ventral white matter, and M–O at the gray/white matter interface. A–C and P–R are composite micrographs, to illustrate the colocalization of some but not all VAChT$^+$ sprouts with CGRP and synaptophysin. **S–Y:** Colocalization of galanin-positive sprouts with the beta1 integrin subunit (S–U) and with CD44 (V–Y). **Z–AK:** Colocalization of Mini-Ruby-labeled growth cones with the alpha7 (Z–AB) and beta 1 (AC–AE) integrin subunits, CD44 (AF–AH), and VAChT (AI–AK). White arrows point to double-labeled sprouts in AC,AD, in AF,AG, and in AI,AJ). Asterisks in AC and AD label a Mini-Ruby$^+$, perivascular macrophage. Micrographs in AI–AK are from the border region between facial nucleus (left) and medial white matter and also show two adjacent, Mini-Ruby-labeled motoneurons (n) at left, surrounded by large, VAChT$^+$ synapses. Z–AH are inside the dorsal white matter, next to the facial nucleus. A magenta/green version of Figure 5 is available as Supporting Information Figure 2. Scale bar = 50 μm for A–C,J–L; 27 μm for Z–AB,AI–AK; 12.5 μm for P–R; 40 μm in all other micrographs.

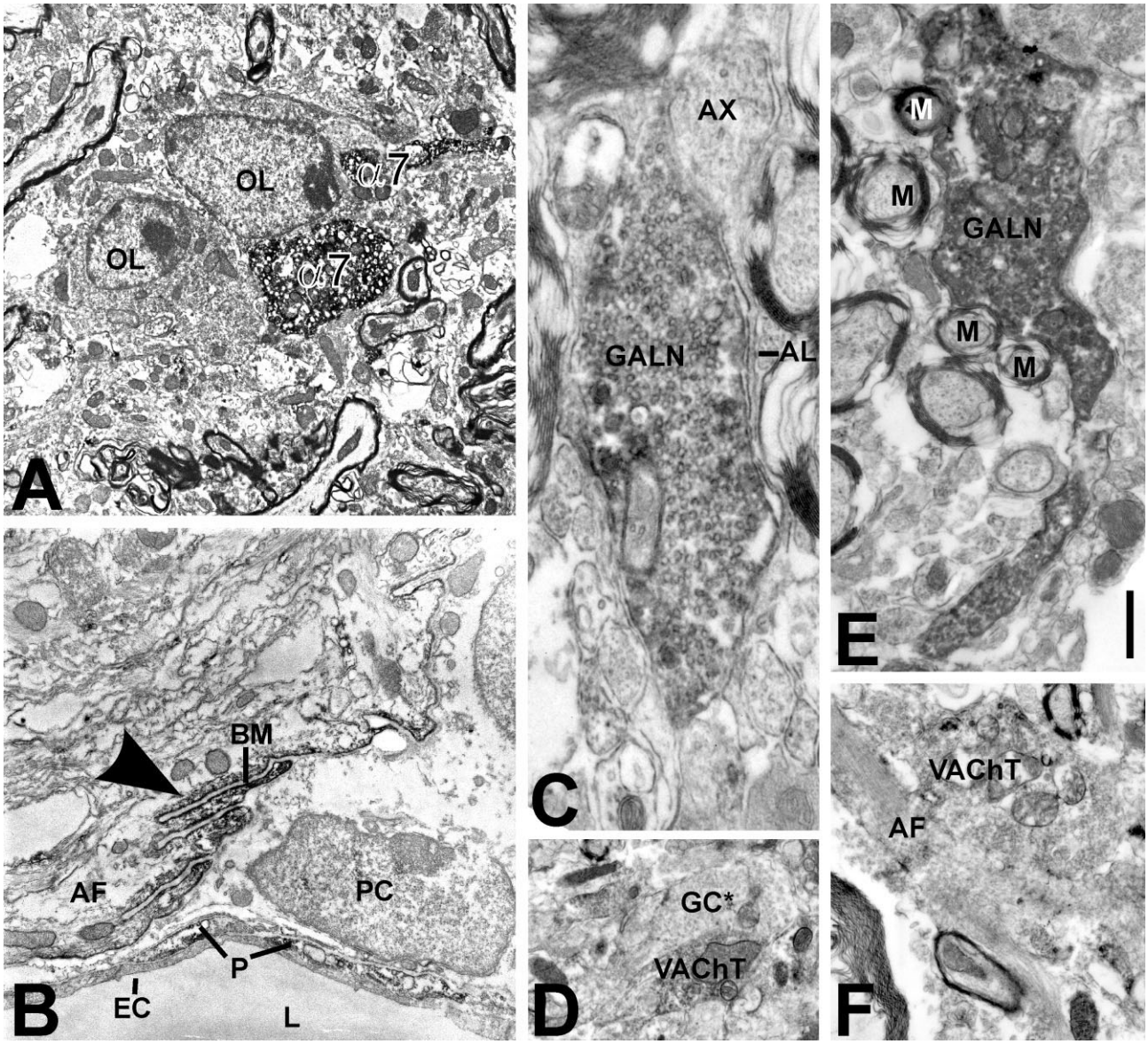

Figure 6. Ultrastructure of axonal growth cones and their cellular contacts using alpha7 (A,B), galanin (C,E), and VAChT (D,F) immunoreactivity in the white matter surrounding the facial motor nucleus, 14 days following facial nerve cut in WT animals. **A:** Intensely cytoplasmically stained axonal growth cones (alpha7), containing numerous (unstained) mitochondria and synaptic vesicles and contacting adjacent oligodendrocytes (OL). **B:** Strong alpha7 immunoreactivity in submembranous astrocyte cytoplasm (arrowhead) next to the finger-like protrusions of the basal membrane (BM). Some alpha7 immunoreactivity was also present in blood vessel pericytes (P). L, blood vessel lumen; EC, endothelial cell; PC, perivascular cell; AF, astrocyte fibrils. **C,E:** Galanin (GALN)-immunoreactive growth cones, here contacting astrocyte lamella (AL; C), unmyelinated axons (AX; C), and numerous myelinated axons (E). **D,F:** VAChT-immunoreactive axonal sprouts growing alongside a VAChT-negative (GC*) growth cone (D) and an astrocyte fibril (AF)-containing process (F). Scale bar = 1 μm for A,B,F; 0.35 μm for C; 1.2 μm for D; 0.6 μm in E.

ous mitochondria and vesicles, demarcating the 2–5-μm large structures characteristic of growth cone morphology and the associated 0.3–0.5-μm thin axonal stalks that were frequently directly in contact with neighboring alpha7-negative oligodendroglial surfaces (Fig. 6A). There was no alpha7 immunoreactivity on the associated myelin or myelinated axons (Fig. 6A), blood vessel endothelia, or large perivascular cells (Fig. 6B). However, some submembraneous alpha7 immunoreactivity was also present on the small pericytes and the astrocytic processes contacting the perivascular basal membranes (Fig. 6B).

Similar sprout ultrastructure was also observed using immunoreactivity for galanin (Fig. 6C, E) and VAChT (Fig. 6D, F). To determine the approximate frequency of different contacts, we analyzed 39 galanin^{+} and 57 VAChT^{+} sprouts at ×10,000 magnification (Table 3). Assessment with these latter, common and unambiguously neuron-specific markers revealed frequent growth cone contacts

TABLE 3.
Utrastructural Growth Cone Contacts

Detected growth cone immunoreactivity	Galanin positive (%)	VAChT positive (%)
Contact with myelin	56 (22/39)	54 (31/57)
Oligodendroglial cell body	3 (1/39)	0 (0/57)
Astrocyte lamella	95 (37/39)	91 (52/57)
Filamentous astrocyte process	23 (9/39)	21 (12/57)
Neighboring axon	97 (38/39)	100 (57/57)
Another growth cone	15 (6/39)	39 (22/57)[1]

[1] $P < 2\%$, χ^2 test comparing this contact type for galanin$^+$ vs. VAChT$^+$ growth cones. Galanin$^+$ and VAChT$^+$ can contact several different structures at the same time, so the total number of different contacts can be higher (approximately three times higher) than the number of the labelled growth cones in either column.

with neighboring unmyelinated axons and astrocyte lamellae (Fig. 6C), other growth cones (Fig. 6D), myelin sheaths (Fig. 6E), and large astrocyte processes containing astrocyte fibrils (Fig. 6F). As shown in Table 3, quantification of identified growth cones and their contacts in the electron microscopic sections of perifacial ventral white matter revealed that they were particularly frequent with neighboring unmyelinated axons (97–100%), astrocyte lamella (91–95%), and outer myelin sheaths (54–56%), and with lower frequency with other growth cones, fibrillar astrocyte processes (21–23%), and oligodendroglial cell bodies (0–3%). This frequency of cellular contacts was very similar for the galanin$^+$ and VAChT$^+$ sprouts. The only exception were contacts with other growth cones, which were approximately 2.5-fold more common in the VAChT$^+$ sprouts (39%) than in galanin$^+$sprouts, with 15% ($P < 2\%$, χ^2 test).

Effects of lipopolysaccharide-induced inflammation and alpha7, brain c-Jun, and TNFR1/2 deletions

Previous studies with the facial axotomy model examining neuronal cell death (Möller et al., 1996; Raivich et al., 2002), leukocyte influx (Raivich et al., 1998; Bohatschek et al., 2001), bystander-activation inflammatory changes in neighboring microglia, and induction of late neuronal regeneration-associated molecules such as galanin and beta1 integrin subunit (Kloss et al., 1999) showed that these events also peak at day 14, coinciding with the currently detected maximum in intracerebral facial axonal sprouting. To determine their effects on the delayed facial sprouting, we next examined the changes resulting from specific gene deletion mutants for alpha7, brain c-Jun, and TNF receptor types 1 and 2 (TNFR1/2) gene deletions, and LPS-induced inflammation, which were previously shown to affect cell death, regeneration, bystander activation, and neural leukocyte recruitment.

In the case of c-Jun, preliminary data suggested a reduction of sprouting in the absence of brain c-Jun (Raivich et al., 2004; Supp. Info. Fig. 2). In the current study, direct quantification of growth cone area using GCD algorithm and visual counting confirmed this effect (Fig. 7A–C), revealing a 97% decrease in area and a 96% decrease in the number of galanin$^+$ sprouts in mice lacking brain c-Jun ($P < 1\%$, Student's *t*-test). Deletion of the alpha7 integrin subunit (Fig. 7G–I) caused a 45% increase in area and 50% increase in the number of galanin$^+$ sprouts in the –/–mice ($P < 5\%$); that of TNFR1/2 (Fig. 7J–L) was associated with a 39% increase in area but minimal change (–3%) in the number of sprouts, with neither change reaching the level of statistical significance ($P = 10.5\%$ and 92%, respectively). Systemic application of 1 mg *E. coli* lipopolysaccharide (LPS) in 0.9% saline (Fig. 7M–R) with a 0.5-, 1-, or 2-day interval preceding day 14 caused an approximately 50% reduction in the area of galanin$^+$ sprouts ($P < 2\%$, one-way ANOVA followed by post hoc Tukey); the effect disappeared at the 4-day interval. Injection of saline alone with a 1-day interval did not affect sprouting (Fig. 7O). Direct visual counting revealed similar, approximately 40% decrease in the number of sprouts 0.5–2 days following exposure to LPS ($P < 5\%$, one-way ANOVA, post hoc Tukey).

Because absence of brain c-Jun also strongly diminished the postaxotomy increase in neuronal galanin immunoreactivity in a previous study (Raivich et al., 2004), it is possible that the currently detected effect of c-Jun was due to galanin-presumptive sprouts carrying very little galanin immunoreactivity and thus escaping detection. This problem appears to be specific for galanin and c-Jun; deletion of alpha7 did not appear affect the overall galanin immunoreactivity (Werner et al., 2000). In the current study, we reconfirmed this lack of effect on the overall galanin immunofluorescence (IF) in the axotomized facial motor nucleus in the alpha7 mutants [10.0 ± 0.4 vs. 9.6 ± 0.7 in optical luminosity values (OLV) for the IF in alpha7+/+ and –/–mice, respectively; $P = 61\%$] and noted similar lack of effect in TNFR1/2 mutants (8.4 ± 0.8 vs 8.6 ± 0.5, $P = 86\%$), or the application of LPS (8.76 ± 0.61 for control, 9.51 ± 0.80 for 0.5 days, 9.88 ± 1.11 for 1 day, 9.55 ± 0.61 for 2 days, and 9.53 ± 0.89 for 4 days, respectively; $P = 90\%$ in one-way ANOVA). In general, brightly fluorescent axonal growth cones showed an approximately 3–3.5-fold higher staining compared with the whole facial motor nucleus (0.50–0.55 in $\log_{10}$ relative intensity of staining and contrast/RISC units). However, unlike the results in the interleukin-6 deletion study (Galiano et al., 2001), we did not observe a statistically significant change in the RISC values of the mutants (jun, alpha7, TNFR1/2) compared with their wild-type littermates (*t*-test) or in LPS-injected animals compared with controls (one-way ANOVA).

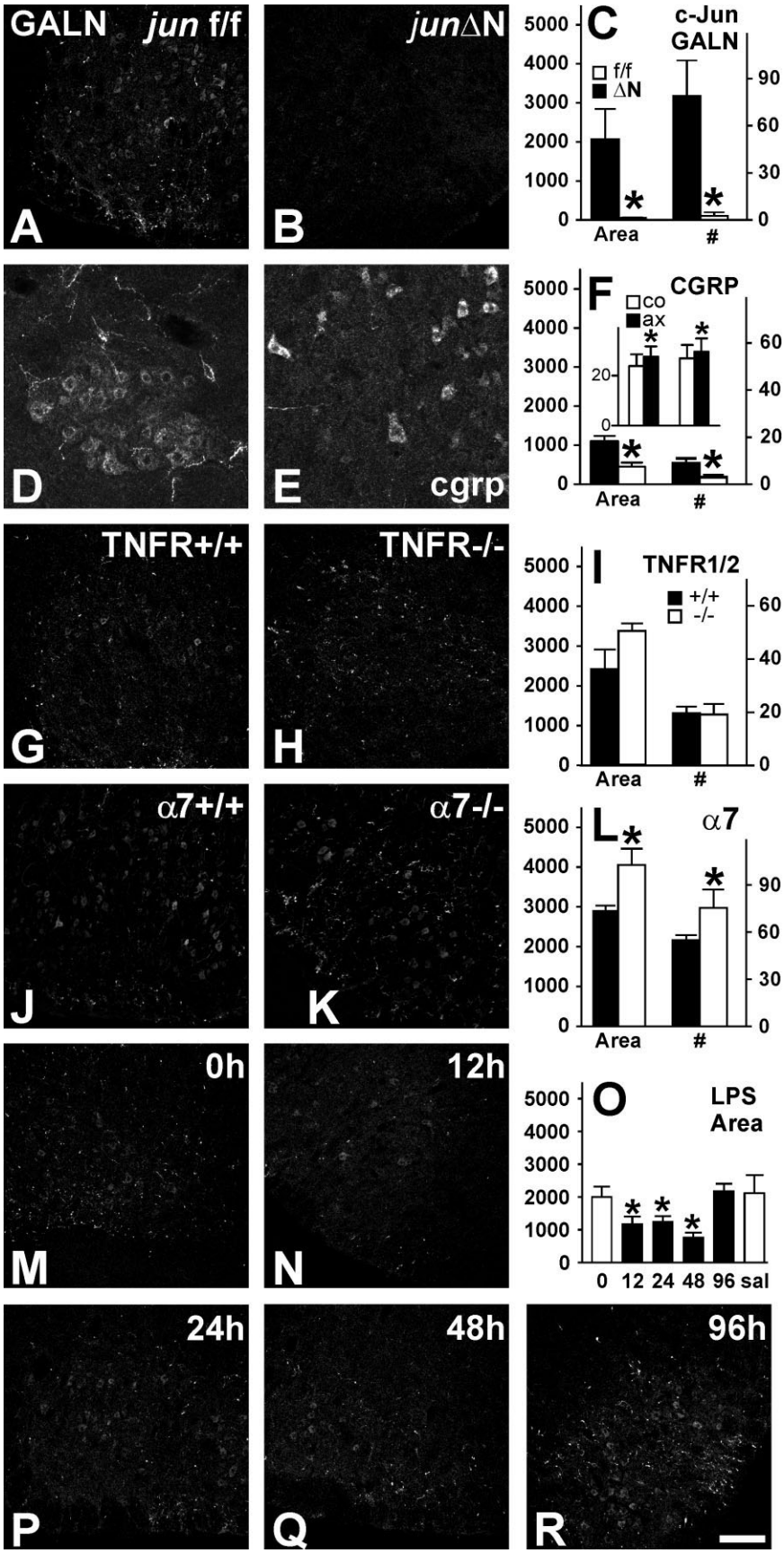
GALN jun f/f
A
junΔN
B
C
c-Jun
GALN
f/f
ΔN
5000
4000
3000
2000
1000
0
90
60
30
0
Area
#
D
E
cgrp
F
CGRP
co
ax
20
0
60
40
20
TNFR+/+
G
TNFR-/-
H
I
TNFR1/2
+/+
-/-
α7+/+
J
α7-/-
K
L
α7
0h
M
12h
N
O
LPS
Area
0 12 24 48 96 sal
24h
P
48h
Q
96h
R

Figure 7

In line with previous data (Moore, 1989; Raivich et al., 1995), quantitative experiments on total CGRP immunoreactivity did reveal constitutively strong staining on the control side and, at 14 days after axotomy, a moderate though significant increase on the injured side in the control *jun*$^{f/f}$ (Fig. 7F, inset, two left bars) as well as in the brain Jun-deficient mice (Fig. 7F, inset, two right bars; $P < 1\%$, Student's *t*-test). Moreover, neither the control nor the axotomized side nor the increase in CGRP staining on the axotomized side was affected by deletion of brain c-Jun.

To validate the effect of brain c-Jun on facial axonal sprouting, we therefore examined the effects on the CGRP^{+} sprouts. As shown in Figure 7D,E, deletion of brain c-Jun brought on a visible reduction in sprouts labeled with CGRP immunoreactivity, while not affecting the intensity of neuronal cell profiles. In the same vein, quantitative comparison of the area covered by CGRP^{+} sprouts (Fig. 7F) showed a 60% decrease in brain Jun-deficient animals compared with their *jun*$^{f/f}$ controls ($P < 2\%$, Student's *t*-test). Direct visual counting revealed a similar, approximately 67% decrease in the number of sprouts ($P < 5\%$).

Changes in beta1 integrin levels

The beta1 integrin subunit is the obligate partner of alpha7 and shows a neuronal expression peak 14 days following facial nerve cut (Kloss et al., 1999), so we next explored the relationship between sprouting response and levels of this regeneration associated molecule. As shown in Figure 8A, absence of the alpha7 integrin caused significantly elevated beta1 integrin levels at day 14 compared with littermate controls (+34%, $P < 5\%$, Student's *t*-test). Similarly, deletion of brain c-jun also showed a 68% decrease in beta1 integrin immunoreactivity following facial axotomy at day 14 (Fig. 8B; $P < 5\%$), in line with the absence in central sprouting observed in these mutants.

Figure 7. Effects of neural c-Jun (*jun*$^{\Delta N}$; **A–F**), TNFR1/2 (**G–I**), and alpha7 (**J–L**) gene deletions and LPS-induced inflammation (**M–R**) on galanin (A–C,G–R)-and CGRP (D–F)-immunoreactive central axonal sprouting in the facial motor nucleus 14 days after cut. Left row, littermate controls; center, mutants; right, quantification of the effects on the area (left Y-axis, parts per million) and number (#, right Y-axis) of galanin-or CGRP-positive sprouts (mean ± SEM, n = 3–6 animals per group). Solid bars, littermate controls; open bars, mutants. In the case of endotoxin (O), single intraperitoneal injection of 1 mg *E. coli* LPS /kg caused a transient decrease of sprouting 12–48 hours after injection (solid bars). Uninjected animals (0) and mice 24 hours after saline (sal) injection served as controls (open bars). *$P <$ 5%, Student's *t*-test (C,I) or ANOVA followed by post hoc Tukey test (O). The **inset** in F shows the overall CGRP immunoreactivity (in OLV values) in the axotomized (ax, solid bars) and contralateral (co, open bars) for the *jun*$^{f/f}$ controls (left) and *jun*$^{\Delta N}$ mutants (right). Scale bar = 200 μm in R (applies to A,C,G–R); 80 μm for D,E.

Administration of LPS did not affect beta1 integrin levels significantly at any of the time points (0.5–4 days) tested (Fig. 8D). There was also no significant difference between cut and crush injury at day 7 or day 14, but there was a 25% increase at day 10 (Fig. 8C). Reinjury paradigms (8 + 6, 14 + 8) caused a significant, 26% and 27% decrease ($P <$ 5%), respectively, compared with their controls at days 14 and 22 (Fig. 8E).

DISCUSSION

Regenerative axonal sprouting is critical for repair of the adult nervous system, but the specific signals involved are only beginning to be understood. The facial nerve axotomy model is a well-characterized paradigm for studying molecular mechanisms involved in successful peripheral regeneration and functional recovery, and previous studies have reported the appearance of central galanin^{+} sprouts inside the facial motor nucleus 14 days after nerve cut (Galiano et al., 2001; Makwana et al., 2007). The aim of the current set of experiments was to establish the neuroanatomical origin and distribution of these growth cone-carrying axons, determine the time course of their sprouting response, and identify physiological causes responsible for its transient appearance and regulation following injury.

As shown in the current study, transection of axons in the peripheral part of the facial motor nerve caused the delayed appearance of sprouting, galanin^{+}, and to a lesser extent CGRP^{+}, neurites inside the central nervous system, in and around the affected facial motor nucleus. These sprouts appeared to originate from axotomized facial motoneurons based on their selective appearance on the injured side; presence of vesicular acetylcholine transporter as a marker of cholinergic phenotype; presence of both galanin^{+} and CGRP^{+} subpopulations of facial motoneurons; and colocalization with the bidirectional, retrograde and anterograde, tracer Mini-Ruby first applied to the proximal stump of the cut facial nerve. As demonstrated in Figure 2H, cell body fluorescence for Mini-Ruby was completely limited to the axotomized facial motor nucleus. Together with the absence of axonal Mini-Ruby staining in sensory projection areas (brainstem, substantia gelatinosa, spinal nucleus of the trigeminal nerve), this argues against a major sensory contribution to the perifacial sprouting. This point is reinforced by the presence of VAChT as a marker of cholinergic phenotype on a large number, although not in all, of sprouts detected here and the fact that VAChT^{+} innervation of motoneurons is not affected by removal of sensory input (Oliveira et al., 2003). Finally, sprouts located outside the nucleus and visualized with their stalk and bulb had their leading structure, the growth cone bulb, in the majority of cases pointing away from the nucleus, suggesting growth away, not growth toward, the nucleus.

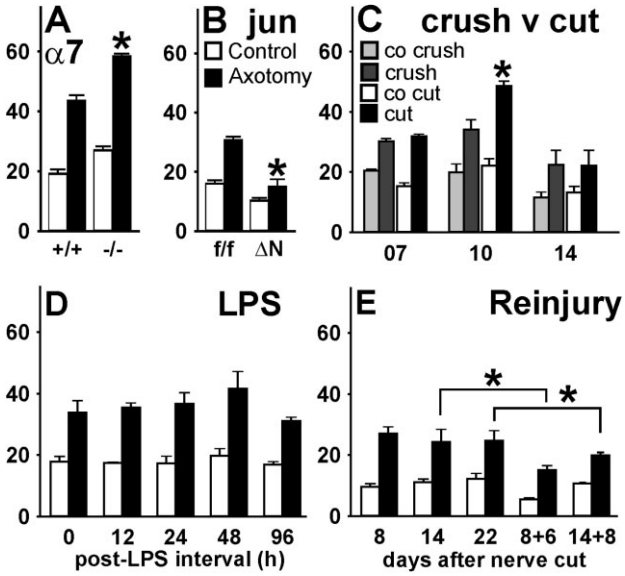

Figure 8. Effects of alpha7 (**A**) and neural *jun* (**B**) deletions, crush vs. cut (**C**), application of LPS (**D**), and additional nerve injury (**E**) on beta1 integrin subunit levels in the axotomized and contralateral facial motor nuclei. $*P < 5\%$, Student *t*-test (A–C) or ANOVA and post hoc Tukey test (E). Beta1 immunoreactivity was quantified by using the Mean-SD algorithm and is shown in OLV values, n = 3–6 animals per group, as in Figure 7. A,B,D show the results from facial motor nuclei 14 days after nerve cut; C compares crush with cut 7–14 days after axotomy; E shows the effects of second (cut) injury. co (C), contralateral side to the lesion.

Neurochemically, the detected sprouts clearly exhibited the profile of growing axon terminals. They contained high levels of anterogradely transported neuropeptides galanin and CGRP, synaptophysin, and VAChT; expressed regeneration-associated CD44 and alpha7beta1 integrin cell adhesion molecules (Werner et al., 2000; Raivich et al., 2004); and lacked MAP2, a typical component of dendritic cytoskeleton (McDermid et al., 2004). The absence of neurofilament H staining is also in line with the fact that neurofilaments do not extend into the terminal growth cone structures (Jacobs and Thomas, 1982; Tetzlaff and Bisby, 1989). Detailed morphological studies in similar models in axotomized cat spinal motoneurons and commissural interneurons showed that these sprouts had a long, axon-like process can project directly from the soma, proximal principal dendrite, or even very distal part of the dendrite, depending on the type of axotomized neuron (MacDermid et al., 2004; Fenrich et al., 2007). Although the current data focus more on the molecular characterization and regulatory dynamics of the sprouting response, it will be of considerable interest to identify in a future study the main subcellular origin of the prolific sprouting response that is observed following mouse facial axotomy.

Sprouting orientation

Theoretically, growth cones associated with the injured facial motor nucleus could be oriented in any direction with respect to the nucleus. In fact, they did show a clearly trimodal distribution (Fig. 1I), with three of the nine segments responsible for 70% of the orientations taken. Sprouts in the largest of these three groups (A, 38%) were oriented away from (0°–20°) and those in the smallest (I, 8%) were oriented directly toward the nucleus (160°–180°). Sprouts in the relatively large intermediate group (E, 24%) oriented themselves roughly perpendicular to the vector from the center of the nucleus and parallel (80–100°) to the outline of the nucleus proper. The overall predominance of outward-pointing sprouts appears to suggest the presence of a strong repellent cue associated with the injured facial motor nucleus, which would be consistent with the lower density of sprouts inside than directly outside the nucleus, as shown in Figure 1H. In the same vein, the presence of a smaller segment of sprouts pointing toward the nucleus (8% in I, 13% in the inward three segments G–I) could be due to a paradoxical reaction, reversing a repellent to an attractant response (Tear, 1998; Gavazzi, 2001) or the presence of bona fide attractors, to which only a smaller subpopulation is sensitive. Finally, instead of a gradual increase from the directly inward-to outward-pointing segments, there is a relatively large, intermediate fraction of "cruising" sprouts that run perpendicular to the vector from the nucleus center. Although at first puzzling, this could suggest that some sprouts lay a decidedly equidistant course between two similarly attractive directions.

At present the identity of signals regulating this orientation distribution are unknown. Injured facial motor neurons are known to change the expression for a series of chemorepellant molecules and their subcellular signalling, with increased semaphorin IIIC and plexin A2 synthesis (Pasterkamp et al., 1998; Spinelli et al., 2007; Oschipok et al., 2008). However, some repellent signals may also originate from neighboring microglia (Schifman and Selzer, 2007), which exhibit maximal activation at day 14 (Bohatschek et al., 2004), together with the peak sprouting response. Here, cell-type-selective deletion of expressed chemorepellent cues will improve insight into the cellular source and specific effects of signals guiding sprouting inside the adult central nervous system.

Effects of regeneration, reinnervation, and recut

The onset and peak of sprouting at day 7 and day 14 after cut occur at roughly the same time as the beginning of facial motoneuron reinnervation of their peripheral target described in previous studies (Werner et al., 2000; Raivich et al., 2004). Moreover, denervated muscle fibers

are a rich source of neutrophins and adhesion molecules (Covault and Sanes, 1985; Koliatsos et al., 1993; Funakoshi et al., 1993; Ishii et al., 1994; Springer et al., 1995) that could provide a transient surge in trophic signals available to axotomized motoneurons during the initial process of reconnection. However, our data do not suggest that reinnervation is responsible for the sudden burst in central axonal sprouting. Although reinnervation is known to occur earlier, more promptly, and with less error after crush than after cut (Nguyen et al., 2002; Witzel et al., 2005), peak levels of sprouting after cut were more than 5-fold higher than after crush. Similarly, the reinterruption of axonal connections with a recut (8 + 6, 14 + 8) led to a significantly stronger sprouting response compared with that observed following a single cut at day 14 and day 22, respectively. This enhanced sprouting could be due to a conditioning effect (Woolf et al., 1992; Gilad et al., 1996). However, the 14 + 8 sprouting was less than at day 14, suggesting that overall duration and presence of recut, rather than the conditioning effect, are the primary variables that define the extent of central sprouting.

Surprisingly, these facial axonal sprouts were particularly numerous in the white matter tissue that appears to inhibit the outgrowth of corticospinal, rubrospinal, or peripheral sensory axons via rapid growth cone collapse (Thallmair et al., 1998; McKerracher, 2001; Cafferty et al., 2008). At the ultrastructural level (Table 1), the facial sprouts showed frequent and close contact with neighboring myelinated sheaths (Fig. 6E, Table 1) and occasionally with the oligodendroglial cell bodies (Fig. 6A), while maintaining an active growth state. Interestingly, and unlike most of the cases mentioned above from previous studies, dissociated sensory neurons microtransplanted into the spinal cord showed almost no inhibition, growing robustly through normal or even through predegenerated white matter (Davies et al., 1999). In fact, they were stopped only by glial scars surrounding CNS lesions. Although these effects appeared to be specific for peripheral sensory neurons—similarly dissociated cortical neurons did not regenerate into white matter (Tom et al., 2004)—the facial sprouting response shown in the current study could suggest that similar resilience to white matter inhibitory signals is inducible in central neurons. Understanding the molecular signals associated with the formation of facial axonal sprouts could thus provide clues to improving regenerative response in the white matter of the central nervous system.

Neuronal cell death and inflammation

The peak in central axonal sprouting in the mouse facial axotomy model also coincides with the maximum in substantial neuronal cell death and also with inflammatory changes in microglia and astrocytes and leukocyte recruitment observed in this CNS injury and repair model. Previous evidence also shows that those subtypes of neurons that are most likely to be programmed to launch a regenerative response after injury, for example, retinal ganglion cells, also exhibit a high rate of cell death (Berkelaar et al., 1994), which is in line with observations in which particular transcription factors such as c-Jun that contribute to cell death are also required for regeneration (Raivich et al., 2004).

In the same vein, brain c-Jun-deficient animals with an absence of neuronal cell death following facial nerve cut (Raivich et al., 2004) do show a reduced sprouting response in the mutant animals. However, this correlation is not maintained in other mutants with effects on cell death in the same model. TNFR1/2 null mice show a 4-fold reduction in cell death (Raivich et al., 2002) and a slight, though not significant, tendency toward higher central sprouting. Transforming growth factor-β1 null mice also show greatly increased cell death, together with a significantly reduced sprouting response (Makwana et al., 2007). A similar lack of linear correlation is also observed for peripheral regeneration, with enhanced sprouting in IL6 null (Galiano et al., 2001) and alpha7 null (Fig 6G–I) animals and reduced sprouting in the brain c-jun-deficient animals (Fig 6A–F); all three groups of mutant mice show a significant reduction in the speed of peripheral nerve outgrowth (Zhong et al., 1999; Werner et al., 2000; Galiano et al., 2001; Raivich et al., 2004).

Current data do show a relatively straightforward correlation between neural inflammation and reduced central axonal sprouting in the facial axotomy model. Systemic application of 1 mg *E. coli* endotoxin causing severe neural inflammation and granulocyte recruitment (Bohatschek et al., 2001), resulted in a 50% reduction in sprouting response 12–48 hours following the intraperitoneal injection (Fig. 6M–R). Enhanced neural inflammation in TGF-beta1 null mice is associated with reduced sprouting (Makwana et al., 2007). This also appears to be true in reverse, with attenuated inflammation and 50% enhanced sprouting in IL6 null mice (Galiano et al., 2001). Finally, reduced inflammatory response in the TNFR1/2 null mice (Hristova et al., 2005; Bohatschek et al., 2005; Liu et al., 2006) coincides with the tendency toward improved sprout outgrowth in these mutant mice shown in the current study and agrees with the appearance of MAP2-negative dendraxon sprouts in permanently axotomized cat motoneurons (McDermid et al., 2004).

Induced inflammation around the cell body has been shown to improve sensory axon outgrowth into the CNS (Lu and Richardson, 1991). However, these results were obtained when inflammatory stimulus was used instead of peripheral nerve injury, unlike the current model in which peripheral injury is followed by a robust inflammatory re-

sponse inside the affected part of the brain (Moran and Graeber, 2004). Central injury frequently produces a mild retrograde reaction, in which additional inflammation will elicit a stimulatory effect (Hossain-Ibrahim et al., 2006), raising the question with regard to those components of neuronal response that specifically enhance neurite outgrowth inside the injured CNS.

Endogenous signals in central axonal sprouting

Up-regulation of neuronal transcription factors such as c-Jun, ATF3, or STAT3 plays an important role in the neural response to injury and the synthesis of molecules required for regeneration and repair (Herdegen and Leah, 1998; Tsujino et al., 2000; Schweizer et al., 2002). As shown in this study, neural expression of c-Jun transcription factor strongly supports the delayed appearance of central axonal sprouting. Although numerous regeneration-associated genes and proteins show an early onset and peak of expression following injury (e.g., ATF3, GAP43, CD44, CGRP, alpha7 integrin subunit) that may allow the different stages in the initiation and execution of neurite outgrowth (Seijffers et al., 2007), there is a second or later group of molecules such as galanin, beta1, and noxa (Kloss et al., 1999; Galiano et al., 2001; Kiryu-Seo et al., 2005; Di Giovanni et al., 2006) with a relatively delayed expression that coincides with central sprouting and neuronal cell death. Moreover, many of the late but also early molecules are brain c-Jun dependent and as shown in the current study are actually expressed in the facial axonal sprouts, for example, CD44, galanin, and alpha7beta1 integrin. These growth-cone-localized molecules support axonal elongation and outgrowth in the peripheral nerve (Werner et al., 2000; Holmes et al., 2000) and may enhance central sprouting as well as allow nascent central growth cones to withstand numerous inhibitory cues such as NOGO, MAG, and OMGP that are present in the white matter (McKerracher, 2001). Although hypothetical, the neurite-outgrowth enhancing properties of galanin could also be involved in the much stronger sprouting observed in the galanin$^+$ compared with the CGRP$^+$ populations of axotomized facial motoneurons.

Deletion of the alpha7 integrin subunit increases central sprouting, which could point to an inhibitory role of the alpha7beta1 integrin. Previous immunohistochemical studies revealed prominent localization of both integrin components, alpha7 and beta1, on the terminal parts of growing axons and the cell bodies of axotomized motor and sensory neurons, with very little expression on most of the axons or in dendritic arborizations (Kloss et al., 1999; Werner et al., 2000). The current study also shows a very similar distribution, with much higher levels of both components in the terminal part of the sprout than in the adjacent axon-like stalk (Fig. 5S–U,Z–AB,AC–AE), pointing to a specific growth cone function. Furthermore, the apparently compensatory up-regulation of beta1 could suggest enhanced activity, for example, via one of the other 11 currently identified beta1-associating alpha subunits (Sixt et al., 2006), by interacting with fibronectin, the main extracellular matrix component associated with the outgrowth of transplanted sensory neurons in central white matter, for example (Tom et al., 2004). Moreover, the strong decrease in posttraumatic neuronal expression of beta1 in brain Jun-deficient mice could also contribute to the reduction in central sprouting in these mutant animals.

This potential involvement of beta1-family integrins is qualified by incomplete overlap of peak beta1 levels (day 10) and sprouting (day 14) in the cut vs. crush experiment. It is possible that the regulatory control exerted by the alpha7beta1 integrin is in fact several steps upstream of the actual sprouting response, particularly inasmuch as the immunoreactivities for beta1 (Fig. 8C) and for alpha7 (Fig. 1b in Werner et al., 2000) both peak between day 7 and day 10 and are already strongly decreased at day 14. Moreover, the significant reduction of beta1 levels in the recut experiment was associated with enhanced sprouting (Fig. 7D,E) and could indicate the presence of additional pathways involved in the regulation of central axonal outgrowth under varying genetic and experimental conditions. Nevertheless, the hypothesis for beta1-integrin-family involvement will have to be tested using central neuronal deletion of the beta subunit to settle this issue. Furthermore, if these experiments do show positive involvement of beta1, identifying the cognate alpha subunit(s) involved in central axonal sprouting could enhance the therapeutic understanding of the repair processes operating in the injured brain and spinal cord.

ACKNOWLEDGMENTS

We gratefully acknowledge the help of Ms. Dietmute Büringer (Neuromorphology, Martinsried) and Mr. Mark Tully (Cell and Developmental Biology Department, UCL) for their expert assistance with electron microscopy and Prof. Horst Bluethmann (Hoffmann-LaRoche, Basel, Switzerland) for providing the TNFR1/2 null mice.

LITERATURE CITED

Behrens A, Sibilia M, David JP, Möhle-Steinlein U, Tronche F, Schütz G, Wagner EF. 2002. Impaired postnatal hepatocyte proliferation and liver regeneration in mice lacking c-jun in the liver. EMBO J 21:1782–1790.

Berkelaar M, Clarke DB, Wang YC, Bray GM, Aguayo AJ. 1994. Axotomy results in delayed death and apoptosis of retinal ganglion cells in adult rats. J Neurosci 14:4368–4374.

Blue ML, Davis G, Conrad P, Kelley K. 1993. Specific cleavage of the α4 integrin associated with activation of peripheral T lymphocytes. Immunol 78:80–85.

Bohatschek M, Werner A, Raivich G. 2001. Systemic LPS injection leads to granulocyte influx into normal and injured brain: effects of ICAM-1 deficiency. Exp Neurol 172:137–152.

Bohatschek M, Kloss CU, Hristova M, Pfeffer K, Raivich G. 2004. Microglial major histocompatibility complex glycoprotein-1 in the axotomized facial motor nucleus: regulation and role of tumor necrosis factor receptors 1 and 2. J Comp Neurol 470: 382–399.

Cafferty WB, McGee AW, Strittmatter SM. 2008. Axonal growth therapeutics: regeneration or sprouting or plasticity? Trends Neurosci 31: 215–220.

Covault J, Sanes JR. 1985. Neural cell adhesion molecule (N-CAM) accumulates in denervated and paralyzed skeletal muscles. Proc Natl Acad Sci U S A 82:4544–4548.

Cotman CW, Geddes JW, Kahle JS. 1990. Axon sprouting in the rodent and Alzheimer's disease brain: a reactivation of developmental mechanisms? Prog Brain Res 83:427–434.

Davies SJ, Goucher DR, Doller C, Silver J. 1999. Robust regeneration of adult sensory axons in degenerating white matter of the adult rat spinal cord. J Neurosci 19:5810–5822.

Di Giovanni S, Knights CD, Rao M, Yakovlev A, Beers J, Catania J, Avantaggiati ML, Faden AI. 2006. The tumor suppressor protein p53 is required for neurite outgrowth and axon regeneration. EMBO J 25:4084–4096.

Diamond J, Coughlin M, Macintyre L, Holmes M, Visheau B. 1987. Evidence that endogenous beta nerve growth factor is responsible for the collateral sprouting, but not the regeneration, of nociceptive axons in adult rats. Proc Natl Acad Sci U S A 84:6596–6600.

Echtermeyer F, Schöber S, Pöschl D, von der Mark H, von der Mark K. 1996. Specific induction of cell motility on laminin by 7 integrin. J Biol Chem 271:2071–2075.

Erickson SL, de Sauvage FJ, Kikly K, Carver-Moore K, Pitts-Meek S, Gillett N, Sheehan KC, Schreiber RD, Goeddel DV, Moore MW. 1994. Decreased sensitivity to tumour-necrosis factor but normal T-cell development in TNF receptor-2-deficient mice. Nature 372:560–563.

Fenrich KK, Skelton N, Macdermid VE, Meehan CF, Armstrong S, Neuber-Hess MS, Rose PK. 2007. Axonal regeneration and development of de novo axons from distal dendrites of adult feline commissural interneurons after a proximal axotomy. J Comp Neurol 502:1079–1097.

Friede RL, Bischhausen R. 1980. The fine structure of stumps of transected nerve fibers in subserial sections. J Neurol Sci 44:181–203.

Funakoshi H, Frisen J, Barbany G, Timmusk T, Zachrisson O, Verge VM, Persson H. 1993. Differential expression of mRNAs for neurotrophins and their receptors after axotomy of the sciatic nerve. J Cell Biol 123:455–465.

Galiano M, Liu ZQ, Kalla R, Bohatschek M, Koppius A, Gschwendtner A, Xu SL, Werner A, Kloss C, Bluethmann H, Raivich G. 2001. Interleukin-6 (IL6) and the cellular response following facial nerve injury: effects on lymphocyte recruitment, early microglial activation and axonal outgrowth in IL6-deficient mice. Eur J Neurosci 14:327–341.

Gavazzi I. 2001. Semaphorin-neuropilin-1 interactions in plasticity and regeneration of adult neurons. Cell Tissue Res 305: 275–284.

Gilad VH, Tetzlaff WG, Rabey JM, Gilad GM. 1996. Accelerated recovery following polyamines and aminoguanidine treatment after facial nerve injury in rats. Brain Res 724:141–144.

Gilmor ML, Nash NR, Roghani A, Edwards RH, Yi H, Hersch SM, Levey AI. 1996. Expression of the putative vesicular acetylcholine transporter in rat brain and localization in cholinergic synaptic vesicles. J Neurosci 16:2179–2190.

Harris J, Ayyub C, Shaw G. 1991. A molecular dissection of the carboxyterminal tails of the major neurofilament subunits NF-M and NF-H. J Neurosci Res 30:47–62.

Hemler ME, Crouse C, Takada Y, Sonnenberg A. 1988. Multiple very late antigen (VLA) heterodimers on platelets. Evidence for distinct VLA-2, VLA-5 (fibronectin receptor), and VLA-6 structures. J Biol Chem 263:7660–7665.

Herdegen T, Leah JD. 1998. Inducible and constitutive transcription factors in the mammalian nervous system: control of gene expression by Jun, Fos and Krox, and CREB/ATF proteins. Brain Res Rev 28:370–490.

Heumann R, Goemans C, Bartsch D, Lingenhohl K, Waldmeier PC, Hengerer B, Allegrini PR, Schellander K, Wagner EF, Arendt T, Kamdem RH, Obst-Pernberg K, Narz F, Wahle P, Berns H. 2000. Transgenic activation of Ras in neurons promotes hypertrophy and protects from lesion-induced degeneration. J Cell Biol 151:1537–1548.

Holmes FE, Mahoney S, King VR, Bacon A, Kerr NC, Pachnis V, Curtis R, Priestley JV, Wynick D. 2000. Targeted disruption of the galanin gene reduces the number of sensory neurons and their regenerative capacity. Proc Natl Acad Sci U S A 97: 11563–11568.

Holzmann B, Weissman IL. 1989. Integrin molecules involved in lymphocyte homing to Peyer's patches. Immunol Rev 108: 45–61.

Hossain-Ibrahim MK, Rezajooi K, MacNally JK, Mason MR, Lieberman AR, Anderson PN. 2006. Effects of lipopolysaccharide-induced inflammation on expression of growth-associated genes by corticospinal neurons. BMC Neurosci 7:8.

Hristova M, Cuthill D, Zbarsky V, Acosta-Saltos A, Wallace A, Blight K, Buckley SM, Peebles D, Heuer H, Waddington SN, Raivich G. 2009. Activation and deactivation of periventricular white matter phagocytes during postnatal mouse development. Glia 58:11–28.

Hu C, Mayadas-Norton T, Tanaka K, Chan J, Salgame P. 2000. Mycobacterium tuberculosis infection in complement receptor 3-deficient mice. J Immunol 165:2596–2602.

Ide C, Kato S. 1990. Peripheral nerve regeneration. Neurosci Res Suppl 13:S157–S164.

Ishii DN, Glazner GW, Pu SF. 1994. Role of insulin-like growth factors in peripheral nerve regeneration. Pharmacol Ther 62: 125–144.

Kalla R, Liu Z, Xu S, Koppius A, Imai Y, Kloss CU, Kohsaka S, Gschwendtner A, Möller JC, Werner A, Raivich G. 2001. Microglia and the early phase of immune surveillance in the axotomized facial motor nucleus: impaired microglial activation and lymphocyte recruitment but no effect on neuronal survival or axonal regeneration in macrophage-colony stimulating factor-deficient mice. J Comp Neurol 436:182–201.

King TE, Pawar SC, Majuta L, Sroka IC, Wynn D, et al. 2008. The role of $\alpha 6$ integrin in prostate cancer migration and bone pain in a novel xenograft model. PLoS ONE 3:e3535.

Kiryu-Seo S, Hirayama T, Kato R, Kiyama H. 2005. Noxa is a critical mediator of p53-dependent motor neuron death after nerve injury in adult mouse J Neurosci 25:1442–1447.

Kloss CUA, Werner A, Shen J, Klein MA, Kreutzberg GW, Raivich G. 1999. The integrin family of cell adhesion molecules in the injured brain: regulation and cellular localization in the normal and regenerating mouse facial nucleus. J Comp Neurol 441: 162–178.

Koliatsos VE, Clatterbuck RE, Winslow JW, Cayouette MH, Price DL. 1993. Evidence that brain-derived neurotrophic factor is a trophic factor for motor neurons in vivo. Neuron 10:359–367.

Li L, Zhou XF. 2001. Pericellular *Griffonia simplicifolia* I isolectin B4-binding ring structures in the dorsal root ganglia following peripheral nerve injury in rats. J Comp Neurol 439:259–274.

Linda H, Risling M, Cullheim S. 1985. "Dendraxons" in regenerating motoneurons in the cat: do dendrites generate new axons after central axotomy? Brain Res 358:329–333.

Liu BP, Cafferty WB, Budel SO, Strittmatter SM. 2006. Extracellular regulators of axonal growth in the adult central nervous system. Philos Trans R Soc Lond B Biol Sci 361:1593–1610.

Liu W, Hirata K, Kawabuchi M. 2005. The occurrence of nitric oxide synthase-containing axonal baskets surrounding large neurons in rat dorsal root ganglia after sciatic nerve ligation. Arch Histol Cytol 68:29–40.

Lu X, Richardson PM. 1991. Inflammation near the nerve cell body enhances axonal regeneration. J Neurosci 11:972–978.

MacDermid VE, Neuber-Hess MS, Rose PK. 2004. The temporal sequence of morphological and molecular changes in axotomized feline motoneurons leading to the formation of axons from the ends of dendrites. J Comp Neurol 468:233–250.

Makwana M, Jones LL, Cuthill D, Heuer H, Bohatschek M, Hristova M, Friedrichsen S, Ormsby I, Bueringer D, Koppius A, Bauer K, Doetschman T, Raivich G. 2007. Endogenous transforming growth factor beta1 suppresses inflammation and promotes survival in adult CNS. J Neurosci 27:11201–11213.

Mayer U, Saher G, Fässler R, Bornemann A, Echtermeyer F, von der Mark H, Miosge N, Pöschl E, von der Mark K. 1997. Absence of integrin alpha 7 causes a novel form of muscular dystrophy. Nat Genet 17:318–323.

McLachlan EM, Hu P. 1998. Axonal sprouts containing calcitonin gene-related peptide and substance P form pericellular baskets around large diameter neurons after sciatic nerve transection in the rat. Neuroscience 84:961–965

McLachlan EM, Janig W, Devor M, Michaelis M. 1993. Peripheral nerve injury triggers noradrenergic sprouting within dorsal root ganglia. Nature 363:543–546.

McKerracher L. 2001. Spinal cord repair: strategies to promote axon regeneration. Neurobiol Dis 8:11–18.

McQuarrie IG. 1985. Effect of conditioning lesion on axonal sprout formation at nodes of Ranvier. J Comp Neurol 231: 239–249.

Mehta A, Reynolds ML, Woolf CJ. 1993. Partial denervation of the medial gastrocnemius muscle results in growth-associated protein-43 immunoreactivity in sprouting axons and Schwann cells. Neuroscience 57:433–442.

Menon B, Krishnamurthy P, Kaverina E, Johnson JN, Ross RS, Singh M, Singh K. 2006. Expression of the cytoplasmic domain of beta-1 integrin induces apoptosis in adult rat ventricular myocytes (ARVM) via the involvement of caspase-8 and mitochondrial death pathway. Basic Res Cardiol 101:485–493.

Möller JC, Klein MA, Haas S, Jones LL, Kreutzberg GW, Raivich G. 1996. Regulation of thrombospondin in the regenerating mouse facial motor nucleus. Glia 17:121–132.

Moore RY. 1989. Cranial motor neurons contain either galanin-or calcitonin gene-related peptidelike immunoreactivity. J Comp Neurol 282:512–522.

Moran LB, Graeber MB. 2004. The facial nerve axotomy model. Brain Res Rev 44:154–178.

Nguyen QT, Sanes JR, Lichtman JW. 2002. Pre-existing pathways promote precise projection patterns. Nat Neurosci 5:861–867.

Oliveira AL, Hydling F, Olsson E, Shi T, Edwards RH, Fujiyama F, Kaneko T, Hökfelt T, Cullheim S, Meister B. 2003. Cellular localization of three vesicular glutamate transporter mRNAs and proteins in rat spinal cord and dorsal root ganglia. Synapse 50:117–129.

Oschipok LW, Teh J, McPhail LT, Tetzlaff W. 2008. Expression of Semaphorin3C in axotomized rodent facial and rubrospinal neurons. Neurosci Lett 434:113–118.

Pasterkamp RJ, Giger RJ, Verhaagen J. 1998. Regulation of semaphorin III/collapsin-1 gene expression during peripheral nerve regeneration. Exp Neurol 153:313–327.

Pinkstaff JK, Detterich J, Lynch G, Gall C. 1999. Integrin subunit gene expression is regionally differentiated in adult brain. J Neurosci 19:1541–1556.

Raivich G, Makwana M. 2007. The making of successful axonal regeneration: genes, molecules and signal transduction pathways. Brain Res Rev 53:287–311.

Raivich G, Reddington M, Haas CA, Kreutzberg GW. 1995. Peptides in motoneurons. Prog Brain Res 104:3–20.

Raivich G, Haas S, Werner A, Klein MA, Kloss C, Kreutzberg GW. 1998. Regulation of MCSF receptors on microglia in the normal and injured mouse central nervous system: a quantitative immunofluorescence study using confocal laser microscopy. J Comp Neurol 395:342–358.

Raivich G, Liu ZQ, Kloss CUA, Labow M, Bluethmann H, Bohatschek M. 2002. Cytotoxic potential of proinflammatory cytokines: combined deletion of TNF receptors TNFR1 and TNFR2 prevents motoneuron cell death after facial axotomy in adult mouse. Exp Neurol 178:186–193.

Raivich G, Bohatschek M, Clive DaCosta C, Iwata O, Galiano M, Hristova M, Wolfer DP, Lipp HP, Aguzzi A, Wagner EF, Behrens A. 2004. Essential role of the AP-1 transcription factor c-jun in axonal regeneration. Neuron 43:57–67.

Ramon y Cajal S. 1928. Degeneration and regeneration of the nervous system. London: Oxford University Press.

Rothe J, Lesslauer W, Lötscher H, Lang Y, Koebel P, Köntgen F, Althage A, Zinkernagel R, Steinmetz M, Bluethmann H. 1993. Mice lacking the tumour necrosis factor receptor 1 are resistant to TNF-mediated toxicity but highly susceptible to infection by *Listeria monocytogenes*. Nature 364:798–802.

Salmon AM, Damaj MI, Marubio LM, Epping-Jordan MP, Merlo-Pich E, Changeux JP. 2001. Altered neuroadaptation in opiate dependence and neurogenic inflammatory nociception in alpha CGRP-deficient mice. Nat Neurosci 4:357–358.

Schifman MI, Selzer ME. 2007. Differential expression of class 3 and 4 semaphorins and netrin in the lamprey spinal cord during regeneration. J Comp Neurol 501:631–646.

Schmits R, Filmus J, Gerwin N, Senaldi G, Kiefer F, Kundig T, Wakeham A, Shahinian A, Catzavelos C, Rak J, Furlonger C, Zakarian A, Simard JJ, Ohashi PS, Paige CJ, Gutierrez-Ramos JC, Mak TW. 1997. CD44 regulates hematopoietic progenitor distribution, granuloma formation, and tumorigenicity. Blood 90:2217–2233.

Schweizer U, Gunnersen J, Karch C, Wiese S, Holtmann B, Takeda K, Akira S, Sendtner M. 2002. Conditional gene ablation of Stat3 reveals differential signaling requirements for survival of motoneurons during development and after nerve injury in the adult. J Cell Biol 156:287–297.

Seijffers R, Mills CD, Woolf CJ. 2007. ATF3 increases the intrinsic growth state of DRG neurons to enhance peripheral nerve regeneration. J Neurosci 27:7911–7920.

Sigurjonsson OE, Perreault MC, Egeland T, Glover JC. 2005. Adult human hematopoietic stem cells produce neurons efficiently in the regenerating chicken embryo spinal cord. Proc Natl Acad Sci U S A 102:5227–5232.

Sixt M, Bauer M, Lammermann T, Fassler R. 2006. Beta1 integrins: zip codes and signaling relay for blood cells. Curr Opin Cell Biol 18:482–490.

Spinelli ED, McPhail LT, Oschipok LW, Teh J, Tetzlaff W. 2007. Class A plexin expression in axotomized rubrospinal and facial motoneurons. Neuroscience 144:1266–1277.

Springer JE, Seeburger JL, He J, Gabrea A, Blankenhorn EP, Bergman LW. 1995. cDNA sequence and differential mRNA regulation of two forms of glial cell line-derived neurotrophic factor in Schwann cells and rat skeletal muscle. Exp Neurol 131:47–52.

Tanigawa N, Saito T, Ogawa K, Iida H. 2005. Origin of regenerated axons in nerve bypass grafts. J Neurotrauma 22:605–612.

Tear G. 1998. Molecular cues that guide the development of neural connectivity. Essays Biochem 33:1–13.

Teixido J, Parkerlf CM, Kassner PD, Hemler ME. 1992. Functional and structural analysis of VLA-4 integrin $\alpha 4$ subunit cleavage. J Biol Chem 257:1786–1791.

Thallmair M, Metz GA, Z'Graggen WJ, Raineteau O, Kartje GL, Schwab ME. 1998. Neurite growth inhibitors restrict plasticity and functional recovery following corticospinal tract lesions. Nat Neurosci 1:124–131.

The UniProt Consortium. 2009. The Universal Protein Resource (UniProt). Nucleic Acids Res 37:D169–D174.

Tom VJ, Doller CM, Malouf AT, Silver J. 2004. Astrocyte-associated fibronectin is critical for axonal regeneration in adult white matter. J Neurosci 24:9282–9290.

Tronche F, Kellendonk C, Kretz O, Gass P, Anlag K, Orban PC, Bock R, Klein R, Schütz G. 1999. Disruption of the glucocorticoid receptor gene in the nervous system results in reduced anxiety. Nat Genet 23:99–103.

Tsujino H, Kondo E, Fukuoka T, Dai Y, Tokunaga A, Miki K, Yonenobu K, Ochi T, Noguchi K. 2000. Activating transcription factor 3 (ATF3) induction by axotomy in sensory and motoneurons: a novel neuronal marker of nerve injury. Mol Cell Neurosci 15:170–182.

Uhlenkott CE, Huijzer JC, Cardeiro DJ, Elstad CA, Meadows GG. 1996. Attachment, invasion, chemotaxis, and proteinase expression of B16-BL6 melanoma cells exhibiting a low metastatic phenotype after exposure to dietary restriction of tyrosine and phenylalanine. Clin Exp Metastasis 14:125–137.

von Ballestrem CG, Uniyal S, McCormick JI, Chau T, Singh B, Chan BM. 1996. VLA-beta 1 integrin subunit-specific monoclonal antibodies MB1.1 and MB1.2: binding to epitopes not dependent on thymocyte development or regulated by phorbol ester and divalent cations. Hybridoma 15:125–132.

Werner A, Willem M, Jones LL; Kreutzberg GW, Mayer U, Raivich G. 2000. Impaired axonal regeneration in a7-integrin deficient mice. J Neurosci 20:1822–1830.

Witzel C, Rohde C, Brushart TM. 2005. Pathway sampling by regenerating peripheral axons. J Comp Neurol 485:183–190.

Woolf CJ, Shortland P, Coggeshall RE. 1992. Peripheral nerve injury triggers central sprouting of myelinated afferents. Nature 355:75–78.

Zhong J, Dietzel ID, Wahle P, Kopf M, Heumann R. 1999. Sensory impairments and delayed regeneration of sensory axons in interleukin-6-deficient mice. J Neurosci 19:4305–4313.